



CRYSTALLOGRAPHIC MECHANISMS OF TOPOTACTIC
STRUCTURE CHANGES, ESPECIALLY IN
INORGANIC NITRATE CRYSTALS

BY

WALTRAUD MARIA KRIVEN B.Sc.(HONS.)

T H E S I S
SUBMITTED FOR THE DEGREE OF
DOCTOR OF PHILOSOPHY

DEPARTMENT OF PHYSICAL AND INORGANIC CHEMISTRY
THE UNIVERSITY OF ADELAIDE
FEBRUARY, 1976.

S U M M A R Y

The transformations $I \rightleftharpoons II \rightarrow III$ in $RbNO_3$ were studied by X-rays, X-ray-optical, optical microscopy and computational methods. The initial product in $I \rightarrow II$ corresponded to the type A orientation previously reported in the NaCl-type to CsCl-type martensite transformation in NH_4Br . In the analogous structure change in $RbNO_3$, further crystallographic information was found through the rhombohedral, phase II intermediate.

Mechanisms were discussed for the type A orientation. To test whether martensite theory applied the relevant features were computed for the lattice invariant shear (L.I.S.) systems of $\{100\}\langle 011 \rangle_I$ and $\{110\}\langle 001 \rangle_I$ which were derived from transformation twinning. The habit plane provides a much more sensitive test of the operative L.I.S. than do the orientation relations. With the reported lattice parameters the predicted habit plane is 4° off $\{102\}_I$ for $(100)\langle 011 \rangle$ L.I.S., and 9° off $\{010\}_I$ for the $(110)\langle 001 \rangle$ L.I.S. Although on the $[100]$ projection, the computed habit plane trace directions based on (100) twinning agreed with observation, whilst with (110) twinning there was a discrepancy of $\pm 6^\circ$, on the $\{111\}$ projection the traces observed can correspond only to the (110) twinning. This is in accordance with the observed subtexture in the main bands. The general agreement between theory and observations confirmed that the $I \rightleftharpoons II$ transformation is martensitic.

The postulated mechanisms were able to illustrate in sets of unit cells, the origin of observed lamellae and their subtexture where it

occurred. They further showed how misfit dislocations assist the accommodation of detwinned product in the parent matrix. Internal strains of the initial product are relieved by annealing or relaxation phenomena analogous to recovery and recrystallization in deformed metals and alloys. The phenomena observed were twin blunting, ballooning of lamellae, and the passage of a detwinning interface. When crystals of II were allowed to anneal before measurement, product crystals contained only one or two grains. Among the orientations found was a type B relation previously reported in NH_4Br .

Six new relations for $\text{I} \rightarrow \text{III}$ exhibited a common crystallographic characteristic. The order-disorder $\text{IV} \rightarrow \text{III}$ transformation was followed in the electron microscope by the disappearance of weak, superlattice reflections. In RbNO_3 at least seventeen orientation relations were experimentally observed.

Electron microscopy of KNO_3 yielded five orientation relations, of which two describe the $\text{II} \rightarrow \text{I}$ transformation. KNO_3 completely decomposes under electron radiation to KNO_2 and K_2O (β). The topotactic process may be regarded as a structure change accompanied by a composition change. One relation corresponded to a martensitically predicted orientation, based on the $\{\text{100}\}\langle\text{011}\rangle_{z=4}$ shear system analogous to that in the isostructural but reverse process in RbNO_3 .

The aragonite-type to calcite-type transformation in KNO_3 $\text{II} \rightarrow \text{I}$ was studied by optical microscopy, X-ray diffraction, electron microscopy and computing. Experimental observations reveal reproducible shape changes and orientation relations. By optical microscopy with

interference contrast, regular, parallel surface traces on $\{b\}_{II}$ faces were found to lie on certain crystallographic zones. Assuming the observed X-ray relation found in three experiments, of $[c]_{II} \parallel [c]_{I,hex}$, $Z=3$, $[b]_{II} \parallel [a]_I$, some of the traces lie on zones which contain the planes $\{110\}_I$ and $\{100\}_I$ or $\{1\bar{1}1\}_I$ of the rhombohedral, $Z=4$ cell.

In the ten experimentally determined relations it was frequently observed that main crystallographic axes in the parent become such in the product. Other irrational orientations also resulted including a pseudo-equivalent of a previously reported relation. With respect to the transformation the pseudo-hexagonal nature of the orthorhombic phase was verified. It was shown that the aragonite-calcite transformation is not necessarily reconstructive but the observations imply a martensite mechanism.

A computer martensite analysis of the $II \rightarrow III$ transformation in zirconia was done to check on the effect of errors in a published analysis. A comparison of the effect of lattice parameters using the same method of calculation, showed that the number and positions of predicted habit planes is sensitive to lattice parameters. This indicated that great care should be taken to use lattice parameters at the transformation temperature.

TABLE OF CONTENTS

	Page No.
TITLE	i
SUMMARY	ii
TABLE OF CONTENTS	v
DECLARATION	viii
ACKNOWLEDGEMENT	ix
<u>CHAPTER 1. INTRODUCTION</u>	1
SECTION 1.1 PHASE TRANSFORMATIONS AND TOPOTAXY	2
SECTION 1.2 MECHANISMS AND MARTENSITE THEORY	10
<u>CHAPTER 2. PHASE TRANSFORMATIONS IN RUBIDIUM NITRATE</u>	22
SECTION 2.1 INTRODUCTION	23
SECTION 2.2 EXPERIMENTAL APPARATUS AND TECHNIQUES	46
SECTION 2.3 CALCITE-TYPE UNIT CELLS	52
SECTION 2.4 $I \rightleftharpoons II$ TRANSFORMATION	58
2.4.1 X-ray Observations	58
2.4.2 Optical Results	66
2.4.3 X-ray - Optical Results	70
2.4.4 Martensite Calculations	72
SECTION 2.5 $I \rightarrow III$ TRANSFORMATIONS, X-RAY OBSERVATIONS	83
SECTION 2.6 $IV \rightarrow III$ TRANSFORMATIONS, ELECTRON MICROSCOPY	85
SECTION 2.7 INTERPRETATION AND DISCUSSION	87
2.7.1 $I \rightleftharpoons II \rightarrow III$ Transformation	87
(a) Interpretation	87
(b) Discussion	104
(i) X-ray and X-ray - Optical Results	104
(ii) Optical Microscopy	131

	Page No.
SECTION 2.8 CONCLUSION	135
<u>CHAPTER 3. THE DECOMPOSITION OF POTASSIUM NITRATE IN AN ELECTRON MICROSCOPE</u>	139
SECTION 3.1 INTRODUCTION	140
SECTION 3.2 METHODS AND RESULTS	145
SECTION 3.3 GRAPHICAL MARTENSITE ANALYSIS	150
SECTION 3.4 INTERPRETATION AND DISCUSSION	154
SECTION 3.5 CONCLUSION	164
<u>CHAPTER 4. THE II \rightarrow I TRANSFORMATION IN POTASSIUM NITRATE</u>	166
SECTION 4.1 INTRODUCTION	167
SECTION 4.2 EXPERIMENTAL APPARATUS AND TECHNIQUES	181
SECTION 4.3 RESULTS	184
4.3.1 $\{110\}_{II}$ Twinning and Premonitory Effects	184
4.3.2 Optical Microscopy	190
4.3.3 Scanning Electron Microscopy	200
4.3.4 Transmission Electron Microscopy	203
4.3.5 X-ray Diffraction	207
SECTION 4.4 CALCULATION OF THE REGION OF COHERENT RE-ARRANGEMENT BY THE METHOD OF ARKHAROV	215
SECTION 4.6 INTERPRETATION AND DISCUSSION	223
4.6.1 Analysis of Previously Reported Orientation Relations	223
4.6.2 Discussion	230
SECTION 4.7 CONCLUSION	245

	Page No.
<u>CHAPTER 5. PART A - A MARTENSITE ANALYSIS OF THE TETRAGONAL TO MONOCLINIC TRANSFORMATION IN ZIRCONIA</u>	246
SECTION 5.1 INTRODUCTION	247
SECTION 5.2 RESULTS	250
SECTION 5.3 DISCUSSION AND CONCLUSION	267
<u>CHAPTER 5. PART B - ELECTRON MICROSCOPY OF MERCURIC SULPHIDE</u>	
SECTION 5.4 INTRODUCTION	270
SECTION 5.5 OBSERVATION	271
APPENDIX A	273
BIBLIOGRAPHY	284
PUBLISHED PAPERS	304

DECLARATION

This thesis describes my own work in the Department of Physical and Inorganic Chemistry, at the University of Adelaide. To the best of my knowledge, it contains no material previously presented for any other degree, at this or any other University, or written or published by any other person, except where due reference is given in the text.

ACKNOWLEDGEMENT

I am sincerely grateful to Dr. S.W. Kennedy for his guidance and supervision during this work, and I appreciate his patience.

To my colleague, Dr. W.L. Fraser, I am also indebted for his friendship and heuristic discussions which significantly helped this work.

Thanks are due to Mr. A. Bowers particularly, and the workshop and electronics staff, for their good work and prompt attention with apparatus and repairs.

I thank Dr. M.R. Snow and Prof. D.O. Jordan for supervision during preparation of this thesis. I commend the accurate typing of Mrs. K. Hardie, the printing of thesis photographs by Mr. K. Tank of the Photographic Services Group of the University, and final copies of diagrams by Mrs. J. Laing. My parents are thanked for financing the production of this thesis.

The award of a University of Adelaide Research Grant for four years and three months is acknowledged.

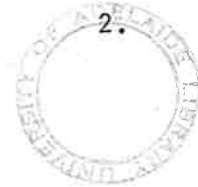
CHAPTER 1.

CHAPTER 1. INTRODUCTION.

	<u>Page No.</u>
SECTION 1.1 PHASE TRANSFORMATIONS AND TOPOTAXY.	2
1.2 MECHANISMS AND MARTENSITE THEORY.	10

CHAPTER 1

INTRODUCTION



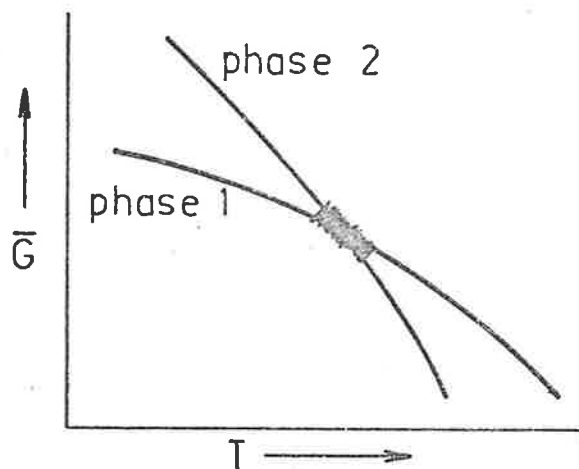
SECTION 1.1 PHASE TRANSFORMATIONS AND TOPOTAXY

Crystalline solids may exist in more than one phase. When one polymorph or modification changes to another, a transformation occurs. The reasons why a structure changes are determined by thermodynamics and kinetic studies. The way a structure changes defines the mechanism. (4)

A treatise on the thermodynamics of transformations is given by Ubbelohde. (1-3) At a given temperature and pressure a one component solid is described by equations of state summarized in the molar free energy function $G = f(T,P)$. The classical approach to defining a transformation considers that two phases, 1 and 2, are in equilibrium but independent of each other. The molar free energy curves intersect when $\bar{G}_1 = \bar{G}_2$. The first derivatives of T and P are related to the molar entropy ΔS and molar volume change ΔV , by the Clausius - Clapeyron equation:

$$\frac{dP}{dT} = \frac{\Delta S}{\Delta V}$$

Experimental observation of crystals indicates that the point of transformation is not always well defined. The graph of free energy curves is "smeared" at their intersection indicating "thermodynamic indeterminacy" in this region.



Classical thermodynamics is modified when the two phases are regarded as mutually dependent with reference to the volume difference between the two structures. Macroscopic samples of solid consist of subgrains in various orientations. With two phases in equilibrium there will be a strain arising from bulk compression or tension energy, χ_{12} , as well as a domain or subgrain boundary energy, σ_{12} , produced by structural misfits at domain interfaces.^(4,8-10) The free energy becomes $\bar{G}_1 = f(T, P, \chi_{12}, \sigma_{12})$. Since the modifying factors depend on the direction of transformation, χ_{12} is not necessarily equal to χ_{21} ; neither does $\sigma_{12} = \sigma_{21}$. This causes hysteresis.

Transformations in a single crystal are also subject to these modifying factors. Ubbelohde⁽¹⁻³⁾ postulates a "hybrid" crystal in which the two phases are mutually oriented to minimize strains.

Discontinuous transformations commence by nucleation and growth.⁽⁴⁻⁷⁾ During the early stage of nucleation, an embryo of the new phase is sensitive to accommodation in the bulk matrix and hence subtexture or grain size. Due to hysteresis in different subgrains, a discontinuous transformation may appear to be "smeared" or continuous.

Thermodynamics shows how the free energy expresses the driving force for a transformation, and affects the kinetics of the process.⁽⁵⁾ It further classifies structure changes as discontinuous or continuous. When there is an abrupt change in the state functions describing a system, for example volume, enthalpy or entropy, the transformation is discontinuous and a corresponding discontinuity appears in the curve of the first derivative of G. When no such discontinuity is found until the second or higher derivative~~s~~ of the free energy function, the transformation is said to be continuous.⁽¹⁾ Further classifications are based on structural considerations.

Mechanisms are of equal importance to thermodynamics and kinetics in describing a transformation. Buerger^(44,34) proposed the following generally accepted terminology. In a "reconstructive" transformation, first coordination bonds are broken and remade to give the new phase (figure 1). Such processes are usually slow to occur, or "sluggish" due to their high activation energy. On the other hand, a "displacive" transformation involves no rupture of first coordinations, but merely a distortion of the lattice. The energy involved is much lower, and the change is relatively fast. Other descriptions which

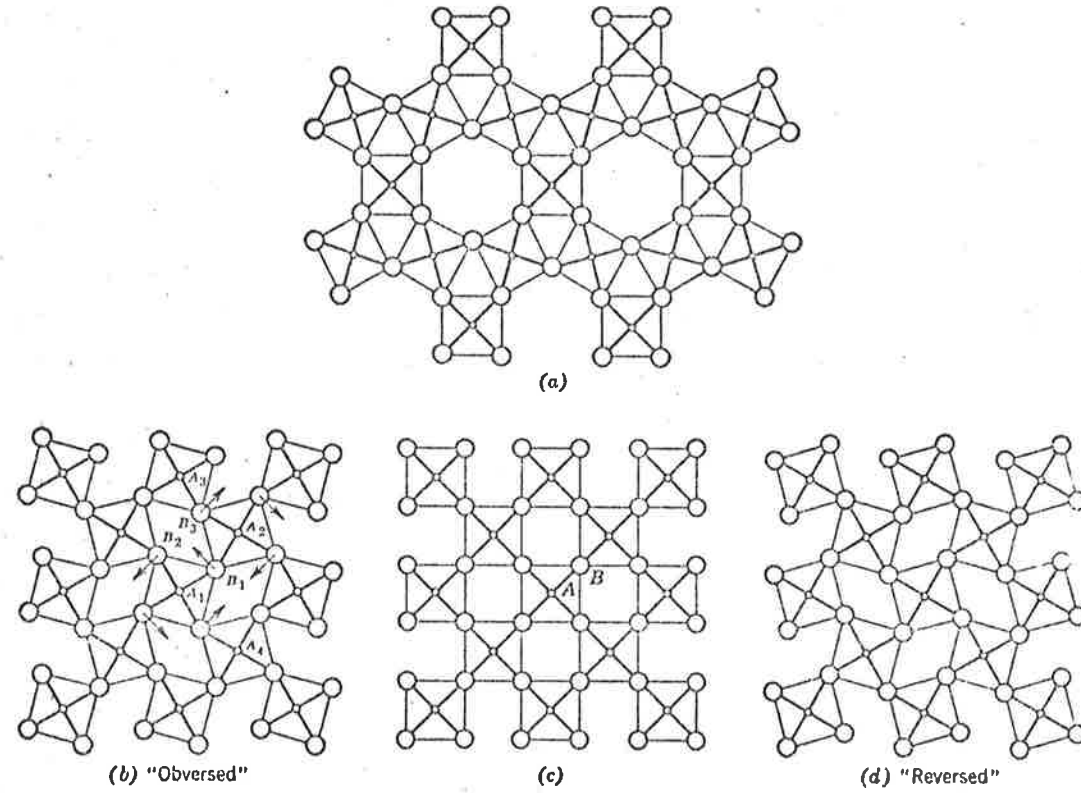


Figure 1. A reconstructive process converts (a) to (c) and involves breaking first-
coordination bonds. A displacive transformation occurs during (c) to (b)
or (d).

have been used for this classification are *topotactic*, *cooperative*, *diffusionless*, *coordinated*, *deformational*, *martensitic* or *military*.

Another more recent type of classification is based on the interface and its manner of propagation. (11,187,337) In a coherent transformation the three-dimensional framework is preserved without rupture. This may occur with migrating twin boundaries, boundaries in crystals undergoing displacive transformations, coherent precipitates, and coherent exsolution lamellae. Where there is not good fit at the interface, it is strained, or, with increasing disregistry the strain is relieved by a grid of dislocations and a semicoherent interface results. (6,337)

The geometry of a coherent interface (11) shows that it propagates by cooperative movement of the row of atoms at the interface. The movement occurs in the direction of a vector whose length is less than the translational vector of the parent lattice. Displacive mechanisms may further be categorized as martensitic and non-martensitic or oriented growth-type mechanisms.

Displacive transformations may also be described as "topotactic". This then includes solid state reactions in which the transformation is accompanied by a composition change. Although the latter term has been used by some workers (14,132) as referring only to reactions involving a composition change, others use it more comprehensively. In a recent review of "Topography and Topology in Solid State Chemistry", Thomas (15) draws a distinction between "topotactic" and "topochemical" reactions. Earlier, Dent Glasser, Glasser and

Taylor⁽¹³⁾ recognized such a distinction, and adopted an intermediate position.

Thomas⁽¹⁵⁾ uses the term "topochemical" for three-dimensional orientation relations between the crystallography of the product and reactant phases, in the same way as epitaxy and epitactic reactions refer to the two-dimensional orientations which occur when a new phase forms on the surface of another. "Topos" is Greek, meaning "a place",⁽³³⁵⁾ whilst "tassein"(Gk.) means "to put in order". Alternatively, "Tassis"(Gk.) is "a stretching" and "epi"(Gk.) means "upon". Hence epitaxy refers to two-dimensional fit of one substrate on another. By analogy with this second root or origin of the word, "topotaxy" used by Dasgupta^(14,132) refers only to those reactions in which the over-all three-dimensional arrangement and morphology of a crystal remains unchanged during the replacement or addition of ions or atoms. It is apparent to the writer that Thomas,⁽¹⁵⁾ and at a compromising stage, Dent Glasser, Glasser and Taylor⁽¹³⁾ are effectively using the first root of the word. This allows for some displacive-type distortion of the lattice during the composition change. The latter usage is preferred and adopted by the writer on the basis of the work described in this thesis, particularly Chapter 3.

Bernal⁽¹²⁾ has categorized topotactic reactions as chemical, in which there is a composition change, or geometrical where there is not. The latter corresponds to a phase transformation.

"Topotaxy" therefore, may be defined as:

a solid state reaction in which there is a three-dimensional lattice correspondence, and hence, an orientation relation between parent and product structures. The process may or may not be accompanied by a composition change.

Such a definition then includes displacive-type transformations, to those accompanying composition changes, to "topochemical" reactions.

Numerous examples of topotaxy have been reviewed. (13-15,349)

The phenomenon of topochemical control was identified early in inorganic compounds, (336) and Thomas (15) comprehensively reviews further examples of such.

In inorganic compounds and minerals, amongst the oxides and mixed oxides, various phases of Fe, Ti, Mn, Si, Al and some of their combinations, are interchanged. This occurs by addition or removal of H₂O molecules from layers of the cation-oxygen lattice. Exsolution phenomena, for example in spinel are classed as topotactic, (13) as are the reactions in hydroxides, oxide hydroxides and silicates of small cations.

The trend in carbonates of Fe, Ca, Mg, Mn, and Zn is to decompose topotaxially to their oxides on heating. (14) Clay minerals and other important rock-forming silicate minerals of pyroxenes, amphiboles and olivines likewise transform pseudo-morphically. These compounds may be pictured as silicon-oxygen layers which have condensed into SiO₄ tetrahedra such as occurs in olivines. Infinite single chains of tetrahedra are found in pyroxenes, while amphiboles are characterized

by double chains which adopt a form repeated at intervals of two tetrahedra. This arrangement allows fit into the cation - oxygen framework of the structures. These chains are called Zweierketten. The silicates of larger cations cause the chains to adopt a structure repeated every three to five tetrahedra, referred to as Dreierketten or Funferketten respectively. Thus, topotactic reactions are widespread in solid, inorganic oxy-compounds.

SECTION 1.2 MECHANISMS AND MARTENSITE THEORY

There is a distinction between structural relations between polymorphs, and the actual mechanism by which a transformation proceeds. Besides its intrinsic interest, the former usually is necessary background for the latter. If one closely examines a structure, a likely transformation mechanism may become apparent, or a choice between them may be facilitated.

Structural analysis by X-rays is a space-averaging and time-averaging procedure. Electron microscopy however, permits considerable insight into the microstructure of solids, and consequently into their behaviour. Numerous, apparently unrelated structures have been unified by the successful application of the metallurgical concepts of dislocations. (4,8,9)

Stacking sequences and faults are intimately connected with partial dislocations and antiphase boundaries. Such extended defects rationalize polytypism (207) and are involved in continuous transformations in minerals (337) as well as in exsolution phenomena such as spinodal decomposition. (160-162,167,169,172)

The arrangement of dislocations into planar faults, and their various combinations in extended defects are the basis of explanations of ultra-microstructural characteristics of a range of metal oxides and mixed oxides. (15) The contemporary trend of high-resolution electron microscopy (338-343) and lattice - image calculations (289,291) provide direct evidence of extended defects in the ultra-micro-structure of solids of metallurgical and chemical interest. Reviews

have been published^(344-346,15) of these faulted structures which are briefly described as follows.

Magnéli phases⁽³⁴⁷⁾ are a homologous series of oxides of the metals W, Mo and Re, which may be represented by a formula such as $M_n O_{3n-1}$ or $M_n O_{3n-2}$, where n is integral and variable. The oxides are grossly non-stoichiometric. Such types of phases are also found in other transition metal oxides, for example, of Ti, V, Cr and in mixed oxides such as W-Nb-O. Wadsley⁽³⁴⁸⁾ explained the series by postulating that the decrease in the ratio of oxygen to metal ions could be accommodated by localized variations in faults, or the manner in which coordination octahedra share atoms. Geometrically, when an oxygen layer is removed from a stoichiometric crystal, the two half crystals fuse and shear on a plane. The direction of shear has a component parallel to the missing layer. Hence, as the oxygen to metal ratio diminishes the coordination number between atoms is still preserved. Proceeding through the series, varying amounts of the usually corner-shared octahedra of $Re O_3$ - type structures become edge-shared, which constitutes a rutile-type structure. Face-shared octahedra occur in other non-stoichiometric solids.

These Wadsley-type planar defects are described as crystallographic shear or (c.s.) planes. Several varieties have since been postulated and experimentally observed. C.S. planes may be single, double or "swinging", that is, pivoting. When single c.s. planes intersect they produce double c.s. planes or "block structures" which also can accommodate a large number of distinct compositions. Cylindrical

antiphase boundaries may be produced by rotation faults.

The above considerations of structural relations in metallurgical and inorganic chemical substances, do not necessarily describe a transformation mechanism. (303,349) However, they substantiate the conclusion that there is a gradation of types of mechanism between the extremes of reconstructive to displacive or topotactic.

Other types of transformation mechanisms have been postulated, which include 0-lattice theory (351,352) and the geometry of coincidence-site lattices. (350) Furthermore, chemical reactions in solids may be mechanically initiated. (353,226)

The term "martensite" originated from the austenite (f.c.c.) to martensite (b.c.t.) transformation in steels. The mechanism of this transformation was subsequently shown to have wider applications so that now it is generally understood that "martensite is defined not by what it is, but by how it forms". (354) Martensite theory is a purely mathematical or geometric method for explaining and/or predicting the crystallographic mechanism and orientation relations of certain types of displacive transformations. Such transformations have the following observable properties:

- (a) There is a homogeneous, shear-like shape change in the product.
- (b) The transformation proceeds at an interface or habit plane on which there is optimum fit by both parent and product structures. Depending on strains in the structures, habit planes sometimes develop as lenticular plates.

(c) There is a precise orientation relation between the two phases.

(d) There is often fine substructure in the product.

The crystallography of martensite transformations was independently formulated as matrix algebra methods, by Wechsler, Lieberman and Read (1953)^(39,17) and Bowles and Mackenzie (1954).⁽²⁷⁻²⁹⁾

Several detailed treatments⁽⁴⁶⁾ and reviews have subsequently been published.^(30,16,355,157,174,333,41) A geometric method was also described by W.L. & R.⁽¹⁷⁾ which was used and is illustrated in Chapter 3 of this thesis. A brief outline of the main concepts only will be given here.

It seems to the writer that a martensite transformation may be likened to a child's game of standing domino pieces in a long line. When the end piece is hit, it knocks down its neighbour and so on along the line. The reaction is fast, yet each piece moves only a short distance. Sometimes the reaction loses momentum and stops, and a new flick is required. Appreciable driving forces required by martensite transformations are provided during superheating or cooling.

In terms of the crystallography the speed of the reaction is due to a coherent plane of fit between the two structures. This is the interface or habit plane which is glissile, and on the average, undistorted and unrotated by the transformation. Given that one structure deforms into another, the problem is to find the usually irrational plane of fit common to both structures. Their mutual

orientation relation is thus defined.

It has been shown,⁽¹⁷⁾ as illustrated in figure 2, that an inhomogeneous transformation with a plane of zero average distortion is energetically more favourable than a homogeneous transformation. An inhomogeneous shear refers to the mechanism in which a lattice variant deformation such as a Bain strain⁽¹⁵⁷⁾ or Buerger deformation⁽⁴⁴⁾ is coupled with a lattice invariant deformation, such as slip or twinning.

The habit plane or interface is produced in an inhomogeneous transformation as follows. Referring to figures 3(a) to (e), a parent lattice (a) is deformed into a product lattice (b) by a lattice variant deformation. The solid undergoes a macroscopic shape change (e), but on closer examination, it is seen not to be the same as the lattice deformation. This is due to compensating lattice invariant shears of slip or twinning (figures 3(d) to (e)), which facilitate accommodation of the product in the bulk matrix. A habit plane or interface (figure 4) separates the parent from the sheared product.

As yet, shear systems are found by examination of the two structures, viewed in terms of a suitable lattice correspondence between cells. A three-dimensional homogeneous strain is characterized by at least one set of mutually orthogonal directions, which remain orthogonal but possibly rotated, after the strain has occurred.⁽⁴⁶⁾ These are defined as the *principal axes* (or eigen vectors) of the strain, and are written as a deformation matrix of the type

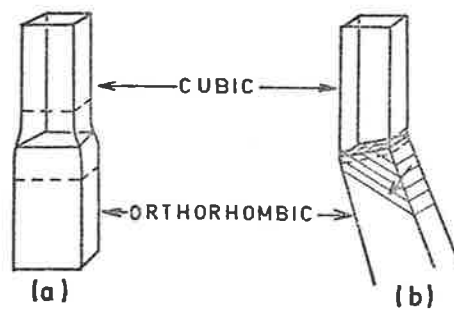


Figure 2. Homogeneous and Inhomogeneous shear

- (a) Homogeneous transformation as in single crystal to single crystal.
- (b) Inhomogeneous transformation as to a set of twin-related regions.
(ref.17).

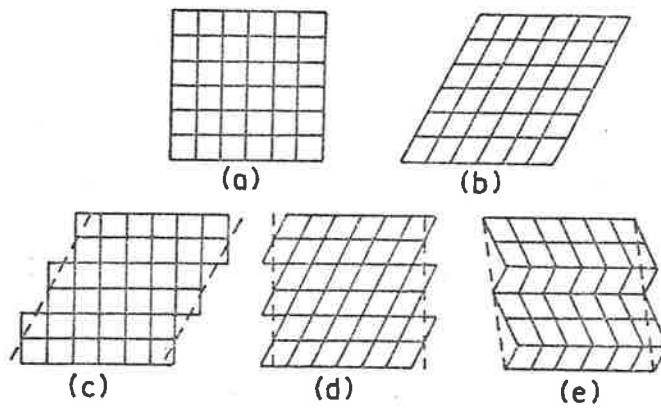


Figure 3. (a) Parent lattice
(b) deformed product lattice
(c) to (e) lattice invariant shear of slip or twinning.

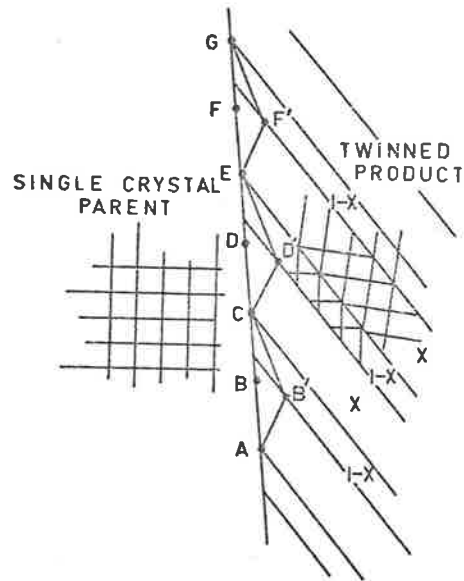


Figure 4. The equal segmented line in the parent $ABCD\dots G$ goes into the broken line $AB'CD'EF'G$ during this two-dimensional analog of the transformation to a twinned product. Note that $AB' \perp AB$ while $B'C \perp EC$, but $ABCD\dots G = AB'CD'EF'G$ and, therefore, this line lies in the habit plane which is, on the average, undistorted. (After reference 17).

$$\begin{vmatrix} \eta_1 & 0 & 0 \\ 0 & \eta_2 & 0 \\ 0 & 0 & \eta_3 \end{vmatrix}$$

Wayman⁽⁴⁶⁾ explains the general construction of martensite theory.

In terms of the geometric method, if an undistorted plane is to result from a homogeneous distortion, one of the principal distortions must be greater than unity, one must be less than unity, and the third must be equal to unity. This condition may be visualized as a sphere containing three mutually orthogonal axes. Since one axis is unchanged in length by the lattice invariant deformation, the description reduces to two dimensions. The circle becomes an ellipse whose axes are given by the remaining two axes of the deformation (figure 5). The point of intersection between a circle and ellipse defines a vector which is undistorted by the transformation. When the angle between any two of the four such vectors remains unchanged, an undistorted and unrotated habit plane is found.

During transformation there is fit of the two structures at the interface. Geometrically, this is obtained by a lattice invariant shear coupled with a rotation, so that the habit planes of parent and product structures coincide. The four solutions thus obtained define the orientation relation. The graphical martensite analysis of Chapter 3 was done by the above method of Wechsler, Lieberman and Read.^(17,49)

The matrix algebra formulation may be summarized in the equation⁽⁴⁶⁾

$$P_1 = R B P$$

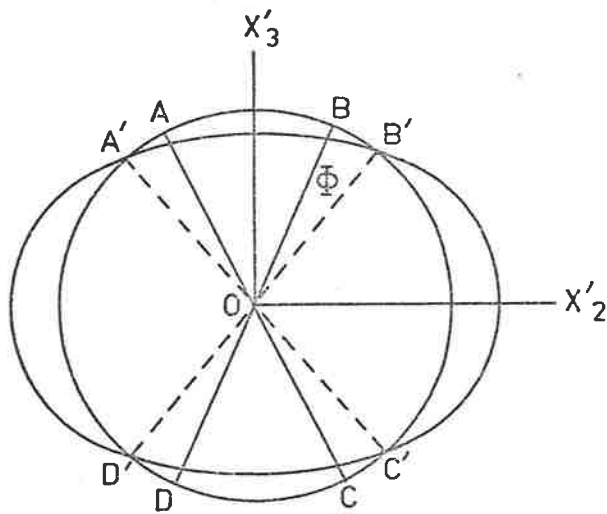


Figure 5. A circular cone of unextended vectors is deformed into an ellipse.

where the above are matrix representations defined as

R = rigid body rotation

B = lattice variant deformation

P = lattice invariant deformation

P₁ = macroscopic shape change.

The algebraic solutions to the above equation and its implications are long and hazardous, but they have been significantly facilitated by use of the computer. Two such programs were available and used in this work, PRØGRAM MRTNST of Ledbetter and Wayman⁽³⁰⁾ and PRØGRAM MARTENS of Fraser.⁽⁴¹⁾ The latter deals with the case where two of the principal deformations are the same, that is, $\eta_1 = \eta_2$. The required input data are

- (i) the lattice parameters determined as accurately as possible at the transformation temperature,
- (ii) the lattice correspondence matrix
- (iii) the magnitudes and directions of the principal deformation axes
- (iv) the shear system, which may be slip or twinning.

The output information is relatively detailed and gives four solutions or variants which include predicted habit planes and orientation relations.

Any shear system may mathematically give a solution but it is not valid unless the shear system is a valid one for the structure. The concept of transformation twinning⁽¹⁸⁶⁾ (see Chapter 2) which has been

successfully applied, however, proposes that a twin plane in the product is derived from a mirror plane in the parent. The geometrical, almost phenomenological predictions of martensite theory are compared with experimental observations, for verification.

Martensite analyses involving two stages or double shears have also been discussed.⁽³³⁴⁾ Recent considerations are concerned with the relationship of martensite theory to the lattice dynamics within solids. Clapp⁽³⁵⁶⁾ discusses a localized soft mode theory in which strains near lattice defects cause a rapid change in local elastic properties, resulting in localized "soft mode" centres. Such regions are proposed as primary nucleation sites for martensitic transformations. Further knowledge of such dynamical lattice instabilities or soft phonons⁽³⁵⁷⁾ may deepen the current understanding of martensite transformations.

The aim of this work, therefore, was to continue in the investigation of transformation mechanisms in inorganic nitrate crystals. Furthermore, it was endeavoured to ascertain the applicability of the metallurgical theories of martensite transformations, in appropriate cases, irrespective of the significant volume change and non-spherical, oppositely-charged ions which constitute inorganic compounds.

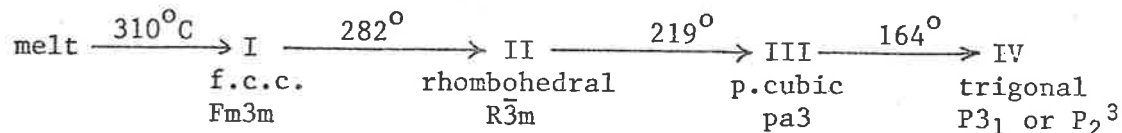
CHAPTER 2

CHAPTER 2PHASE TRANSFORMATIONS IN RUBIDIUM NITRATE

	<u>Page</u>
SECTION 2.1 INTRODUCTION	23
2.2 EXPERIMENTAL APPARATUS AND TECHNIQUES	46
2.3 CALCITE-TYPE UNIT CELLS	52
2.4 $I \rightleftharpoons II$ TRANSFORMATION	58
2.4.1 X-ray Observations	58
2.4.2 Optical Results	66
2.4.3 X-ray - Optical Results	70
2.4.4 Martensite Calculations	72
2.5 $I \rightarrow III$ TRANSFORMATIONS, X-RAY OBSERVATIONS	83
2.6 $IV \rightarrow III$ TRANSFORMATION, ELECTRON MICROSCOPY	85
2.7 INTERPRETATION AND DISCUSSION	87
2.7.1 $I \rightleftharpoons II \rightarrow III$ Transformation	87
(a) Interpretation	87
(b) Discussion	104
(i) X-ray and X-ray - Optical Results	104
(ii) Optical Microscopy	131
2.8 CONCLUSION	135

SECTION 2.1 INTRODUCTION

Rubidium nitrate exists as the following polymorphs at one atmosphere pressure.



A further phase V occurs below -45°C , where the $\text{IV} \rightleftharpoons \text{V}$ transformation involves only minor structural rearrangements. As partly summarized in Tables 1 to 4, and elsewhere⁽⁷²⁻⁷⁵⁾ the above phases have been investigated by X-rays,⁽⁴⁸⁻⁵⁷⁾ differential thermal analysis,^(61,65) calorimetry,^(62,63) dilatometry,⁽⁶⁴⁾ optical microscopy,^(49,64,78,79) neutron diffraction,⁽⁶⁰⁾ image intensification,⁽⁴⁵⁾ dielectric properties,^(66,68,69) infra-red absorption and Raman spectroscopy,^(59,85-89) ultra violet absorption spectroscopy,⁽⁶⁴⁾ electrical conductivity,^(49,67,76,77,84) proton magnetic resonance,⁽⁷⁰⁾ and pyroelectric properties.⁽⁵⁸⁾ Another phase also exists above 16 Kb at room temperature.⁽⁸¹⁾ The phase diagram of RbNO_3 over a temperature range of 700°C and pressure range of 60 Kb, has been investigated,⁽⁸²⁾ the latest work being by Cleaver and Williams.⁽⁸³⁾

There is a distinction between structural relations between polymorphs, and the actual mechanism by which the transformation proceeds. Besides its intrinsic interest, the former usually is necessary background for studies of the latter. If one closely examines a structure, a likely transformation mechanism may become apparent, or a choice between several may be facilitated.

TABLE 1
STRUCTURAL DATA ON RbNO₃

Phase	System	Lattice Parameters (Å)	Space Group	No. of Formula Units	Density (g/cc)	Temp. of (°C) Analysis	Reference
I	cubic	a = 7.32		4	2.50	295	(49)
	cubic	a = 7.32		4		290	(50)
	f.c.c.	a = 7.32		4	305	(51)	
		a = 7.29			→ 291	(51)	
	NaCl-type		Fm3m	4		(52)	
II	hexagonal	a = 5.48 c = 10.71	R $\bar{3}$ m(c.f. NaNO ₃ I, KNO ₃ I)	3		250	(53)
	(rhombohedral)	a = 4.77 α = 70°10'		1			(53)
	tetragonal	a = 6.19 c = 8.74		4	2.92		(49)
	rhombohedral	a = 4.79 α = 70°12'		1		250	(50)
	(Hexagonal)	a = 5.51 c = 10.74		3		(50)	
				R $\bar{3}$ m		(52)	

Continued/.....

TABLE 1 (cont.)

Phase	System	Lattice Parameters (Å)	Space Group	No. of Formula Units	Density (g/cc)	Temp. of (°C) Analysis	Reference	
III	cubic	a = 4.371		1		210	(54)	
	cubic	a = 8.74	Pa3(T _h ⁶)	8			(55)	
	cubic	a = 4.36		1	2.96	180	(49)	
	cubic	a = 4.37		1		180	(50)	
				lower symmetry than Pm3m	1			(52)
IV	rhombohedral	a = 7.37 α = 109°28'	C _{3v} ⁵	4			(56)	
	(pseudo-cubic)	a = 4.26		1				
	hexagonal	a = 10.45 c = 7.38	H3m (C _{3v} ²)	9	3.134	room temp.	(57)	
	trigonal	a = 10.48 c = 7.45	P3 ₁ 12 or P3 ₂ 12	9	3.11		(49)	
	trigonal	a = 10.49 c = 7.44		9		29	(51)	
				P3 ₁ or P3 ₂				(58)
				D _h ³ symmetry for nitrate group				(59)
			P3 ₁ (C ₃ ²) or P3 ₂ (C ₃ ³)				(60)	
			(C ₃ ²) or (C ₃ ³)				(85)	

TABLE 2
TEMPERATURE OF PHASE TRANSFORMATIONS IN RbNO₃ AT ONE
ATMOSPHERE (°C) where (c) denotes cooling and (h) heating

melt ↔ I	I ↔ II	II ↔ III	III ↔ IV	Method of Determination	Reference
314 (h)	291(h)	219(h)	164(h)	d.t.a.	(61)
310	281	211(c) 218(h) 219.2-220.7	160 164	calorimetry direct differential calorimetry	(62) (63)
	282+1(h)	219+2(h)	161+2(h)	optical microscopy	(64)
	270(c) 278(h)	202(c) 228(h) 218+2(c) 222+2(h)	153(c) 166(h) 161+2(c) 168+4(h)	d.t.a. dielectric constant	(65) (66)
	281+1.5(h)	219+1.5(h)	161+1.5(h)	resistivity	(66)

TABLE 3
THERMODYNAMIC DATA ON RbNO₃ TRANSFORMATIONS

(c) denotes cooling (h) denotes heating (x) denotes name of phase

Parameter	melt \longleftrightarrow I	I \longleftrightarrow II	II \longleftrightarrow III	III \longleftrightarrow IV	Method of Determination	Reference
ΔH (Kcal/mole)	1,109 \pm 1.5%	0.23 \pm 6.5%	0.767 \pm 2%	0.932 \pm 1.5%	calorimetry	(62)
			0.774 \pm 1.5%	0.923 \pm 1.5%	direct differential calorimetry	(63)
		0.300(h)	0.650(h)	0.950(h)	d.t.a.	(65)
ΔS (cal/g.deg)	1.9 \pm 1.5%	0.42 \pm 6.5%	1.53 \pm 2%	2.15 \pm 1.5%	calorimetry	(62)
ϵ (a)(Kcal/mole)		55(h)	50(h)	165(h)	d.t.a.	(65)
Volume(\AA^3)	98.06	92.88	83.45	(Phase IV) 77.55		(52)
$\frac{\Delta V_x}{V_{x-1}}$ (%)	-5.58%(C)	-10.15%(c) 5.58%(h)	-7.07%(c) 11.30%(h)	7.61%(h)		

TABLE 4

PHYSICAL PROPERTIES OF THE FOUR PHASES OF RbNO_3

where (c) denotes cooling and (h) denotes heating, and (rev) denotes reversible

Parameter	I	II	III	IV	Reference
Electrical Properties				pyroelectric	(80)
		antiferroelectric	paraelectric		(68)
				antiferroelectric	(69)
				pyroelectric	(58)
Conductance (σ) in (ohm^{-1}) or (mho)	only observed transformation $\text{I} \rightleftharpoons \text{II}$ as change of slope in plot of $\log \sigma$ vs. $1/T$ ($^{\circ}\text{K}$)	σ	3σ (h)	0.03σ (h), (rev)	(49,74)
		σ	30σ (rev)	0.03σ (rev)	
Specific conductance	4.5×10^5	7.8×10^{-1}	1.8×10^2	2.5	(67)
Crystal morphology and optical properties		calcite-type, with strong, negative birefringence			(78)
	isotropic	anisotropic	isotropic	needles with triangular cross-section	(49)
		rhombohedral, high birefringence			(79)

continued/....

TABLE 4 (Cont.)

Parameter	I	II	III	IV	Reference
Thermal expansion coeff. $\alpha(^{\circ}\text{C}^{-1})$ (curve)			85×10^{-6}	$\alpha_c = 101.5 \times 10^{-6}$	(48)
				$\alpha_a = 97.1 \times 10^{-6}$ at 164°C	(68)

Phase IV is an ordered structure of 9 formula units per cell. The trigonal cell slightly deviates from being hexagonal⁽⁵⁷⁾ but could also be pseudo-cubic, $a = 4.26 \text{ \AA}$.⁽⁵⁶⁾ Low temperature infrared and Raman spectroscopy⁽⁸⁹⁾ reveal nitrate anions librating about the trigonal axis, in a planar torsional oscillation. Early studies depict two thirds of the NO_3^- in site symmetry⁽⁹⁰⁾ C_3 and one third in C_{3V} , (C_8),⁽⁵⁹⁾ but subsequent researchers^(86,59,88) find all the nitrates on general C_1 sites. Since a crystallographic C_1 site can accommodate only three nitrate groups, it is argued from Raman spectra⁽⁸⁵⁾ that the nitrates lie in three, non-equivalent sites. It is inferred that these sites approximate to a C_3 or C_2 site and the static fields at two of the distinct sites are similar but not identical.

The IV to III reversible⁽⁵³⁾ transformation is accompanied by changes in the internal frequency region of Raman spectra;^(86,89) in particular, the loss of weaker components in the 1300 to 1400 cm^{-1} band and the broadening of all bands. The conclusion that RbNO_3 IV \rightarrow III is an order-disorder type of transformation^(89,92) grows from the following observations: a large increase in conductance^(49,67) (even in Cs^+ or K^+ doped specimens⁽⁷⁶⁾), sharp dielectric anomalies,^(68,91) a deep minimum in the expansion coefficient,⁽⁶⁸⁾ only a slight change in lattice dimensions,⁽⁷⁵⁾ entropy considerations, and ferroelectric phase IV converting to para-electric phase III.⁽⁶⁸⁾

Pauling's⁽⁹³⁾ concept of free rotation of atomic groups in solids was adopted⁽⁸⁹⁾ to explain X-ray data on nitrate and carbonate structures.

However, Lander⁽⁹⁴⁾ argued that a disordered arrangement of non-spherical ions, as opposed to complete spherical rotation, would also do this.

The ordering of librating NO_3^- units in the nitrate system depends on oxygen-oxygen interaction between neighbouring groups. In a given crystal,⁽⁸⁹⁾ the anion should orient itself in the potential field so that its oxygen atoms are at a maximum distance from the neighbouring oxygens. This position is not unique, however, as equivalent positions can be obtained by a rotation about the trigonal axis. Potential maxima occur at every 120° or 60° depending on the symmetry of the site. If sufficient energy is available a librating anion can surmount the energy barrier imposed by the repulsive forces of neighbouring oxygen atoms. It either rotates freely, or, on losing energy it takes up an equivalent position displaced by 120° or 60° from the original position. Therefore, the librational bands should terminate at a frequency corresponding to the "free rotation" energy barrier.

It is likely therefore, that on heating, the relatively ordered, librating nitrate groups of phase IV receive sufficient thermal energy to overcome this barrier, so losing their orientational order, and rotate freely enough to become mutually indistinguishable. Phase III then results. The IV to III transformation observed in the electron microscope and described in Section 2.6 of this Chapter, tests whether this hypothesis is consistent with experimental findings.

An alternative view of the disorder⁽⁵⁴⁾ of phase III holds that due

to the rather small space available to the anions, their rotation is the expression of the disturbance of their mobility by the surrounding cations; the interaction of the anions amongst themselves also has to be considered. X-ray measurements⁽⁵⁵⁾ and thermodynamic considerations,⁽⁷⁵⁾ however, depict a cube of phase III in which the NO_3^- group lies perpendicular to the body diagonal, slightly shifted from the centre, on site symmetry C_3 .⁽⁷⁶⁾ By adding ionic radii it is seen⁽⁸⁴⁾ that free movement along the body diagonal is possible. Increased conductance on $\text{IV} \rightarrow \text{III}$ is partly due to positional randomisation of Rb^+ ions,^(49,58) but this is felt to be a minor factor compared to anion disorder which has a more significant effect on entropy.⁽⁵²⁾ The alternative view of disorder, therefore, is not wholly convincing.

Similarly, according to Korhonen,⁽⁵⁵⁾ phase III can be described by 8 primitive unit cells, has space group $\text{Pa}3$, and is assumed to be an orientationally ordered structure. Strømme,⁽⁵²⁾ for several reasons, modified this model to incorporate orientational randomness, giving a statistical unit cell of one molecule, with symmetry less than space group $\text{Pm}3\text{m}$.

Phase II is rhombohedral, S.G. $\overline{R}3\text{m}$, and isostructural with calcite-type NaNO_3I or KNO_3I .^(53,52) Although there is an increase in thermal energy and nitrates rotate around the trigonal axis,^(53,54) a decrease in conductance accompanies the $\text{III} \rightarrow \text{II}$ transformation.⁽⁴⁹⁾ Salhotra et al.⁽⁷⁶⁾ explain this as due to the nitrates of III librating off-centre but along the body diagonal of the cubic unit cell. In phase II, the

[2.1]

nitrate is locked in an off-centre position where its movement is hampered, resulting in a decrease in conductance after transition. This view is consistent with its antiferroelectric properties.⁽⁹⁶⁾

Although it is suggested that phase II is ordered,^(53,49,96) a precise structure analysis⁽⁵²⁾ discusses extended disorder on the basis of entropy changes. This is plausible in view of phase II being an intermediate structure between I and III, and more in keeping with the understanding in physics^(97,98) of order-disorder phenomena. The calcite-type model where all the three-fold axes of the nitrate groups are aligned in the same direction, is modified to a structure based on this extended disorder.

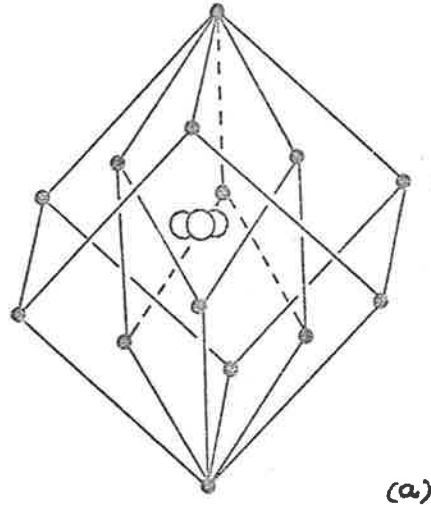
In the series III \rightarrow II \rightarrow I most of the volume change occurs in III \rightarrow II⁽⁷⁵⁾ which is not as reversible a transformation as IV \rightarrow III.⁽⁵³⁾ A volume change of 10.0% was measured by dilatometry.^(64,49) In fact, as observed in an optical microscope⁽⁴⁹⁾ crystals crack and bend during this transformation both on heating and cooling.

Phase I is face-centred cubic, with 4 formula units per cell.⁽⁴⁹⁻⁵²⁾ In the NaCl-type structure,⁽⁵¹⁾ librating ions are placed with their centres on Cl⁻ positions and their planes perpendicular to the body diagonal of the cubic cell. X-ray observation suggests that the nitrate ions librate and tilt with large amplitude, but from lattice parameters it is evident that there is insufficient space for spherical free rotation, which agrees with the prediction⁽⁷⁵⁾ that the entropy is too low for such rotation.

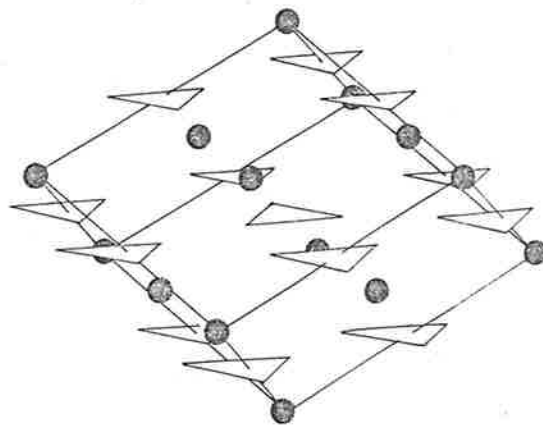
Fig. 1

Phase I.

face centred cubic,

 $Z = 4, a = 7.32 \text{ \AA}$ $\alpha = 90^\circ$ 

Phase II

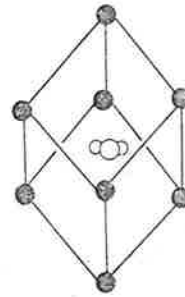
Rhombohedral, $Z = 4$ $a = 7.30 \text{ \AA}$ $\alpha = 97.98^\circ$ (scale: $2 \text{ \AA} = 1 \text{ cm}$)

Phase III

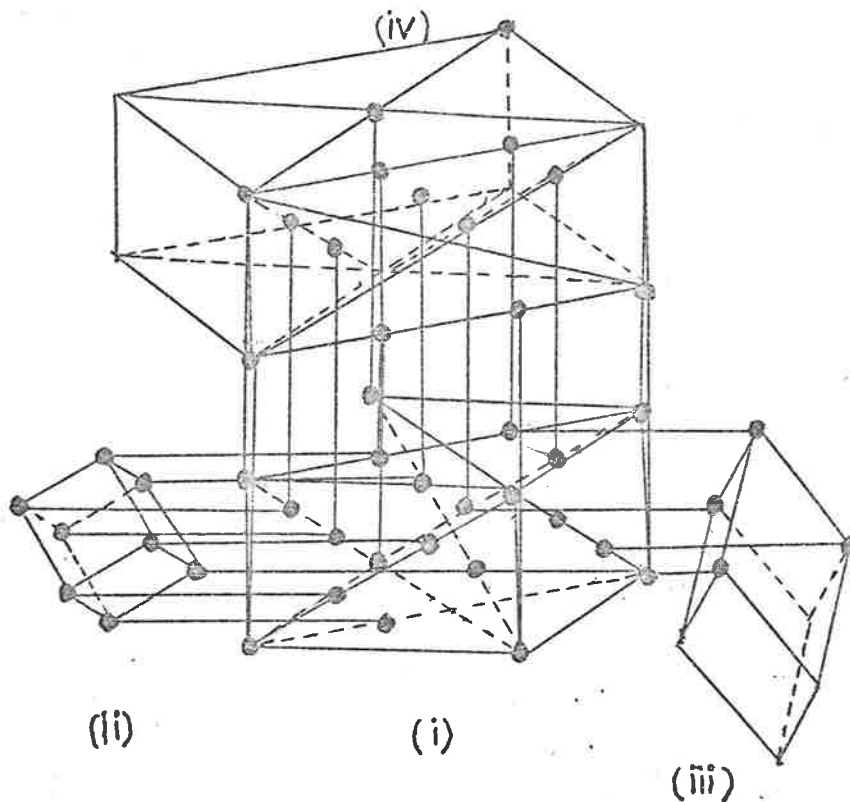
Primitive cubic,

$Z = 1$, $a = 4.37 \text{ \AA}$

$\alpha = 90^\circ$



(c)



(d)

Phase IV. Trigonal, $Z = 9$, $a = 10.49 \text{ \AA}$, $c = 7.44 \text{ \AA}$

cell (i), trigonal, $Z = 9$; cell (ii), pseudo cubic, $Z = 1$;

cell (iii), rhombohedral, $Z = 2$; cell (iv), orthorhombic,

$Z = 18$. (diagram after reference (53)).

In each of the four phases of RbNO_3 therefore, the nitrate executes a different state of libration - rotation depending on the energy of the system, and other factors, such as mutual interaction and the geometry of the cation cage. This may be significant in the mechanism of these planar-ion type transformations. According to Kennedy,⁽⁵¹⁾ the structure type of the polymorphs is sensitive to a temperature dependent "effective ionic radius" of the anion. A complete picture of the mechanism also involves tilting of this planar group.

Figure 1(a)to(d) illustrates the unit cells of the four polymorphs of RbNO_3 under consideration. Z indicates the number of formula units in the chosen cell. At the centre of each primitive sub-cell, a nitrate ion is librating in a relatively ordered manner, (phase IV), or rotating-librating in a progressively more disordered manner in going from phases IV to I.

Rao and Rao⁽⁶⁵⁾ studied thermal hysteresis by d.t.a. in reversible transformations of the nitrates, and found that its magnitude was related to the volume change. They concluded that the origin of hysteresis probably lies in the strain energies associated with the transformations. Approximate energies were estimated from analyses of d.t.a. data and shown to be a function of ΔV , and related to $\Delta T \times \Delta S$.

In view of the close structural similarity of phases IV and III, it is not surprising that the pseudohexagonal form converts to the cubic form without shattering,⁽⁸⁰⁾ the easily reversible process resulting in

a crystal of domains of all the possible C-axis orientations. (75)

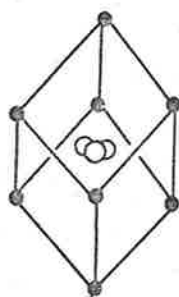
Brown and McLaren (49) report the X-ray orientation relation:

$$[0001]_{\text{IV}} \parallel [111]_{\text{III}} , (10\bar{1}1)_{\text{IV}} \parallel [100]_{\text{III}}$$

where this corresponds to an unaltered cation arrangement with the disorder in the anions.

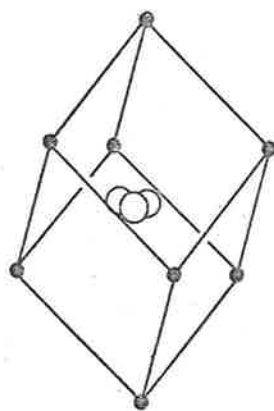
The series of transformations $\text{III} \rightarrow \text{II} \rightarrow \text{I}$ in RbNO_3 is a progressive conversion from CsCl-type to NaCl-type structures. (50,75,79,95)

The relationship between the structures, (50) illustrated below, can be described as a progressive elongation of the body diagonal, the so-called Buerger deformation. (44)



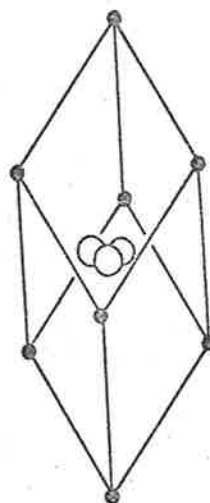
Phase III

$$a = 4.37 \overset{\circ}{\text{Å}}, \alpha = 90^\circ$$



Phase II

$$a = 4.79 \overset{\circ}{\text{Å}}, \alpha = 70.20^\circ$$



Phase I

$$a = 5.176, \alpha = 60^\circ$$

The primitive CsCl-type sub-cell changes from a 'rhombohedral' angle of 90° in phase III, to 70° in the calcite-like phase II, to 60° in the NaCl-type phase I.

In this laboratory, several investigations on the transformations in RbNO_3 were made by optical microscopy, X-ray diffraction and corresponding image intensification, and by martensite computations. Prior to this, as seen above, most investigations were of a chemical or physical nature with no determinations of orientation relations.

Kennedy⁽⁴⁵⁾ reported that when a melt-grown specimen of phase I was carefully cooled and the transformation to II followed in an image intensifier, a strict orientation relation was maintained in a way which strongly suggested that the cation framework remains unaltered. By combination of the polarizing microscope with X-ray precession and front-reflection Laue photographs, Iversen and Kennedy^(95,82) found in repeated experiments, that the structure change $\text{I} \rightarrow \text{II} \rightarrow \text{III}$ proceeds topotaxially. The relation

$$(001)_{\text{I}} \parallel (011)_{\text{III}}, [100]_{\text{I}} \parallel [100]_{\text{III}}$$

was found. It was a mean orientation, the reflections actually being split into several components corresponding to individual orientations differing from this mean by up to 5° . Experimentally, melt-grown phase I was cooled slowly and annealed in II, before conversion to III.

With polarized light microscopy Kennedy⁽⁵¹⁾ found that the interface between I and II is very mobile, suggesting close correspondence of structures. When a good crystal of I is transformed quickly to II, the inter-

face consists of a series of long needles or laths and complex lamellar twinning results. Within about 10 minutes extensive detwinning occurs, often with the formation of several grains. If the interface is cycled or the specimens retransformed, it is usually smooth and several discrete options appear. Twins are common. Some lamellar mechanical twinning occurs on cooling, sometimes followed by slip or cleavage.

Iversen and Kennedy⁽⁸²⁾ followed the sequence of transformations $I \rightleftharpoons IV$. In the $I \rightarrow II$ transformation they observed that the size of lamellae depends on cooling rate; the faster the cooling, the thinner the lamellae. It is probable that slow cooling results in the strain being taken up by the lattice, so that large lamellae then result. Fast cooling produces larger strains and more twin lamellae per unit area are required to relieve the strain. Twins are observed within larger lamellae and may be the result of similar phenomena in that the larger lamellae relieve their own stresses by twinning.

As mentioned previously, the $II \rightarrow III$ transformation involves large strains and volume change. Slow cooling and annealing is necessary for the transformation to occur in an ordered manner. If cooling is too fast, transformation often causes cracking. There appeared to be two mechanisms for $II \rightarrow III$. A "random" mechanism is usually nucleated at twins, slip lines or subgrain boundaries. In the other mechanism phase III forms as oriented platelets in clear, well annealed blocks of II, which are cooled slowly. There are three orientations of these

platelets per extinction angle block, and in some cases they were observed to be parallel to twin traces. The platelets show some variance around the three orientations, and are initially small and regular needle-shaped, but soon elongate, thicken and become irregular, coalescing to form phase III.

The III \rightarrow II transformation is accompanied by distortion and bending of crystals. Infra-red spectra of cooled melts and X-ray irradiated crystals did not reveal any decomposition products such as RbNO_2 .

Following the work by Iversen and Kennedy, Courtenay and Kennedy⁽⁷⁹⁾ were successful in growing small crystals of RbNO_3 II above 220°C , by crystallizing from a mixture of polyethylene glycols above 219°C . The crystals had edge-lengths of 14-30 μm , and the obtuse rhombohedral angle measured from photomicrographs was 98° . The fast extinction direction bisected this rhombohedral angle and the birefringence was high. This morphology corresponds to the ($Z = 4$) "morphological rhombohedron",⁽⁹⁹⁾ which is ideal for comparison with ($Z = 4$) f.c.c. phase I.

These crystals undergo a regular large shape change in the transformations II \rightarrow I \rightarrow II, in a spectacular manner. The rhombs superheat slightly and then change quite suddenly to a rectangular (or square) shape as seen in projection, corresponding to the cubic symmetry of phase I. The following account summarizes some work done by E.W. Courtenay in this laboratory.

"The transformation is preceded by a decrease in birefringence sometimes throughout the crystal, and sometimes just as a band preceding

the interface which makes a trace on the $\{100\}_{Z=4}$ rhomb faces, parallel to a $\langle 100 \rangle_{II}$ direction. Sometimes the transformation is difficult to observe as the crystals' surfaces flow plastically at these high temperatures; this was expected by Brown and McLaren.⁽⁴⁹⁾ If a partially transformed crystal is cooled the shape change is reversible.

The transformed crystals changed back to phase II in two ways. On cooling slowly, 2°/hour, some of the more perfect looking crystals retained their orthogonal shape by means of transformation twinning; that is, in a series of laths making traces parallel to $\langle 100 \rangle$ on the $\{100\}$ face of the square platelets. The I → II interface was parallel to the II → I interface. The laths (or lamellae) grew from the edges inwards. They were accompanied by lines on the surface of the crystal and changes in shape which were apparent at the edges. The resulting product crystals were not as strongly birefringent as those grown in phase II from solution. On cycling the crystals through the transformation the interface direction was either maintained or changed to a direction at right angles to it.

Other crystals transformed so as to give a twinned product with the trace of the twin plane being parallel to $\langle 100 \rangle$ on the $\{100\}$ face. One crystal began to transform at the centre, with two interfaces spreading in opposite directions. The appearance of the product twin resembled a solution-grown growth twin of phase II. The measured angles of the transformation twins were approximately the same as the measured angles of the growth twins. Some crystals which had transformed by laths

Figure 2(a).

RbNO_3 II rhomb. Reflected polarized light,
bright field image. Neg. mag. X140.

Total mag. X1230

Figure 2(b), (c) and (d).

RbNO_3 II (\leftarrow I \leftarrow II). Reflected polarized light
Neg. mag. X200. Total mag. X1760.

Phase I transforms to II by twinning
so as to preserve cubic shape.

(Photographs - Courtesy of Mr. E.W. Courtenay)

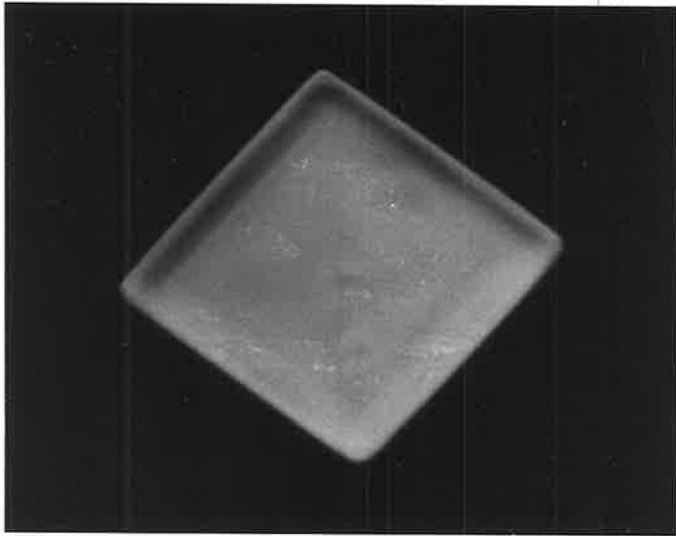


Figure 2(a)



Figure 2(b)

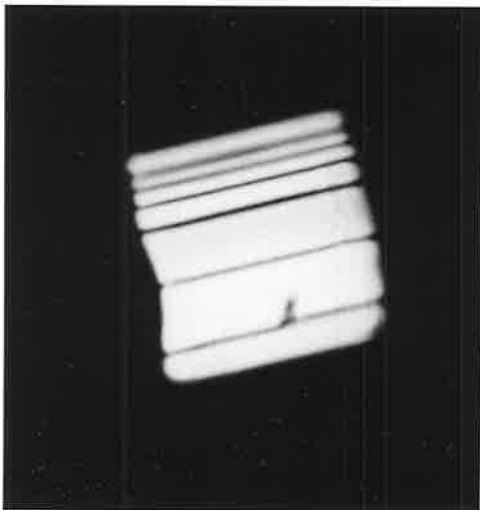


Figure 2(c)

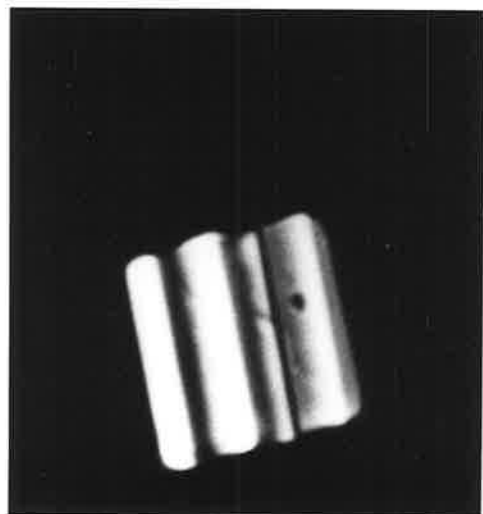


Figure 2(d)

Figure 3(a)

Reflected, polarized light,
bright field

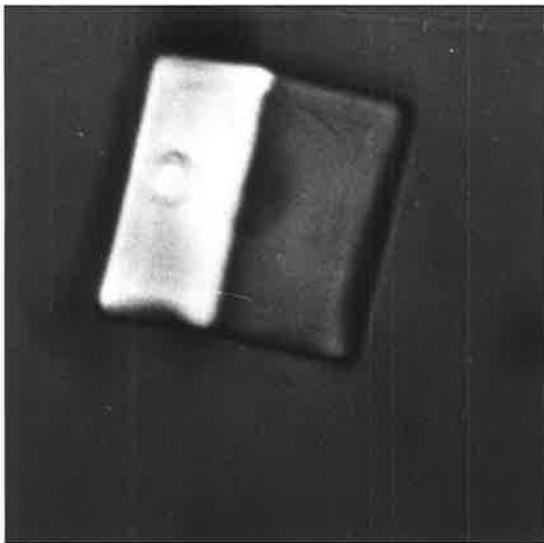
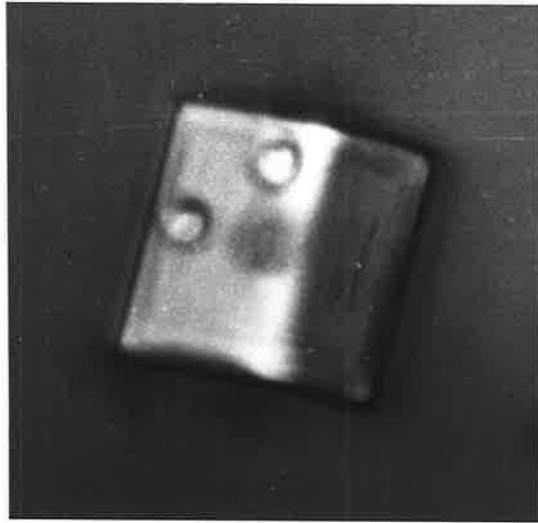


Figure 3(c)

RbNO_3 II \rightarrow I
A birefringent phase II rhomb
transforms to an isotropic
phase I cube

neg. mag. X140
total mag. X1230

Figure 3(c)

(Photographs - Courtesy of
Mr. E.W. Courtenay)

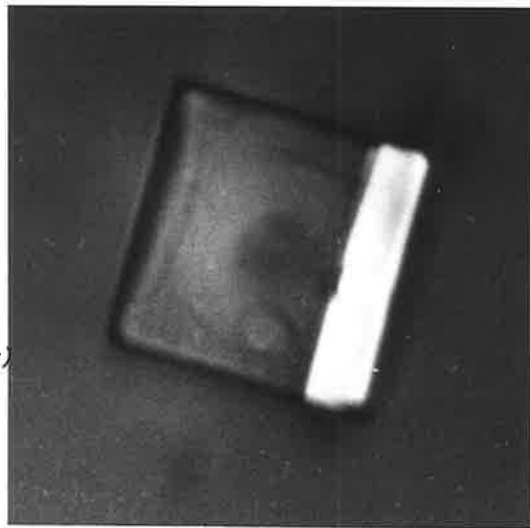


Figure 4(a).

Reflected polarized light,
bright field image.

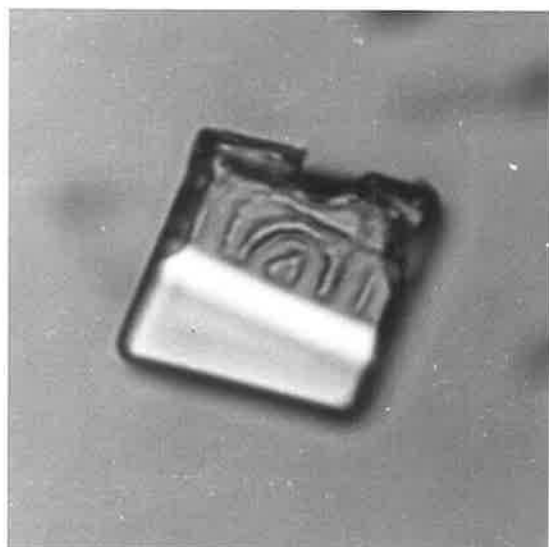
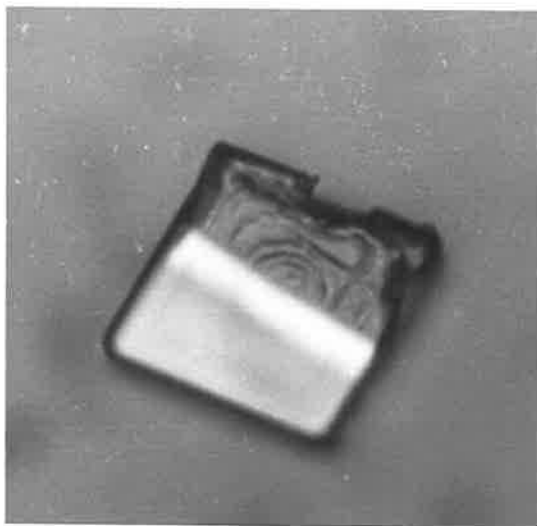


Figure 4(b)

RbNO_3 II \rightarrow III
A birefringent phase II rhomb
transforms to an isotropic
phase III ~~cube~~, via an interface
at $\pm 87^\circ$ to $\langle 100 \rangle_{\text{II}, Z=4}$.

Neg. mag. X140
Total mag. X1230

(Photographs - Courtesy of
Mr. E.W. Courtenay)

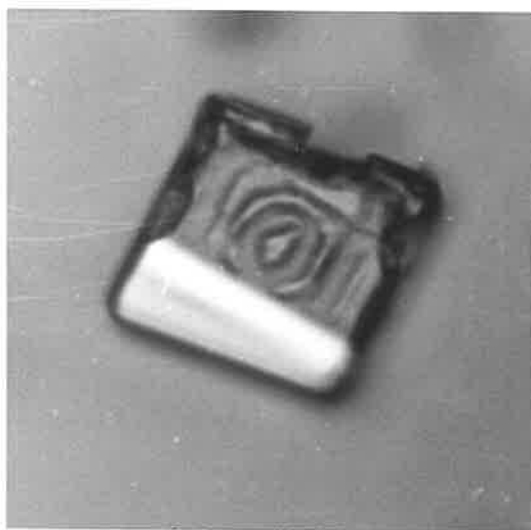


Figure 4(c)

Figure 4(d).

RbNO_3 II \rightarrow III
Transmitted, polarized light,
Neg. mag. X140
Total mag. X1230

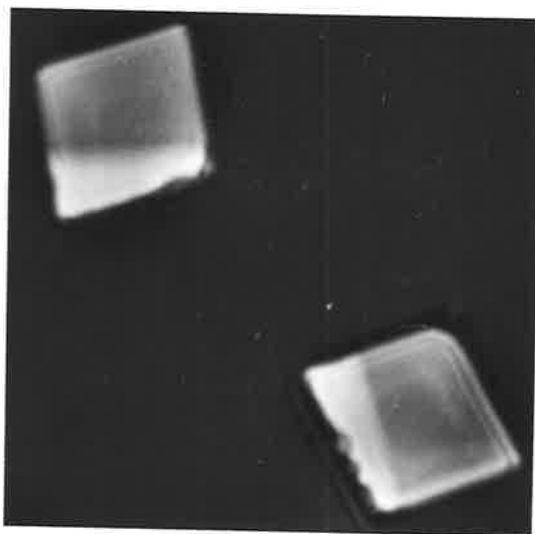


Figure 4(e).

RbNO_3 II \rightarrow III
Transformation interface
|| to $\langle 1\bar{1}0 \rangle_{\text{II}}$, $z=4'$

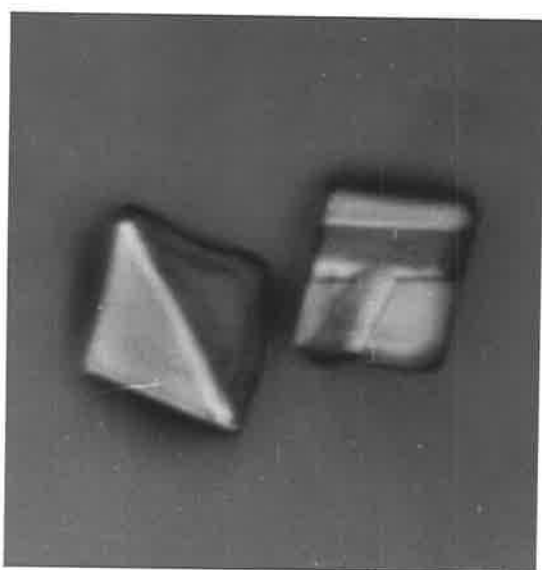
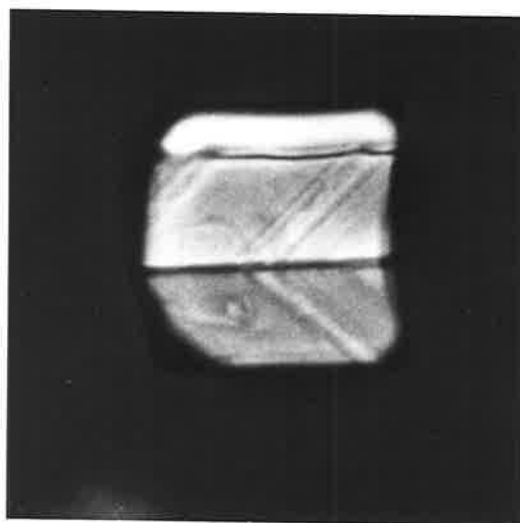


Figure 4(f).

RbNO_3 I \rightarrow II (twinned)
Reflected, polarized light,
bright field image. Angle
of subtexture traces
to main lamellae is
 40.6°



(Photographs - Courtesy of Mr. E.W. Courtenay)

(lamellae), on being left, changed shape so as to have the appearance of the transformation twinned product".

Figures 2, 3 and 4 illustrate the above observations. In general, a regular shape change is valuable evidence of the persistence over substantial distances, of coordinated displacements of atoms in the mechanism of transformation. During this sudden cooperative structure change the planes of the anions re-orient. This large regular shape change of a crystal is the first observed in a structure containing planar complex ions.

Continuing, "In observing the II \rightarrow III transformation, crystals of phase II were left within $\pm 5^{\circ}\text{C}$ of the transformation temperature for about half an hour. A band of differing birefringence appeared on the crystals along certain defined directions. These either grew within the crystal or from the edges. On cooling slightly, a dark line appeared in the centre of the coloured band. This dark band then moved slowly through the crystal preceded by the band of colour. The transformed crystal etched to a much greater extent than either phase I or phase II crystals. There appeared to be some shape change inclined at an angle to the $\{100\}$ face. The directions of the interfaces were at $\pm 87^{\circ}$ to a $\langle 100 \rangle_{\text{II}}$ ($Z=4$) or parallel to a $\langle 1\bar{1}0 \rangle_{\text{II}}$, as illustrated in figures 4(a) to (e). On transforming rapidly the crystals deformed with large distortions".

Fraser and Kennedy⁽³⁹⁻⁴²⁾ of this laboratory comprehensively studied the I (NaCl-type) to II (CsCl-type) transformation in NH_4Br ,

[2.1]

by optical microscopy, X-ray diffraction, scanning electron microscopy and martensite computation, with which they also considered the ammonium halides in general. They overcame the problem of dendritic growth of ammonium bromide by growing well-formed cubic crystals from an ethylene glycol solution above 137°C.

Two types of orientation relation were found^(41,42) which were irrational;

$$\text{type A: near } \{001\}_I \parallel \{1\bar{1}1\}_{II}, \quad \langle 100 \rangle_I \parallel \langle 10\bar{1} \rangle_{II}$$

$$\text{type B: } \{010\}_I \wedge \{010\}_{II} \approx 4^\circ, \quad \langle 100 \rangle_I \wedge \langle 101 \rangle_{II} \approx 9^\circ$$

The volume decreased by $\frac{\Delta V}{V_I} = 15\%$, and was accompanied by a shape change or formation of plates of product. Fraser⁽⁴¹⁾ wrote a computer program PROGRAM MARTENS, for a martensite analysis in which $\eta_2 = \eta_1$ (see Chapter 1). It enabled the prediction of orientation relations, habit planes and shape changes for the NaCl-type \rightarrow CsCl-type structure change in the ammonium halides, using lattice invariant shears of slip and twinning. With it, also, the multiplicity of symmetry equivalent solutions was clearly explained. Comparison of observed orientation relations, interface orientations and shape changes with computed predictions for NH_4Br , showed that the mechanism was consistent with the expected structural relations.

Prior to these studies, in inorganic compounds only a few orientation relations were reported for the $\text{NaCl} \rightleftharpoons \text{CsCl}$ structure change; partial relations from electron microscopy of $\beta\text{-CsCl}$ to

α -CsCl, ⁽³⁸⁾ references in Fraser and Kennedy, ⁽⁴⁰⁻⁴²⁾ that of Iversen and Kennedy ⁽⁹⁵⁾ and those discussed in Chapter 3 of this thesis.

The reverse II (CsCl-type) to I (NaCl-type) transformation has also been studied by X-rays, in ammonium halides, in particular, by Kennedy, Patterson, Chaplin and Mackay, ⁽⁴³⁾ mostly in this laboratory. A spread of $\pm 2^\circ$ or sometimes $\pm 5^\circ$ from the mean orientation relationship was noted. A common relation was

$$A: (11\bar{1})_I \parallel (100)_{II} , (011)_I \parallel (001)_{II} ;$$

others observed were

$$B: \{11\bar{1}\}_I \parallel (\bar{1}\bar{1}0)_{II} , \langle 011 \rangle_I \parallel [001]_{II}$$

$$C: \{100\}_I \parallel (100)_{II} , \langle 011 \rangle_I \parallel [001]_{II} .$$

In cubic structures however, plane poles and directions are indistinguishable, and one is unable to assign indices as planes or directions.

The aim of studying RbNO₃ by X-rays therefore, was to see whether any reported orientation relations could be observed in this analogous structure change. If so, by reference to the rhombohedral intermediate (phase II) where planes can be distinguished from directions, it was hoped to provide more information about the transformation mechanism.

In conclusion therefore, RbNO₃ is an exceedingly interesting and fruitful transformation to investigate for information on the NaCl-type to CsCl-type structure change. As a transparent, birefringent inorganic compound, it has an advantage over metallic compounds, through the

added information obtained from extinction directions, twin bands, and polarization colours. RbNO_3 provides a test of whether the planes of triangular oxyanions tilt or can be re-oriented during structure changes while the general arrangement (e.g. of cations) is merely deformed. This understanding may then be used to interpret other, possibly more complicated transformations, such as the aragonite-calcite type, where a structural relationship is not so evident (see Chapter 4).

SECTION 2.2 APPARATUS AND TECHNIQUES

The apparatus for the combined X-ray diffraction and optical microscopy used in this approach is shown in figure 5(a). A Buerger X-ray precession camera⁽¹⁰⁷⁾ was aligned on its base, to the beam from a molybdenum tube, whilst for specimen manipulation and photography, it could be carefully rotated sideways and then back into alignment.

A heater, figure 5(b), was constructed from nichrome wire (30 s.w.g. or 0.0092 inch diameter) which was wound into a coil and mounted on an asbestos support, itself screwed on to the goniometer. An asbestos paper shield was fixed around it with water-glass to reduce temperature fluctuations during precession. The heater was joined in series to an ammeter by light, cotton-covered copper wire (30 s.w.g.). The heating circuit, figure 5(c), shows two step-down voltage transformers which were used for better temperature control. It is evident that the apparatus was not highly sophisticated, and considerable experimental difficulty was experienced, particularly with phase I which exists in a narrow temperature range of 28°C.

Specimen handling conformed to an idea first developed in this laboratory from J.H. Patterson's work on $TlNO_3$ ⁽³⁶⁾ of using very small single crystals. Even a crystal of approximate size $\frac{1}{2}mm \times 1mm \times \frac{1}{2}mm$ would have a large number of dislocations and nucleation sites, and hence possibly orientations. If the transformation is accompanied by shape changes^(35,41) (and Chapter 4 of this thesis), the result is a complex diffraction pattern which is very difficult to interpret.



Figure 5(a). The apparatus for combined X-ray diffraction and optical microscopy.

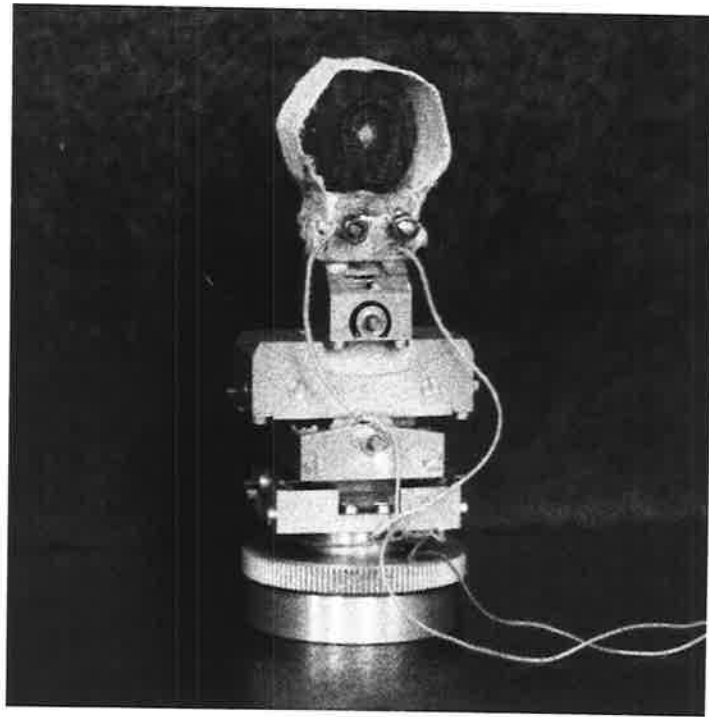


Figure 5(b). The X-ray heated mounted on the goniometer.

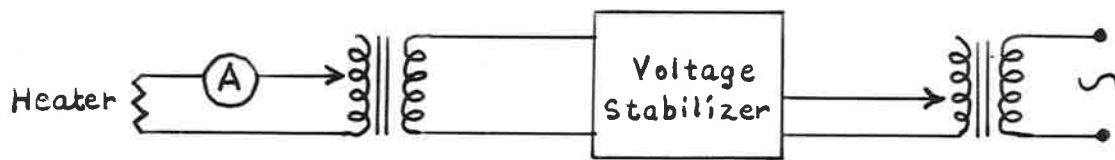


Figure 5(c). The heating circuit.

Small samples of RbNO_3 of approximate size 1mm x 1mm were therefore grown from the melt on the glass coverslip in order to avoid handling and cutting of specimens, which would introduce strain and nucleation sites. Rubidium nitrate of very high purity from E. Merck AG. Darmstadt was used throughout.

Whilst previous workers of this laboratory took care to construct heaters with no thermal gradients, for example by using a temperature controller, this was not done for the present experiments. Rather, it was felt that a thermal gradient would promote preferential nucleation of the new phase at a certain region of the specimen, and so be more likely to result in a product phase of only one subgrain. Furthermore, the passage of the interface could then be anticipated and observed more readily.

With the supporting coverslip in a horizontal position and use of the polarizing microscope, the heater was calibrated for the melt and transformation temperatures. However, when the heated coverslip was in a vertical position the specimen was cooled and the current settings for the transformation temperatures were different, due to the different thermal environment. Repeated trials were necessary for familiarization with the heater. The temperature of the specimen differed slightly with position on the coverslip; hence the thermal gradient.

To protect against ambient temperature fluctuations such as wind draughts due to air conditioning and people walking about, etc., a plastic cabinet was constructed about the apparatus.

In these experiments, speed of manipulations and interpretation of X-ray photographs for identifying the orientation was an essential factor. Hence Polaroid Land Film, type 57 was used rather than ordinary Ilford Industrial G film. With less time in the near-melt region, phase I would be less likely to be contaminated or decompose as was previously feared,⁽⁴⁵⁾ although no nitrite decomposition products were found by Raman spectroscopy.⁽⁸²⁾ Nevertheless, if the melt was heated very much above 310°C small specks were noticed moving in it. As a compromise therefore, the crystal was not held in the melt or phase I for longer than necessary, and the melt was not heated far above 310°C. Coverslips of hard Matsunami glass rather than silica were used since the former would not be as reactive.

Rubidium nitrate usually grew from the melt in the low index projection $\{100\}_I$, or on remelting, sometimes $\{111\}_I$, or on repeated remelting the specimen could sometimes be "rolled into" a $\{112\}_I$ or $\{110\}_I$ projection. By X-ray precession and unfiltered Mo radiation, or Zr- filtered monochromatic radiation, phase I was aligned with a main crystal direction parallel to the spindle axis. As previously observed in this laboratory, Laue photographs at such a high temperature showed considerable glare or scatter of radiation, as distinct from thermal asterism. Precession photographs, particularly Zr- filtered, were quite clear, however.

The transformations of phase I \rightleftharpoons II \rightarrow III were observed mainly by unfiltered and filtered X-ray precession photographs, Laues, and on some

occasions by manual oscillation of the spindle, to track and check a product orientation. Occasionally, due to the narrow temperature range of I, it would transform to II as observed in unfiltered precession photographs, but the product orientation could still be discerned from $K\alpha$ reflections.

In experiments combining X-rays and optical microscopy, the spindle axis was found by optically aligning a glass fibre. A polarizing microscope fitted with a Practica IV camera was positioned so that the horizontal cross-hair of the microscope eyepiece (6X) and the camera eyepiece cross-hair were all parallel to the spindle axis. There was some small wobble in the microscope eyepiece giving an error of deviation from the spindle axis, as found by comparison of photographs, of $\pm 2^\circ$. The microscope was usually fitted with a 20X objective, although sometimes for larger magnifications a long working distance 40X objective was used. Planar 10X or 12.5X microscope eye pieces were also used, although with the 40X objective, light intensity was weak. White light collected on a small lens-shaped mirror below the specimen. Above the mirror a plastic sheet of polarizing material combined with the analyser in the microscope to provide plane polarized light.

The experiment was conducted as follows. The heater supporting X-ray oriented phase I in any of the above-mentioned projections was quickly turned to a horizontal position, corresponding to an "ad hoc" decrease of current, juggling so as to keep the specimen in that phase. The microscope was then quickly focused on to the specimen. Ideally the

[2.2]

transformation to phase II with the passage of an interface, was then followed and photographed. Sometimes, however, interfaces were not observed but the remaining surface traces were photographed.

In view of the relatively expensive use of Polaroid film, preliminary investigations were also made with an X-ray image intensifier. It was found that for the types of specimen used, there was not too much glare from the coverslips at these temperatures, so that Bragg reflections could be discerned although they were close to the centre of the image. It is suggested that in further investigations this technique be incorporated, since it has an added advantage of speed of specimen manipulation and data collection, as well as possible recording of movement of reflections during transformation.⁽⁴⁵⁾

Optical microscopy of the I \rightarrow II transformation was done with the Reichert Zeotopan Research microscope, which has the facility of both transmitted and reflected polarized light. A Nomarski interference contrast⁽²⁷⁰⁾ and a multi-beam interferometer⁽²⁶⁹⁾ attachment were used for surface observations.

The heaters used in these experiments were prepared by E.W. Courtenay and consisted of a conducting transparent film^(102,104) deposited on a pyrex glass slide. At the edges terminals were painted, and the heater was varied by means of a sensitive constant voltage heating circuit. Molten crystals were slowly cooled to phase I and then to phase II.

In some X-ray precession experiments, an accurately set parent phase transformed to a product in an irrational projection which could not

readily be interpreted, or two projections, one of which was irrational. In these cases the product was set to a rational projection by manipulating the goniometer arcs and noting the value and direction of the readings, as had been done for the parent. These spatial manipulations were then repeated with the aid of a globe and cap, the globe being graduated in 5° intervals along both great circles and small circles. These graduations were traced on the cap as well. A value of $\pm 4^{\circ}$ was a reasonable estimate of the accuracy. In this way, one was able to follow the determination of the spatial position of the product more directly and quickly than could be done with a series of two-dimensional stereograms.

For interpretation of data throughout the work described in this thesis, stereograms of planes and directions were calculated and plotted at any specified radius, by means of the University of Adelaide, controlled Data Corporation (C.D.C.) 6400 computer. This was done by means of a program written in FORTRAN, PROGRAM STEREO, by Mr. A. Pearce of the Engineering Department. PROGRAM ANGLES, also used, was translated by W.L. Fraser of this laboratory from a Cambridge program in the language TITAN, and it computes d spacing and angles between specified planes.

SECTION 2.3 CALCITE-TYPE UNIT CELLS

Prior to presenting orientation relations, it is beneficial to understand the relationship between the different sub-cells of the calcite-type structure of RbNO_3 II, it being isostructural with NaNO_3 I and KNO_3 I, and the different terminology currently used to describe them. This elaboration is necessary for Chapters 3 and 4 as well.

Table 5 summarizes descriptions and terminology of the sub-cells, (99,105,41) whilst Table 6 gives their lattice parameters as measured or calculated for RbNO_3 . Figure 6 depicts, to the scale $1 \text{ cm} = 2\text{\AA}$, the relationship between them. For simplicity the convention used during this work and in this thesis is to refer to the sub-cells by the crystal system and Z, the number of formula units per cell; e.g., rhombohedral, $Z = 4$, or hexagonal, $Z = 6$.

When discussing correspondences between $Z = 4$ and $Z = 1$ rhombohedral subcells, the choice of axes adopted in this thesis is such that

$$(111)_{\text{Rh},Z=4} \parallel (111)_{\text{Rh},Z=1}, \quad (1\bar{1}0)_{Z=4} \parallel (0\bar{1}1)_{Z=1}$$

that is, the $[a_1]$ rhombohedral axis of the $Z=1$ cell is rotated 60° anticlockwise from the $[a_1]$ of the $Z=4$ cell, when both are viewed down the vertical $[111]$ axes.

Matrices for interconversion of planes and directions between cells are given in Table 7, whilst the formula for interconversion of rhombohedral to hexagonal lattice parameters can be found in text books. (99)

TABLE 5

DESCRIPTION AND TERMINOLOGY OF SOME CALCITE-TYPE SUB-CELLS

Z	Name	Index of cleavage face	Reference
2	X-ray rhombohedral cell	{211}	(99) (105)
6	X-ray hexagonal cell	{10 $\bar{1}$ 4}	(99) (105)
4	(i) Cleavage rhombohedral pseudo-cell	{100}	(105)
	(ii) Morphological rhombohedron	{100}	(99)
	(iii) distorted NaCl-type cleavage cell	{100}	
12	Hexagonal morphological pseudo cell	{10 $\bar{1}$ 1}	(105)
32	Cleavage rhombohedron, true cell for calcite	{100}	(99) (105)
96	Hexagonal Cleavage rhombohedral true cell	{10 $\bar{1}$ 1}	"
1	(i) primitive rhombohedron	{101}	(51) (41)
	(ii) rhombohedral cell	{110}	(101) (102)
3	hexagonal cell	{01 $\bar{1}$ 2}	(99) (100)

TABLE 6
LATTICE PARAMETERS OF RbNO₃ II SUB-CELLS

Z	Crystal System	Lattice Parameters (Å)		Reference
1	rhombohedral	$a_r = 4.79$	$\alpha = 70^\circ 12'$	(50)
3	hexagonal	$a_h = 5.51$	$c_h = 10.74$	(50)
2	rhombohedral	$a_r = 7.84$	$\alpha = 41^\circ 15'$	(50), (99)
6	hexagonal	$a_h = 5.53$	$c_h = 21.48$	"
4	rhombohedral	$a_r = 7.30$	$\alpha = 97.98^\circ$	"
12	hexagonal	$a_h = 11.017$	$c_h = 10.746$	"

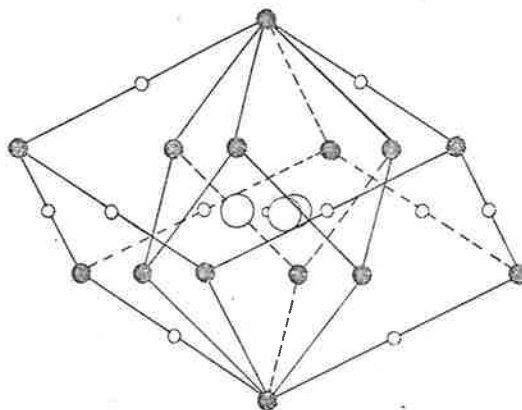
CALCITE TYPE UNIT CELLS.

Fig. 6(a).

Rhombohedral, $Z = 1$

and rhombohedral,

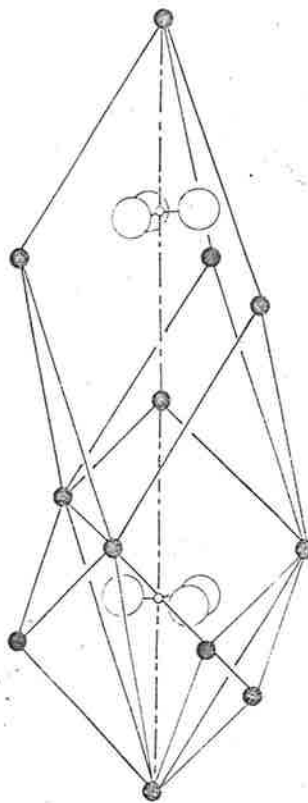
 $Z = 4$ cells

Fig. 6(b).

Rhombohedral, $Z = 1$

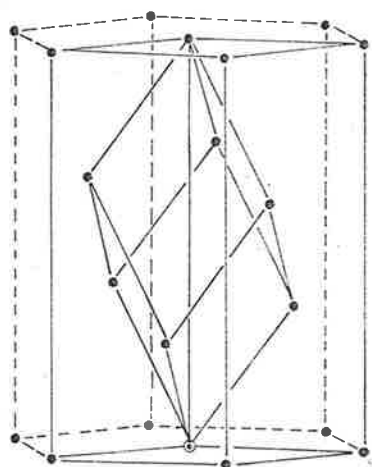
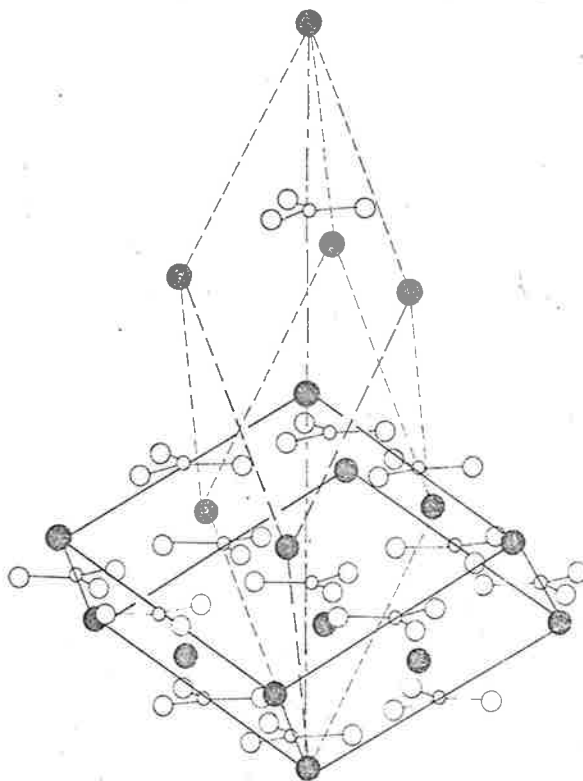
and rhombohedral

 $Z = 2$ cells.(Scale: $1 \text{ cm} = 2\overset{\circ}{\text{A}}$)

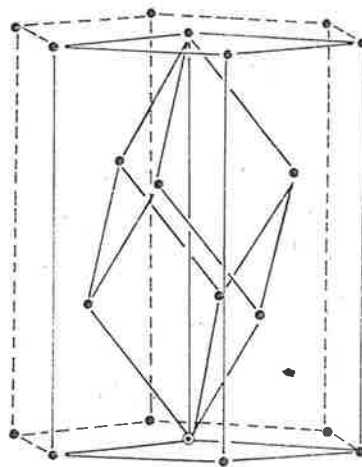
Fig. 6(c).

Rhombohedral, $Z = 4$

and rhombohedral,

 $Z = 2$ cells. ⁽¹⁰⁵⁾

(i)



(ii)

Fig. 6(d). Rhombohedral, $Z = 1$ and hexagonal, $Z = 3$ cells
in obverse (i) and reverse (ii) settings (after
ref. (100)).

TABLE 7

MATRICES FOR INTERCONVERSION OF CALCITE-LIKESUB-CELLS (99,47,105)

Rhombohedral to Hexagonal

e.g. (Z=1) to (Z=3)
(Z=2) to (Z=6)
(Z=4) to (Z=12)

$$\begin{vmatrix} 1 & \bar{1} & 0 \\ 0 & 1 & \bar{1} \\ 1 & 1 & 1 \end{vmatrix} \quad \Delta = 3$$

Hexagonal to Rhombohedral

e.g. (Z=3) to (Z=1)
(Z=6) to (Z=2)
(Z=12) to (Z=4)

$$\begin{vmatrix} 2 & 1 & 1 \\ 3 & 3 & 3 \\ \frac{1}{3} & \frac{1}{3} & \frac{1}{3} \\ \frac{1}{3} & \frac{2}{3} & \frac{1}{3} \end{vmatrix} \quad \Delta = \frac{1}{3}$$

For rhombohedral (Z=2) to rhombohedral (Z=4)

$$\begin{vmatrix} 3 & \bar{1} & \bar{1} \\ \bar{1} & 3 & \bar{1} \\ \bar{1} & \bar{1} & 3 \end{vmatrix}$$

For rhombohedral (Z=4) to rhombohedral (Z=2)

$$\begin{vmatrix} \frac{1}{2} & \frac{1}{4} & \frac{1}{4} \\ \frac{1}{4} & \frac{1}{2} & \frac{1}{4} \\ \frac{1}{4} & \frac{1}{4} & \frac{1}{2} \end{vmatrix}$$

For rhombohedral (Z=6) to hexagonal (Z=96)

$$\begin{vmatrix} 4 & 0 & 0 \\ 0 & 4 & 0 \\ 0 & 0 & 1 \end{vmatrix}$$

SECTION 2.4 I \rightleftharpoons II \rightarrow III TRANSFORMATIONS2.4.1 X-ray Observations

In this section, orientation relations obtained by precession and associated techniques are described and numbered [n], with experimental reproducibility indicated.

Relation [1]:

An $[010]_I$ projection was aligned with the $\langle 110 \rangle$ direction parallel to the spindle axis. The Laue photograph is shown in figure 7(a) whilst a corresponding, typical $[100]_I$ projection precession photograph is seen in figure 7(b). In the latter, the weaker double reflections towards the edge of the pattern are due to upper layers, analogous to first and second order Laue zones observed in electron microscopy. ⁽¹⁰⁶⁾ Due to the thickness of the polaroid cassette holder, layer screens could not be used, but these reflections could be discerned since they did not occur regularly on reciprocal lattice points.

On fast cooling to phase II, a single crystal product orientation was obtained. Since arc settings on the goniometer were small, it was considered to be reasonably accurate to rotate the specimen by 13° in the plane of the film bringing reflection "b" in figure 7(c) into a vertical position. This is a $\mu = 12^\circ$ precession photograph. At this stage a non-standard technique, of confirming the orientation by "tracking the Bragg reflection" was applied, and is described as follows.

A $\pm 4^\circ$ oscillation photograph about the spindle axis, and a $\mu = 12^\circ$ "precessing Laue" photo did not show the vertical reflection "b". The

Fig. 7(a) X-ray Laue photograph of RbNO_3I . [010] projection with $\langle 101 \rangle$ direction horizontal. Mo radiation.

Fig. 7(b) Corresponding zero layer precession photograph [010] direction. Mo/Zr filter.



Figure 7(a).

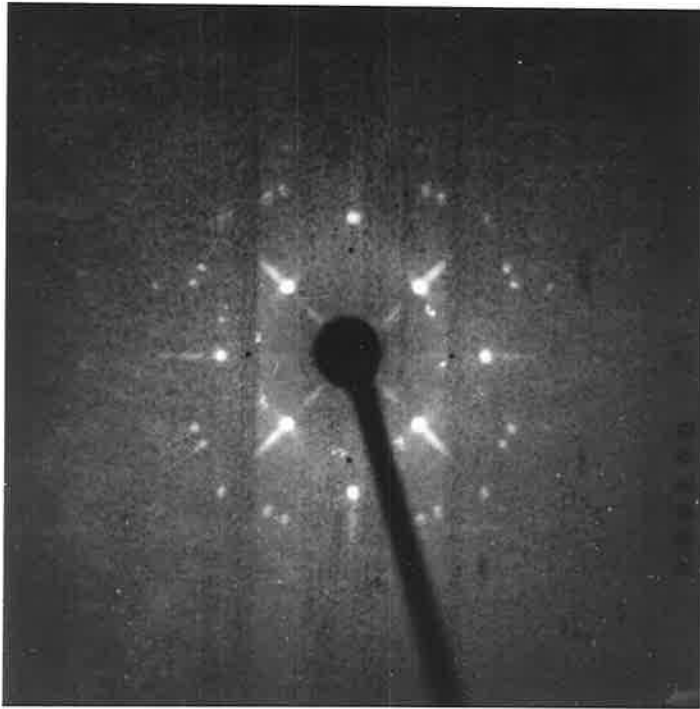


Figure 7(b).

Figure 7(c). A $\mu = 12^\circ$ precession photo of detwinned RbNO_3II in a $[3\bar{1}\bar{1}]_{\text{II},Z=1}$ projection. Reflection "b" is vertically above the origin. Mo/Zr filter. Relation [1].

Figure 7(d). A zero layer precession photo of RbNO_3II in the second projection of $[2\bar{1}0]_{\text{II},Z=1}$. X-ray beam now proceeded down the Bragg reflection "b". Mo/Zr filter.

reflection "b"

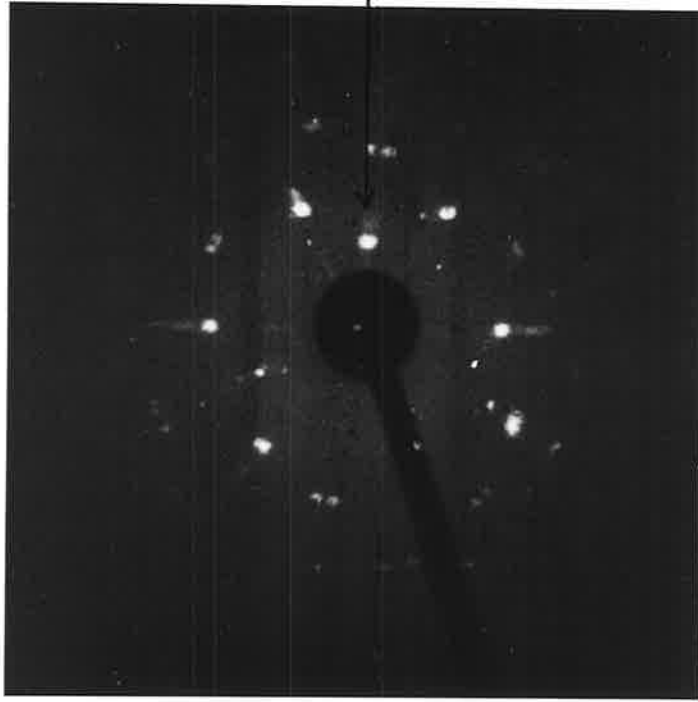


Figure 7(c)

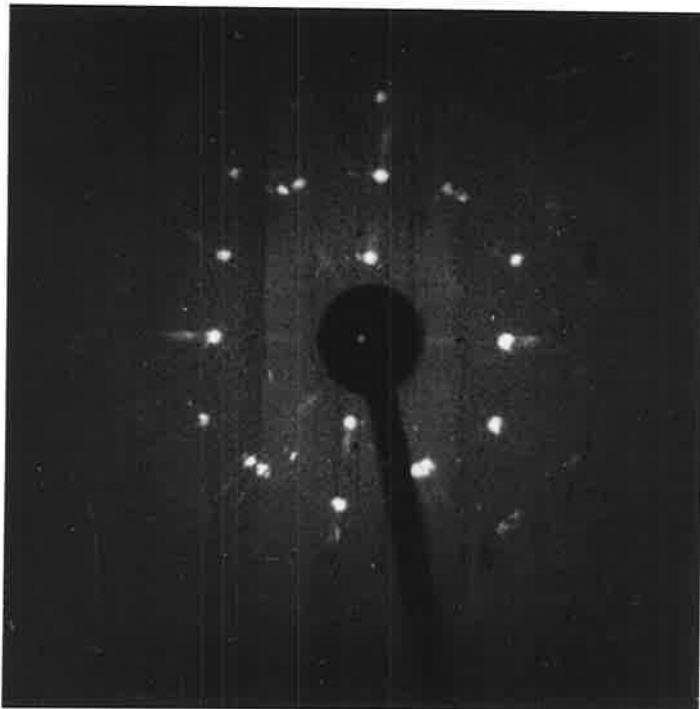


Figure 7(d)

spindle was reset so that the top of the specimen was tilted 10° forward and a $\mu = 3^\circ$ filtered precession photograph captured it. From a Laue photograph at this spindle setting and a $\pm 3^\circ$ oscillation photo, the distances of reflection "b" (figure 7(c)) from the centre were measured and converted to angles ($\tan \theta = \text{distance}/D$ (cms)). A correction of 0.5° on the spindle axis was deduced, which thus gave the Bragg setting for reflection "b" at 9.5° from the first, product orientation.

The Bragg reflection was then brought to the centre by rotating the specimen forward 5° (measured from its converted distance from the centre), so that the beam proceeded along the normal to the plane which gave that reflection. An excellent single crystal parallelogram pattern, figure 7(d) was obtained, which was easier to interpret than the first product orientation.

Laue photographs were taken, but due to streaking and splitting of reflections, or the polycrystalline nature of the product, they were difficult to interpret, and most orientation relations were determined from precession photographs.

During the three hours of this experiment the single crystal product orientation did not change. The first projection of the product, figure 7(c), was $[3\bar{1}\bar{1}]_{II}$, given in terms of the rhombohedral, $Z = 1$ unit cell, and abbreviated $[3\bar{1}\bar{1}]_{II(Z=1)}$; the spindle axis corresponded to the $\{112\}_{II(Z=1)}$ pole. The second projection, the parallelogram of figure 7(d) was indexed as $[2\bar{1}0]_{II(Z=1)}$.

According to the correspondence between $Z = 4$ and $Z = 1$ rhombohedral

cells, described in Section 2.3, $(100)_{Z=1} \wedge [3\bar{1}\bar{1}]_{Z=1} = 8^\circ$. From photographs and stereograms therefore, the orientation relation was deduced to be

$$\begin{aligned} (100)_{I(Z=4)} \wedge (100)_{II(Z=1)} &= 8^\circ \\ [010]_{I(Z=4)} \wedge [01\bar{1}]_{II(Z=1)} &= 7^\circ \quad \text{-----}[1] \end{aligned}$$

The limit of accuracy of $\pm 4^\circ$ was established as follows. On a $[111]_{II(Z=1)}$ stereogram the experimental projection $[3\bar{1}\bar{1}]_{II(Z=1)}$ is denoted by a point A; the goniometer arcs and spindle manipulations, when followed with a two dimensional Wulff net, anticipate a point at B; the second experimental point indicated by the $[2\bar{1}0]_{II(Z=1)}$ projection is labelled C. The angle between B and C is $3\frac{1}{2}^\circ$. In this orientation relation $[111]_I \wedge [111]_{II} = 40^\circ$, and the relation was observed on one occasion.

Relation [2]

This was obtained in 4 separate experiments, and was referred to as the "multiple orientations" or "split spot pattern".

As observed by optical microscopy (Section 2.1,⁽⁵¹⁾ and 2.4), when phase I transforms quickly to II, complex lamellar twinning is produced. Within about 10 minutes, with the passage of an interface, extensive detwinning occurs giving several grains. Figure 8 is a diffraction pattern corresponding to such an unrelaxed phase. Lamellae were aligned with an optical microscope at $\sim \pm 45^\circ$ to the cross-hairs. The pattern was indexed as three mutually-rotated superimposed

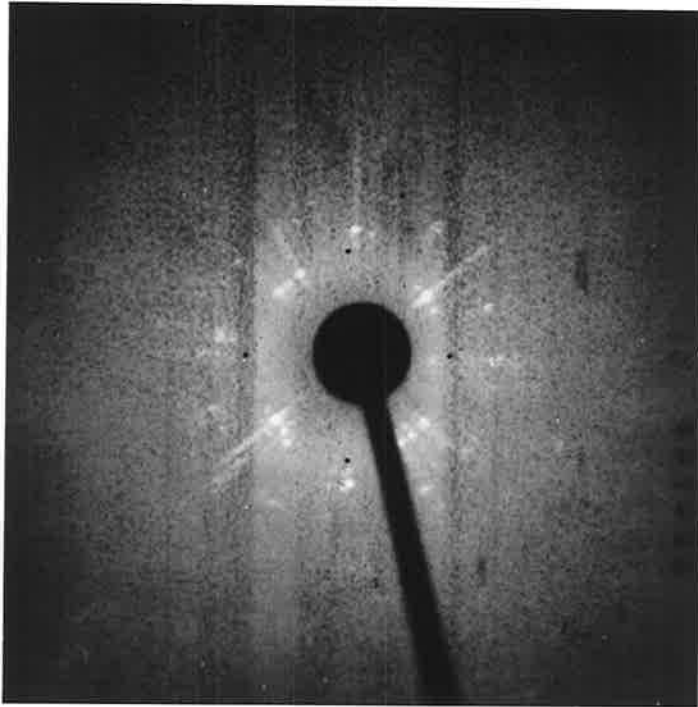


Figure 8. An X-ray precession photo of $\text{RbNO}_3^{\text{II}}$ in a $[100]_{\text{II},Z=4}$ projection. The "multiple orientations" or "split spot pattern" where $\{100\}_{\text{I},Z=4}^{\wedge}$ $\{100\}_{\text{II},Z=4} = 0^\circ, \pm 8^\circ$, corresponds to an initial twinned product of phase II. Mo/Zr filter. Relations [2] and [2]'

projections of $\langle 1\bar{1}1 \rangle_{II(Z=1)}$, or the corresponding $\langle 100 \rangle_{II(Z=4)}$. Typically, a $\langle 100 \rangle_{I(Z=4)}$ projection such as in figure 7(b) was replaced by this multiple pattern of $\langle 100 \rangle_{II(Z=4)}$ projections of figure 8. The exposure time for a precession photograph with polaroid film was 6 to 8 minutes.

The $\{010\}_{Z=4}$ reflections of an almost oriented $[100]_I$ projection, on orientation, appear to split by $\pm 8^\circ$. This value was also found by averaging several photographs from different experiments. The $\{010\}_{I(Z=4)}$ reflections themselves remain stationary, and a set of triplet spots is produced. This type of pattern was observed previously in this laboratory.⁽¹⁰⁸⁾ Any movement of $\{110\}_{I(Z=4)}$ reflections was too small to be accurately determined in these experiments.

From comparison of photographs and experimental, computed stereograms, $[111]_I \wedge [111]_{II} = 7^\circ$ and the orientation relation can be described as

$$[001]_{I(Z=4)} \parallel [1\bar{1}1]_{II(Z=1)} \text{ i.e. } [001]_{II(Z=4)},$$

$$(010)_I \parallel (011)_{II(Z=1)} \text{ i.e. } (010)_{II(Z=4)} \quad \text{-----} [2]$$

Relation [2]'

In the reverse approach to the $I \rightarrow II$ structure change, forming from phase I by discrete jumps of the interface, lamellae of phase II were observed through the polarizing microscope, figure 9 ; they were aligned parallel to the horizontal and vertical cross-hairs. The

specimen was then carefully turned, and maintained in phase II, within the experimental conditions. The triplet spot pattern of a $\langle 1\bar{1}1 \rangle_{II(Z=1)}$ projection was found. On slowly heating to phase I, a slightly mis-oriented cubic $[100]_{I(Z=4)}$ pattern resulted giving relation [2] which was thus shown to be reversible. In the corresponding Laue photographs of the two projections the direction of a $\{100\}_{II(Z=4)}$ reflection remained unchanged, to become that of a $\{100\}_{I(Z=4)}$ reflection, further confirming relation [2].

Relations [3] and [4]

A $[111]_I$ projection transformed to phase II in a complex twin array, with lamellae parallel to $\langle 1\bar{1}0 \rangle$ directions. The detwinned phase was found to contain two orientations, the first in the relation:

$$\begin{aligned} [111]_I & \parallel [01\bar{1}]_{II(Z=1)} , \\ (\bar{1}\bar{1}2)_I & \wedge (011)_{II(Z=1)} = 3^\circ \text{ --- --- --- [3]} \end{aligned}$$

with a missetting of about $\pm 5^\circ$ at most. This gave $[111]_I \wedge [111]_{II(Z=1)} = 90^\circ$, $[11\bar{1}]_I \wedge [111]_{II} = 24^\circ$, $(001)_I \wedge (010)_{II} = 17^\circ$, $[100]_I \wedge [10\bar{1}]_{II} = 14^\circ$, and $(110)_I \wedge (00\bar{1})_{II} = 4^\circ$.

The second orientation was related to the first by a common $\{110\}_{II(Z=1)}$ or $\{100\}_{II(Z=4)}$ plane. With the aid of a cap and globe, the relation found was

$$\begin{aligned} [111]_I \wedge [\bar{1}\bar{1}\bar{1}]_{II(Z=1)} & \text{ i.e. } [\bar{1}00]_{II(Z=4)} = 12^\circ \\ (\bar{1}\bar{1}2)_I \wedge (011)_{II(Z=1)} & \text{ i.e. } (011)_{II(Z=4)} = 3^\circ \text{ --- --- --- [4]} \end{aligned}$$

Relations [3] and [4] were obtained once.

Relation [5] and [6]

Phase I in a [100] projection transformed to a multiple orientation or split spot pattern, figure 10(a), according to relation [2].

Figure 10(b) is a Laue photo of the twinned phase. On further cooling the single crystal patterns of figure 10(c). (d) appeared which were indexed as a $[101]_{II(Z=1)}$ or $[2\bar{1}\bar{1}]_{II(Z=4)}$. Since it was unlikely that thermal gradients had increased the temperature significantly, it was assumed that phase II had detwinned in a single orientation. With the aid of the cap and globe, it was found that

$$[1\bar{1}1]_{II(Z=1)(M.O.)} \wedge [101]_{II(Z=1)(S.O.)} = 7^\circ$$

or

$$[100]_{II(Z=4)(M.O.)} \wedge [112]_{II(Z=4)(S.O.)} = 7^\circ,$$

such that

$$(10\bar{1})_{II(Z=1)(M.O.)} \wedge (10\bar{1})_{II(Z=1)(S.O.)} = 4^\circ \text{ --- [5]}$$

where (M.O.) denotes multiple orientations phase and (S.O.) denotes single orientations phase. The magnitude of uncertainty here is about $\pm 4^\circ$, and the relation was obtained once. Similarly, one deduced the relation between phase I and detwinned phase II to be

$$[100]_I \wedge [101]_{II(Z=1)} = 6^\circ$$

$$(011)_I \wedge (10\bar{1})_{II} = 4^\circ (\pm 4^\circ) \text{ --- [6]}$$

Relation [7]

Phase I in a [111] projection was left in phase II for $2\frac{1}{2}$ hours and annealed in phase I for 3 hours. The structure change was not

Figure 10(a) RbNO_3II , a "multiple orientations pattern" with $\langle 110 \rangle_{\text{I}}$ directions vertical and horizontal. Zero layer precession, Mo/Zr filter.

Figure 10(b) The corresponding Laue photograph.

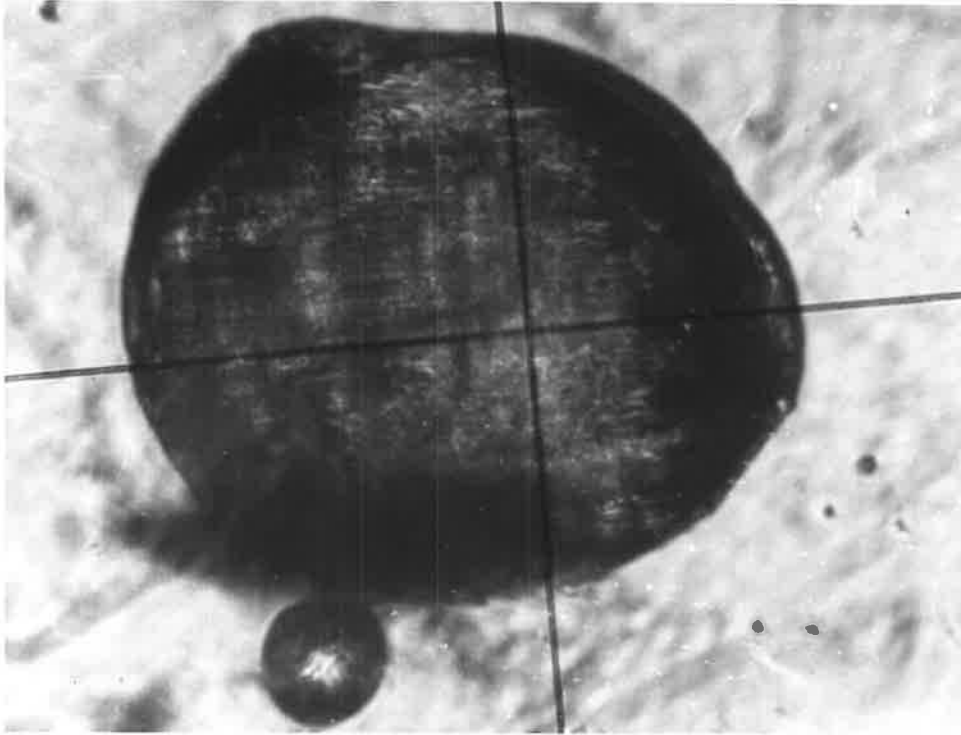


Figure 9. Combined X-ray - optical microscopy of the initial, $RbNO_3$ phase II product. Twin lamellae are parallel to $\langle 100 \rangle_I$ directions. Transmitted, polarized light, negative mag. X60.

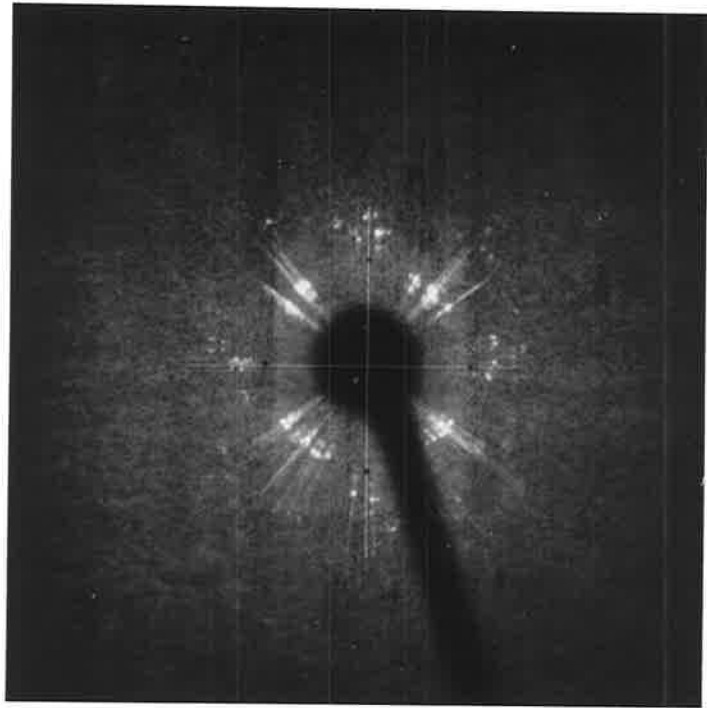


Figure 10(a)



Figure 10(b)

Figure 10(c). Laue photo of subsequent single crystal of detwinned $\text{RbNO}_3^{\text{II}}$. Mo radiation. Relation [5].

Figure 10(d). Corresponding zero layer precession photo in $[101]_{\text{II}, Z=1}$ or $[2\bar{1}\bar{1}]_{\text{II}, Z=4}$ projection. Mo/Zr filter.

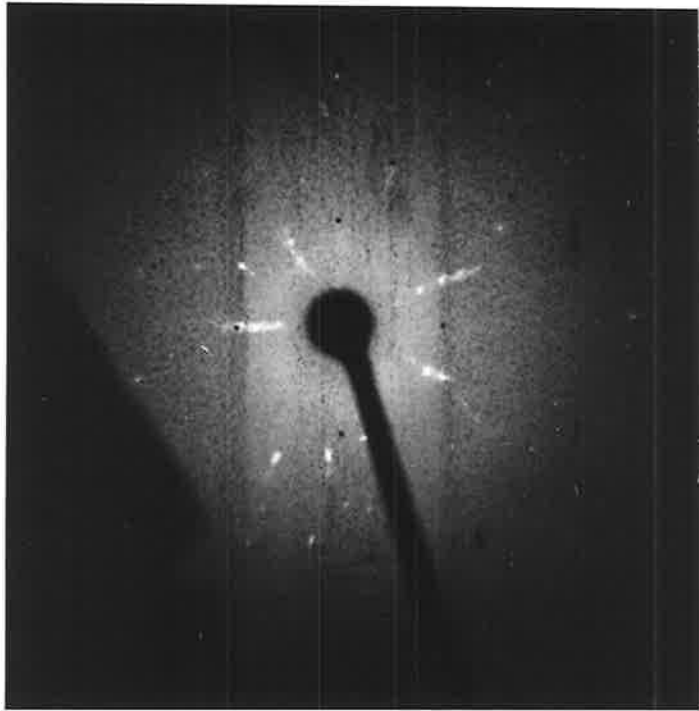


Figure 10(c)

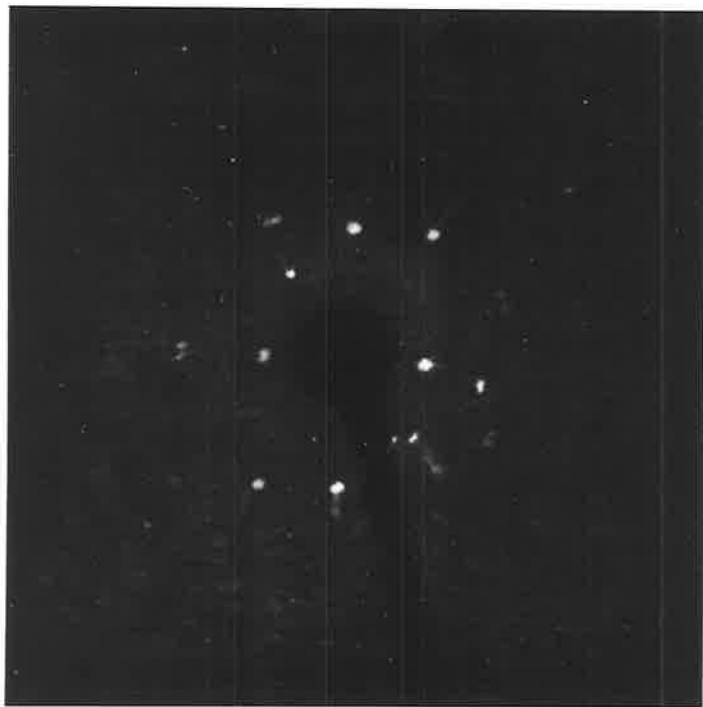


Figure 10(d)

reversible, but gave

$$\begin{array}{l} [111]_{\text{I}} \parallel [001]_{\text{I(c)}} , \\ (1\bar{1}0)_{\text{I}} \parallel (1\bar{1}0)_{\text{I(c)}} \text{ ----- [7]} \end{array}$$

(c) denoting cycled. The $[001]_{\text{I(c)}}$ projection was not exactly set with one set of (220) reflections being absent, implying missetting of about $\pm 5^\circ$. This relation was found once.

Relations [8], [9] [10]; (phases I \rightarrow II \rightarrow III)

A $(110)_{\text{I}}$ projection, was aligned with $[\bar{1}\bar{1}1]_{\text{I}}$ horizontal and $[\bar{1}12]_{\text{I}}$ vertical. Lamellae traces were found inclined at -32° to the horizontal, in the detwinned phase II, figure 24 of Section 2.4.3. The product was a slightly misset $(3\bar{1}3)_{\text{II}(Z=1)}$ i.e. $[100]_{\text{II}(Z=4)}$ projection, which gave to the relation

$$\begin{array}{l} (100)_{\text{I}} \wedge (011)_{\text{II}(Z=1)} \text{ i.e. } (001)_{\text{II}(Z=4)} = 1^\circ \\ [010]_{\text{I}} \wedge [1\bar{1}0]_{\text{II}(Z=1)} = 4^\circ \text{ ----- [8]} \end{array}$$

Neglecting the small discrepancy of angles this is the same as relation [1] described earlier.

The specimen was further cooled to phase III, giving a polycrystalline pattern, which contained the main projection of $[100]_{\text{III}(Z=1)}$. With respect to phase I, the orientation was

$$\begin{array}{l} [110]_{\text{I}(Z=4)} \parallel [001]_{\text{III}(Z=1)} \\ (1\bar{1}0)_{\text{I}} \wedge (210)_{\text{III}} = 3^\circ \text{ ----- [9]} \end{array}$$

which gives $(1\bar{1}0)_{\text{I}} \wedge (100)_{\text{III}} = 24^\circ$. The orientation between phases

II detwinned, and III was measured as

$$\begin{aligned}
 & [1\bar{1}1]_{\text{II}(Z=1)} \quad \text{i.e.} \quad [100]_{\text{II}(Z=4)} \quad || \quad [001]_{\text{III}(Z=1)} \quad , \\
 & (10\bar{1})_{\text{II}(Z=1)} \quad \wedge \quad (\bar{1}\bar{2}0)_{\text{III}(Z=1)} = 1^\circ \quad \text{-----} [10] \\
 \text{giving} & (111)_{\text{II}(Z=1)} \quad \wedge \quad (1\bar{1}1)_{\text{III}} = 16^\circ .
 \end{aligned}$$

SECTION 2.4.2 Optical Results of the I \rightarrow II Transformation

Kennedy⁽⁵¹⁾ and Kennedy and Iversen^(82,95) have already reported that the I \rightarrow II transformation is accompanied by complex Lamellar twinning which was observed in macroscopic samples by Courtenay and Kennedy,⁽⁷⁹⁾ as described in section 2.1. The width of lamellae depends on cooling rate. With slow cooling larger lamellae are formed, together with a herring-bone subtexture. It was reported that after about 10 minutes, detwinning occurs depending on as yet undetermined factors including temperature. Kennedy⁽¹⁰⁸⁾ states that closer examination of the herring-bone subtexture, reveals twin thickening (to be published). The I \rightarrow II transformation, including this phenomenon was investigated. Previous observations^(51,82,95) were noted.

The interface and nascent phase II were observed through crossed polars at magnifications of the order of 450X. A small-scale relaxation becomes apparent within seconds of the passage of an interface. The new phase grows in at least two ways depending on the region of observation. Parallel to lamellae, the interface is propagated by discrete jumps perpendicular to the length of the lamellae. At the ends of other lamellae, a herring-bone pattern grows in the lamellae direction. Figure 11(a) illustrates the latter region, while figure 11(b) shows with reflected polarized light that the lamellae and herring-bone subtexture are visible on the surface, and hence are shape changes. These effects are reversible only if the crystal is cooled within about 10 seconds after the transformation.

Figures 11 (a),(b),(c) also illustrate the impression that phase II grows in a zig-zag manner, which is reversible only within up to 10 to 15 seconds after transformation, but after which the "zags flip and become zigs", and the interface is no longer reversible.

Not all lamellae have subtexture, as confirmed by optical interferometry of thin lamellae and for example, figure 12. Figures 13(a) to (d) illustrate how an interface of the detwinning phase II moves at an irregular rate within adjacent lamellae joining them into the same orientation. Since the interface is perpendicular to the lamellae direction, this is referred to as "perpendicular small-scale relaxation", by the writer. This process also occurred in the crystal of figures 14(a),(b). From the edge of this crystal, as well as in figure 15, it is seen that lamellae mark individual plates which may be variants, probably symmetry related, of the product (see later, Section 2.4.5).

In the herring-bone pattern of figure 16 subtexture striations are inclined at an average angle of 41° to lamellae.

The slow growth of lamellae with stable subtexture which is apparently different from the "twin flipping" of figures 11(a),(b) and (c), is followed in figures 17(a) to (d). The new phase appears to grow on subtexture striations. The interface between striations or lamella boundary has a zig-zag nature, figure 17(e). The herring-bone pattern here is not symmetrical which may be due to the projection. Subtexture striations were measured at an average angle of $+22^{\circ}$, -58° to lamellae directions or $+25^{\circ}$, -64° towards the centre (or in the

Figure 11(a). *Optical microscopy of $\text{RbNO}_3 \text{ I} \rightarrow \text{II}$.
Phase II appears to grow in a zig zag
manner at the ends of lamellae.
Transmitted, polarized light.*

Figure 11(b). *Corresponding reflected polarized light
showing surface effects. Neg. mag.
X450, total mag. approx. 4000X.*



Figure 11(a)

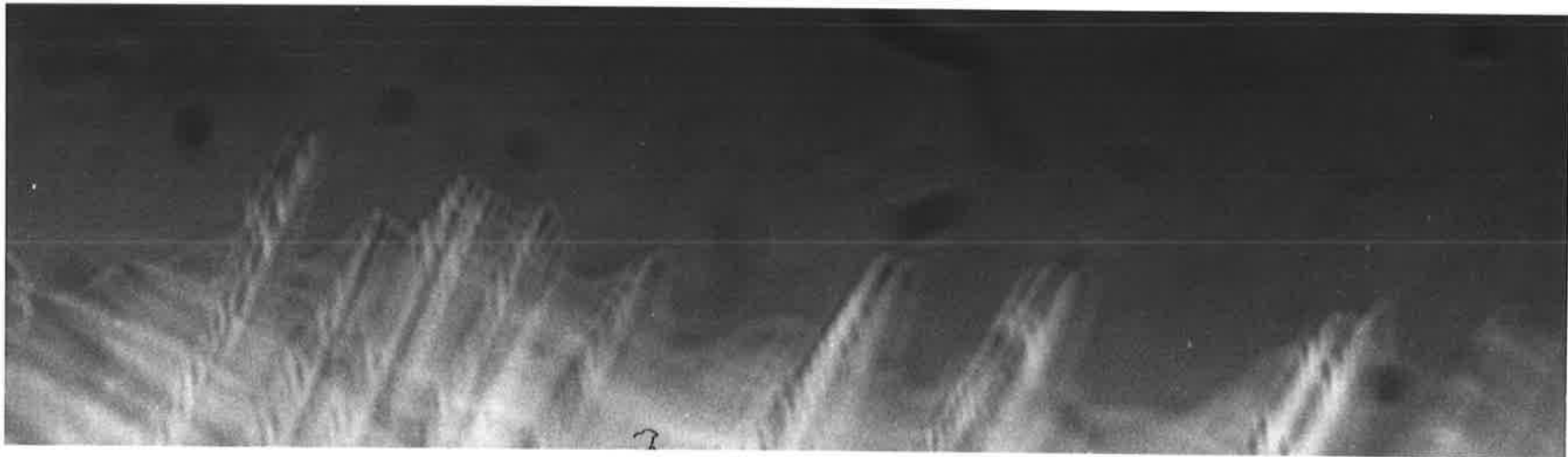


Figure 11(b)

Figure 11(c). The following photograph of RbNO_3 I \rightarrow II.
Transmitted, polarized light. Neg. mag.
X450, total mag. approx. 4000X.

Figure 11(d). RbNO_3 I \rightarrow II. Initially lamellae and
subtexture are not well defined.
Transmitted polarized light, neg. mag. X450.



Figure 11(c)



Figure 11 (d)

Figure 12. Lamellae without subtexture in small
crystallite. Transmitted polarized light.
Neg. mag. X450, total mag. X6440.

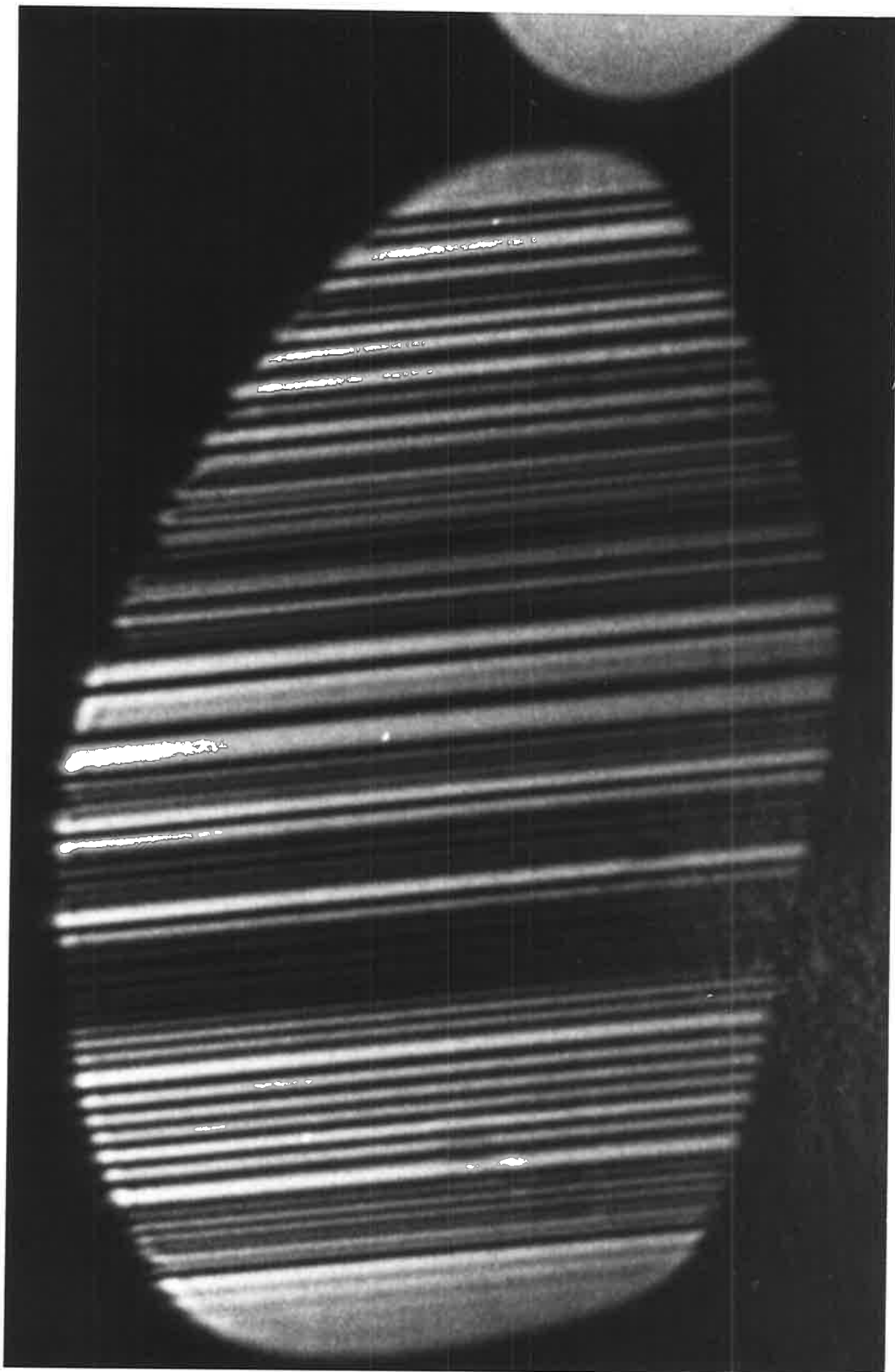


Figure 12.

Figure 13(a)

Figure 13(b)

*"Twin blunting" or "perpendicular
small-scale relaxation"*

Figure 13(c)

Figure 13(d)

*Transmitted polarized light,
neg. mag. X450, total mag. X1410.*

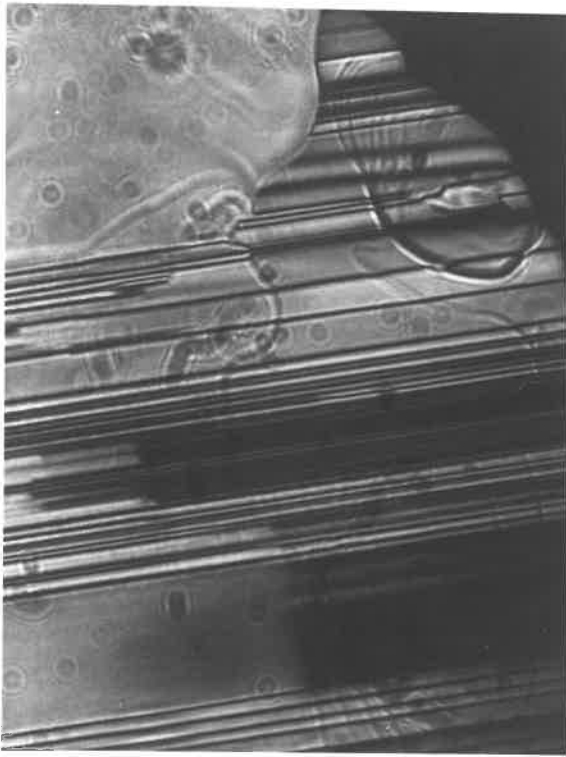


Figure 13(a)

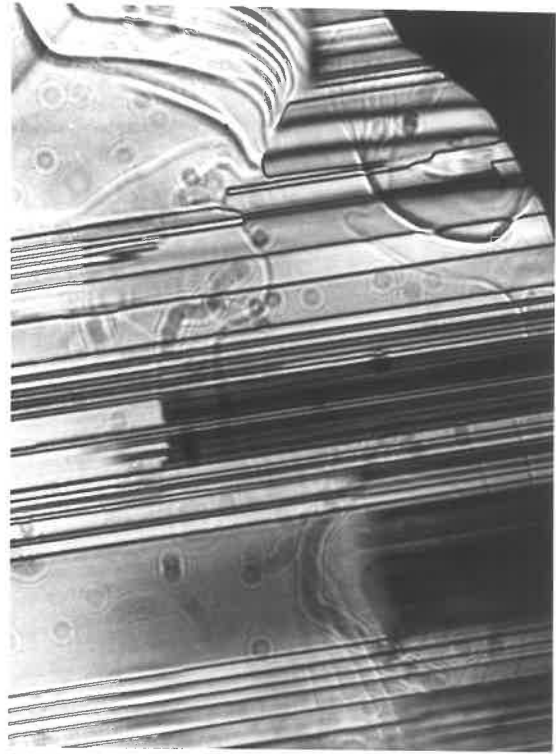


Figure 13(b)



Figure 13(c)

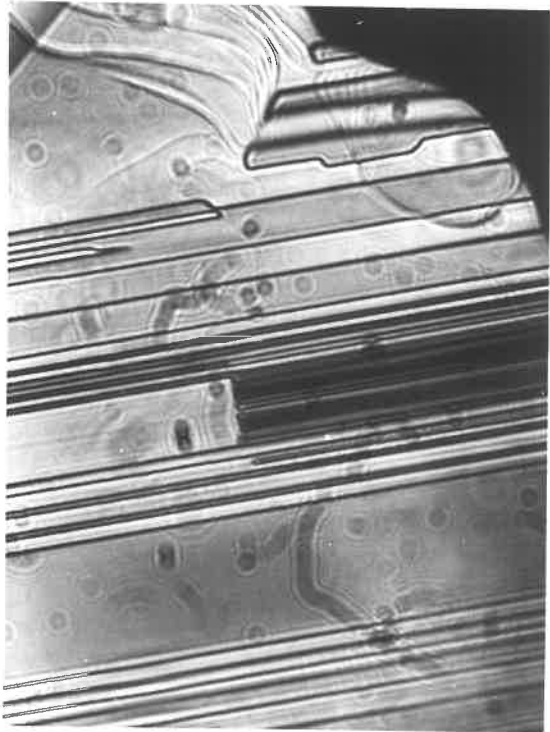


Figure 13(d)

Figure 14(a). RbNO_3 II. Initially lamellae are not well defined. Transmitted, polarized light. Neg. mag. X450, total mag. approx. 4000X.



Figure 14(a)

Figure 14(b). RbNO_3II . A perpendicular small-scale relaxation "interface" joins neighbouring lamellae, which then widen and become more evident. Total mag. approx. 4000X.



Figure 14(b)

Figure 15. RbNO_3 . Lamellae mark individual plates
of product. Transmitted polarized light.
Neg. mag. X450, Total mag. approx. 7000.

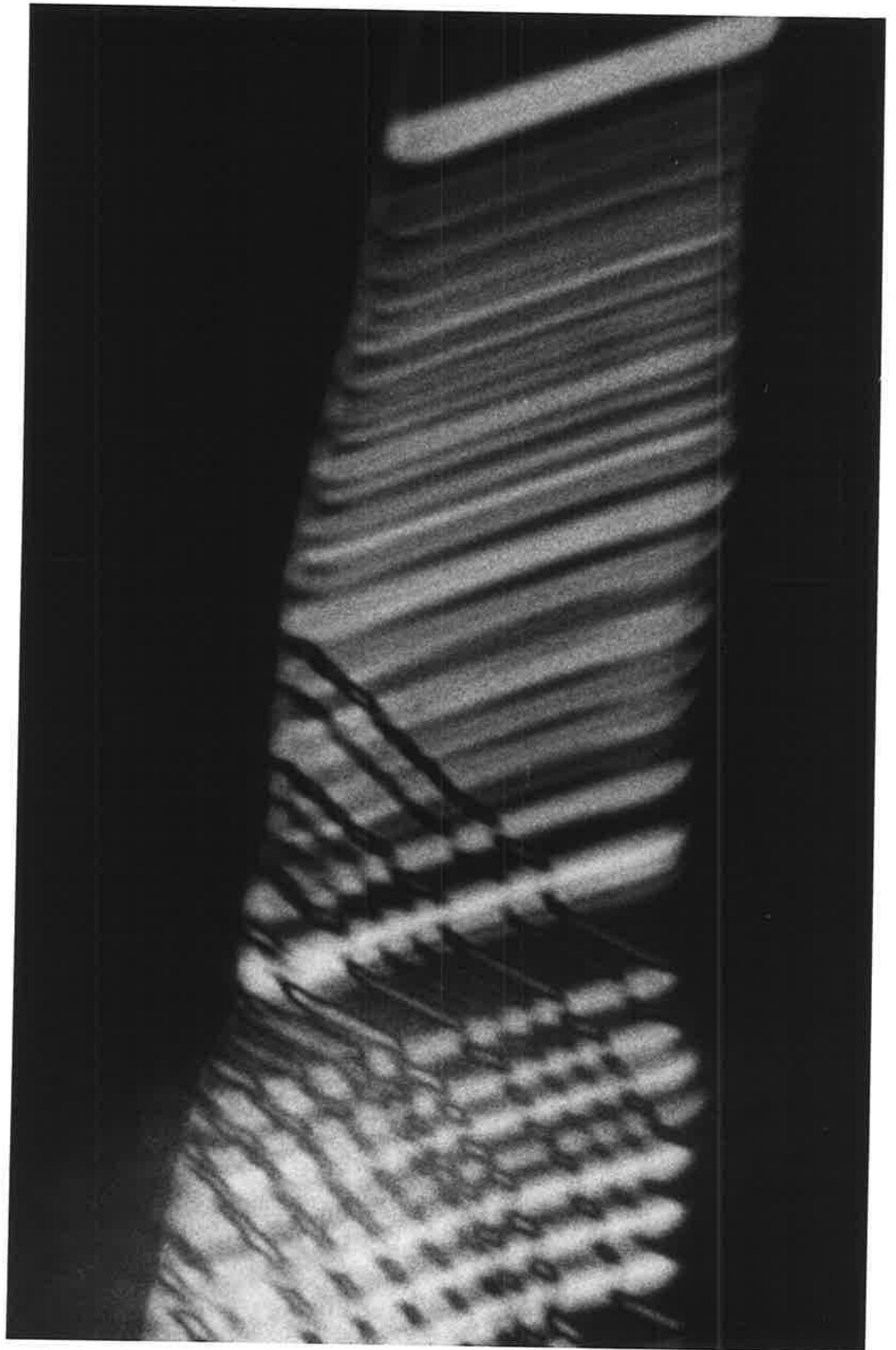


Figure 15.

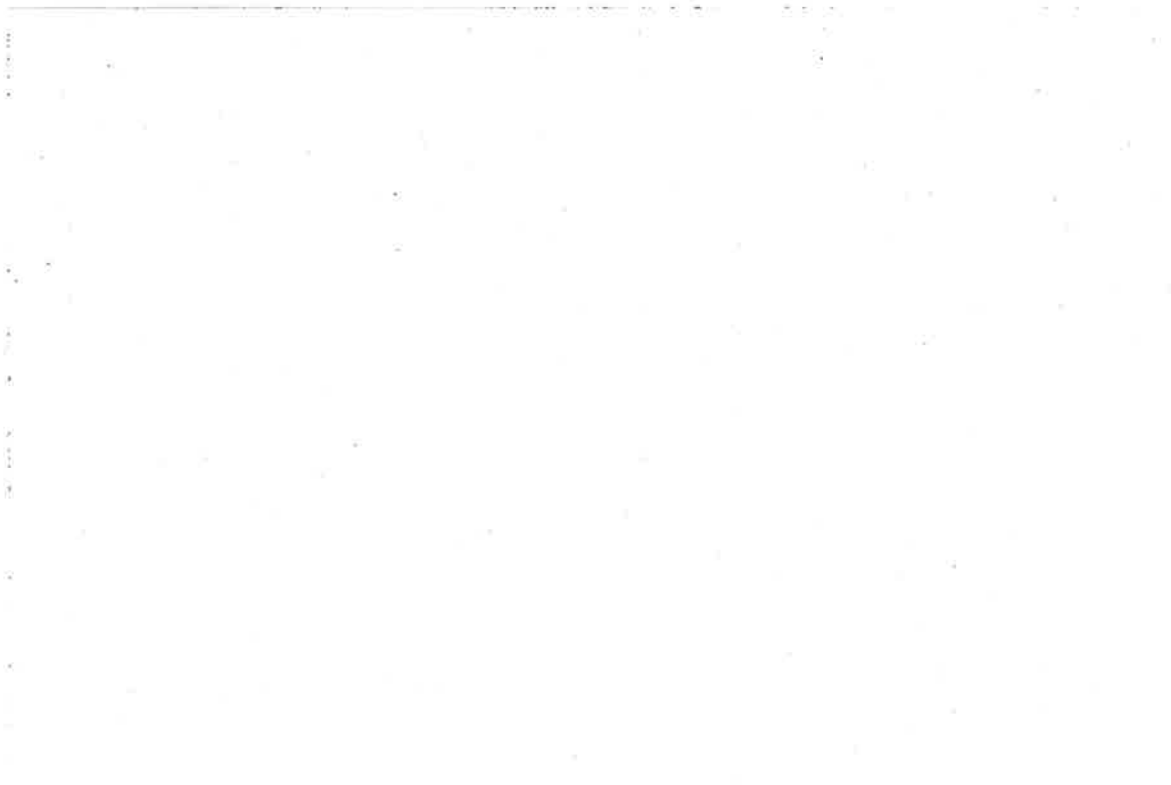
The image area is mostly blank, suggesting the micrograph content is either missing or extremely faint. The text below describes the intended content.

Figure 16. *Optical microscopy of main lamellae with subtexture striations. Transmitted polarized light. Neg. mag. X450. Total mag. X2700.*



Figure 16.

Figure 17(a). RbNO_3 II from I. Lamellae with "stable" subtexture. Transmitted polarized light. Neg. mag. X450, total mag. X2780.

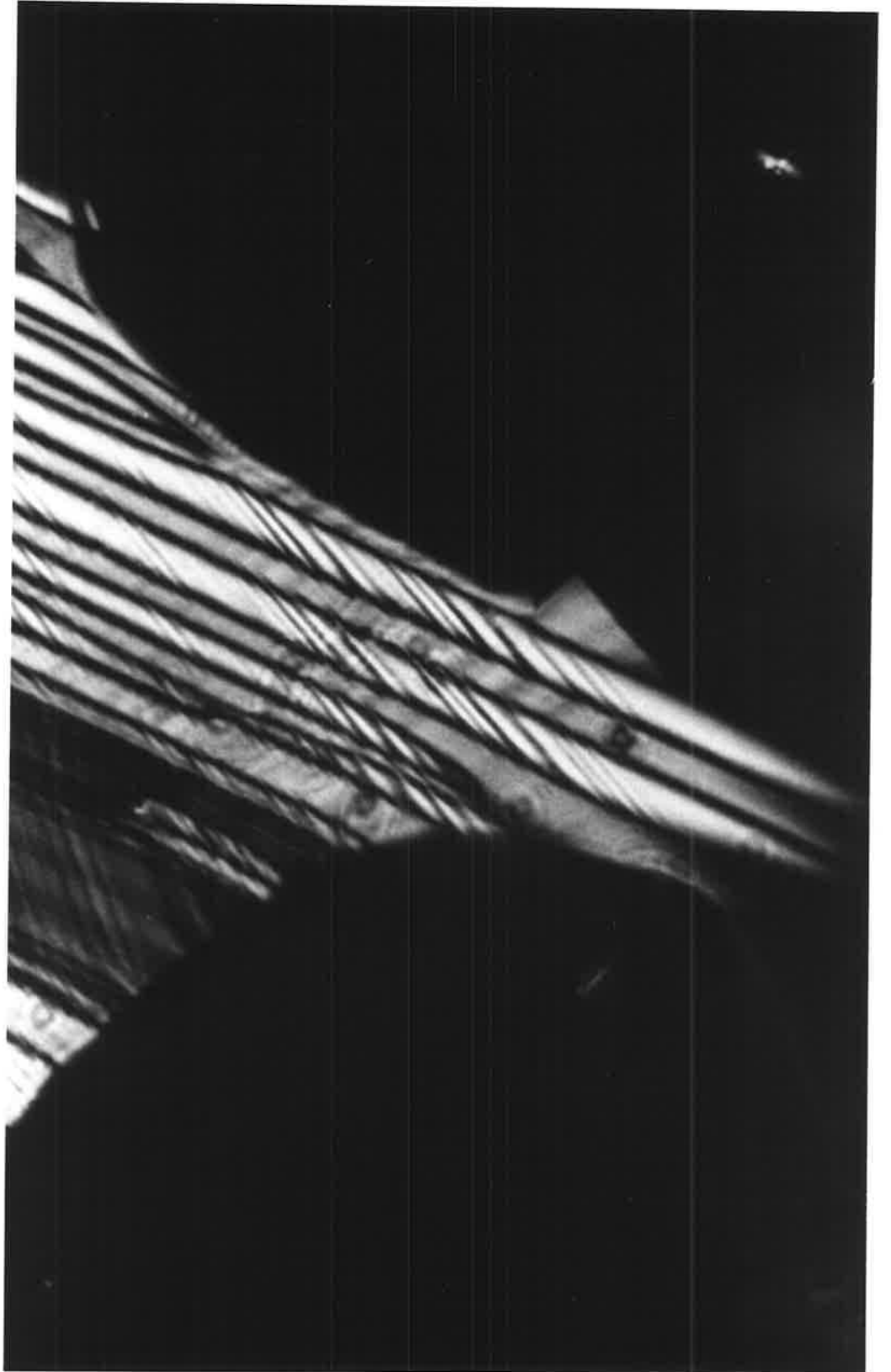


Figure 17(a)

Figure 17(b).

Reflected, polarized
light.
Neg. mag. X450,
total mag. X3840.

Figure 17(c)

Transmitted, polarized
light.
Neg. mag. X450,
total mag. X3840.

Oblique, slow growth of lamellae

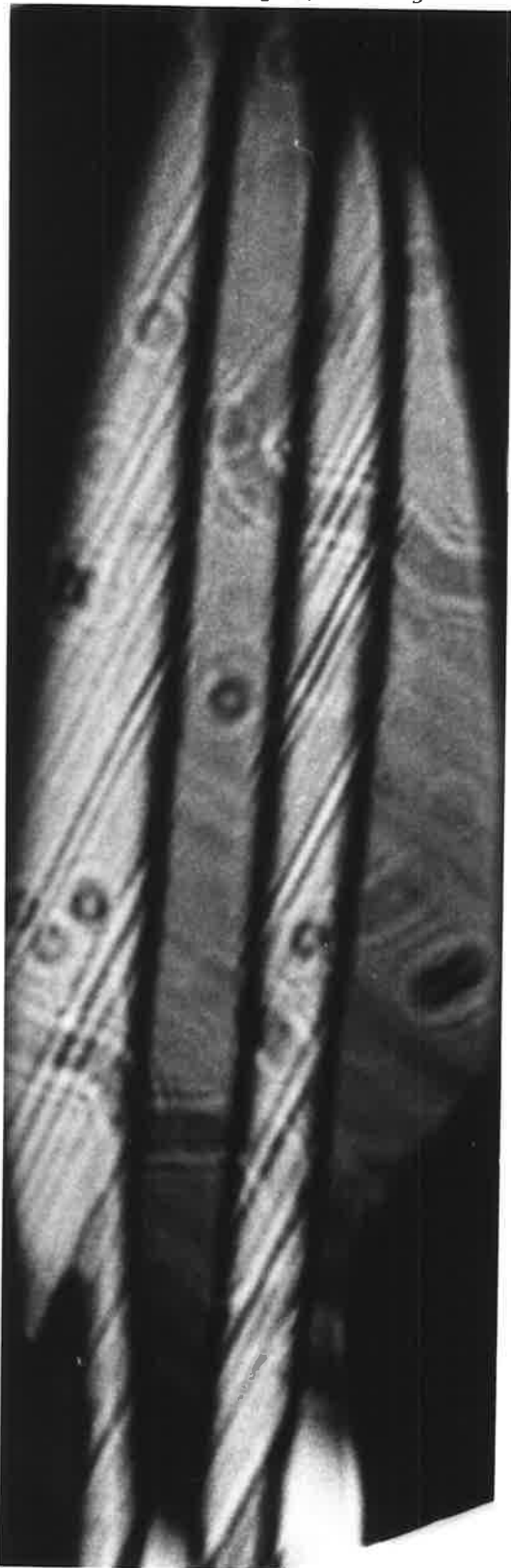


Figure 17(b)

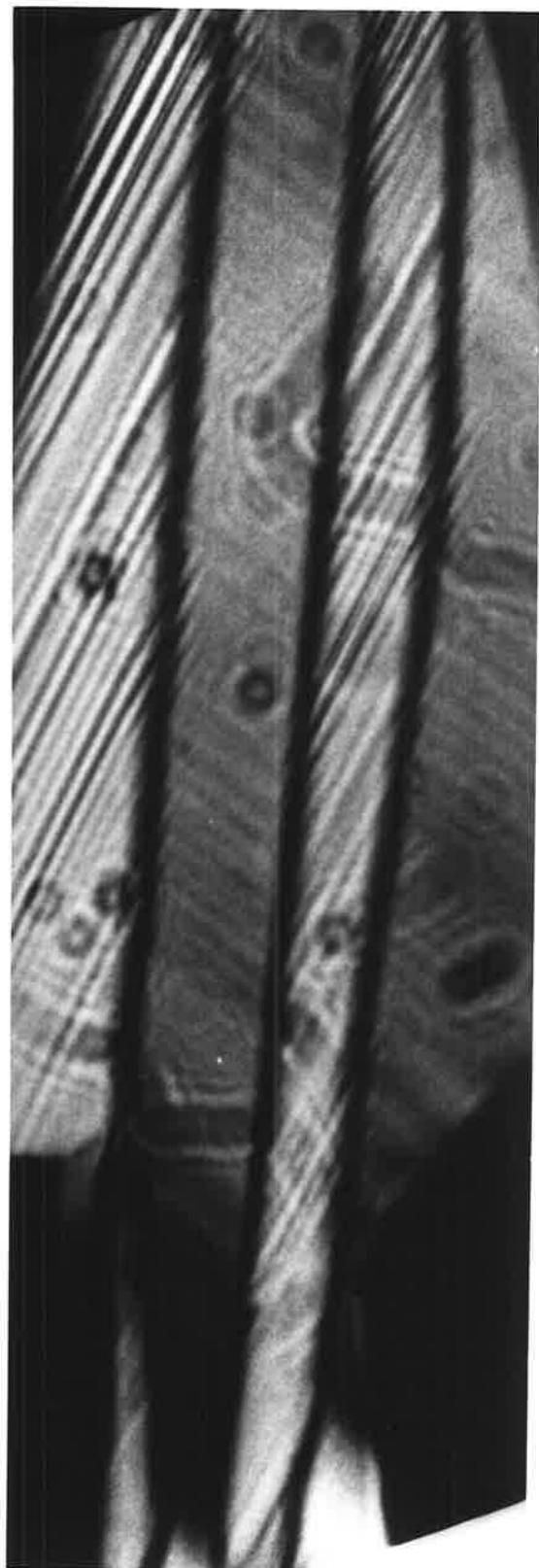


Figure 17(c)

Figure 17(d).

RbNO_3 II growing from
phase I.
Transmitted,
polarized light.
neg. mag. X450,
total mag. ~ 4000

Figure 17(e).

Accommodation at
lamellae boundaries.
Transmitted
polarized light.
neg. mag. X450,
total mag. X4350.

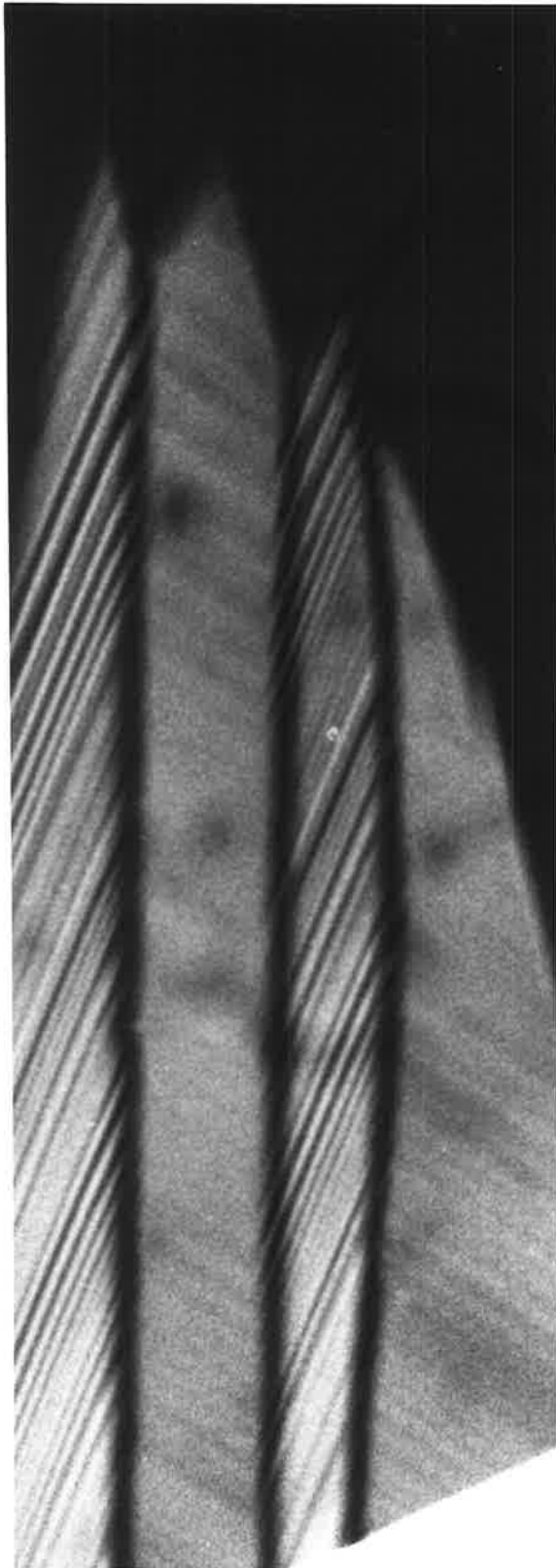


Figure 17(d)

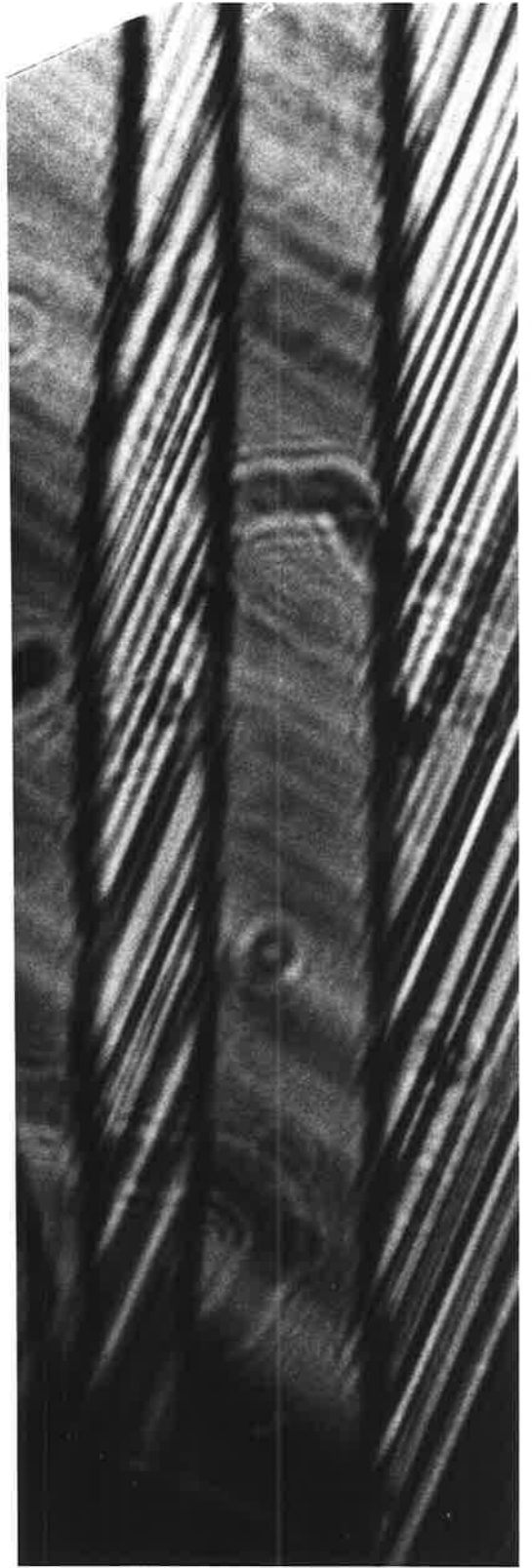


Figure 17(e)

photograph, the base) of the new phase matrix. The total magnification of figure 17(e) is 4350X.

Crystals frequently transform so that there are more than one set of thin lamellae; the figure below graphically presents various observed angles of intersection.

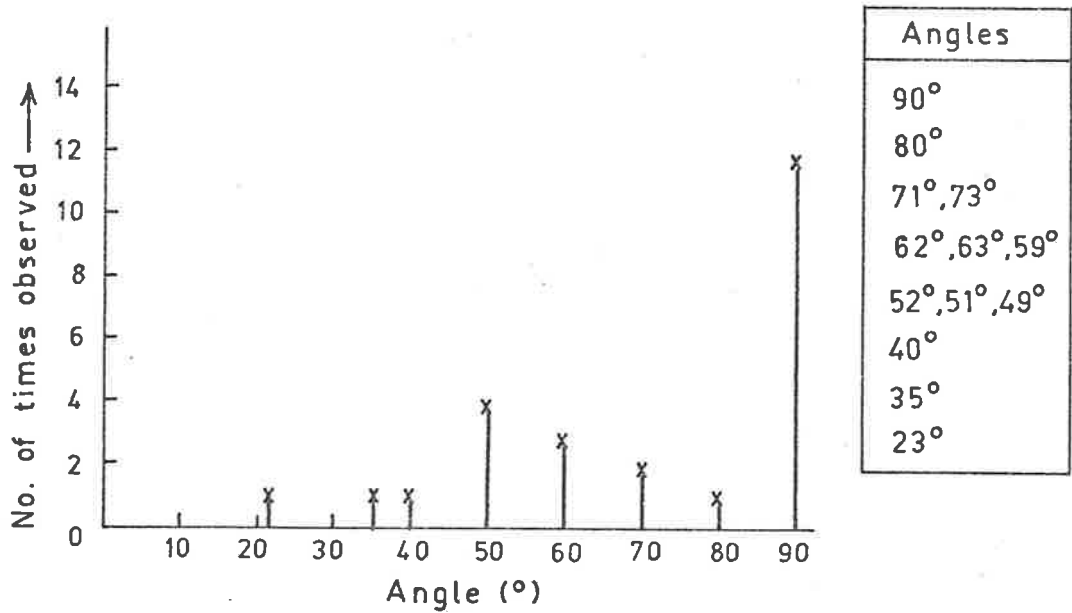


Figure 19. Phase II lamellae sometimes "balloon" out during medium-scale relaxation. Transmitted polarized light. Neg. mag. X450. Total mag. X1800.

Figure 18. A detwinning or large-scale relaxation interface leaves behind a single crystal orientation. Transmitted, polarized light. Neg. mag. X450, total mag. X1750.

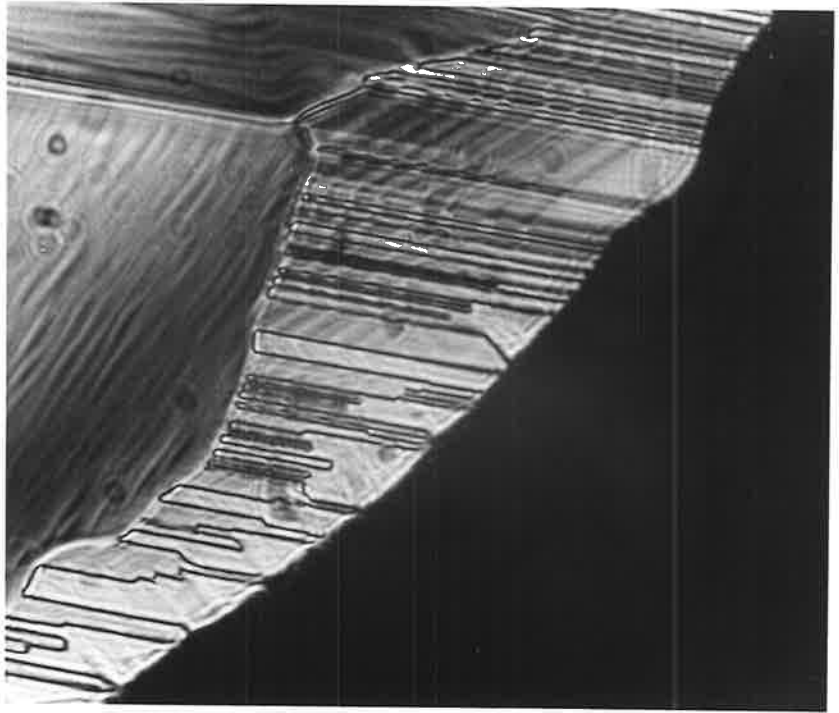


Figure 19.

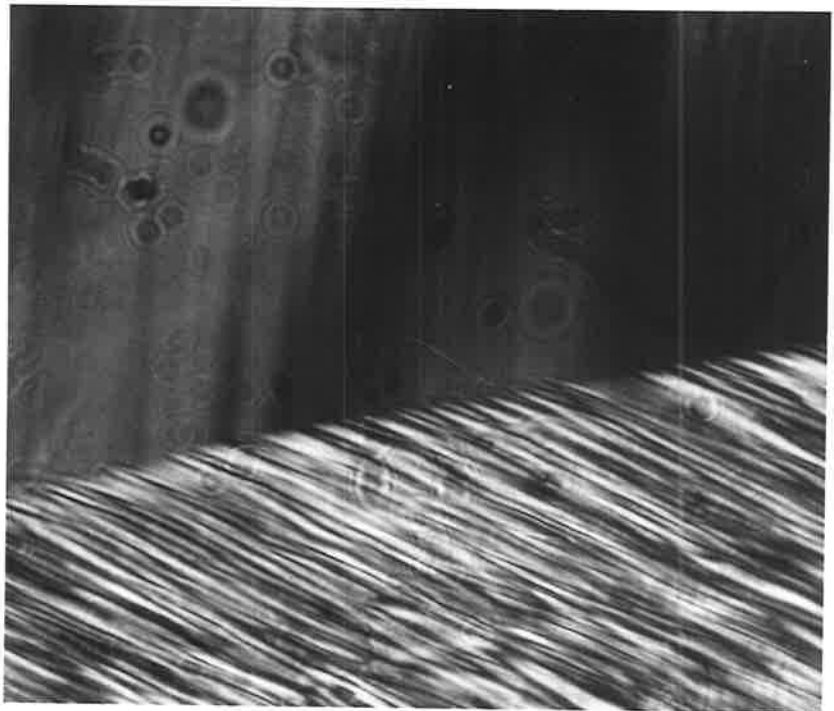


Figure 18.

Within seconds after some transformations, thin lamellae superimpose and thicken so as to give the appearance of Moiré patterns. "Small scale relaxation" follows in the form of a blob which moves along lamellae directions joining and broadening them. In figure 18 such a Moiré pattern is being removed by the detwinning interface. In this investigation this detwinning is referred to as "large-scale relaxation", since it occurs over many sets of unit cells, and in fact the entire crystal. "Small-scale relaxation" described above occurs on a scale comparable to much smaller sets of unit cells. Figure 19 depicts an intermediate form of relaxation which sometimes occurs at the edge of crystals where lamellae widen or "balloon" out. This is referred to as "medium-scale relaxation" by the writer.

Finally, as discussed in Section 2.1, the $II \rightleftharpoons III$ transformation is accompanied by distortion and bending since it involves a large strain and volume change. Figure 20 is an example where fragmentation occurred at the edge of a specimen during quick cooling and transformation $II \rightarrow III$. The shape of the fracture does not appear random but makes an angle of 64° in the matrix. Fragments like this were observed on several occasions.

SECTION 2.4.3 X-ray - Optical Results

The experimental method is described in Section 2.2. Negative magnifications were usually of the order of 120X. The herring-bone patterns of figure 17(a) of the previous section were magnified some 12 times more. Hence, it was difficult to observe fine subtexture in these experiments and usually only lamellae directions were noted with respect to oriented phase I. Table 8 summarizes positions of lamellae in unrelaxed phase II or their traces in the large-scale relaxed phase, as indicated. A measured clockwise rotation is designated positive.

TABLE 8(a)

ORIENTATION OF PHASE II LAMELLAE WITH RESPECT TO PHASE I

Projection in phase I	Location	Number of Observations	Figure
{100}	to $\langle 100 \rangle$ 14° to $\langle 100 \rangle$ (?)	4 1	21
{111}	to $\langle 1\bar{1}0 \rangle$ 4° to $\langle 1\bar{1}0 \rangle$ 2°, 3° to $\langle 1\bar{1}0 \rangle$	6 1 1	24
{112} with $(1\bar{3}1)$ vertical and $(1\bar{1}0)$ at -31° to vertical	inclined at +82° and -70° to vertical (detwinned phase)	1	
{110} with $\{1\bar{1}\bar{1}\}$ horizontal and $(1\bar{1}2)$ vertical	inclined at -32° to horizontal (detwinned phase)	1	22

TABLE 8(b)

LAMELLAE WITH SUBTEXTURE

{100}	Lamellae to $\langle 100 \rangle_I$ with subtexture striations at -40° and +42° to main lamellae, and hence at 5°, 3° to $\langle 110 \rangle_I$	1	23
-------	---	---	----

(?), early experiment

Figure 21. Twinned RbNO_3II from a $\langle 100 \rangle_I$ projection. Crosswires \parallel to $\langle 110 \rangle$ directions, lamellae to $\langle 010 \rangle$ directions. Transmitted polarized light, neg. mag. X60, total mag. X250.

Figure 22. Detwinned RbNO_3II , from a $\langle 110 \rangle_I$ projection. Horizontal crosswires $\parallel \langle 1\bar{1}2 \rangle_I$. Lamellae traces at -32° to horizontal. Transmitted polarized light, neg. mag. X60, total mag. X250.

Combined X-rays - optical microscopy

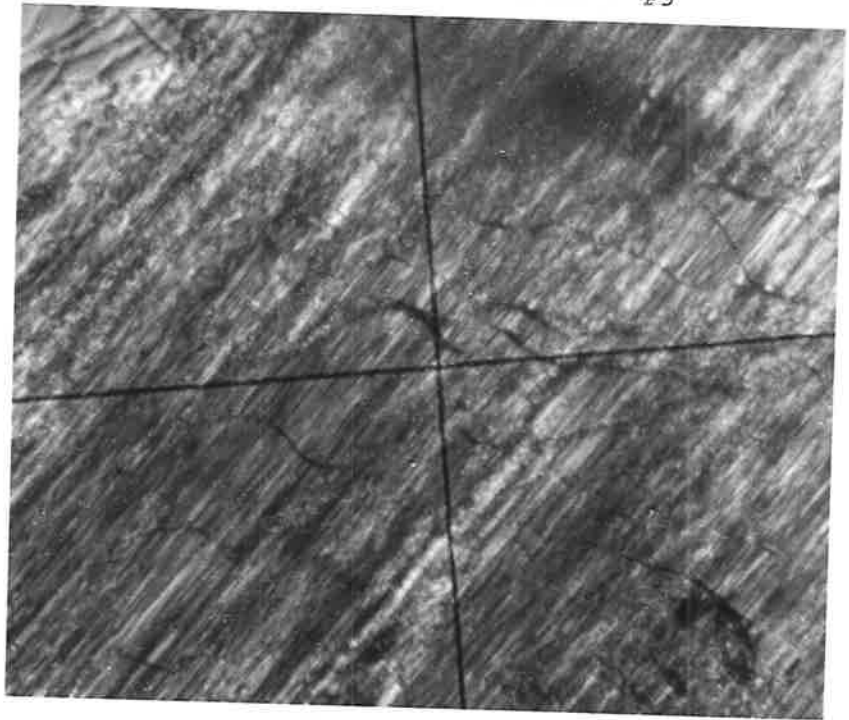


Figure 21.

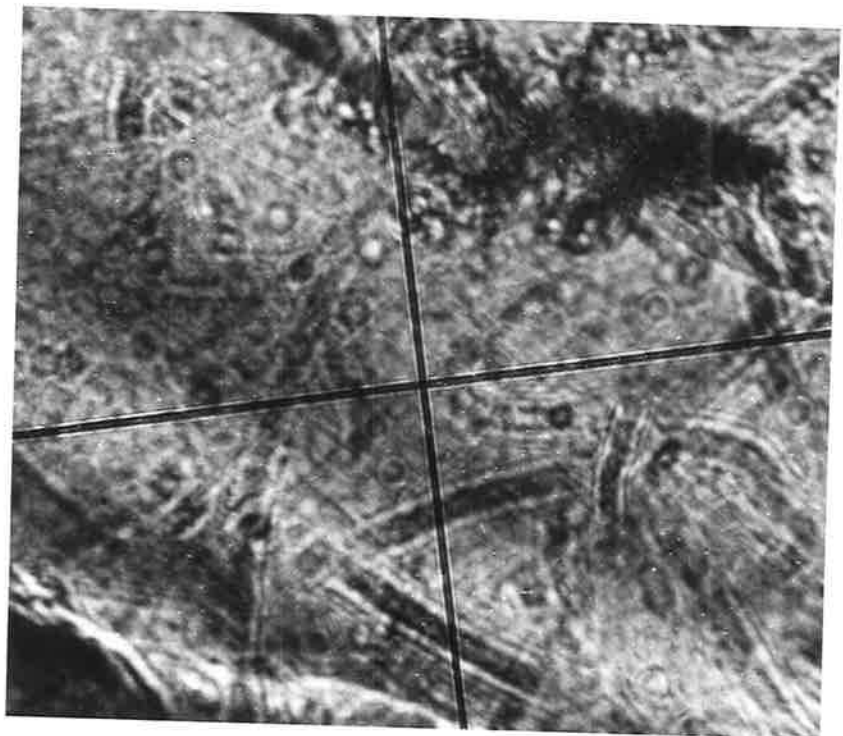


Figure 22.

Figure 23. RbNO_3II from a $\langle 100 \rangle_I$ projection. Lamellae are \parallel to $\langle 100 \rangle$ with oblique set at 5° and 3° to $\langle 110 \rangle_I$. Transmitted polarized light. Neg. mag. X60, total mag. X250.

Figure 24. Twinned RbNO_3II from a $\langle 111 \rangle_I$ projection. Lamellae \parallel to $\langle 1\bar{1}0 \rangle_I$ directions. Transmitted polarized light, neg. mag. X60, total mag. X250.

combined X-rays - optical microscopy

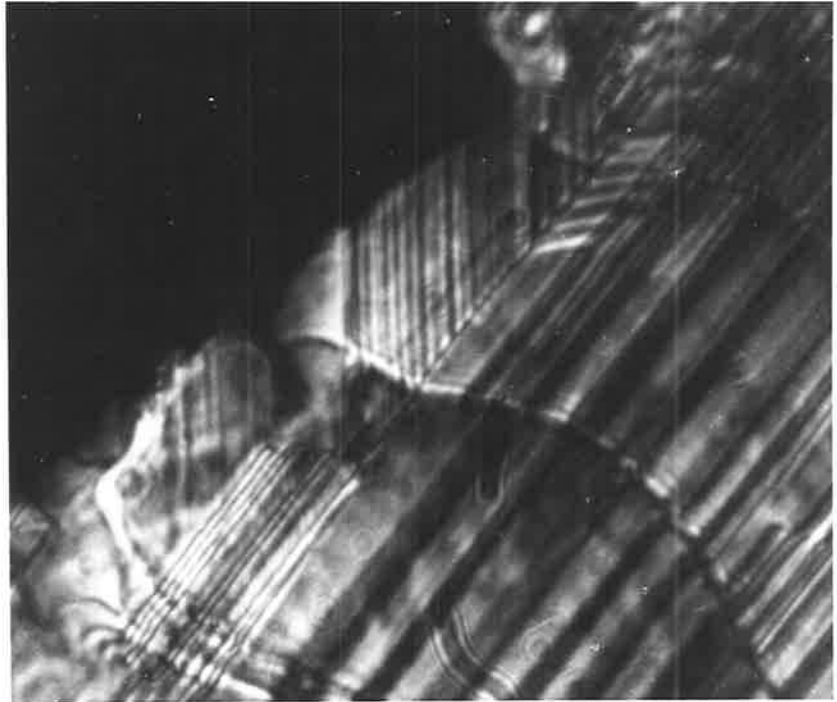


Figure 23.

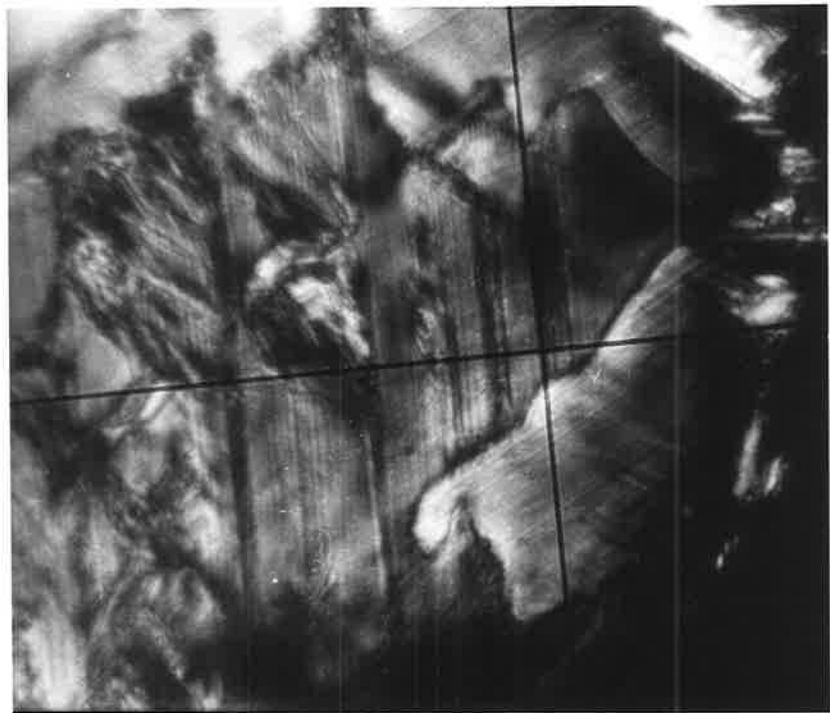


Figure 24

SECTION 2.4.4 Martensite Calculations

The reasons for undertaking martensite calculations for the shear systems considered are discussed in Section 2.7.1. This section summarizes data used in conjunction with PROGRAM MARTENS of Fraser.⁽⁴¹⁾ The theoretical basis of the analysis has been given in Chapter 1. The face-centred cubic to rhombohedral structure change was analysed in terms of $Z = 4$ cells, in the lattice correspondence

$$\begin{array}{l} [1\bar{1}0]_{\text{I}} \quad || \quad [1\bar{1}0]_{\text{II}}, \\ [11\bar{2}]_{\text{I}} \quad || \quad [11\bar{2}]_{\text{II}} \quad \eta_1 = \eta_2 = 1.0643 \\ [111]_{\text{I}} \quad || \quad [111]_{\text{II}} \quad \eta_3 = 0.8476 \end{array}$$

The shear systems considered were twinning of the type $(100)[011]_{\text{I}}$ and $(110)[001]_{\text{I}}$.

Predicted orientation relations were displayed on computerized stereograms, and are summarized in Tables 9 and 10.

The dependence of habit plane orientation on lattice parameters of parent and product phases was investigated. Table 11 summarizes various reported lattice parameters and their derived η values. Table 12 shows that for the $(100)[011]$ shear system, the average predicted habit plane is $4^\circ \pm 2^\circ$ off $\{102\}_{\text{I}}$, whilst for the $(110)[001]$ shear system is $10^\circ \pm 4^\circ$ off $\{001\}_{\text{I}}$. Integer descriptions of the irrational habit planes were facilitated by the use of PROGRAM ANGLES.⁽¹⁷⁹⁾

Traces corresponding to predicted habit planes were drawn on computerized standard cubic stereograms, in the projections $\{100\}_{\text{I}}$, $\{111\}_{\text{I}}$, $\{112\}_{\text{I}}$, and $\{110\}_{\text{I}}$, which were experimentally observed. The

TABLE 9

ORIENTATION RELATIONS PREDICTED BY A MARTENSITEANALYSIS of the I → II Transformation, in terms of Z=4 cells

<u>{100} Twinning</u>	<u>{110} Twinning</u>
variant (i)	variant (i)
$[111]_I \wedge [111]_{II} = 9^\circ$	$[111]_I \wedge [111]_{II} = 6^\circ$
$(010)_I \parallel (010)_{II}$	$(100)_I \parallel (100)_{II}$
$(0\bar{1}1)_I \wedge (0\bar{1}1)_{II} = 5^\circ$	$(011)_I \wedge (011)_{II} = 12^\circ$
$(011)_I \wedge (011)_{II} = 5^\circ$	$(0\bar{1}1)_I \wedge (0\bar{1}1)_{II} = 4^\circ$
variant (ii)	variant (ii)
$[111]_I \wedge [111]_{II} = 10^\circ$	$[111]_I \wedge [111]_{II} = 7^\circ$
$(001)_I \parallel (001)_{II}$	$(100)_I \parallel (100)_{II}$
$(011)_I \wedge (011)_{II} = 5^\circ$	$(101)_I \wedge (101)_{II} = 4^\circ$
	$(110)_I \wedge (110)_{II} = 8^\circ$
variant (iii)	variant (iii)
$[111]_I \wedge [111]_{II} = 6^\circ$	$[111]_I \wedge [111]_{II} = 7^\circ$
$(010)_I \parallel (010)_{II}$	$(100)_I \parallel (100)_{II}$
$(011)_I \wedge (011)_{II} = 5^\circ$	$(101)_I \wedge (101)_{II} = 2^\circ$
	$(\bar{1}01)_I \wedge (\bar{1}01)_{II} = 2^\circ$
variant (iv)	variant (iv)
$[111]_I \wedge [111]_{II} = 7^\circ$	$[111]_I \wedge [111]_{II} = 6^\circ$
$(001)_I \parallel (001)_{II}$	$(100)_I \wedge (100)_{II} = 2^\circ$
$(011)_I \wedge (011)_{II} = 4^\circ$	$(110)_I \wedge (110)_{II} = 2^\circ$
	$(0\bar{1}1)_I \wedge (0\bar{1}1)_{II} = 5^\circ$
Predicted habit plane 4° off {102}	Predicted habit plane 10° off {100}

TABLE 10

MARTENSITE SOLUTIONS FOR THE I \rightarrow II TRANSFORMATION FOR

$$\eta_1 = 1.064 ; \eta_2 = .847$$

L.I. Shear angle in parent ($^{\circ}$)	Rotation axis	Rotation ($^{\circ}$)	Habit Plane Indices	Direction of shape strain	Magnitude of shape strain
<u>Lattice Invariant Shear System (100)[011]_I</u>					
(a) 9.12 $^{\circ}$.383	10.0 ₄	-.369	.064	.163
	.806		.021	-.149	
	-.451		.929	-.016	
(b) 3.89 $^{\circ}$.690	.59 ₄	.369	-.064	.163
	.201		.021	-.149	
	-.695		.929	-.016	
<u>L.I. Shear System (011)[100]_I</u>					
(a) 6.57 $^{\circ}$.551	8.2 ₇	.138	-.024	.163
	-.541		-.079	.159	
	.636		-.987	.026	
(b) 4.66 $^{\circ}$	-.669	6.7	.138	-.024	.163
	-.407		.987	-.026	
	.622		.079	-.159	

TABLE 11

VARIOUS REPORTED LATTICE PARAMETERS AND THEIR DERIVED η VALUES(1968) Salhotra et al⁽⁵⁰⁾

I	(Z=1) rhombohedral	$a = 5.176 \text{ \AA}$	$\alpha = 60^\circ$
	(Z=4) cubic,	$a = 7.32 \text{ \AA}$	$\alpha = 90^\circ$
	(Z=12) hexagonal,	$a_h = 12.679$	$c_h = 10.352$
II	(Z=1) rhombohedral,	$a = 4.79$	$\alpha = 70^\circ 12'$
	(Z=4) rhombohedral,	$a = 7.30$	$\alpha = 97.982$
	(Z=12) hexagonal,	$a_h = 11.0172$	$c_h = 10.746$
		$\eta_1 = 1.0643$	$\eta_3 = 0.8475$
II	(Z=3) hexagonal,	$a_h = 5.51$	$c_h = 10.74$
	(Z=12) hexagonal,	$a_h = 11.02$	$c_h = 10.74$
		$\eta_1 = 1.065$	$\eta_3 = 0.8471$

(1969) Salhotra et al⁽⁸⁴⁾

II	(Z=1) rhombohedral,	$a = 4.80$	$\alpha = 70^\circ 28'$
	(Z=12) hexagonal,	$a_h = 10.90$	$c_h = 10.75$
		$\eta_1 = 1.070$	$\eta_3 = 0.8471$
II	(Z=3) hexagonal,	$a = 5.45$	$c = 10.75$
	(Z=12) hexagonal,	$a_h = 10.90$	$c_h = 10.75$
		$\eta_1 = 1.0529$	$\eta_2 = 0.8475$

(1968) Salhotra et al⁽⁵⁰⁾

III	(Z=1) cubic,	$a = 4.37$	$\alpha = 90^\circ$
	(Z=4) rhombohedral,	$a_r = 7.569$	$109^\circ 28'$
	(Z=12) hexagonal,	$a_h = 12.360$	$c = 7.569$
	(Z=3) hexagonal,	$a_h = 6.189$	$c_h = 7.569$
		$\eta_1 = 1.1940$	$\eta_3 = 0.73116$

TABLE 12
VARIATION OF HABIT PLANES AND CONES OF UNEXTENDED VECTORS, WITH η 's

η_1	η_3	ϕ_1	ϕ_2	Shear System	Habit Plane	Approximate Habit Plane	More precise description
1.064, 0.8475		55.640, 61.44		(100)[011]	{.394, .021, .929}	{1, 0, 2.5}	4.8° off {102}
				(011)[100]	{.138, .078, .987}	{1, 0, 7}	8° off {001}
1.065, 0.850		55.18, 60.97		(100)[011]	{.358, .010, .934}	{1, 0, 2.6}	5.5° off {102}
				(011)[100]	{.098, .069, .993}	{1, 0, 10}	6° off {001}
1.0529, 0.8479		58.135, 63.409		(100)[011]	{.408, .075, .910}	{1, 0, 2.2}	2° off {102}
				(011)[100]	{.261, .122, .957}	{2, 1, 8}	15° off {001}
1.070, 0.8471		54.387, 60.444		(100)[011]	{.345, .008, .939}	{1, 0, 2.7}	6° off {012}
				(011)[100]			no solution

where ϕ_1, ϕ_2 denote angle of cones of unextended vectors of parent and product phase respectively.

Average habit plane for (100)[011] system is $4^\circ + 2^\circ$ off {102} while for the (011)[100] system it is $10^\circ + 4^\circ$ off {001}.

TABLE 13

TRACES CORRESPONDING TO PREDICTED HABIT PLANES FOR (100)[011] AND (110)[001] SHEAR SYSTEMS IN SOME SPECIFIED PROJECTIONS

<u>Projection in Phase I</u>	<u>(100)[011] 4° off{102}</u>	<u>(110)[001] 9° off {001}</u>
{100}	⊗ <010> +22° to <010>	<110> +6°, +7° to <010>
{111}	+16°, +24° to <011̄>	⊗ <110> +13° to <110̄>
{112} with (13̄1) vertical and (110) at -31° to vertical	inclined w.r.t. vertical at: +6°, +8°, +34°, +40° +76°, ⊗+83°, -4°, -12° -52°, -58°, ⊗-72°	+10°, +16°, +22° +29°, -16°, -31° -46°, ⊗-74°, -80° -86°, -93°
{110} with (11̄1) horizontal and (11̄2) vertical	inclined w.r.t. horizontal at +18°, +52°, ⊗-25° -55°, -85°	+26°, +35°, +44° -46°, -64°, -66°

A positive angle indicates a clockwise rotation. ⊗ denotes experimentally observed lamellae, as seen from comparison with Table 8(a).

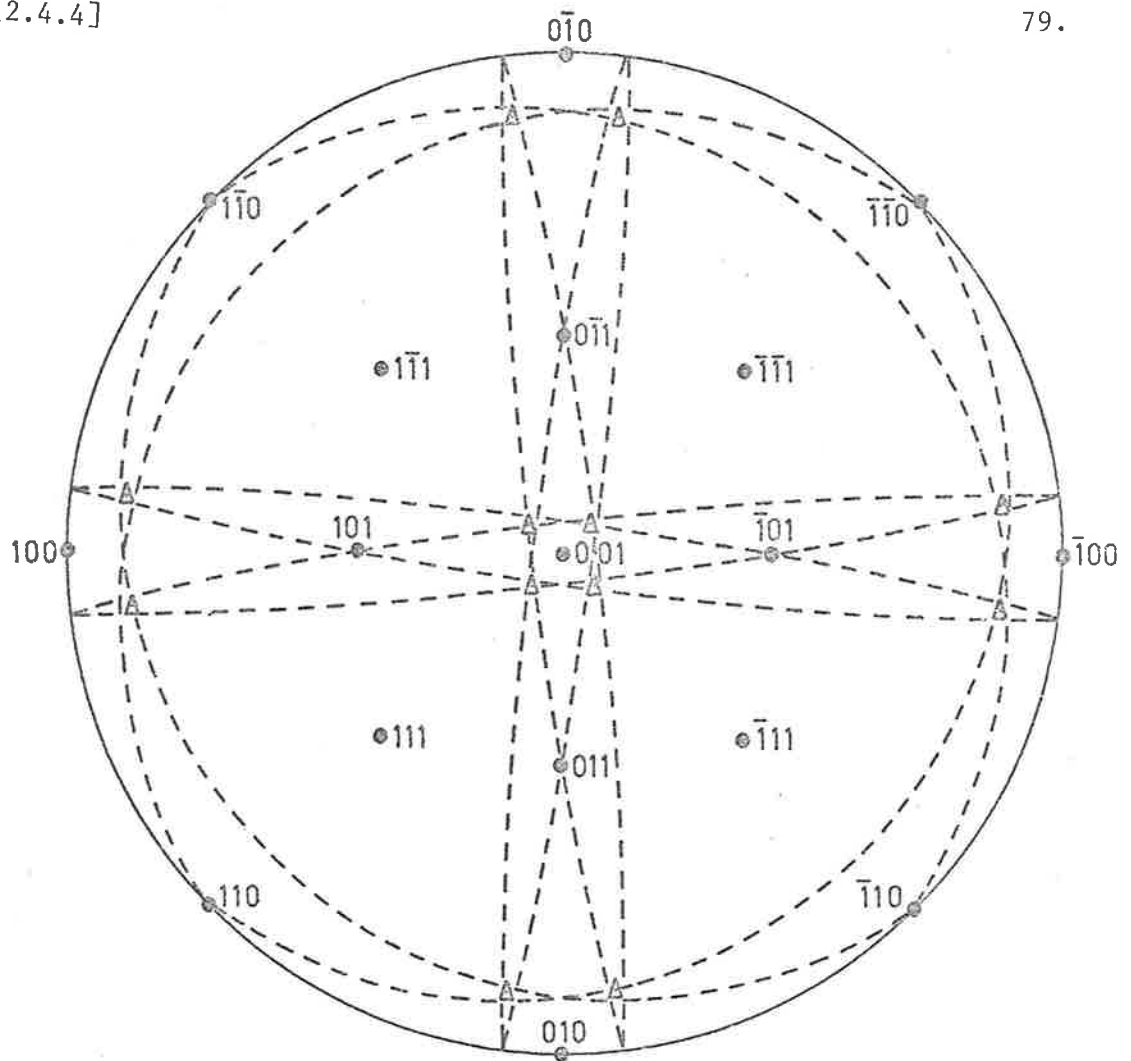


Fig. 25(b). (001) projection of $RbNO_3$ I, f.c.c.

Δ indicates the 10° off $\{010\}$ habit plane predicted by $\{110\}$ twinning. Traces occur at $\parallel \langle 110 \rangle$ and at $\pm 6^\circ, \pm 7^\circ$ to $\langle 010 \rangle$.

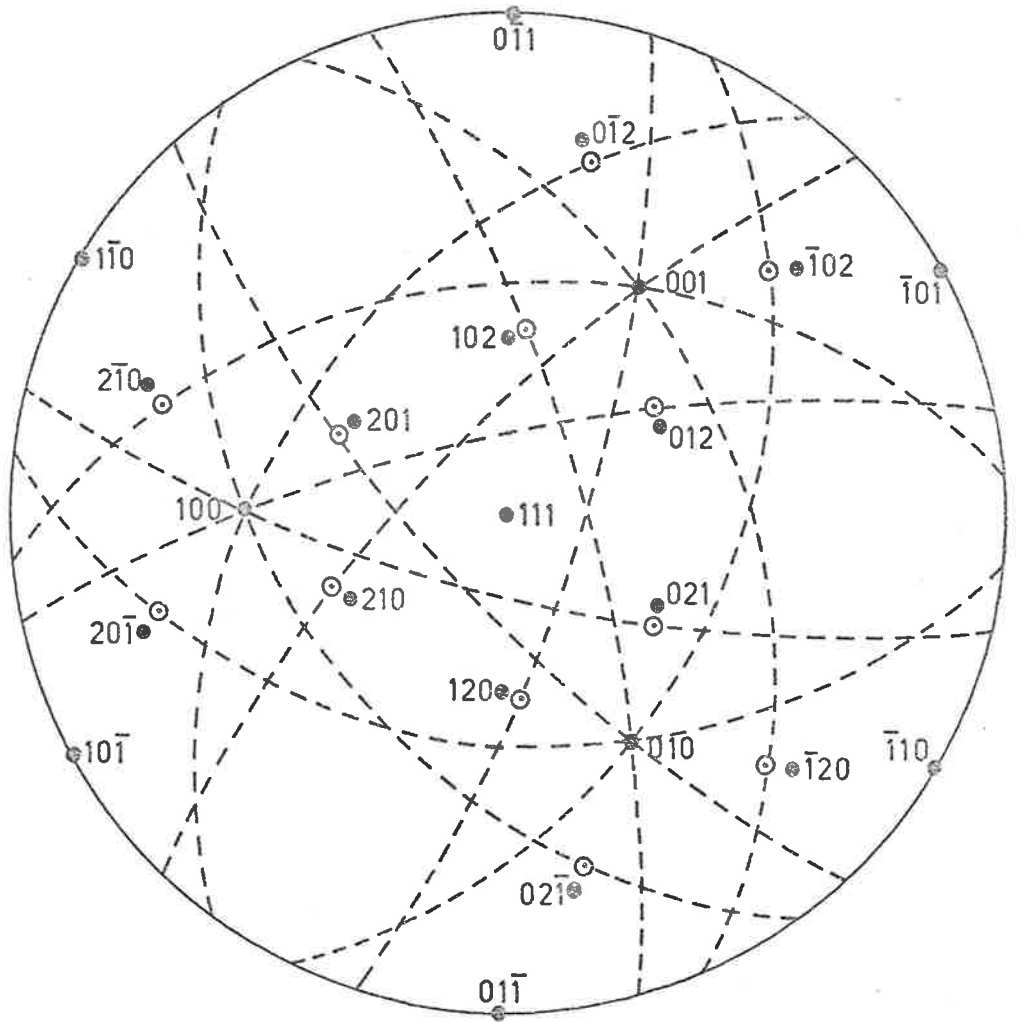


Fig. 25(c). (111) projection of RbNO_3 I, f.c.c.

⊙ indicates the 4° off $\{012\}$ habit plane predicted by $\{100\}$ twinning. Traces occur at $\pm 16^\circ$ and $\pm 24^\circ$ to $\langle 1\bar{1}0 \rangle$.

method is illustrated in figures 25(a) to (d). The results for the two shear systems are given in Table 13. They are subject to approximately $\pm 3^\circ$ error due to stereogram manipulations and uncertainty in habit plane locations. Angles marked with an asterisk are those experimentally observed within a small margin of error, as seen by comparison with Table 8 of Section 2.4.3.

Other shear systems, in particular $(1\bar{1}0)[110]_I$, $(011)[11\bar{1}]_I$ and $(011)[2\bar{1}\bar{1}]_I$ gave mathematical solutions but were not further investigated since there was no experimental or theoretical basis for their consideration. As seen from Table 11, the transformation $I \rightarrow III$ may be analysed martensitically with the same lattice correspondence as for $I \rightarrow II$. The structure change is the NaCl-type to CsCl-type transformation in ammonium bromide which was quantitatively analysed and observed.⁽⁴¹⁻⁴²⁾ The lattice invariant shear $\{100\}\langle 011\rangle_I$ from transformation twinning, produced a 5° off $\{102\}_I$ habit plane which was experimentally observed.

SECTION 2.5 I → III TRANSFORMATION, X-RAY OBSERVATIONS

This section continues in the manner of Section 2.4.1. Phase I is referred to in terms of the $Z = 4$ cell, and phase III in terms of $Z = 1$, both cells being cubic.

Relation [11]

In five different experiments, phase I was cooled quickly to phase III. From the opaque appearance of twinned phase II in two of these experiments, it was seen that the specimen existed in the twinned phase for only about one second. In two other experiments, the specimen was held for some time in the relaxed state. On these seven occasions phase I transformed to a polycrystalline phase III, in which no single orientation could be found, even after prolonged standing to allow for annealing or recrystallization.

Relation [12]

A crystal in a $[100]_I$ projection was cooled straight to phase III, which appeared in a $[100]_{III}$ projection, figures 26(a),(b), and gave the relation

$$[100]_I \parallel [100]_{III}, \quad (010)_I \wedge (210)_{III} = 1^\circ \text{ --- [12]}$$

where $(010)_I \wedge (110)_{III} = 18^\circ$.

Relation [13]

Phase I in a $[100]$ projection was quickly cooled into phase III by blowing on it and switching down the heater to keep it in that phase. At $[110]_{III}$ projection resulted, figure 27(a),(b), in the orientation,

Figure 26(a). RbNO_3I , [100] projection.
Zero layer precession, Mo
radiation, Zr filter.

Figure 26(b). RbNO_3III transformation product
in a [100] p.c. projection.
Mo/Zr filter, relation [12].

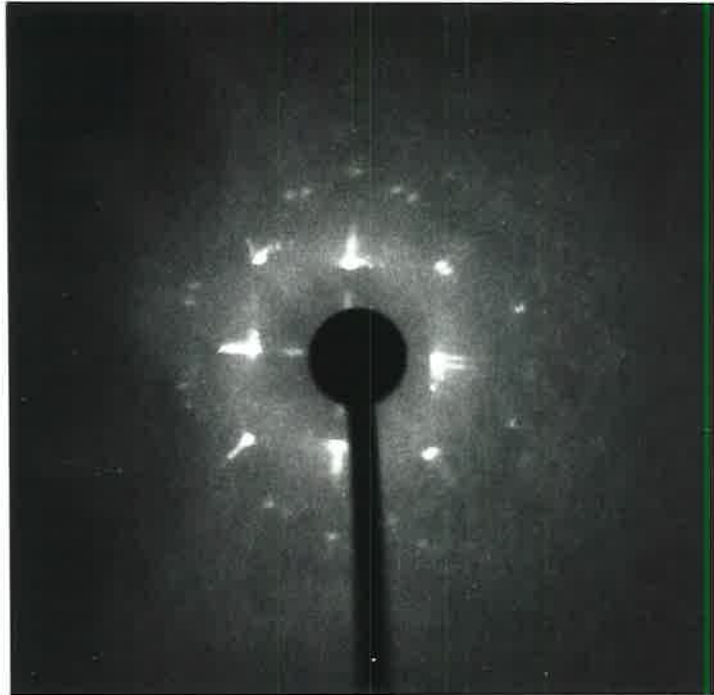


Figure 26(a)



Figure 26(b)

Figure 27(a). RbNO_3I , [100] projection.
Zero layer precession,
Mo radiation/Zr filter.

Figure 27(b). RbNO_3III , transformation product
in a [110] p.c. projection.
Mo/Zr filter, relation [13].

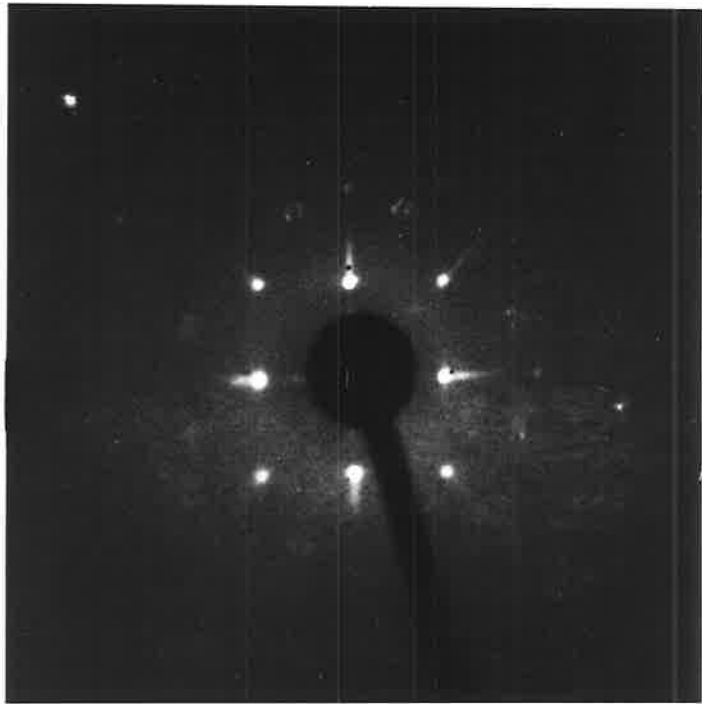


Figure 27(a)

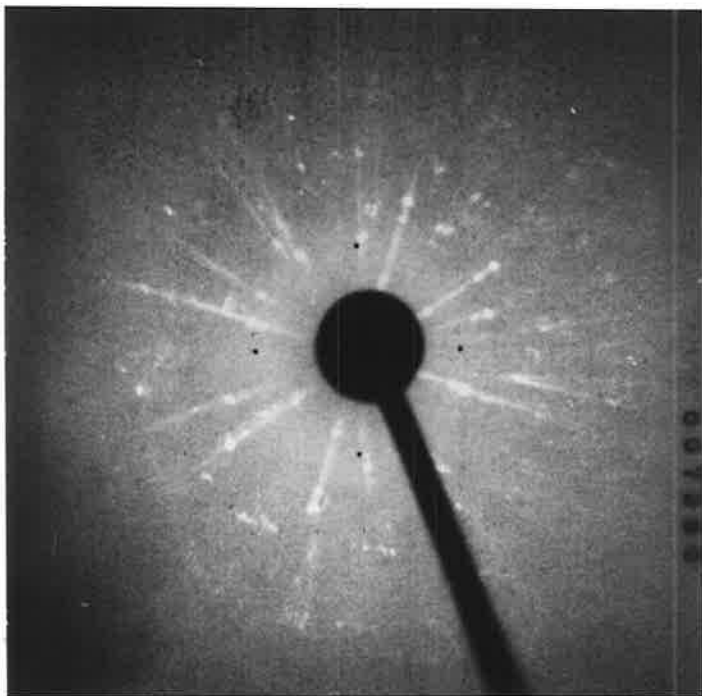


Figure 27(b)

Figure 28(a). RbNO_3I , $[111]$ projection.
Zero layer precession,
Mo radiation/Zr filter.

Figure 28(b). RbNO_3II , multiple product
orientations of $[111]$ p.c.
pattern. Relation [14].

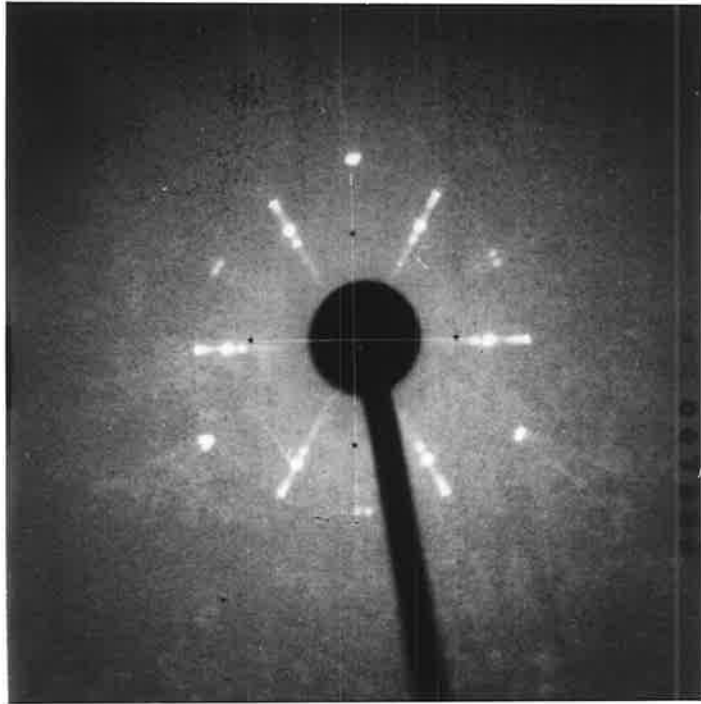


Figure 28(a).

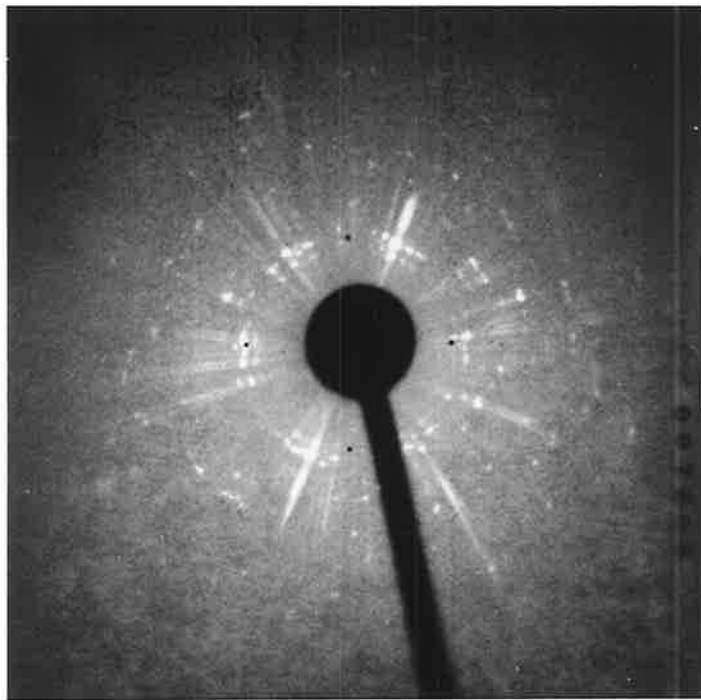


Figure 28(b).

$$[100]_I \parallel [110]_{III}, (010)_I \wedge (100)_{III} = 19^\circ \text{ --- [13]}$$

Relation [14]

Phase I in a [111] projection was cooled quickly to phase III, figures 28(a),(b), and a split spot pattern was obtained, reminiscent of relation [2]. In the resultant orientation,

$$[111]_I \parallel [111]_{III}, \langle 1\bar{1}0 \rangle_I \wedge \langle 1\bar{1}0 \rangle_{III} = 0^\circ, \pm 8^\circ \text{ --- [14]}$$

the observed ratio of (1 $\bar{1}$ 0) d spacings between the parent and product was 1.18 which corresponds to 1.19 for phase III as product, rather than 1.06 for phase II as product.

Relation [15]

Phase I in a [111] projection was rapidly cooled, passing through unrelaxed phase II for one second, and resulted in phase III in the orientation

$$[111]_I \parallel [100]_{III}, (1\bar{1}0)_I \wedge (100)_{III} = 7^\circ \text{ --- [15]}$$

Relation [16]

Finally, with less confidence, due to missetting of about $\pm 6^\circ$ in the parent, an early orientation relation is presented as

$$[111]_I \parallel [011]_{III}, (10\bar{1})_I \parallel (21\bar{1})_{III} \text{ --- [16]}$$

SECTION 2.6 THE IV \rightarrow III TRANSFORMATION, ELECTRON MICROSCOPY

Experimental Method

A dilute solution of RbNO_3 was made with doubly distilled, deionized water and ethanol, from which thin crystallites with numerous extinction contours were grown on carbon-coated gold grids, and dried over silica gel in a dessicator for one day. The Philips EM200 electron microscope was calibrated for the camera constant, λL , with gold deposited under vacuum on to grids carrying Formvar films. The double-tilt stage was used as well as a heating stage where the temperature was regulated by a Philips PW6310 temperature control unit. The electron beam was set at 100 KV.

Results

It was found by selected area diffraction, using the double-tilt stage, that at low beam intensities crystallites give stable diffraction patterns of phase IV, as for example in figure 29(a). When the beam is focused to maximum intensity and deflected about on the specimen, the fainter reflections disappear leaving the crystal in phase III, figure 29(b). Further irradiation causes decomposition, figure 29(c), eventually giving powder rings. Figure 29(a) is a $(1\bar{1}00)_{\text{IV}(Z=9)}$ projection which becomes the $(1\bar{1}0)_{\text{III}(Z=1)}$ projection of figure 29(b). The orientation relation was found to be

$$\begin{array}{l} [1\bar{1}00]_{\text{IV}(Z=9)} \quad || \quad [1\bar{1}0]_{\text{III}(Z=1)} \quad , \\ (0001)_{\text{IV}} \quad || \quad [111]_{\text{III}} \quad \text{-----} \quad [17] \end{array}$$

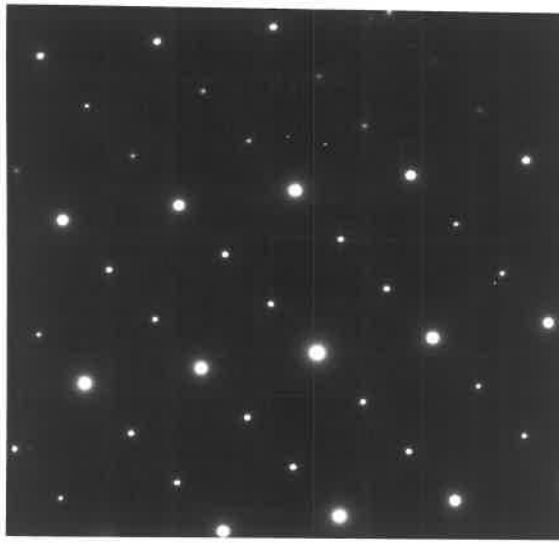


Figure 29(a)

Electron microscope
selected area
diffraction pattern
of RbNO_3 IV in a
 $(1\bar{1}0)_{z=9}$ projection.

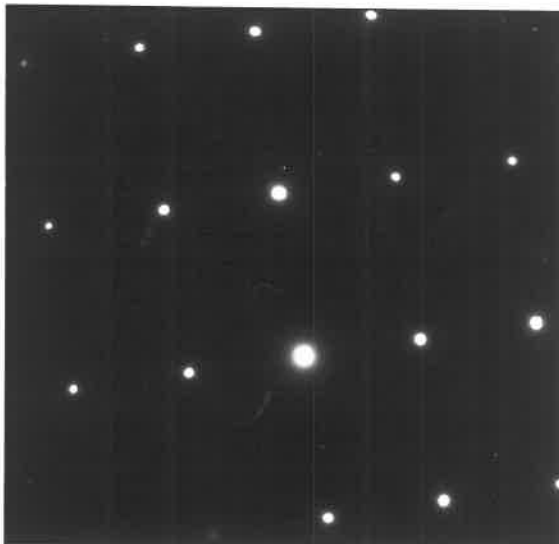


Figure 29(b).

An order-disorder
transformation to
 $(1\bar{1}0)_{III, z=1}$
Relation [17].

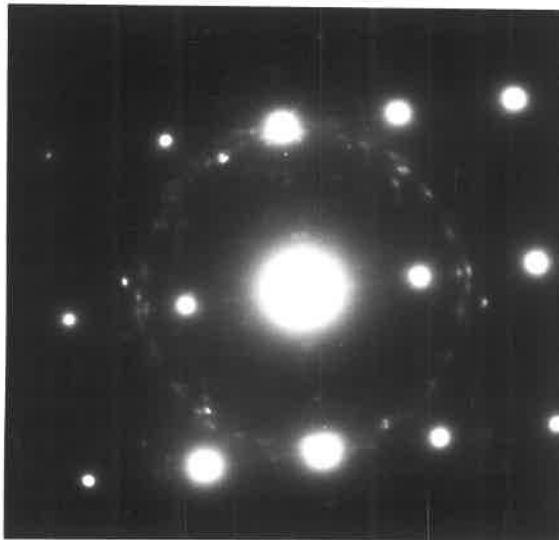


Figure 29(c)

RbNO_3 III.
commencing
decomposition.

Figure 30. Electron micrograph of RbNO_3IV .
Bright field image, 100 kV electrons.
Negative mag. X750.

Figure 31. Radiation and heating in an electron
microscope cause the specimen to become
porous. Neg. mag. X750.



Figure 30.



Figure 31.

Again, a $(5\bar{4}\bar{1}1)_{IV(Z=9)}$ projection was replaced by a $(2\bar{1}0)_{III(Z=1)}$ projection, such that $(11\bar{2}1)_{IV} \parallel (001)_{III}$. Comparison on standard computed stereograms showed that this again, was relation [17] above.

Figures 30 and 31 follow the process in the bright field image, and it is seen that with radiation the specimen becomes porous. Heating of the specimen accelerates the decomposition of phase III, and so no further transformations can be studied.

SECTION 2.7.1 Interpretation and Discussion of the I \rightleftharpoons II \rightarrow III
Transformation in RbNO₃

(a) Interpretation

The X-ray orientation relations described in Section 2.4 were compared with those previously reported for similar structure changes and listed in the introduction to this chapter, Section 2.1.

It was found that within a small angular difference, relations [1] and [8] are the same as the orientation relation type B of Fraser and Kennedy, ^(41,42) viz.

$$\begin{array}{rcccl} \{010\}_I \wedge \{010\}_{II(Z=1)} & = & 4^\circ & (8^\circ) & (1^\circ) \\ [100]_I \wedge [101]_{II(Z=1)} & = & 9^\circ & (7^\circ) & (4^\circ) \\ & & & \text{observed in} & \text{observed in} \\ & & & [1] & [8] \end{array}$$

Due to the use of the globe and cap to follow goniometer manipulations in relation [8], it is not considered to be as accurate as relation [1] which is illustrated stereographically in figure 32. Both experiments describe the orientation between phase I and large-scale relaxed phase II. As planes and directions are distinguishable in rhombohedral phase II, it is seen that their assignation in the type B orientation of Fraser and Kennedy ^(40,41) is correct.

Relations [2] and [2]' between phase I and twinned or unrelaxed phase II as expressed in Section 2.4.1, correspond to Fraser and Kennedy's type A orientation and show that the previous assignation of planes and directions should be reversed. In terms of Z = 4 cells, relation [2] can be expressed as

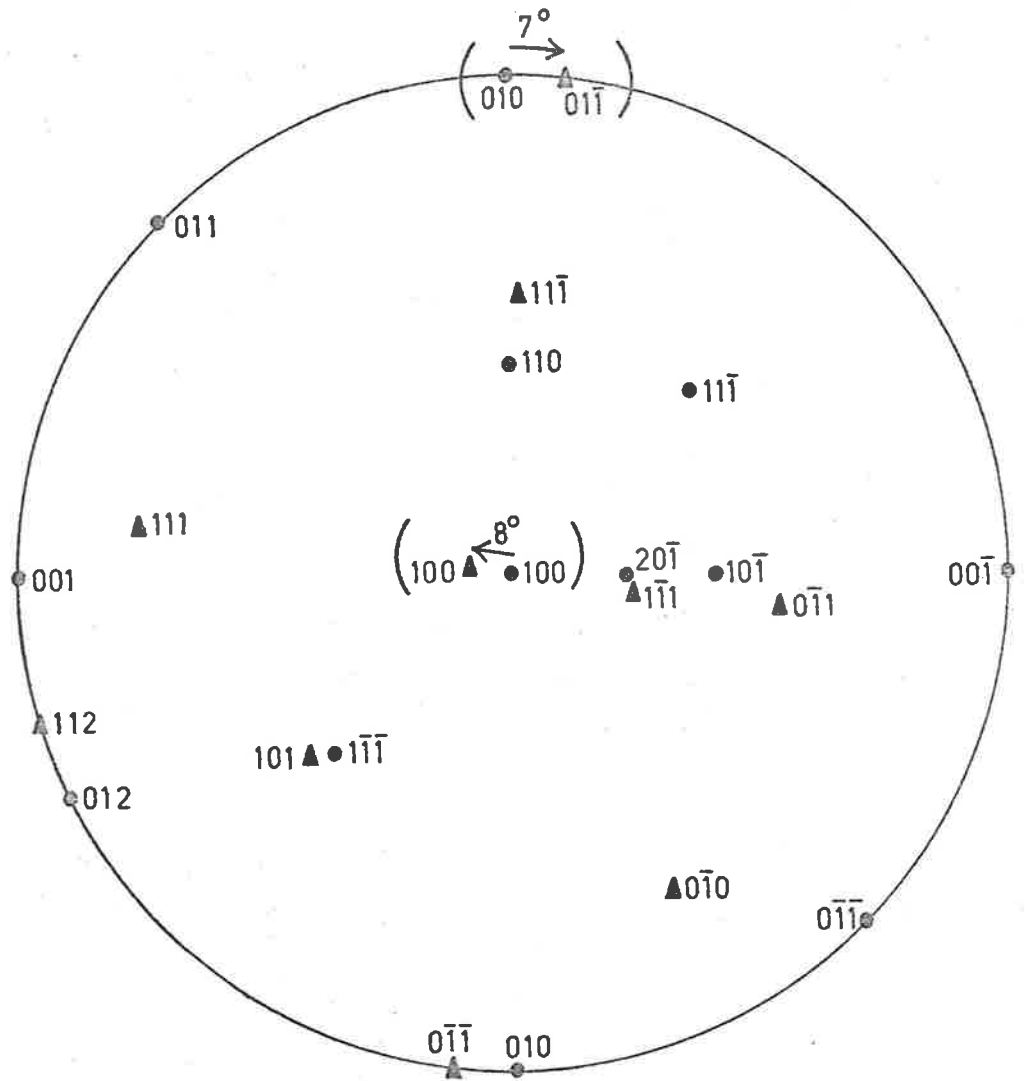


Fig. 32. A planes stereogram of RbNO_3 I \rightarrow II (detwinned), according to relation [1].

● phase I, (f.c.c.), $Z = 4$

▲ phase II, (rhombohedral, $Z = 1$).

$$[100]_I \parallel [100]_{II} , \{010\}_I \wedge \{010\}_{II} = 0^\circ$$

In detwinned or large-scale relaxed phase II, relation [3] was found in one of two coexisting product grains. When expressed as $[111]_I \parallel [01\bar{1}]_{II(Z=1)} , (110)_I \wedge (01\bar{1})_{II} = 4^\circ$, it corresponds within a small angular discrepancy to $(1\bar{1}\bar{1})_I \parallel (110)_{II(p.c.)}$, $(110)_I \parallel (001)_{II}$; since in cubic cells (110) and $(1\bar{1}0)$ planes are indistinguishable. The latter relation is the previously reported type B orientation of Kennedy, Patterson, Chaplin and Mackay,⁽⁴³⁾ figure 33(a),(b),(c). The second product grain, (ii), described by relation [4], viz.

$$[111]_I \wedge [\bar{1}\bar{1}\bar{1}]_{II(Z=1)} = 12^\circ , (\bar{1}\bar{1}2)_I \wedge (011)_{II(Z=1)} = 3^\circ$$

is not the same as any previously reported, but is related to the first by the common $(011)_{II(Z=1)}$ i.e. $(001)_{II(Z=4)}$ plane.

In terms of $Z = 4$ cells,

$$[111]_I \parallel [1\bar{1}0]_{II} , (\bar{1}\bar{1}2)_I \wedge (001)_{II} = 3^\circ \text{ --- [3]}$$

and

$$[111]_I \wedge [\bar{1}00]_{II} = 12^\circ , (\bar{1}\bar{1}2)_I \wedge (001)_{II} = 3^\circ \text{ --- [4]}$$

imply that the relation between the two grains is

$$[\bar{1}10]_{II(i)} \wedge [\bar{1}00]_{II(ii)} = 12^\circ , (001)_{II(i)} \parallel (001)_{II(ii)} \text{ --- [3a]}$$

where (i) denotes grain (i). Examination of relation [3a] stereographically, as shown in figure 33(c), reveals that the two grains are further related by reflection or twinning across a plane whose pole is 8° from $(\bar{1}20)_{II(i)}$ or 7° from $(2\bar{1}0)_{II(ii)}$, and hence very close to the

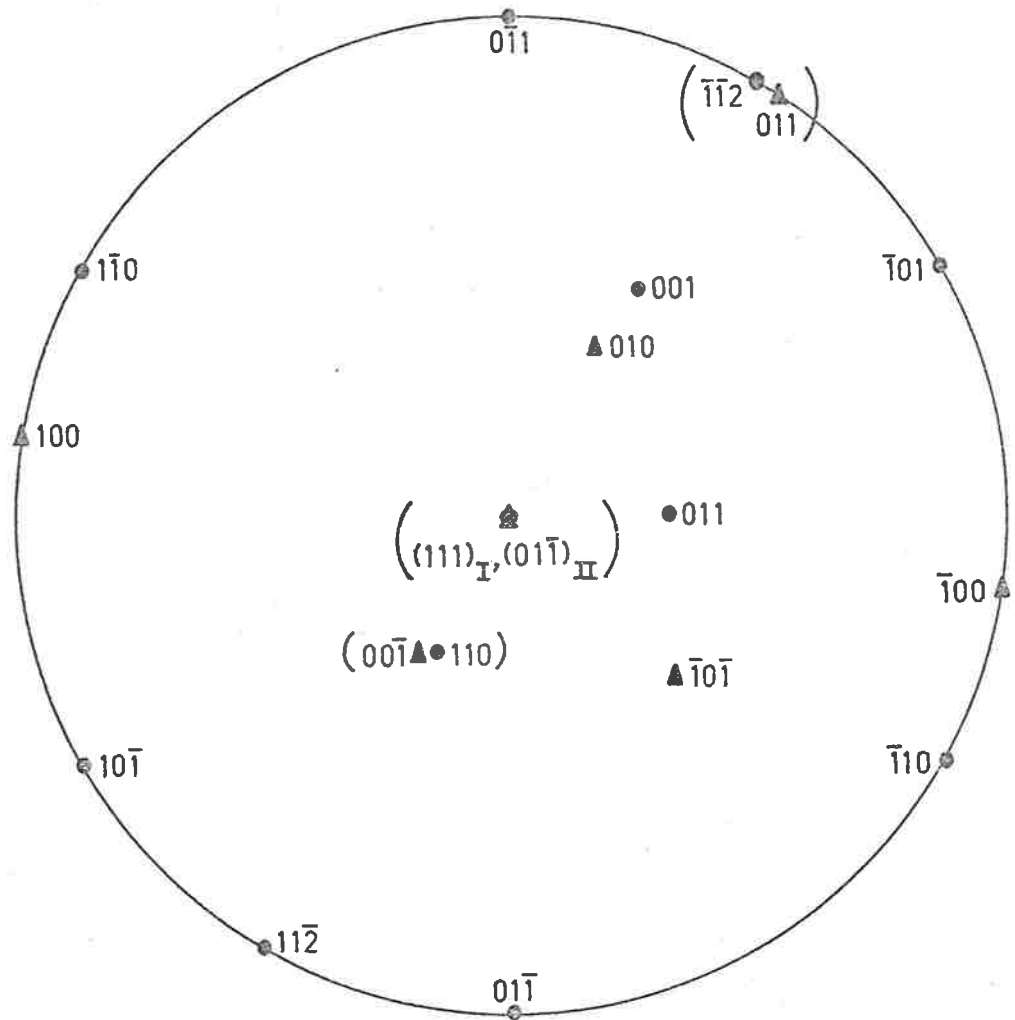


Fig. 33(a). A planes stereogram of RbNO_3 $I \rightarrow II$ (detwinned) according to relation [3].

● phase I, f.c.c., $Z = 4$

▲ phase II, rhombohedral, $Z = 1$

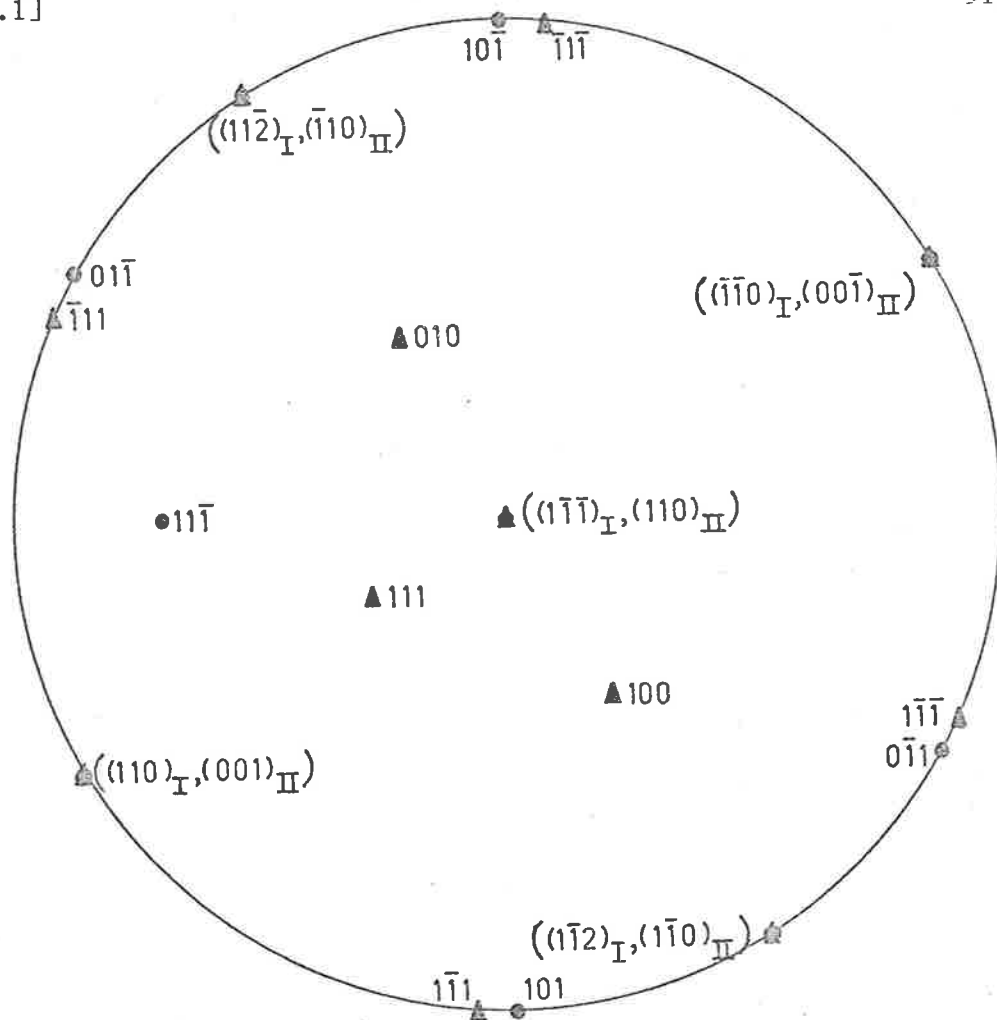


Fig. 33(b). A planes stereogram of the previously reported type B orientation of Kennedy, Patterson, Chaplin and Mackay, ⁽⁴³⁾ for RbNO_3 $I \rightarrow II$.

● phase I, f.c.c. $Z = 4$

▲ phase II, rhombohedral, $Z = 1$.

4° off $\{210\}_I$ habit plane predicted martensitically for a twinning shear $\{100\} \langle 011 \rangle$. In phase I the pole lies in no apparently significant position being 13.5° from $[111]$ and 6° from (323) .

Similarly the pole has no apparent significance in the $Z = 1$ cell of rhombohedral phase II of grain (i), being 13.5° from $(01\bar{1})$.

Detwinning or large-scale relaxation is observed in relation [5], where a product of multiple orientations produced via relation [2] is replaced by a single crystal phase II. The orientation was examined for correspondence between planes or directions in both $Z = 1$ and $Z = 4$ rhombohedral cells, the implied relations being

$$[1\bar{1}1]_{II(Z=1)m.o.} \wedge [101]_{II(Z=1)s.o.} = 7^\circ, (10\bar{1})_{m.o.} \wedge (10\bar{1})_{s.o.} = 4^\circ \quad [5]$$

$$(3\bar{1}3)_{II(Z=1)m.o.} \wedge (212)_{II(Z=1)s.o.} = 7^\circ, (10\bar{1})_{m.o.} \wedge (10\bar{1})_{s.o.} = 4^\circ \quad [5a]$$

$$[100]_{II(Z=4)m.o.} \wedge [211]_{II(Z=4)s.o.} = 7^\circ, (01\bar{1})_{m.o.} \wedge (01\bar{1})_{s.o.} = 4^\circ \quad [5b]$$

$$(9\bar{1}\bar{1})_{II(Z=4)m.o.} \wedge (311)_{II(Z=4)s.o.} = 7^\circ, (01\bar{1})_{m.o.} \wedge (01\bar{1})_{s.o.} = 4^\circ \quad [5c]$$

$$[100]_{II(Z=4)m.o.} \wedge [101]_{II(Z=1)s.o.} = 7^\circ, (01\bar{1})_{m.o.} \wedge (10\bar{1})_{s.o.} = 4^\circ \quad [5d]$$

$$(9\bar{1}\bar{1})_{II(Z=4)m.o.} \wedge (212)_{II(Z=1)s.o.} = 7^\circ, (01\bar{1})_{m.o.} \wedge (10\bar{1})_{s.o.} = 4^\circ \quad [5e]$$

There appear to be no apparent significant correspondence, other than those above defining the relation, and the following;

$$\text{in } [5] \quad [111]_{II(Z=1)m.o.} \wedge [010]_{II(Z=1)s.o.} = 2^\circ$$

$$[5b] \quad [111]_{II(Z=4)m.o.} \wedge [011]_{II(Z=4)s.o.} = 3^\circ$$

$$[5c] \quad (110)_{II(Z=4)m.o.} \wedge (\bar{1}11)_{II(Z=4)s.o.} = 4^\circ$$

According to relation [2] the multiple orientation phase II consists

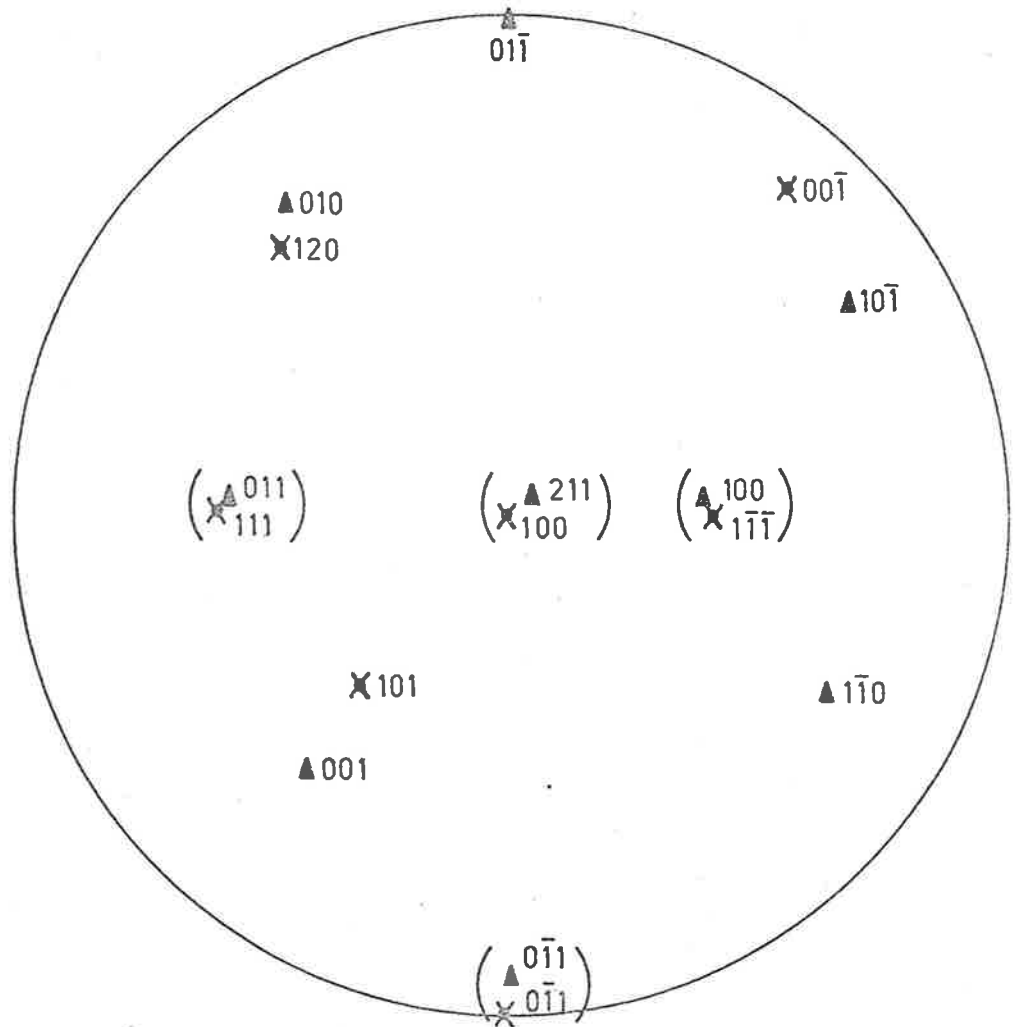


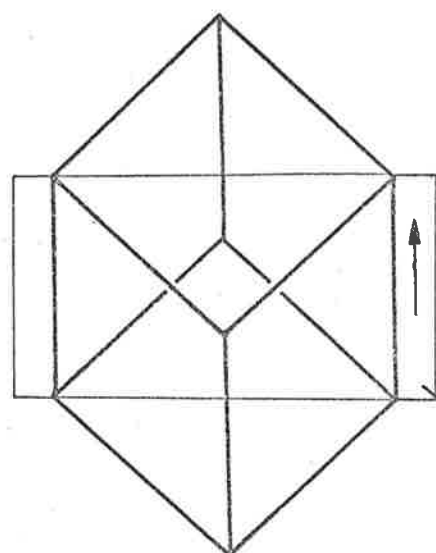
Fig. 34. A directions stereogram of RbNO_3 II (multiple orientations) in terms of the rhombohedral, $Z = 4$ cell, according to relation [5].

X II, multiple orientations

▲ II, single orientation

of three superimposed $[100]_{II(Z=4)}$ projections such that $\{010\}_{II(Z=4)}$ planes are mutually rotated by $-$ and $+ 8^\circ$ about a central $\{010\}_{II(Z=4)}$ which is parallel, and hence rotated 0° , with respect to the $\{010\}_{I(f.c.c.)}$. Referring to the above as options (ii), (iii) and (i) respectively, relation [5] is re-defined as [5]', [5]" and [5]. Examination of [5]' and [5]" as for [5] above gave no apparently significant correspondences other than the direction of projection, common throughout, and for [5b]",

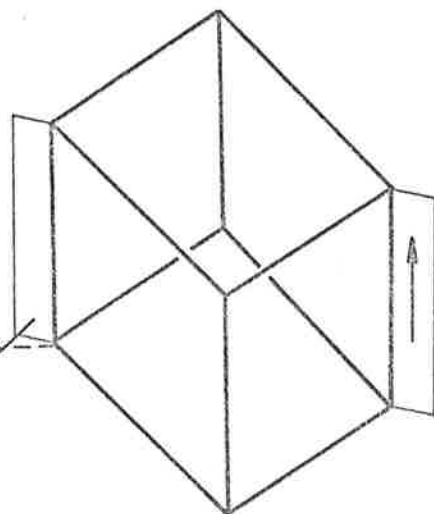
$[111]_{II(Z=4)m.o.} \wedge [011]_{II(Z=4)s.o.} = 6^\circ$. Figure 34 illustrates stereographically relation [5] and the observed structure change is diagrammatically presented below.



I (f.c.c.)

$[100]$
 $a = 7.32 \text{ \AA}$

$(01\bar{1})$

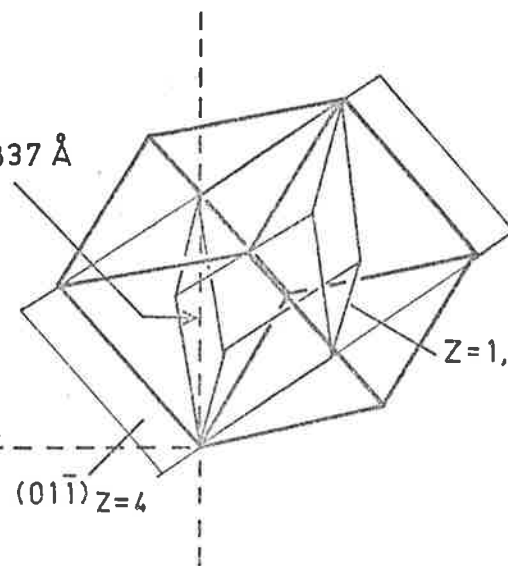


II Rh, Z=4
 m.o.

$[100]$
 $a = 7.30 \text{ \AA}$

$(01\bar{1})$ Z=4

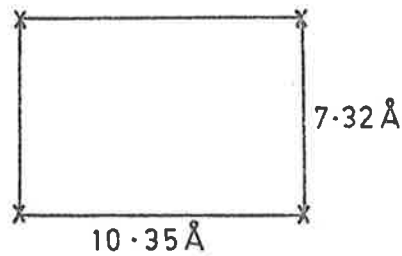
$[10] = 7.837 \text{ \AA}$



II Rh, Z=1
 s.o.

Z=1, Rh

10.35 Å



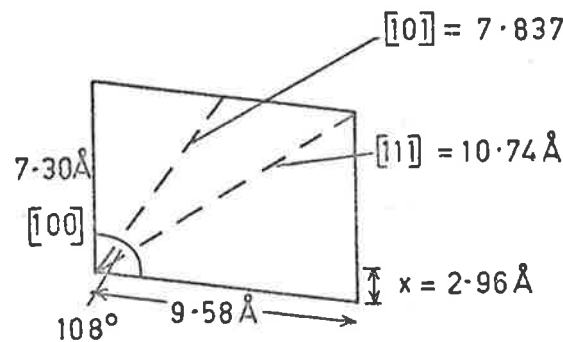
(011) plane

I

Vertical height

7.32 Å

9.364 Å

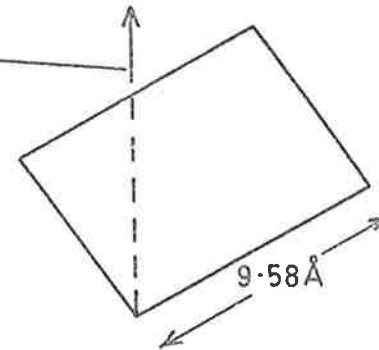


(011)_{Z=4} plane

II (m.o.)

7.30 + 2.96 = 10.26 Å

12.358 Å



(011)_{Z=4} plane

II (s.o.)

7.837 + 1.986 = 9.823 Å

[2.7.1]

In a unit cell, $[111]_{II(Z=4)} = 10.74 \text{ \AA}$, $[100]_{II(Z=4)} = 7.30 \text{ \AA}$,
 $[101]_{II(Z=1)} = 7.837 \text{ \AA}$, $[010]_{II(Z=1)} = 4.79 \text{ \AA}$, giving $[110]_{II(Z=4)} =$
 $2 \times 4.79 = 9.58 \text{ \AA}$.

Looking at corresponding (011)_{Z=4} planes, the process can be pictured as the above.

Percentage deformations in main directions and their differences with reference to the above diagram, for relation [5] were examined. From models illustrating the $\{100\}\langle 011\rangle_I$ twinning mechanism, figures 39(a) to (c), it is seen that the largest strain occurs in the $\langle 100\rangle_{Z=4}$ direction; a deformation of 40.16% was calculated. Replacement by a $[101]_{II(Z=1)}$ decreases the overall strain in this direction. The unit cell width in the horizontal direction increases, but the shape of the $(01\bar{1})$ plane suggests that the misfit may not be as large as the values indicate. Nevertheless, such considerations do not suggest a definite explanation for the detwinned orientation.

Relation [6], and to a lesser extent, relation [5], may not be as experimentally reliable as relations [1] to [10], since it was deduced on the basis of six sets of goniometer arc manipulations which were followed on the cap and globe. The relation does not correspond to type B of Fraser and Kennedy.⁽⁴²⁾ It is similar within 11° to Kennedy, Patterson, Chaplin and Mackay's⁽⁴³⁾ type A orientation.

Relation [7] between phase I and I cycled through large-scale relaxed phase II, shows a tendency for major rows of ions to align, and is further confirmation of the observation^(41,303) that in real crystals, hexagonal \rightleftharpoons square net deformations occur. Epitaxial growth of an abnormal f.c.c. Mg structure on a NaCl-type MgO was observed⁽¹⁸⁴⁾ with the orientation $(111)_{Mg} \parallel (100)_{MgO}$, such that $[1\bar{1}0]_{Mg} \parallel [1\bar{1}0]_{MgO}$, which is relation [7].

In a single crystal passing from phase I, through large-scale relaxed phase II, to phase III, relations [8], [9] and [10] were found;

[8] being Fraser and Kennedy's^(41,42) type B orientation. Relation [9] is not the same as Iversen and Kennedy's⁽⁹⁵⁾ orientation for RbNO_3 I \rightarrow III, nor similar to any of the previously reported NaCl-type \rightleftharpoons CsCl-type orientations. Relation [10] between large-scale relaxed phase II and III, has also not been previously reported.

Interesting correspondences between the structures are:

$$\begin{aligned} [100]_{\text{II}(Z=4)} & \parallel [001]_{\text{III}(\text{p.c.})} \\ (110)_{\text{II}(Z=4)} & \wedge (0\bar{1}1)_{\text{III}(\text{p.c.})} = 10^\circ \\ (001)_{\text{II}(Z=1)} & \wedge (111)_{\text{III}(\text{p.c.})} = 6^\circ \\ (0\bar{1}1)_{\text{II}(Z=1)} & \wedge (011)_{\text{III}(\text{p.c.})} = 10^\circ. \end{aligned}$$

Examination of the I \rightarrow III orientations shows that relation [15], observed in a single crystal product, is the same as [14] in a composite crystal for the case where $[1\bar{1}0]_{\text{I}} \wedge [1\bar{1}0]_{\text{III}} = 8^\circ$. Iversen and Kennedy's⁽⁹⁵⁾ orientation was not reproduced. None of the relations have been previously reported. Relations [9] where $[1\bar{1}1]_{\text{I}} \wedge [100]_{\text{III}} = 11^\circ$, and [15] where $[0\bar{1}1]_{\text{I}} \wedge [001]_{\text{III}} = 7^\circ$ are reminiscent of Kennedy, Patterson, Chaplin and Mackay's,⁽⁴³⁾ type A orientation, the appropriate angular difference being 0° in both cases, but this may only be a coincidence.

However, except in [14], for the case of $\langle 1\bar{1}0 \rangle_{\text{I}} \parallel \langle 1\bar{1}0 \rangle_{\text{III}}$, and considering the lower experimental reliability of [16], it is interesting to note that all the other relations have $\{102\}_{\text{I}}$ close to a $\{110\}_{\text{III}}$.

Specifically,

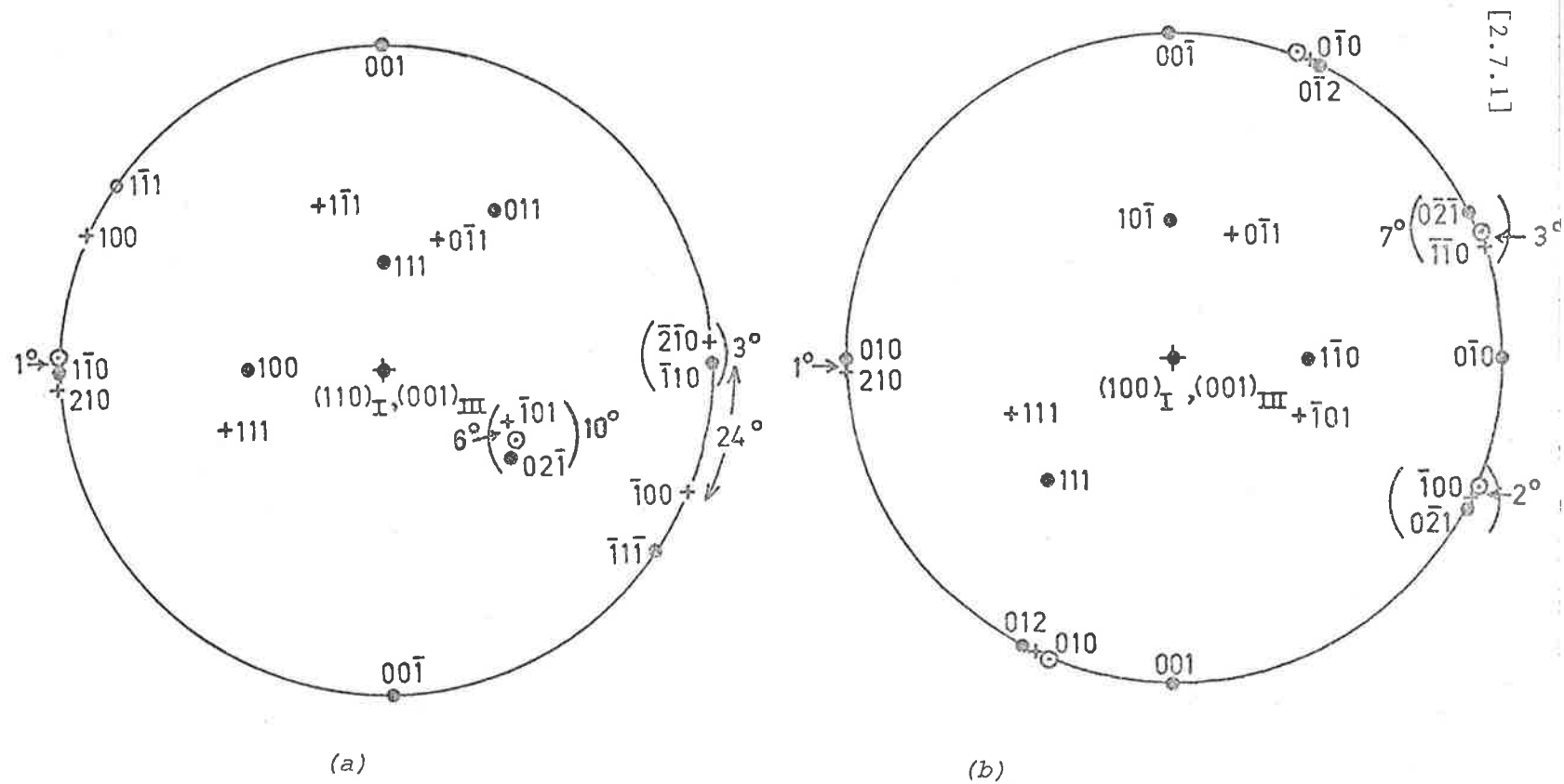


Fig. 35(a). (b). Planes stereograms of RbNO_3 I \rightarrow III, according to relations [9] and [12] respectively.

- phase I, f.c.c.
- + phase III, p.c.
- ⊙ 4° off $\{012\}_I$ habit plane.

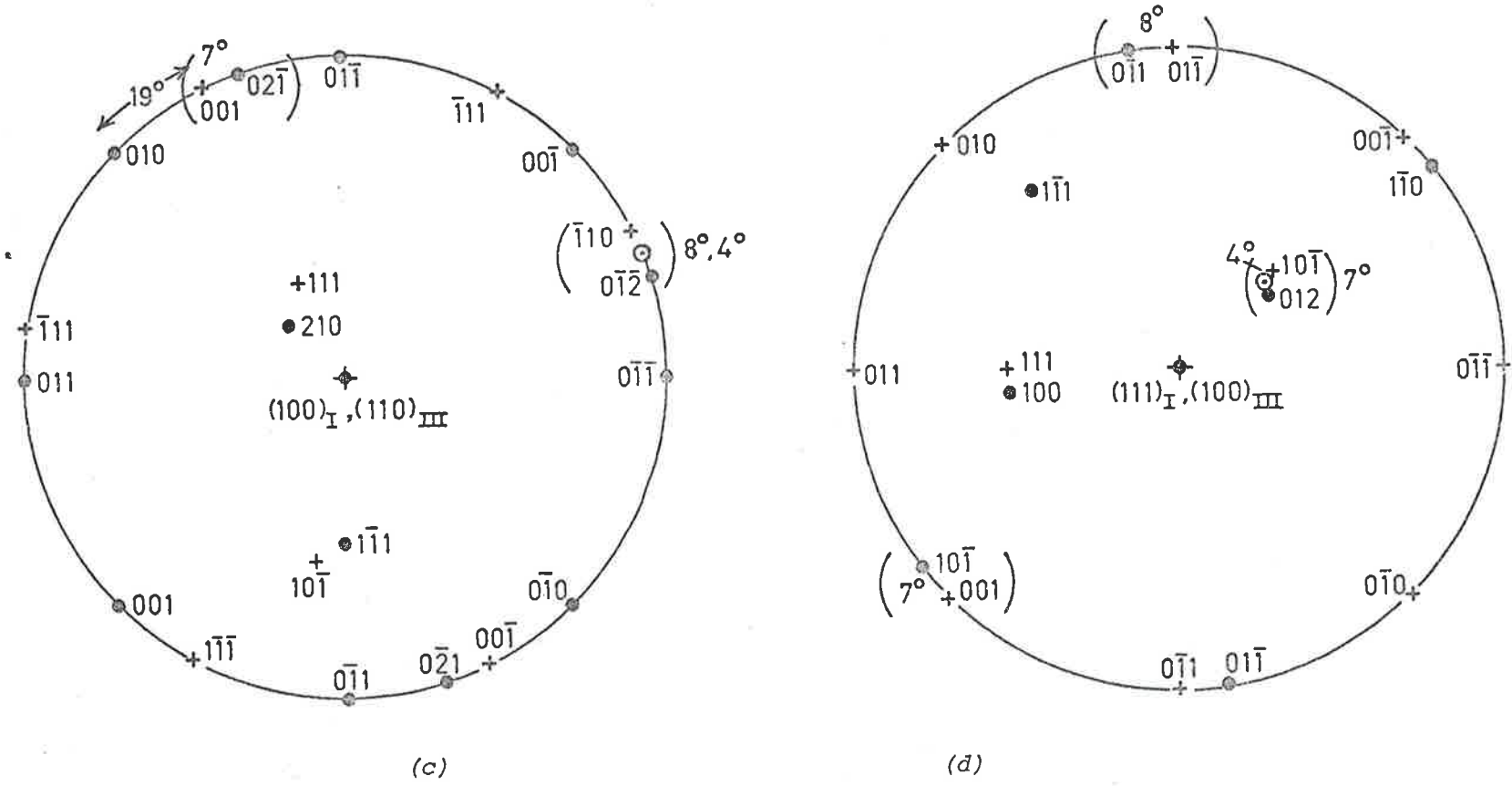
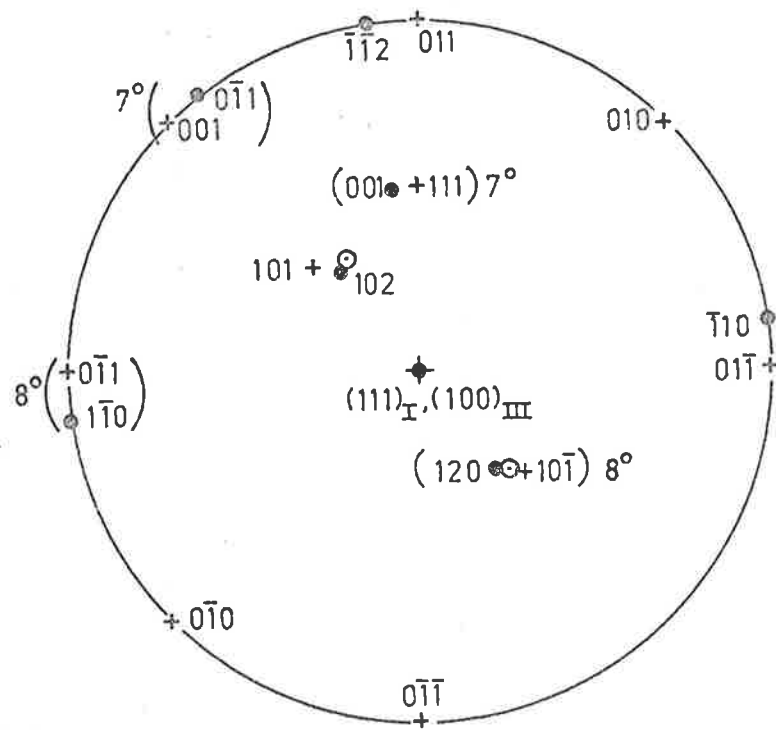
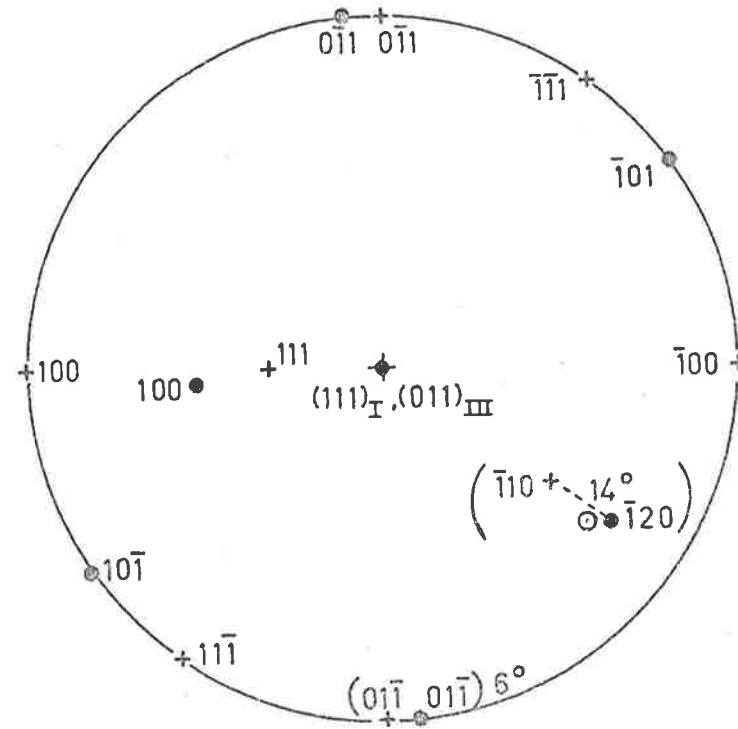


Fig. 35 (c), (d). Planes stereograms of $RbNO_3$ I \rightarrow III according to relations [13] and [14] respectively.

- phase I, f.c.c.
- + phase III, p.c.
- ⊙ 4° off $\{012\}_I$ habit plane.



(e)



(f)

Fig. 35(e), (f). Planes stereograms of RbNO_3 I \rightarrow III according to relations [15] and [16] respectively.

● phase I, f.c.c.

+ phase III, p.c.

⊙ 4° off $\{012\}_I$ habit plane.

[9]	$(02\bar{1})_I \wedge (\bar{1}01)_{III} = 10^\circ$	(6°)	(after goniometer manipulations for phase II)
[12]	$(021)_I \wedge (110)_{III} = 7^\circ$	(3°)	
[13]	$(021)_I \wedge (1\bar{1}0)_{III} = 8^\circ$	(4°)	
[14]	$(012)_I \wedge (10\bar{1})_{III} = 7^\circ$	(4°)	
[15]	$(102)_I \wedge (101)_{III} = 8^\circ$	(4°)	
[16]	$(\bar{1}20)_I \wedge (\bar{1}10)_{III} = 14^\circ$	(10°)	(missetting error)

Furthermore, as seen from the bracketed angles, $\{110\}_{III}$ or $\{1\bar{1}0\}_{III}$ (being equivalent in cubic), are even closer to the 4° off $\{102\}_I$ habit plane pole predicted martensitically for a (100)[011] twinning shear. Figures 35(a) to (f) illustrates the observed I \rightarrow III orientations in stereograms. Except for relation [9], phase III was cooled directly from phase I.

SECTION 2.7.1 (b) Discussion(i) X-ray and X-ray-Optical Results

Examination of the phase I f.c.c., and phase II, rhombohedral, $Z = 4$ structures suggests several mechanisms by which the transformation could occur. A Buerger⁽⁴⁴⁾ deformation relates the two structures, but as yet it has not been observed as a complete mechanism for transformations involving significant volume changes such as occurs here.

Shôji⁽¹⁷⁸⁾ postulated a shear-type mechanism interconverting 8-coordinated CsCl-type and 6-coordinated NaCl-type structures. A shear of half a CsCl unit cell length on the $(110)_{\text{CsCl}}$ plane in an $[011]_{\text{CsCl}}$ direction is preceded by a contraction in $[\bar{1}\bar{1}0]_{\text{CsCl}}$ and followed by a dilation in the two directions perpendicular to this. The NaCl to CsCl change proceeds in the reverse manner and $(100)_{\text{NaCl}} \rightarrow (011)_{\text{CsCl}}$, $(011)_{\text{NaCl}} \rightarrow (01\bar{1})_{\text{CsCl}}$, $[010]_{\text{NaCl}} \rightarrow [\bar{1}11]_{\text{CsCl}}$. Shôji further suggested that the $(110)_{\text{CsCl}}$ can become a (100) or a (110) plane in the NaCl lattice.

Fraser and Kennedy⁽¹⁷⁹⁾ of this laboratory reported the first complete orientation relation for the NaCl to CsCl transformation in NH_4Br , observing by X-rays and optical microscopy, that it is consistent with a Shôji mechanism. The relation

$$(001)_{\text{NaCl}} \parallel (101)_{\text{CsCl}}, (010)_{\text{NaCl}} \parallel (\bar{1}11)_{\text{CsCl}}, (100)_{\text{NaCl}} \parallel (12\bar{1})_{\text{CsCl}}$$

was found.

On subsequent closer examination of NH_4Br , contemporary with the work for this thesis, Fraser and Kennedy⁽⁴⁰⁻⁴²⁾ found the irrational

orientations types A and B, as mentioned in Section 2.1. By optical and scanning electron microscopy they measured macroscopic shape changes and the orientation of phase II platelets in the phase I matrix. They analysed martensitically the NaCl-type to CsCl-type structure change and clearly showed how the large number of product orientations could arise.

Fraser and Kennedy elaborated on the concept of transformation twinning considered earlier by Cahn,⁽¹⁸⁰⁾ Buerger⁽¹⁸⁶⁾ and Christian⁽¹⁷⁴⁾, who postulated that martensite shear systems could be found where mirror planes in the higher symmetry parent became twin planes in the product. Hence, pairs of $\langle 111 \rangle_{\text{NaCl}}$ are related by $\{100\}_{\text{I}}$ or $\{110\}_{\text{I}}$ mirror planes which become twin planes in the product. The twin direction can be calculated as shown by Bowles and Mackenzie.⁽¹⁸¹⁾

Fraser and Kennedy⁽⁴⁰⁻⁴²⁾ found that transformation twin systems derived from $(100)[011]_{\text{I}}$, $(010)[101]_{\text{I}}$ and $(001)[110]_{\text{I}}$ are $(110)[001]_{\text{II}}$, $(011)[100]_{\text{II}}$, and $(101)[010]_{\text{II}}$ respectively, while a $\{110\}_{\text{I}}$ plane implies $(121)[1\bar{1}1]_{\text{II}}$, $(211)[\bar{1}11]_{\text{II}}$ and $(112)[11\bar{1}]_{\text{II}}$ systems. The Buerger⁽⁴⁴⁾ deformation converts the primitive rhombohedron of the NaCl cell to a primitive cube of CsCl, about which cube a $Z = 4$ rhombohedron can be depicted. Examination of such a model shows that the $\{121\}\langle 1\bar{1}1 \rangle_{\text{II}}$ corresponds to $\{011\}[100]_{\text{I}}$ shear system.

In NH_4Br , the initial and final cones of unextended vectors include an angle of $\phi_1 = 51^\circ 39'$ and $\phi_2 = 68^\circ 0'$, while the angles of $\{100\}_{\text{I}}$ and $\{110\}_{\text{I}}$ from $[111]_{\text{I}}$ are 54.74° and 35.26° respectively. Therefore

the $\{100\}_I$ plane cuts the initial cone but the $\{110\}_I$ does not, by 3.1° . For this reason $\{110\}$ twinning shear was not considered by Fraser and Kennedy.

Slip occurs in the product CsCl phase on the six $\{110\}\langle 001\rangle_{II}$ systems. Three are geometrically equivalent to the $\{100\}\langle 011\rangle_I$ above and three, $(\bar{1}\bar{1}0)[001]_{II}$, $(0\bar{1}1)[100]_{II}$ and $(\bar{1}01)[010]_{II}$ correspond to $\{1\bar{1}0\}[110]$ in phase I.

It was found⁽⁴⁰⁻⁴²⁾ that the $\{1\bar{1}0\}\langle 001\rangle_I$ slip systems yield two distinct types of solutions, ("types 1,2") each having 24 crystallographically equivalent but physically distinct variants. The $\{100\}\langle 011\rangle_I$ twin systems produce another type of solution, type 3, with 24 physically distinct variants. All three types of solutions would thus result in 72 variants. Possible habit planes are approximately 5° to $\{310\}_I$, 10° to $\{\bar{1}11\}_I$ and 5° to $\{210\}_I$ for solution types 1, 2 and 3 respectively.

The observation of X-ray orientation type A, shape changes and directions of phase II plates in NH_4Br I \rightarrow II conform to the predictions of solution type 3. Hence the mechanism of transformation of NH_4Br I \rightarrow II is martensitic with a lattice invariant shear of twinning on $\{100\}\langle 011\rangle_I$.

In view of the above, while many mechanisms can be proposed for the I \rightarrow II transformation in RbNO_3 , the twin shear systems are obvious candidates for consideration and comparison with experimental observations. RbNO_3 II is not a CsCl-type cubic structure, so that the

the $\{110\}\langle 001\rangle_{\text{II}}$ slip systems need not be considered.

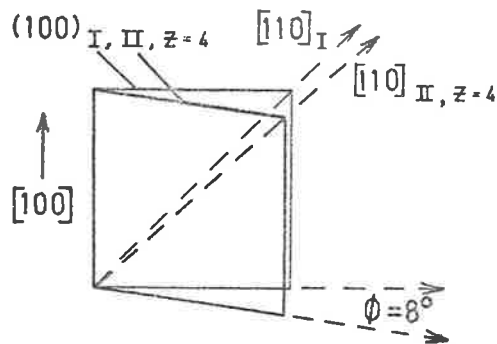
In RbNO_3 , the initial and final cones of unextended vectors are $\phi_1 = 55.64^\circ$ and $\phi_2 = 61.44^\circ$. The angles of $\{100\}_{\text{I}}$ and $\{110\}_{\text{I}}$ to $[111]_{\text{I}}$ are 54.74° and 35.26° respectively, phase I being cubic. Therefore, the $\{100\}_{\text{I}}$ plane cuts the initial cone of unextended vectors and $\{110\}_{\text{I}}$, unlike in NH_4Br , also intercepts this locus by 0.9° . Different lattice parameters producing other ϕ values generally confirm this, as shown in Table 12 of Section 2.4.4. The fact that no solution was found for the $(011)[100]$ shear for η values 1.070, 0.8471 (Table 12) can be explained by the observation that (011) is 0.35° from intercepting the initial cone.

On the basis of X-ray results alone, one may conclude that relation [2] in RbNO_3 was produced by a Shôji-type mechanism, without any recourse to martensite theory. The structure change would proceed as follows.

[2.7.1]

108.

$\{100\} \langle 011 \rangle_I$ Twinning:



$$\alpha_r (I) = 90^\circ$$

$$\alpha_r (II) = 97.98^\circ$$

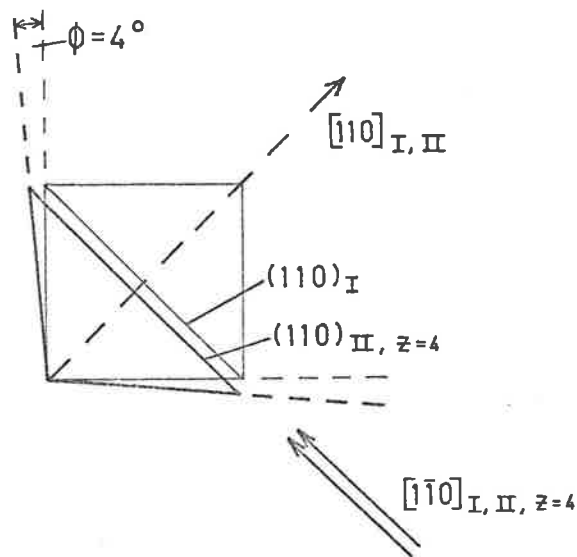
$$\langle 100 \rangle_I \wedge \langle 1\bar{1}0 \rangle_{II} (z=4) = 45^\circ$$

$$\langle 100 \rangle_I \wedge \langle 1\bar{1}0 \rangle_{II} (z=4) = 49.5^\circ$$

$$\delta = \langle 1\bar{1}0 \rangle_I \wedge \langle 1\bar{1}0 \rangle_{II} = 4.5^\circ$$

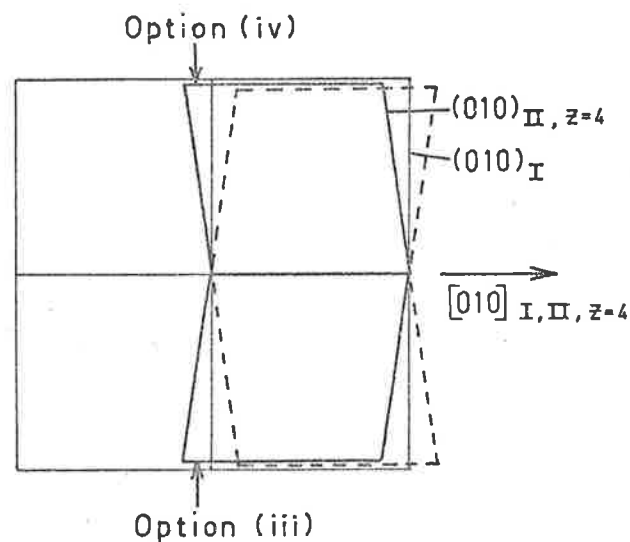
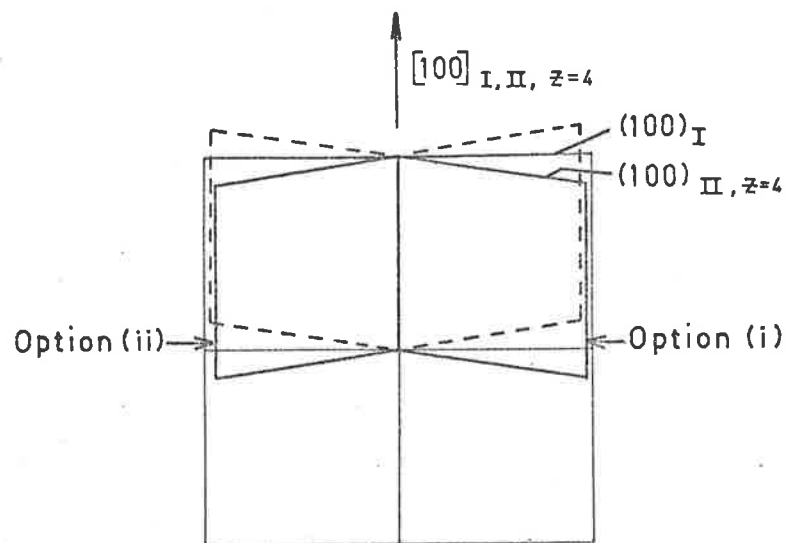
$$\phi = 8^\circ$$

$\{110\} \langle 001 \rangle_3$ Twinning



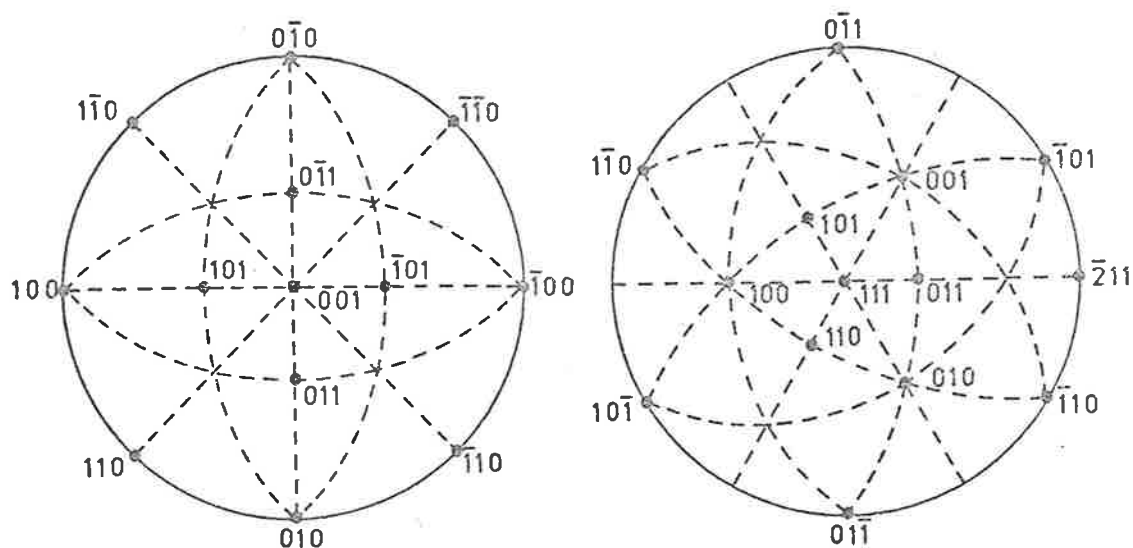
$$\delta' = (110)_I \wedge (110)_{II} = 0^\circ$$

$$\delta = [1\bar{1}0]_I \wedge [1\bar{1}0]_{II} = 0^\circ$$



The "multiple orientations" or "split spot pattern" of relation [2] can then be explained as simultaneously occurring options of the $\{100\} \langle 011 \rangle_I$ mechanism. When $[100]_I \parallel [100]_{II(z=4)}$, $(100)_I \wedge (100)_{II} = \pm 8^\circ$ because $(100)_I$ or $(\bar{1}00)_I$ become $(100)_{II(z=4)}$. Similarly, $[010]_I \parallel [010]_{II(z=4)}$ so that $(010)_I \wedge (010)_{II(z=4)} = \pm 8^\circ$ since either $(010)_I$ or $(0\bar{1}0)_I$ become $(100)_{II(z=4)}$.

The main lamellae directions (or habit plane traces) were found by X-ray-optical means to be parallel to $\langle 100 \rangle_I$ and $\langle 1\bar{1}0 \rangle_I$ in $\{001\}_I$ and $\{111\}_I$ projections respectively. That is, they may be produced by both $\{100\}_I$ or $\{110\}_I$ planes as suggested by Shôji⁽¹⁷⁸⁾, and illustrated stereographically below.



$\{100\}$ planes produce
traces $\parallel \langle 100 \rangle$

$\{110\}$ planes produce traces
 \parallel to $\langle 100 \rangle_I$ and $\langle 1\bar{1}0 \rangle_I$

$\{100\}$ planes produce
traces at $\parallel \langle 1\bar{1}0 \rangle$

$\{110\}$ planes produce traces
at $\langle 1\bar{1}0 \rangle_I$ and $\langle \bar{2}11 \rangle_I$

X-ray orientations and main lamellae directions in $\{100\}$ and $\{111\}$ projections therefore conform to a Shôji mechanism, but they cannot show whether only $\{100\}\langle 011 \rangle_I$ twinning or both shear systems occur.

The picture is altered however, when one considers the orientation

of subtexture striations within lamellae and the direction of lamellae traces in $\{110\}_I$ and $\{112\}_I$ projections. As illustrated in figures 36(a) and (b), traces were found at 14° and 22° from $\{100\}$ or $\{110\}$ loci. In $\{100\}$ projections, subtexture striations were observed at 5° from anticipated $\{110\}$ traces, figure 37, but parallel to $\{110\}_{II(Z=4)}$ traces. The angle $\{010\}_{II(Z=4)} \wedge \{110\}_{II}$ calculated as 40° , agrees with the angle measured between lamellae and subtexture as 40° , 42° (Section 2.1 and 2.4.3). Hence, a simple Shôji mechanism does not explain experimental observations.

Keeping the above considerations in mind, one notes the beautiful illustration of the ordered shape change accompanying the $I \rightleftharpoons II$ transformation in RbNO_3 , furnished by Courtenay and Kennedy,⁽⁷⁹⁾ Section 2.1, and computer calculations of the NaCl-type to CsCl-type structure change by Fraser and Kennedy,⁽⁴⁰⁻⁴²⁾ with the experimental verification in NH_4Br . One is therefore led to the conclusion that RbNO_3 $I \rightarrow II$ should be interpreted as a martensite mechanism. The results are given in Section 2.4.4.

The orientation relations predicted martensitically by the two shear systems are very similar, as seen in Table 9, Section 2.4.4. Relation [2] as expressed in Section 2.4.1 is

$$[100]_I \parallel [100]_{II(Z=4)}, (010)_I \parallel (010)_{II}$$

so that $(111)_I \wedge (111)_{II} = 7^\circ$ and $(01\bar{1})_I \wedge (01\bar{1})_{II} = 4.5^\circ$. This corresponds to any of the four variants of both mechanisms, considering the multiplicity of solutions and in view of the experimental accuracy

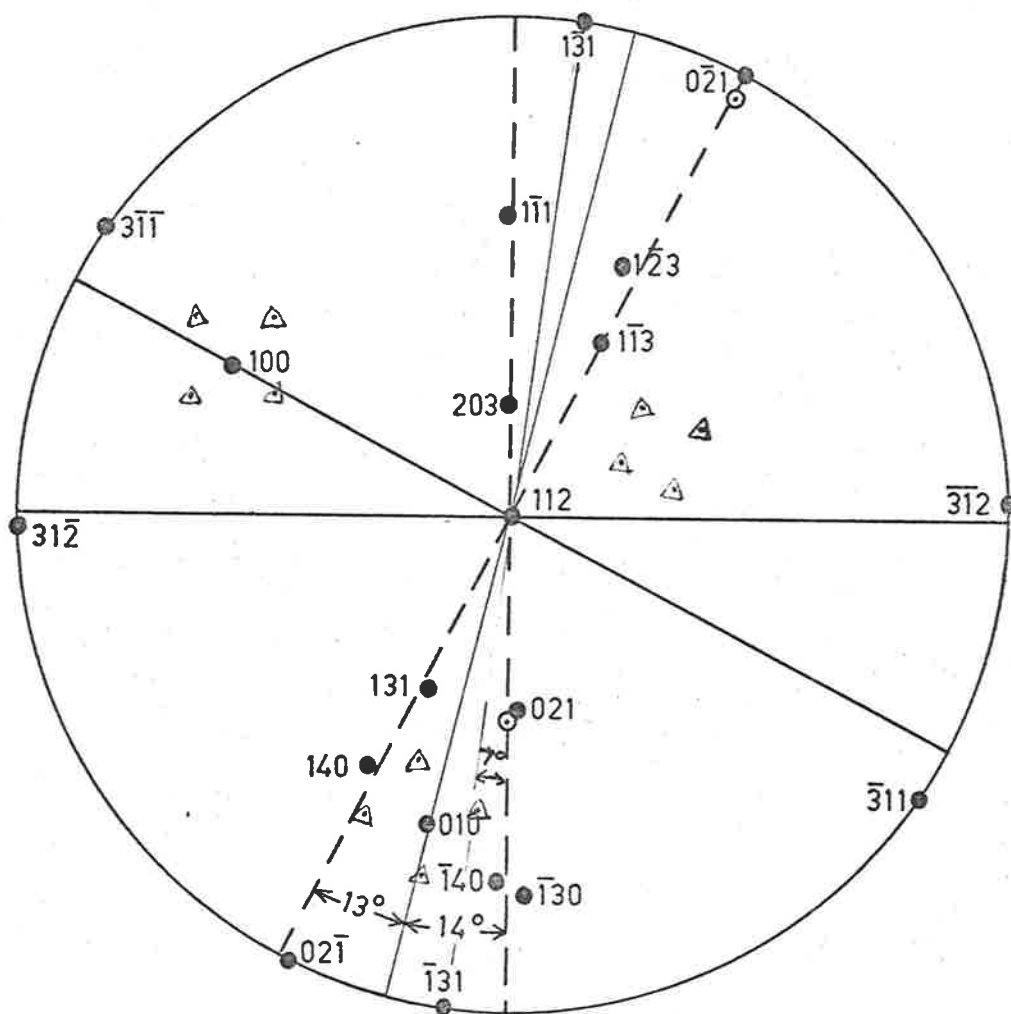


Figure 36(b). Observed traces in (112) projection of $RbNO_3I$. f.c.c.

- Lamellae traces
- Zones corresponding to Lamellae traces
- ⊙ 4° off $\{012\}_I$ habit plane
- Δ 10° off $\{010\}_I$ habit plane

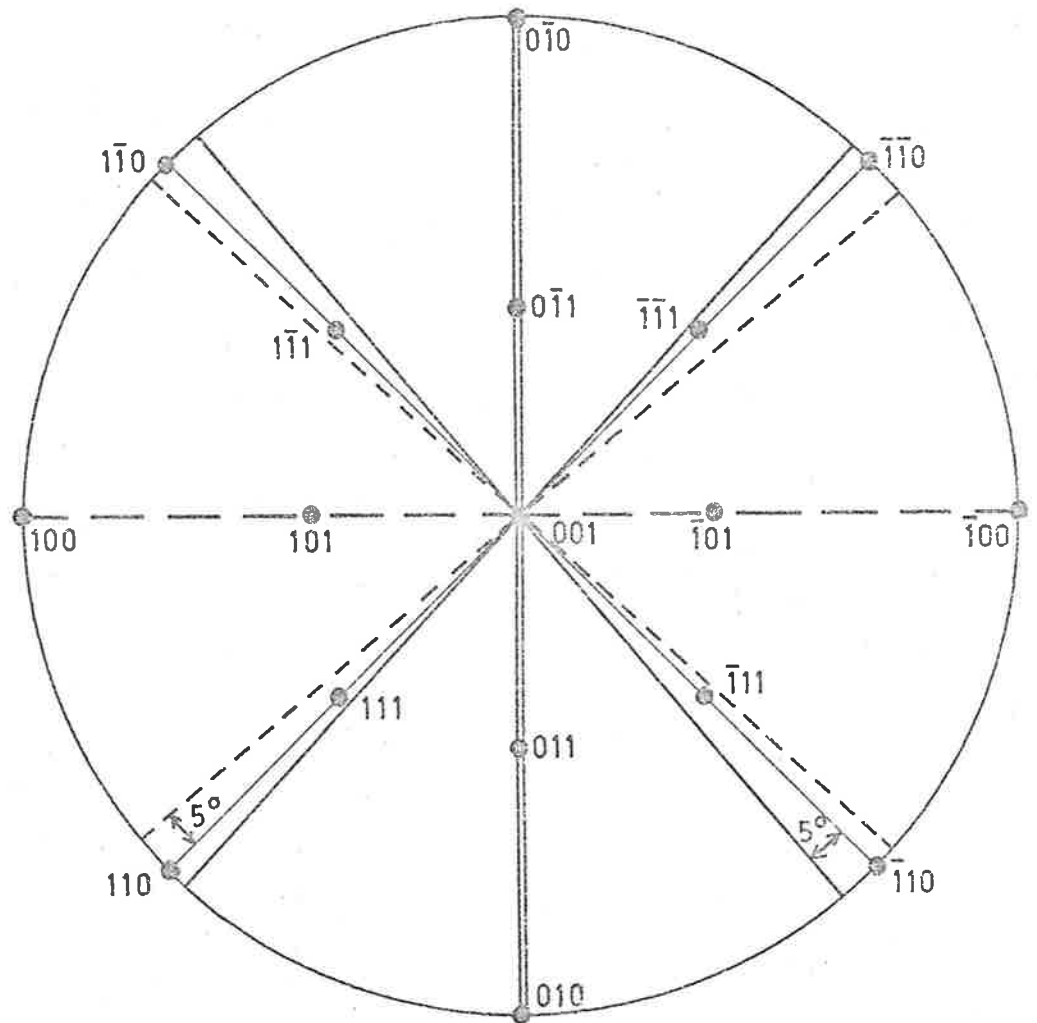


Fig. 37:

Lamellae and subtexture striations observed in an
(001) projection of RbNO_3 I, f.c.c.

- lamellae traces
- zones corresponding to lamellae traces
- subtexture striations
- zones corresponding to traces of subtexture striations.

of the X-ray precession method given earlier as $\pm 4^\circ$, although the accuracy is improved in Laue photographs; the experimental value of $\{010\}_I \wedge \{010\}_{II(Z=4)} = \pm 8^\circ$ was found by averaging over five separate experiments.

The martensite mechanism for RbNO_3 I \rightarrow II is confirmed by habit plane orientations given by X-ray optical evidence. As seen in figures 36(b) and 38(a) depicting $\{112\}_I$ and $\{100\}_I$ projections, the lamellae traces are parallel to traces anticipated from the 4° off $\{012\}$ habit planes predicted by the $\{100\}$ twinning lattice invariant shear (L.I.S.) system. Lamellae in the $\{110\}_I$ projection, figure 36(a) are close to both 4° off $\{012\}_I$ and 10° off $\{010\}_I$ traces, allowing for some experimental missetting. Lamellae traces parallel to $\langle 1\bar{1}0 \rangle_I$ direction in six $\{111\}_I$ projections however, figure 38(b), indicates that the transformation occurs by a $\{110\}\langle 001 \rangle_I$ twinning mechanism.

These results imply that both the $\{100\}$ and $\{110\}$ lattice invariant shear systems provided by transformation twinning, martensitically achieve the RbNO_3 I \rightarrow II structure change. This interpretation conforms to lamellae with herring-bone subtexture. In an $\{001\}_I$ projection, figure 38(a), main lamellae traces are parallel to $\{100\}_{L.I.S.}$ habit planes, whilst subtexture are parallel to $\{110\}_{L.I.S.}$ habit planes. According to this interpretation therefore, both sets of traces are interfaces which, in the case of subtexture, are aligned into a regular herring-bone arrangement. Furthermore, at the magnifications used in this work, traces due to L.I. twinning shear systems are too fine to

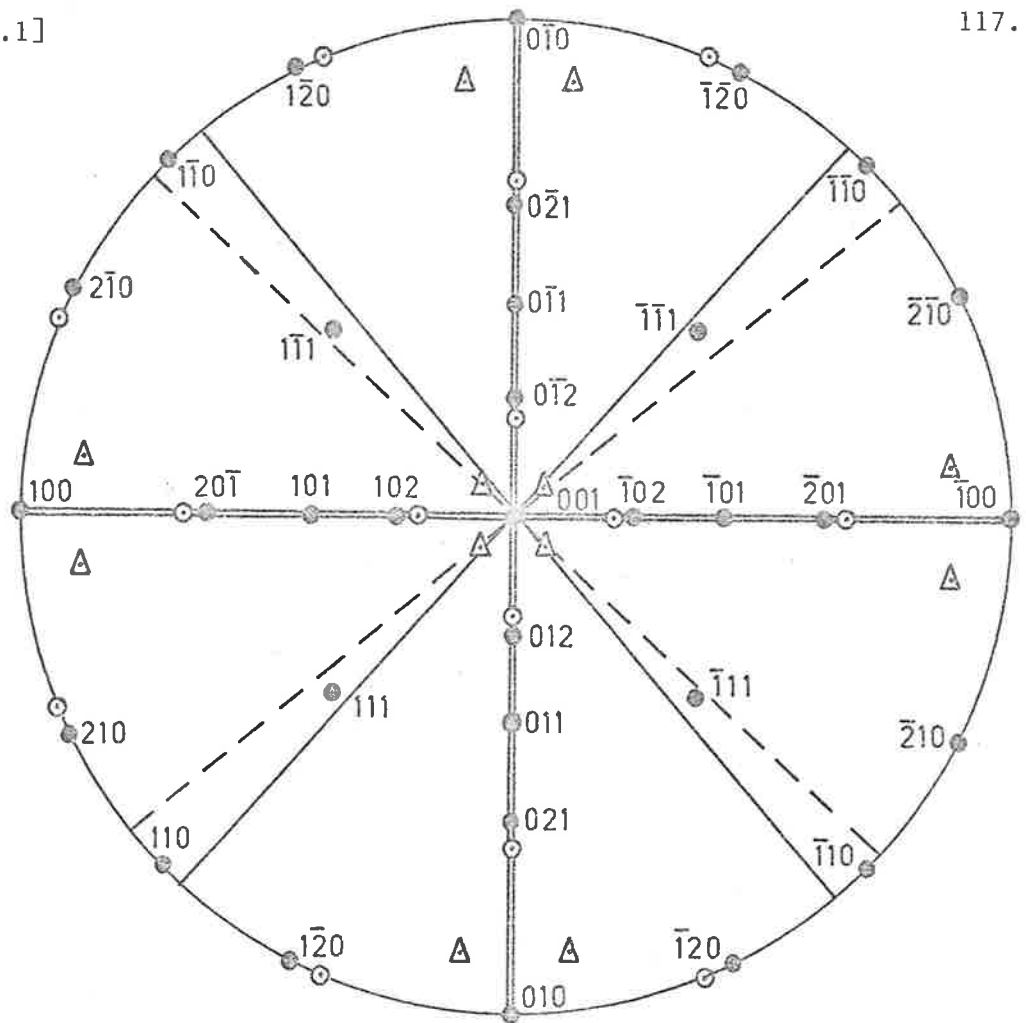


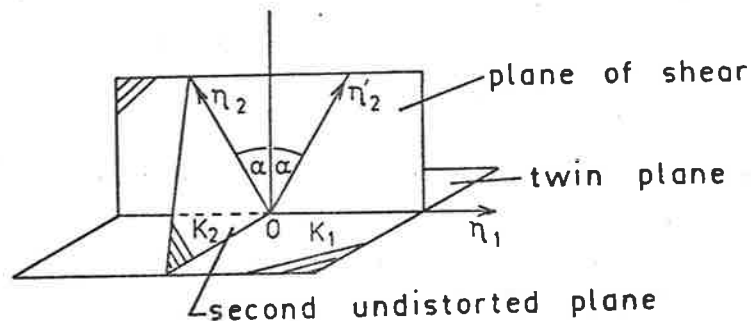
Fig. 38(a). Experimental stereogram corresponding to table 8(b) of section [2.4.3]. An (001) projection of RbNO_3 I, f.c.c., showing main lamellae and subtexture striations together with habit planes predicted by $\{100\}_I$ and $\{110\}_I$ twinning.

- ==== main lamellae traces \odot 4° off $\{012\}_I$ habit plane predicted by
- ==== zones corresponding to lamellae traces
- traces of subtexture striations $\{100\}_I$ twinning
- zones corresponding to traces of subtexture striations Δ 10° off $\{010\}_I$ habit plane predicted by
- striations $\{110\}_I$ twinning.

be observed. The implication that two separate lattice invariant shear systems operate, is novel. It differs from current theories of multiple-shear lattice invariant deformations^(334,350) since either $\{100\}$ or $\{110\}$ L.I.S. system is able to transform the structure.

It is interesting, however, that a $\{110\}_{\text{L.I.S.}}$ mechanism was not observed from main lamellae traces in a $\{100\}_{\text{I}}$ projection, or a $\{100\}_{\text{I}}$ shear system in a $\{111\}_{\text{I}}$ projection. This may be due to different strains in the matrix, depending on the projection. A memory effect is not as likely an explanation; a $\{111\}_{\text{I}}$ projection is usually found in remelted specimens, as is a $\{112\}_{\text{I}}$ projection, whilst a $\{100\}_{\text{I}}$ is the usual projection found on first cooling of the melt. Table 13 of Section 2.4.4. shows that a $\{100\}\langle 011\rangle_{\text{I}}$ mechanism may occur in a $\{112\}_{\text{I}}$ as in a $\{100\}_{\text{I}}$ projection.

It is further interesting to note that $\{100\}$ and $\{110\}$ twins have a mutual relationship in that they are conjugate twins in the cubic structure. This is illustrated below



$$K_1 = (100) \quad K_2 = (011) \quad \eta_1 = [011] \quad \eta_2 = [100]$$

As discussed in Chapter 4 of this thesis, in calcite, with which RbNO_3 II is isostructural, twinning takes place on $\{110\}_{\text{Rh}, Z=4}$ planes, and slip or gliding on $\{100\}_{\text{Rh}, Z=4}$ planes. However, a recent report⁽¹⁶⁵⁾ describes plastic deformation by heat pulses on low index faces of calcite crystals. Based on microscope and X-ray analyses, the reverse is found; twinning predominates on (100) and slip on (110) and (111) faces. However, transformation twins in RbNO_3 differ from other such types of twins as considered above, and both are valid L.I.S. systems according to martensite theory (Section 2.4.4).

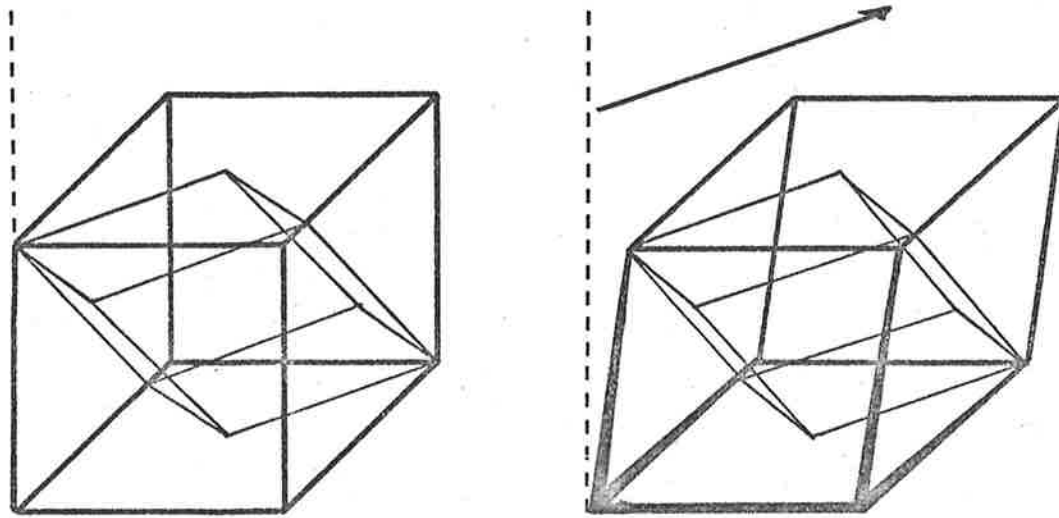
Nevertheless, Christian⁽¹⁷⁴⁾ reviews the characteristics of martensite transformations, and considers that lattice invariant shears can be twinning or slip which is associated with very low energy stacking faults, or a combination of these. Slip and twinning are mathematically equivalent as shear systems producing a martensite solution.

The experimental X-ray and X-ray optical observations therefore, may be re-examined according to the following interpretation. Lamellae traces in a $\{111\}_{\perp}$ projection accurately correspond to the 10° off $\{010\}$ habit planes predicted by $\{110\}_{\perp}$ twinning as L.I.S. system, and $\{110\}_{\perp}$ and $\{112\}_{\perp}$ projections they are relatively close, (10° and 7° respectively, figures 36(a),(b)). In $\{100\}_{\perp}$ projections, there is a discrepancy of at least $\pm 6^\circ$ between observed and calculated traces of main lamellae. Herring-bone subtexture corresponds to $\{110\}_{\text{II}(Z=4)}$ twinning or habit planes predicted by the $\{110\}_{\perp}$ L.I.S. system. Hence, there is general agreement between X-ray - optical observations

of interfaces and theoretical predictions based on $\{110\}_{L.I.S.}$ if one neglects the small angular differences described above.

A scatter of habit planes was observed in the microstructure of Fe - 32% Ni martensite crystals, ⁽³⁵⁹⁾ where a second set of etch traces corresponded to bands of slip dislocations. It was there concluded that current martensite theories involving a single L.I.S. system needed to be modified to explain this scatter. This phenomenon may similarly be found in $RbNO_3 I \rightarrow II$.

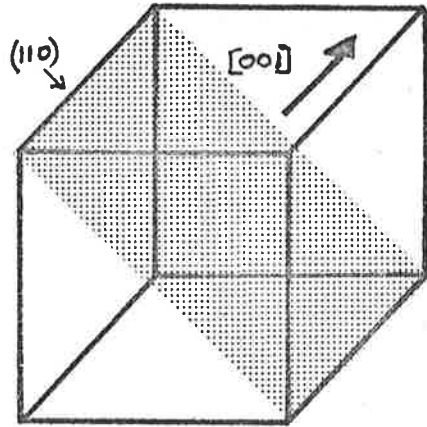
In terms of X-ray patterns, the "multiple orientations" pattern of relation [2] may be explained as follows. Both $\{110\}_I$ and $\{100\}_I$ L.I. shears martensitically predict type A orientation relations. Assuming that two variants may be found which share the same habit plane close to $\{010\}_I$, they may be arranged so as effectively to be reflected across it, and the habit plane appears to be a mirror plane or twin plane. Once an interface is nucleated, it influences the preferential choice of variants which will provide best fit in the matrix. Hence only a small number of sets of lamellae are experimentally observed in a given projection. This apparent twinning across the habit plane is illustrated in figure 39(c), where it is also shown how $\{110\}_{II}$ twinning and $\{100\}_{II}$ twinning are indistinguishable in an X-ray pattern. Figure 39(a) and (b) illustrate the separate $\{100\}\langle 011 \rangle_I$ and $\{110\}\langle 001 \rangle_I$ lattice invariant shear systems. Hence reflection of variants and twins of variants across a habit plane or interface close to $\{100\}_I$ (figure 39(c)), also corresponds to the multiple orientations pattern similar to that previously discussed for $\{100\}_I$



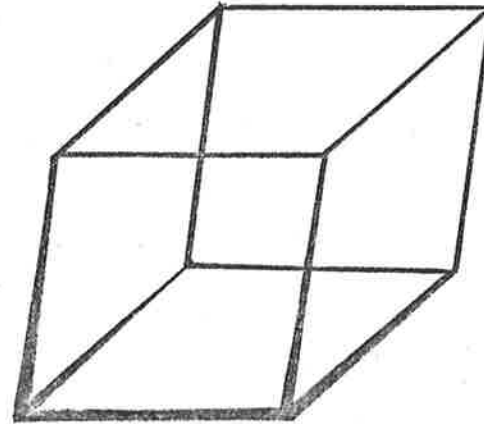
I (f.c.c.)

II (rhombohedral, $Z = 4$)

Fig. 39(a). $\{100\} \langle 011 \rangle$ Twinning in RbNO_3 .

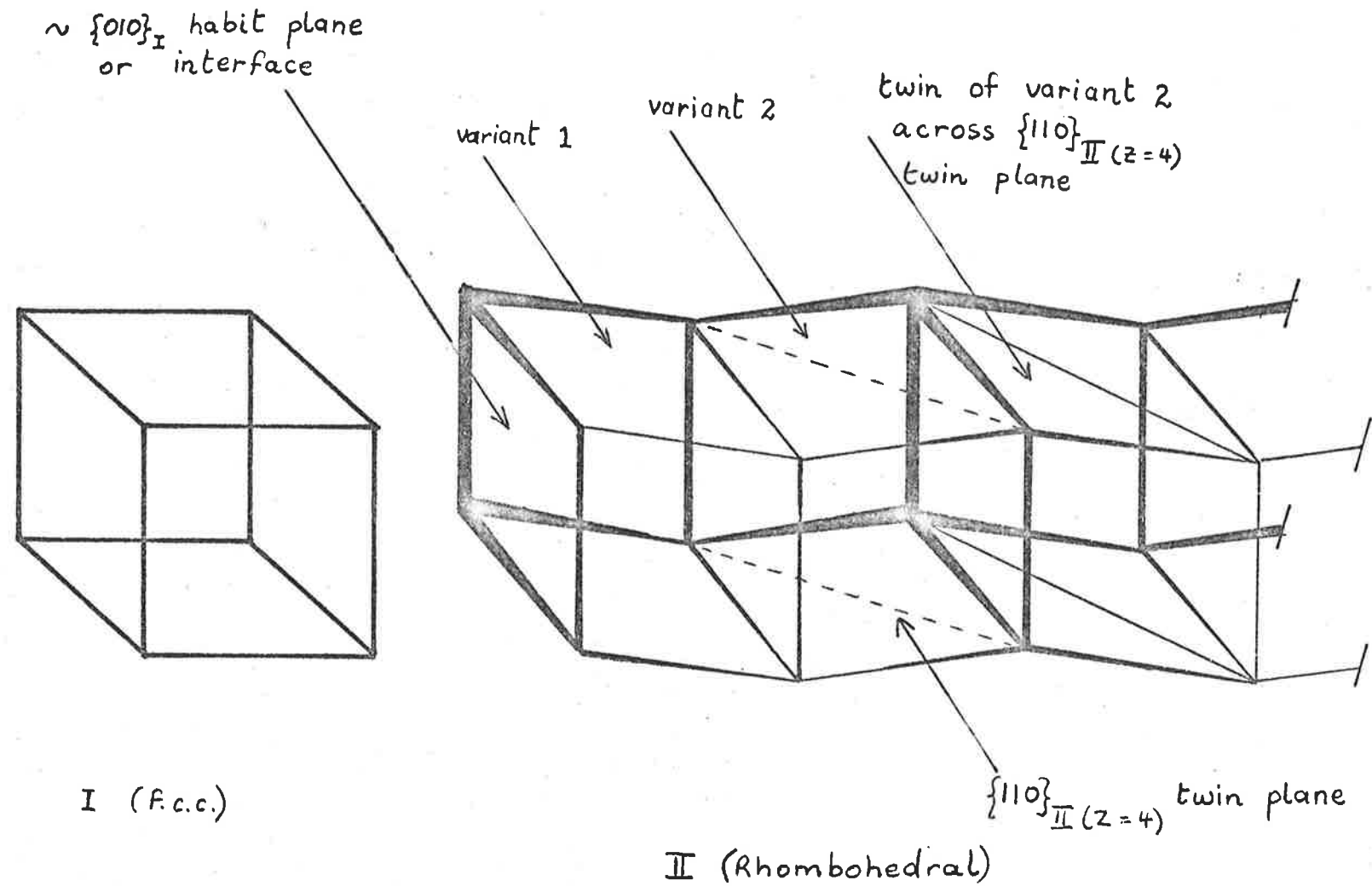


I (f.c.c.)



II (rhombohedral, z=4)

Figure 39(b). $\{110\}\langle 001\rangle_I$ twinning in $RbNO_3$



[2.7.1]

Figure 39(c). $RbNO_3 I \rightarrow II$ by the $\{110\}\langle 011\rangle_I$ lattice invariant shear system. A similar arrangement of $Z = 4$ rhombs may be obtained from $\{100\}_I$ twinning in a "concertina mechanism".

twinning. This is true considering the experimental accuracy of $\pm 4^\circ$.

Figures 39(a) to (c) also illustrate how symmetry equivalent options facilitate fit of product in the parent lattice. Considering figure 39(a), the perpendicular distance between $(100)_I$ planes is 7.32 Å, while that of $(100)_{II(Z=4)}$ is 7.134 Å, indicating a contraction in $[100]_I$. One may calculate the natural misfit^(154,187) relative to phase I, as

$$\delta = \frac{[x]_I - [x]_{II}}{[x]_I} = 0.0254$$

where $[x]_{I,II}$ are the perpendicular distances in phase I and II respectively. The periodicity $p = \frac{1}{1-\delta}$ is 1.0700 and indicates coincidence of planes. There is a misregistry of one unit cell (I) every 39.35 unit cells (II) which may be corrected by an edge dislocation with a $[100]_{I,II(Z=4)}$ Burgers⁽¹⁶⁴⁾ vector. This implies a dislocation frequency of 3.56×10^5 dislocations per cm. Hence, the two dimensional misregistry along $[100]_I \rightarrow [100]_{II(Z=4)}$ is 2.5% and compares well with the analogous 3.1% deduced by Fraser and Kennedy⁽⁴¹⁾ for NH_4Br .

Relations [1], [3], [6] and [8] were found as single product orientations in RbNO_3II . As suggested earlier in this section, [6] may be experimentally unreliable. Relation [3] corresponds to Kennedy, Patterson, Chaplin and Mackay⁽⁴³⁾ type B orientation. Relations [1] and [8] essentially are in agreement, and correspond

to Fraser and Kennedy's⁽⁴⁰⁻⁴²⁾ type B orientation. Since $\{100\}\langle 011\rangle$ and $\{110\}\langle 001\rangle$ shear mechanisms produce very similar orientations corresponding to type A, the $\{110\}\langle 001\rangle$ mechanism cannot explain relations [1] and [8]. This was also concluded by the above workers for other low index lattice invariant shear systems.

Kennedy⁽³⁷⁾ endeavoured to explain the type B orientation by a mechanism of shearing of alternate $\{100\}_I$ planes so that a NaCl structure "unfolds" and the cation and anion layers separate, giving a CsCl structure. Hyde and O'Keefe⁽¹⁸³⁾ describe a mechanism of shear on $\{100\}\langle 011\rangle$ similar to that of Shôji, which was considered for the type A orientation, except that the initial structural correspondence chooses primitive rhombs of NaCl which are twinned on $\{100\}_{II}$. Orientation B should not be explained by any of these mechanisms.

If one considered that a given variant of the type A orientation experienced an "instrumental" rotation⁽¹⁵¹⁾ due to the macroscopic shape change, an apparent orientation is observed. One such variant thus gave $\{010\}_I \wedge \{010\}_{II(Z=1)} = 7^\circ$, $\langle 100\rangle_I \wedge \langle 110\rangle_{II} = 3^\circ$. This was the only likely explanation for orientation B found by Fraser and Kennedy.⁽⁴¹⁾

The writer, while having no reason to disagree with this finding, offers another explanation. All observations report that the $I \rightarrow II$ transformation occurs by the formation of a complex twin array. After about 10 minutes, depending on the temperature, the complex twin array is removed by a detwinning or large-scale relaxation interface

which leaves behind a product of a few, usually only one or two grains. Relation [1] was found on fast cooling to phase II which was a single crystal product. During the three hours of the experiment, it remained unchanged. Similarly, relation [8] was found in detwinned phase II of one product orientation, with lamellae surface traces presumably due to the twinned precursor.

In relation [1], phase I was in a (100) projection, while in [8] the transformation proceeded from a $(110)_I$ projection. Yet, noting some angular discrepancy, relation B was found in both. The "instrumental" rotation⁽¹⁵¹⁾ producing an apparent orientation is based on a premise that the reference plane for the determination of the orientation relation is the surface of the substrate on which the crystal is mounted. It may be that another variant of type A could be found to combine with the "instrumental" rotation corresponding to a (110) substrate plane to produce a type B orientation. Fraser's⁽⁴¹⁾ predicted angular difference for a $(100)_I$ substrate is $7^\circ, 3^\circ$; his observed difference is $9^\circ, 4^\circ$; relation [1] in RbNO_3 gives $8^\circ, 7^\circ$; relation [8] gives $1^\circ, 4^\circ$. Experimental error given by both Fraser and the writer is $\pm 4^\circ$.

Type B orientation is not the only one found in the detwinned phase as seen by relations [3] and [4], discussed earlier in this section. Similarly, relation [5] describes the detwinning process, although no definite explanation has been found for the orientation. The single product orientation [6] is not a type B of Fraser and

Kennedy.⁽⁴¹⁾

The work by Kennedy et al.⁽⁴³⁾ is a complementary study of the CsCl to NaCl-type structure change in ammonium halides, in which three orientations were reported, types A, B and C. Kennedy et al.⁽⁴³⁾ postulate a mechanism for type A, focusing attention on the primitive $Z = 1$ cube transforming to the primitive rhombohedral sub-cell of the NaCl structure. Cooperative movements of atoms are discussed which involve twinning on $(100)_{\text{CsCl}}$ faces. The predicted orientation corresponds to that obtained by calcite-type $\{110\}\langle 001 \rangle_{\text{II}(Z=4)}$ twinning (discussed earlier in this section) with the Shôji-like $\{100\}\langle 011 \rangle$ mechanism accomplishing the reverse structure change.

Kennedy et al.⁽⁴³⁾ propose two explanations for their type B and C orientations. A combination of variants of type A without any "instrumental" rotation⁽¹⁵¹⁾ can be found within a small angular discrepancy. Alternatively, orientations B and C indicate activated rearrangements to help provide accommodation near the transformation temperature. In ammonium iodide it was deduced from continued changes that initially the product of transformation is not at all in an equilibrium minimum energy state. It was concluded that a decision between alternative geometries needed to await further data.

On the basis of this discussion of the types B and C orientations, and relations [1], [3], [4], [8] and [6] in RbNO_3 , the writer suggests that the second explanation is appropriate. Optical observations, discussed in the following section (2.7.1(b), part (ii)) substantiate the view of the second explanation, that the orientations are produced

by relaxation phenomena analogous to recovery and recrystallization^(180, 189,190,191) which have been extensively studied in metals and alloys. The necessary dislocations which can produce plastic relaxation in the regions in which the transformation has led to large strains,⁽¹⁸⁸⁾ are provided by the misfit dislocations. Cahm⁽¹⁸⁰⁾ considers that extensive accommodation slip accompanying intense twinning, may be the important source of recrystallization nuclei. It is reasonable to assume that dislocations play an essential part in the nucleation and development of transformation twins produced martensitically as they do in mechanical twinning.⁽¹⁸⁰⁾

The six orientations found in RbNO_3 for the $\text{I} \rightarrow \text{III}$ transformation, are self-consistent in that a $\{110\}_{\text{III}}$ is about 4° from the habit plane (4° off $\{120\}_{\text{I}}$), which is predicted martensitically for $\{100\}\langle 011 \rangle_{\text{I}}$ twinning, or 8° from $\{120\}_{\text{I}}$ itself. The above do not include Iversen and Kennedy's⁽⁹⁵⁾ relation which was not reproduced in this work. The two types of $\{110\}_{\text{III}}$ correspond to three sets of $(0\bar{1}1)_{\text{I}}$ containing $[111]_{\text{I}}$ and three $(110)_{\text{I}}$ that do not.

The polycrystalline orientations of phase III are consistent with several options and/or variants occurring together, without time for relaxation into a single grain during its existence in phase II. The non-random fragmentation during $\text{I} \rightarrow \text{III}$ illustrated in figure 20 of Section 2.4.2, also supports this interpretation. A single phase III product may have one of the following explanations: a single phase I grain is cooled directly to a single phase III orientation; the

separate options and variants of phase II degenerate in the high symmetry phase III; one martensite variant of II grows to phase III at the expense of, or in preference to others; or, finally, during slow cooling with time for annealing or relaxation in phase II, a grain of II may produce a single grain of III.

SECTION 2.7.1 (b) Discussion(ii) Optical Microscopy

At this stage it is clear that RbNO_3 I \rightarrow II occurs by a martensite mechanism with transformation twinning on $\{110\}$, or on both $\{110\}_I$ and $\{100\}_I$, corresponding to main lamellae bands. Immediately after the passage of an interface, the product is in a higher energy state similar to that produced by deformation twinning. The internal strains are then relieved by annealing in the form of "small, medium and large-scale relaxation".

Annealing processes in deformed metals have been categorized^(189, 190, 191) as recovery, recrystallization, grain growth, and secondary recrystallization. Recovery, the first change that occurs on annealing has no incubation period, and the rate decreases as the reaction proceeds. Recovery includes the process of polygonization but not the restoration of physical properties by grain boundary migration. In thin lamellae, a process similar to polygonization, that is dislocation rearrangement leading to sub-boundary formation,⁽¹⁹²⁾ is observed as blunted twin lamellae.⁽¹⁸⁰⁾ Dislocations are arranged as a wall approximately normal to the twin direction, and this short wall ends abruptly inside the crystal. "Perpendicular small-scale relaxation" in RbNO_3 therefore corresponds to this twin blunting or recovery stage of the annealing process.

The "medium-scale relaxation" or "ballooning" effect has been observed in pure iron, zinc and uranium, and Cahn⁽¹⁸⁰⁾ considered it distinctly unusual. "Large-scale relaxation" corresponds to re-

crystallization, a phenomenon of practical and theoretical interest in metallurgy. Recrystallization resembles a phase transformation in that it can be described in terms of a nucleation frequency and a linear rate of growth. After an incubation period, strain-free grains start to grow from a number of sites until they have consumed the matrix.

The interpretation of "relaxation" phenomena as a mechanism for release of internal strain is substantiated by the following observation of RbNO_3 . While large-scale relaxation occurs in normal-sized specimens that is the bulk matrix, at the edges medium-scale relaxation is sufficient, whereas in single crystallites of a small size (Section 2.4.2), perpendicular small-scale relaxation alone is necessary to release internal strain.

Twinning in RbNO_3 is comparable to that in In-Tl alloys. (192-194)
The cubic to tetragonal transformation has been studied extensively, and found to proceed by twinning on two sets of $\{110\}$ planes. Main bands of a given set of $\{110\}$ twins contain sub-bands of twins on $\{101\}$ planes at 60° to the first set. By ciné-photography it was found that the transformation proceeds by a single interface or double "X, Y and possibly V" interfaces. (192-194)

Figure 17(e) of Section 2.4.2 is a closer view of the habit plane than can be seen in the In-Tl study, and one can see how the sub-texture striations or sub-bands are accommodated by the zig-zag nature of the habit plane.

SECTION 2.7.2 Electron Microscopy of the IV \rightarrow III Transformation

The electron microscopy of RbNO_3 illustrates an order-disorder transformation. Weak superlattice reflections which are difficult to observe by X-ray diffraction, are clearly evident in the electron microscope, and are due to ordered nitrate groups, and their subsequent disappearance accompanies anion randomization. Relation [17] is the same as that reported by Brown and McLaren⁽⁴⁹⁾ who used X-rays. Subsequent decomposition is indicated by powder rings and a porous appearance similar to that of the decomposing KNO_3 , which is described in the next chapter. Radiolysis of RbNO_3 at 164° by protons has been reported elsewhere.⁽¹⁷⁷⁾

SECTION 2.8 CONCLUSION

In conclusion, therefore, one may summarize the results of this investigation of phase transformations in RbNO_3 . The aim of this work has been achieved in so far as previously reported orientation relations for the NaCl-type \rightleftharpoons CsCl-type structure change were observed. Through the rhombohedral intermediate of RbNO_3 II where planes and directions are distinguishable, the orientations reported for NH_4Br are clarified in terms of the appropriate assignation of planes and directions. In particular, the assignation of the type B orientation of Fraser and Kennedy⁽⁴⁰⁻⁴²⁾ is correct, whilst that for type A should be reversed.

17 different and sometimes reproducible orientation relations were found by X-rays, and electron microscopy. Furthermore, with X-rays, and optical and X-ray - optical microscopy, it was shown that the initial transformation product in RbNO_3 II produces relation [2] which corresponds to a type A orientation⁽⁴⁰⁻⁴²⁾ for the NaCl-type to CsCl-type structure change in ammonium bromide. Martensite mechanisms of transformation were computed and discussed in terms of transformation twinning on $\{100\}_I$ and $\{110\}$. These twin systems in the lower symmetry product are derived from mirror planes in the parent.

One mechanism based on the $\{110\}_I$ L.I.S. system is consistent with all the experimental observations if one allows a scatter of habit plane traces of about 7° , from those predicted. As illustrated in Chapter 5 of this thesis, habit planes are sensitive to lattice parameters at the transformation temperature. However, this interpretation

indicates that conventional martensite theory may need to be modified if other L.I.S. systems such as slip cause a scatter in habit plane orientations. The $\{110\}\langle 001\rangle$ has not previously been reported for such structure changes.

Another mechanism which agrees more closely with experimental observations is that either or both $\{100\}_I$ and $\{110\}_I$ L.I.S. systems operate. The interpretation assumes that traces of the operating L.I.S. are too fine to be observed at the magnifications used in this work. All the observed traces therefore correspond to interfaces which sometimes align in a herring-bone subtexture.

Both of the above mechanisms agree with X-ray patterns for the Type A orientation relation, or relation [2], which contain "multiple orientations". The origin of lamellae may be illustrated in terms of sets of $Z = 4$ f.c.c. and rhombohedral cells, in which a concertina effect results from $\{100\}_I$ L.I.S. twinning. Similarly it may arise when two variants produced by $\{110\}_{L.I.S.}$ share a common habit plane close to $\{010\}_I$ which then effectively becomes a twin plane. Twinning on $\{110\}_{II(Z=4)}$ is then indiscernible from the X-ray observations, particularly in view of experimental accuracy of $\pm 4^\circ$.

The "concertina mechanisms" above further show how misfit dislocations assist the accommodation of twinned product in the parent matrix. The internal strains of the initial transformation product are relieved by means of these dislocations, and annealing occurs in the form of relaxation phenomena. These are analogous to recovery and recrystallization which occur in deformed metals and alloys.

The relaxation phenomena observed are:

- (i) twin blunting of thin lamellae corresponding to a polygonization-type process and requiring no incubation period,
- (ii) ballooning of lamellae,
- (iii) after an incubation period dependent on temperature and rate of transformation, the passage of a detwinning interface.

These effects are described by the writer as perpendicular small-scale relaxation, medium-scale relaxation, and large-scale relaxation respectively.

Relations [1] and [8] or the type B orientations⁽⁴⁰⁻⁴²⁾ may be explained as resulting from such relaxation or annealing processes. One such orientation, relation [3], corresponding to type B of Kennedy et al.,⁽⁴³⁾ is accompanied by a second product grain, (relation [4]), which is related to the first by a common $\{001\}_{II(Z=4)}$ plane, or approximately, as a twin across the 4° off $\{120\}_I$ martensite habit plane predicted by $\{100\}$ L.I.S. system.

Twinning in RbNO_3 is comparable to that in In-Tl alloys where main bands with herring-bone sub-bands result from two sets of $\{110\}$ lattice invariant shear systems. A closer view of the main lamellae habit plane illustrates its accommodative nature.

The order-disorder $IV \rightarrow III$ transformation is clearly observed by the disappearance of weak superlattice reflections in electron diffraction patterns. The relation is the same as that reported earlier using X-rays. RbNO_3 decomposes on further heating and

radiation in an electron microscope.

Fraser and Kennedy⁽⁴⁰⁻⁴²⁾ were the first workers to analyse and quantitatively observe a martensite transformation mechanism for the NaCl-type to CsCl-type structure change in ammonium halides containing spherical ions. A martensite mechanism was shown to occur in perovskite-type inorganic oxides such as BaTiO_3 , and a mixture of KTaO_3 and KNbNO_3 .

(32) The volume change here is negligible and the cubic to tetragonal lattice deformation is small. The work on RbNO_3 I \rightarrow II is the first quantitative observation of a martensite mechanism in an inorganic compound of planar oxy-anions involving a large change. The transformation is related to NaCl-type to CsCl-type structure change, and is the first example of an inorganic compound in which more than one type of shear system occurs.

The observation of annealing or relaxation phenomena analogous to those in deformed metals and alloys shows that the behaviour of solids may be governed to a large extent, by principles which are independent of the nature of the solid. Hence, a martensite mechanism predicting best geometrical fit between two structures applies equally in metals and alloys as in inorganic compounds which consist of oppositely charged ions, and even non-spherical ions. The difference between the nature of metals and "softer" inorganic compounds is perhaps reflected in the rate of transformation, the latter change being slower than in metals some of which can transform with the speed of sound. A natural extrapolation then, is to consider the behaviour of minerals and covalent organic compounds. (196, 15)

The work in this laboratory, therefore, has wider implications. It illustrates the advantage of studying solids by several disciplines. Problems may be simplified by studying single crystals which are more likely to produce single product grains; in some cases specimen preparation may be easier, and inorganic crystals have the advantage of purity (as compared to minerals) and transparency, which is not possible in comparable samples of metals and alloys.

CHAPTER 3

CHAPTER 3THE DECOMPOSITION OF POTASSIUM NITRATEIN AN ELECTRON MICROSCOPE

	Page
SECTION 3.1 INTRODUCTION	140
3.2 METHODS AND RESULTS	145
3.3 GRAPHICAL MARTENSITE ANALYSIS	150
3.4 INTERPRETATION AND DISCUSSION	154
3.5 CONCLUSION	164

CHAPTER 3

SECTION 3.1 INTRODUCTION

The decomposition of solid potassium nitrate affords an example of how far crystal chemical relations result in topotaxy in reactions of compounds of complex ions. The change of lattice in this reaction is the same as in the decomposition of calcite-type carbonates to give NaCl-type oxides, but as the change of composition is less ($\text{KNO}_3 \rightarrow \text{KNO}_2$) there may be less accompanying disruption of the specimen than in the decomposition of either carbonates or hydroxides. (109)

Comparison with a polymorphic structure transformation having the same change of symmetry should help to show which of several processes such as surface nucleation or homogeneous decomposition controls the topotaxy in the reaction. The II \rightarrow I transformation in RbNO_3 (Chapter 2) provides such a comparison.

Studies have been made^(110-113,117) of the decomposition of KNO_3 under various radiations. KNO_2 is produced in an open system where O_2 is removed, although complete replacement by the nitrite has not been reported. The effect of 1.2 MeV electrons has been investigated. (110) Studies of thermal and radiative decompositions of other solid (142-150,176) and fused^(140,141) nitrates all indicated the appearance of nitrite or related excited states, although no orientation relations were mentioned.

In the present work, orientation relations were investigated for the reaction



as it occurs under 100 KV electrons in an electron microscope. A less clearly defined accommodation of structural misfits than in a transformation, was found. K_2O is a further decomposition product.

KNO_2 I stable from $40^\circ C$ to the melting point at $440^\circ C$, achieves a cubic NaCl-related structure through randomization of the anion orientations; ^(136,231) the lattice parameter is $a = 6.66 \text{ \AA}$, $Z = 4$. The structure of KNO_3 I can be regarded as a rhombohedral deformation of this cell, symmetry $R\bar{3}m$, the rhombohedral angle becoming $100^\circ 46'$ with a cell edge of $a = 7.037 \text{ \AA}$; again there are 4 molecules per cell. KNO_3 I has the calcite structure described in Section 2.3, but has greater thermal motion of the anions and disorder within their plane. ⁽¹¹⁸⁾ In the reaction KNO_3 I \rightarrow KNO_2 I there is a decrease in molar volume

$$\frac{\Delta V}{V} \text{ KNO}_3(\text{I}) = 9.7\%$$

K_2O has the antifluorite structure at room temperature, but a series of other phases at higher temperatures, including an ordered cubic phase β above $317^\circ C$ and disordered rhombohedral α phase from $372^\circ C$ to $646^\circ C$. ⁽¹¹⁹⁾

$CaCO_3$ and KNO_3 were investigated by S.W. Kennedy in an AEI M6G electron microscope at Cambridge University, and the behaviour of KNO_3 in the Philips EM200 was the subject of part of an Honours thesis by the writer. ⁽¹²⁰⁾ Both workers found that a reaction occurred soon after irradiation. Kennedy noticed that crystals initially developed small, triangular etch pits. This was immediately followed

by porosity in the image. Both workers found that extinction contours in the parent phase remained fixed when the temperature stabilized, but soon broadened and then obscured. The product diffraction pattern gradually superimposed and then replaced that of the single crystal parent. This process occupied three to five minutes depending on radiation intensity and crystal thickness. No specimen shape change was observed. On further gradual irradiation the porous areas grew larger and gave way to sub-porosity. At magnifications X17,000 - X20,000 the resulting areas were seen to be crystallites since their extinction contours moved when the beam was deflected.

Early work by the writer⁽¹²⁰⁾ showed that an ordered, apparently topotactic decomposition occurs with the production of KNO_2 and K_2O . A diamond-shaped KNO_3 I electron diffraction pattern was replaced by a square KNO_2 I pattern, such that in both phases the direction of projection was $[100]$ in $Z = 4$ cells, and gave the relation

$$\begin{array}{l} [100]_{\text{KNO}_3\text{I,Rh,Z=4}} \quad \parallel \quad [100]_{\text{KNO}_2\text{I,cubic,Z=4}} \\ (011)_{\text{KNO}_3\text{I}} \quad \wedge \quad (011)_{\text{KNO}_2\text{I}} = 2^\circ \quad \text{---[1]} \end{array}$$

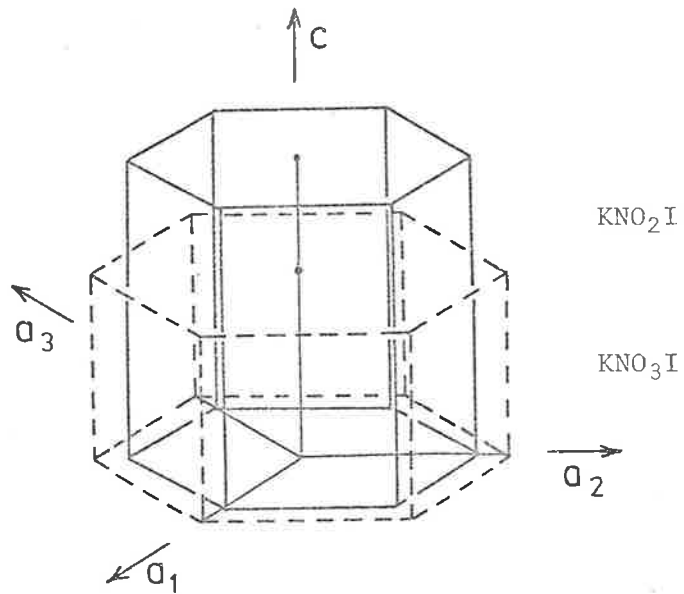
where $[111]_{\text{KNO}_3\text{I}} \wedge [111]_{\text{KNO}_2\text{I}} = 9^\circ$. The trigonal axis tilt indicates that the structure change was not achieved merely by a Buerger deformation⁽⁴⁴⁾ or elongation along the body diagonal of the $Z=4$ cell. The existence of more than one phase of K_2O was suggested by a powder pattern in which more lines appeared than could be attributed to one phase only.

Kennedy used heating stages in earlier experiments but they were

found to be unnecessary for KNO_3 . Normally with gradually increasing but minimum beam intensity, porosity appeared within 10 minutes of irradiation. In experiments with a liquid nitrogen cooling stage, crystals and carbon film appeared darker than normal. One crystal in a $[100]_{I,Z=4}$ was irradiated under such cooling conditions, with a beam of reasonable intensity, for 15 minutes. The diffraction pattern remained unaltered and no porosity was evident, indicating that the decomposition rate was decreased. However, in practice it was difficult for one person to monitor this effect and orient the specimen simultaneously. Hence most experiments were done under normal conditions.

Bright field images were examined at magnifications of X13,100 and X20,000. High magnifications were limited by the necessary low beam intensity. To measure radiation intensity the electron microscope exposure meter was inserted into the beam circuit. Apertures of known dimensions were placed at the specimen position, and the electron current transmitted at standard lens settings was read on the meter. A radiation intensity of approximately 2×10^9 electrons $\text{sec}^{-1} \text{mm}^{-2}$ corresponds to the minimum intensity used. McConnell⁽¹²¹⁾ gave a figure for illumination focused on the specimen, which was calculated to be 2.5×10^{16} electrons $\text{sec}^{-1} \text{mm}^{-2}$, and which approximated to maximum beam intensity.

The lattice correspondence illustrated below, was given^(120,105) in terms of $Z = 12$ hexagonal cells which are based on the $Z = 4$ rhombohedral and f.c. cubic cells of KNO_3I and KNO_2I respectively.



	KNO_3I	KNO_2I
a_{hex}	10.846	9.418
c_{hex}	9.639	11.535
Vol.	981.9	886.78

SECTION 3.2 METHODS AND RESULTS

Crystals of analytical grade potassium nitrate of high purity were grown on to carbon-coated electron microscope grids from aqueous solution using doubly-distilled deionized water. Specimens were dried over silica gel in a desiccator for several hours. KNO_3 crystals usually grew as orthorhombic phase II, metastably as phase I, ⁽¹²²⁾ or in the closely related form III which, on heating, immediately transforms to I in the same orientation. The experimental methods were the same as for the previous studies described in Section 3.1.

Three types of orientation relations were found for $\text{KNO}_3\text{I} \rightarrow \text{KNO}_2\text{I}$, and they are expressed in $Z = 4$ rhombohedral and f.c. cubic cells respectively.

Relation [1]

$$[100]_{\text{KNO}_3\text{I}} \parallel [100]_{\text{KNO}_2\text{I}}, \text{ (direction of beam)}$$

$$(011)_{\text{KNO}_3\text{I}} \wedge (011)_{\text{KNO}_2\text{I}} = 2^\circ \text{ --- --- --- --- --- [1]}$$

$$\text{giving } [111]_{\text{KNO}_3\text{I}} \wedge [111]_{\text{KNO}_2\text{I}} = 8.6 \pm 1.6^\circ$$

$$\text{and } (0\bar{1}1)_{\text{KNO}_3\text{I}} \wedge (0\bar{1}1)_{\text{KNO}_2\text{I}} = 2^\circ$$

The relation which was earlier reported, ⁽¹²⁰⁾ was again found with the two phases coexisting, although reflections were randomized by 5° along powder rings, in the second observation.

[3.2]

Relation [2]

From a product of two orientations in which reflections were spread by up to 17° along powder rings, only one orientation was solved giving the relation

$$(100)_{\text{KNO}_3\text{I}} \parallel (\bar{1}\bar{1}0)_{\text{KNO}_2\text{I}}, [011]_{\text{KNO}_3\text{I}} \parallel [100]_{\text{KNO}_2\text{I}} \text{ --- [2]}$$

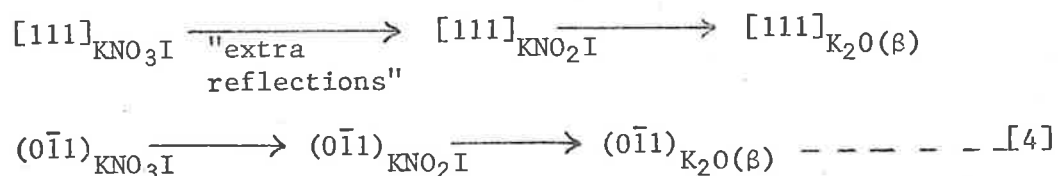
and that $[111]_{\text{KNO}_3\text{I}} \wedge [111]_{\text{KNO}_2\text{I}} = 9^\circ$

Relations [3], [4] and [5]

The relation

$$[111]_{\text{KNO}_3\text{I}} \parallel [111]_{\text{KNO}_2\text{I}}, (0\bar{1}1)_{\text{KNO}_3\text{I}} \parallel (0\bar{1}1)_{\text{KNO}_2\text{I}} \text{ --- [3]}$$

was observed in three separate experiments. In two of these KNO_2I further decomposed to cubic $\text{K}_2\text{O}(\beta)$ as illustrated in figure 1(a) to (c), giving the relation



In the third experiment relation [3] was observed in a crystal transformed from orthorhombic phase II according to the relation, depicted in figure 2(a), (b),

$$(001)_{\text{KNO}_3\text{II}} \parallel (111)_{\text{KNO}_3\text{I}(Z=4)}, [100]_{\text{KNO}_3\text{II}} \parallel [0\bar{1}1]_{\text{I}} \text{ --- [5]}$$

In figures 1 and 2 it is seen that in the trigonal axis projection extra reflections appeared during the process $\text{KNO}_3\text{I} \rightarrow \text{KNO}_2\text{I}$. Their average interplanar spacing was $3.02 \pm 0.1 \overset{\circ}{\text{Å}}$, and they are streaked

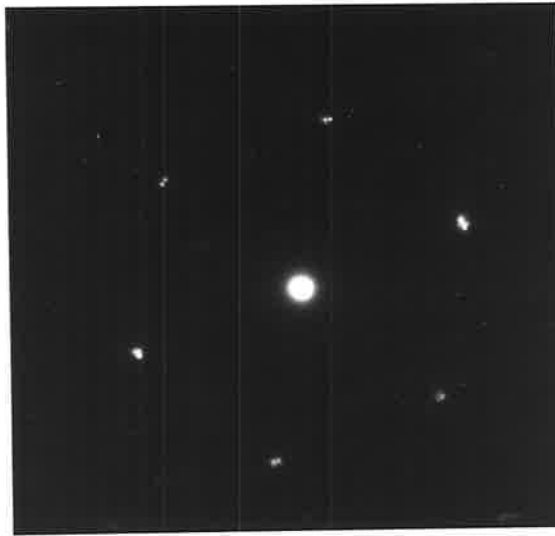


Figure 1(a)
 KNO_3I in
 $(111)_{Rh, Z=4}$
projection

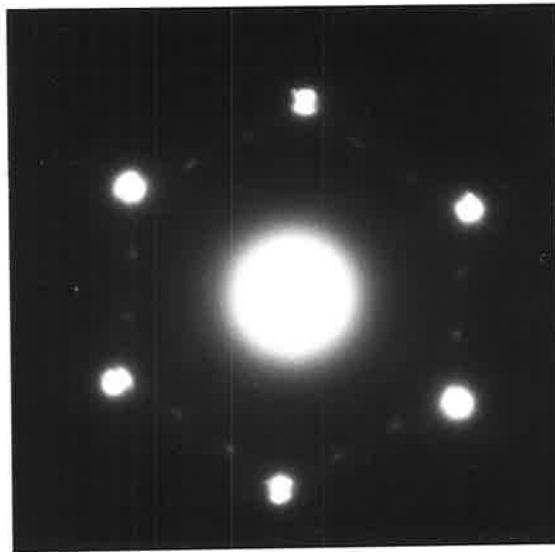


Figure 1(b)
 $KNO_3 \rightarrow KNO_2I$
with product in
 $(111)_{f.c.c.}$ and
"extra reflections"

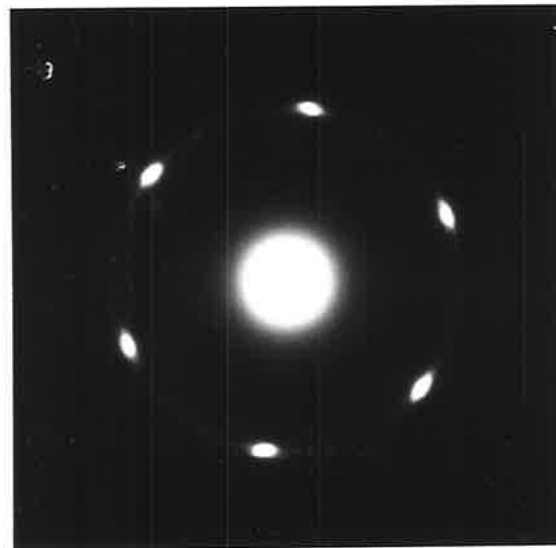


Figure 1(c)
 $K_2O (\beta)$
 $(111)_{cubic}$
projection.

Figure 2(a). Electron diffraction pattern of KNO_3II in (001) projection.

Figure 2(b). KNO_3I product in $(0001)_{\text{hex}, Z=3}$ projection, with "extra reflections"

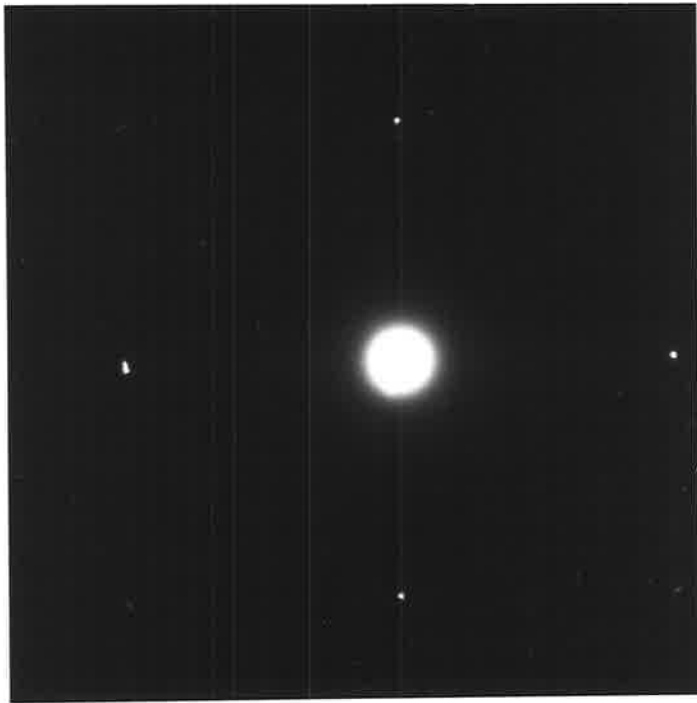


Figure 2(a)

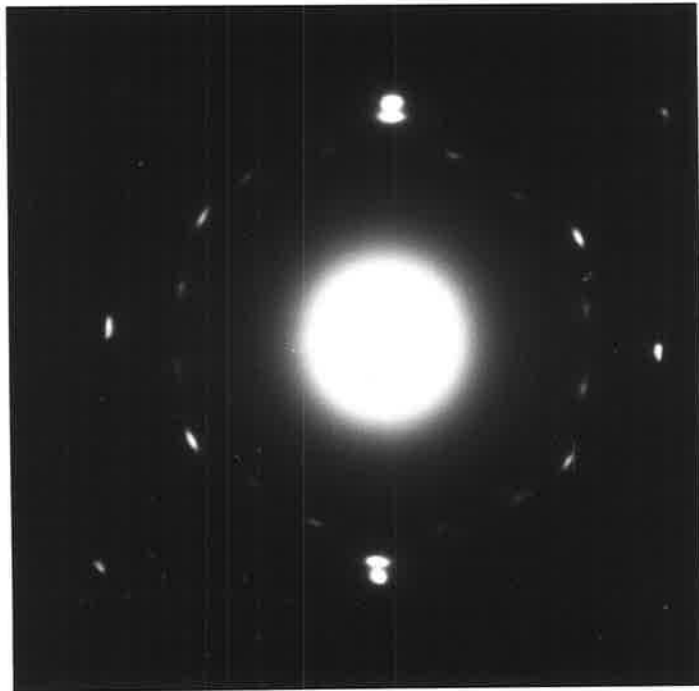


Figure 2(b)

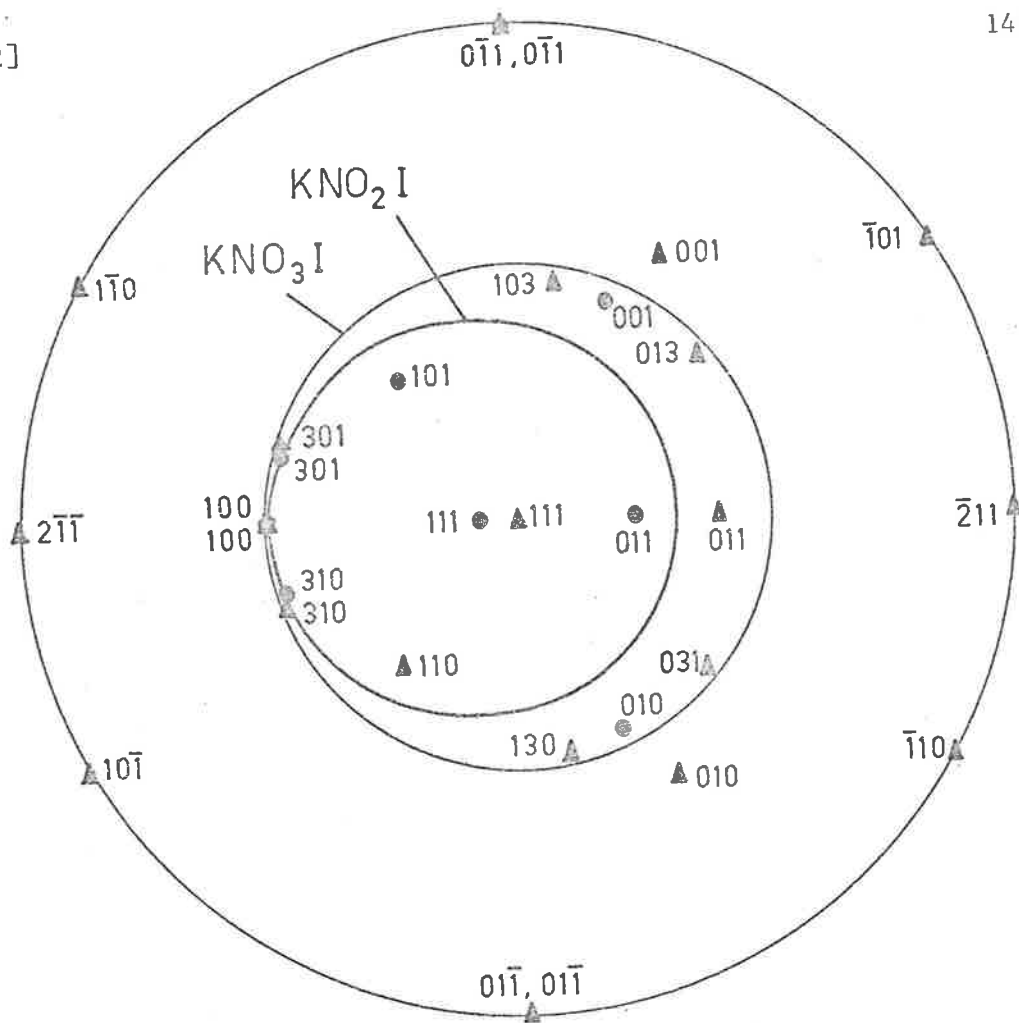


Fig. 3(b). Directions stereogram of $KNO_3 I \rightarrow KNO_2 I$ according to relation [1]. Cones of unextended vectors touch (within $39'$) at $[100], Z = 4$ directions of both structures.

- ▲ $KNO_3 I$, rhombohedral, $Z = 4$
- $KNO_2 I$, f.c.c., $Z = 4$.

[3.2]

along straight lines joining adjacent $\{1\bar{1}0\}_{I,Z=4}$ reflections and hence parallel to $\langle 0\bar{1}1 \rangle$ directions, at positions of $\pm 19^\circ$ ($\pm 1^\circ$) to $\{1\bar{1}0\}$ reflections. Similar reflections of interplanar spacing $2.86 \pm 0.2 \text{ \AA}$ also accompanied $\text{KNO}_3\text{II} \rightarrow \text{I}$, (figure 2).

In the previously reported relation [1], a good single crystal pattern of KNO_3I was replaced by a clear pattern of KNO_2I , with little streaking of reflections. In the second experiment giving this relation however, product reflections were spread over 5° along powder rings. $\{1\bar{1}0\}$ reflections of KNO_2I in relation [3], were spread over 9° along powder rings. Rather larger spread of up to 17° occurred in the experiment giving relation [2]. Nevertheless, a reasonably intense row of reflections in the parent diffraction pattern frequently was maintained under a new index in the product pattern.

Directions stereograms of relations [3] and [1] are presented in figure 3(a) and (b) respectively, where loci of cones of unextended vectors are indicated for the two structures. The Buerger deformation⁽⁴⁴⁾ of elongation of the trigonal axis together with contractions perpendicular to it, provides no plane of fit between the two structures other than the basal plane. When two cones intercept they define an undistorted and unrotated plane of fit. In relation [1], figure 3(b) the cones touch within $39'$. This is a negligible discrepancy in view of the uncertainty of temperatures and hence exact cell parameters, as well as the composition change. A graphical martensite analysis therefore was made.

SECTION 3.3 GRAPHICAL MARTENSITE ANALYSIS

In comparison with the analogous but reverse structure change in $\text{RbNO}_3 \text{ I} \rightleftharpoons \text{II}$, a graphical martensite analysis was carried out by the method of Wechsler, Lieberman and Read,⁽³⁹⁾ for known slip and twin systems.

Cleavage cell experiments on calcite by petrography⁽¹²³⁾ and dislocation etch pits⁽¹²⁴⁻¹²⁷⁾ show that twin gliding occurs on $\{110\}$ $[110]$, and that the $\{2\bar{1}\bar{1}\}[0\bar{1}1]$ glide system dominates when calcite is subject to severe distortion, (as for example, during the onset of solid state thermal decomposition). The cubic twin systems $\{2\bar{1}1\}$ $[0\bar{1}1]$ and $(100)[011]$ and that appropriate for the c/a ratio of $Z = 3$ hexagonal cells,⁽⁴⁷⁾ were investigated, as well as slip on $\{110\}\langle 110\rangle$ which is frequently observed in f.c.c. metals.⁽¹⁵²⁾ The structures of KNO_3I and KNO_2I are related by an extension of the trigonal axis, (Section 3.1) with the $Z = 12$ hexagonal $[a]$ axes parallel. In terms of $Z = 4$ cells the rhombohedral angle changes from $100^\circ 46'$ in KNO_3I to 90° in KNO_2I .

Only the shear system $(100)[011]_{\text{I},Z=4}$ and its conjugate⁽⁴⁷⁾ $(\bar{1}22)[411]_{\text{I},Z=4}$ gave a solution within $39'$, as seen in figure 4(a),(b). Each shear system predicts four solutions, two of which are degenerate due to the geometry of the analysis. Furthermore, these two sets of solutions (a) and (b) are crystallographically equivalent due to the $(0\bar{1}1)_{\text{I},Z=4}$ mirror plane. The four solutions of the $(\bar{1}22)[411]$ shear system are identical with those for $(100)[011]$ shear.

Predicted orientation relation (a) in terms of $Z = 4$ cells, is

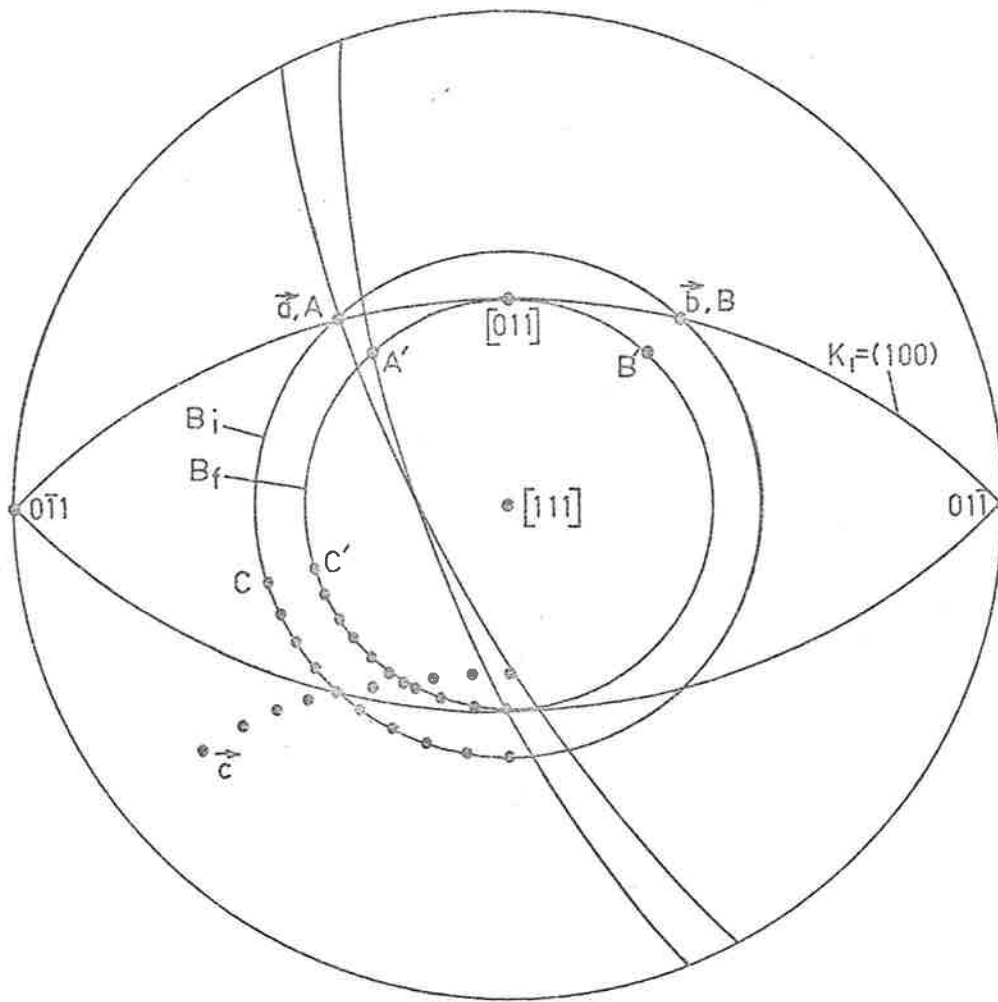
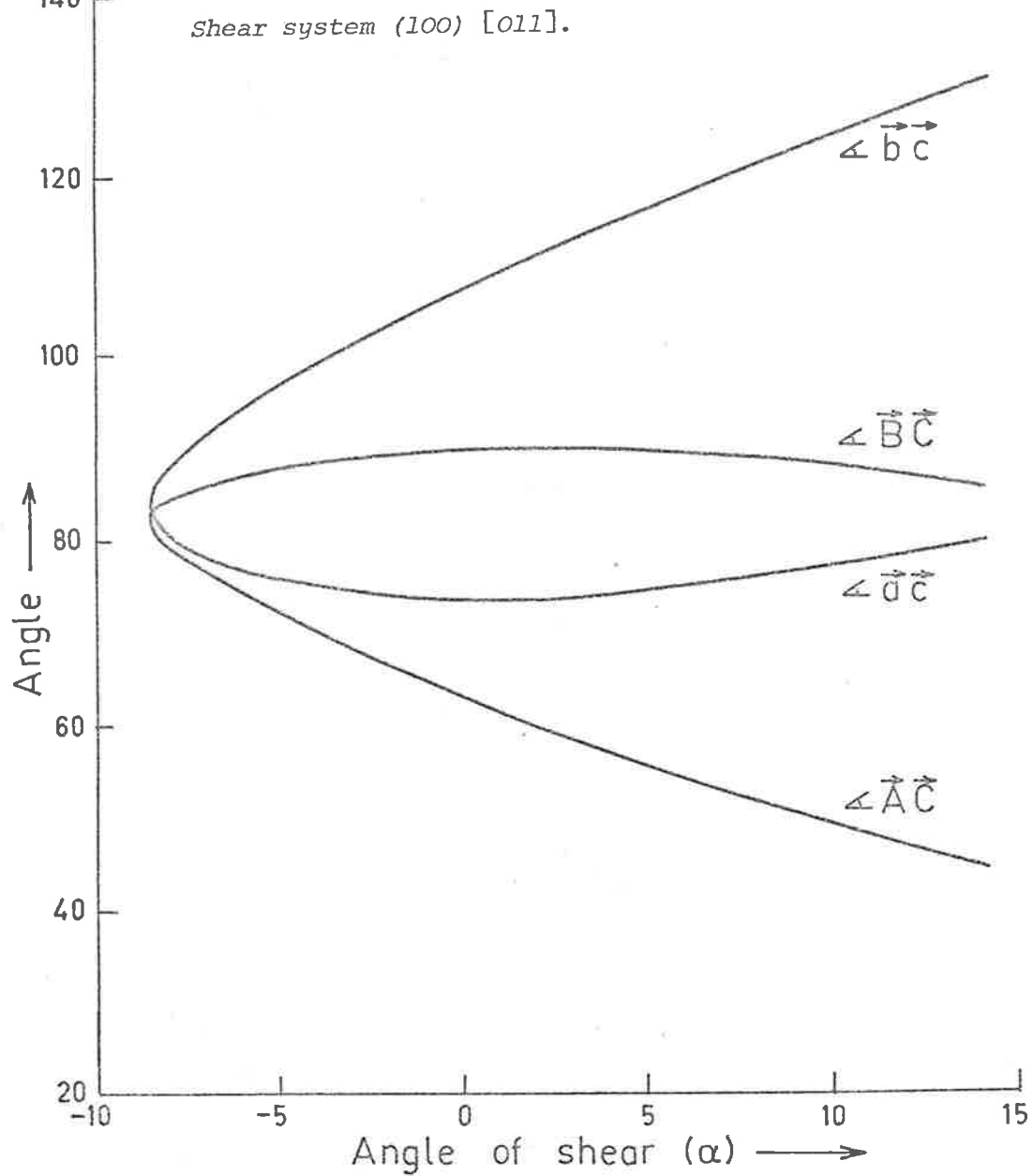


Fig. 4(a). Graphical Martensite Analysis of

KNO_3 I, (Rh, $Z = 4$) \rightarrow KNO_2 I (cubic, $Z = 4$)

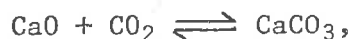
[111] projection of directions.

Fig. 4(b). Graphical Martensite Analysis of KNO_3 I, (Rh, $Z = 4$) →
(cubic, $Z = 4$).



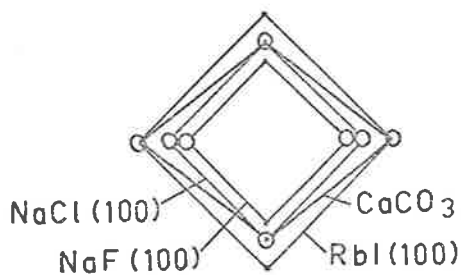
SECTION 3.4 INTERPRETATION AND DISCUSSION

Several observations of the thermal decomposition of calcite⁽¹²⁸⁻¹³⁰⁾ indicate that it proceeds at a well-defined interface, which in the case of



is reasonably mobile at sufficiently high temperatures. Equilibrium can be readily approached from either direction. The rate of interface travel⁽¹²⁹⁾ implies that the reaction is not controlled by a chemical step at the interface, but rather by heat and mass transfer.

Epitaxy between calcite-type and NaCl- and CsCl-type structures has been experimentally investigated by Schultz.⁽¹⁵³⁾ Crystals of 10 alkali halides were grown from vapour or solution on cleavage surfaces of CaCO_3 and NaNO_3 , and the orientations observed by electron diffraction. All compounds deposited according to atomic matching along rows of like ions. As illustrated below, one of the $[110]$ and $[\bar{1}\bar{1}0]$ directions was superimposed.



reference⁽¹⁵³⁾

This was expected from the short range orienting forces. No orientation exhibited a tendency for overall match of both $\langle 110 \rangle$

directions, or gave a cube $\langle 100 \rangle$ axis parallel to a $\langle 100 \rangle_{\text{Rh}, Z=4}$ axis.

Simultaneous evaporation and oxidation of magnesium has been studied directly in an electron microscope.⁽¹⁵⁴⁾ Both on the basal and $\{10\bar{1}0\}$ planes of a h.c.p. magnesium foil, MgO of c.c.p. structure was deduced from a spread of reflections along powder rings. This suggested epitaxial growths of small crystallites in the orientation

$$(0001)_{\text{Mg}} \parallel (111)_{\text{MgO}}, [11\bar{2}0]_{\text{Mg}} \parallel [2\bar{2}0]_{\text{MgO}}$$

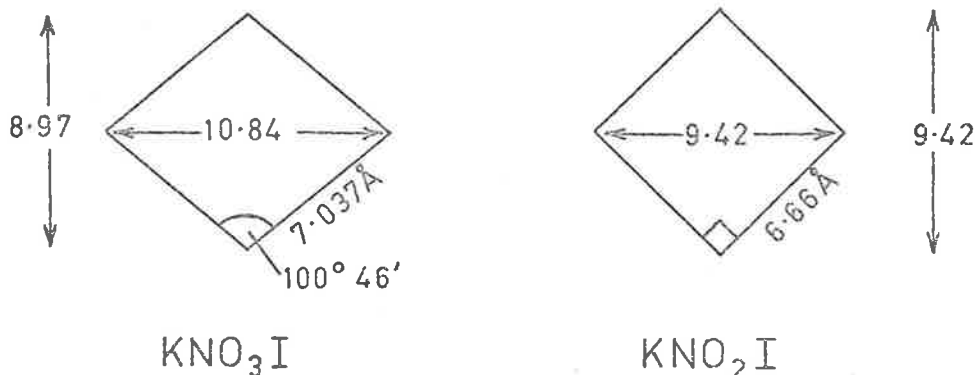
On the $\{11\bar{2}0\}$ plane of Mg, the oxide appeared in an (001) projection such that $[0001] \parallel [0\bar{1}0]_{\text{MgO}}$. The conversion of calcite to pseudomorphic fluorite by inversion in hydrofluoric acid⁽¹⁵⁵⁾ results in the cleavage face of a calcite rhomb becoming a (110) plane of CaF_2 . A similar slower reaction occurs with sodium fluoride solution. Gard⁽¹⁵⁶⁾ examined a sample of freshly prepared perfect calcite rhombs with flat faces and sharp edges, and then the reacted specimens, in an electron microscope. Stereomicrographs indicated that the general shape was preserved during the reaction, but the new surfaces were puckered and perforated with channels about 200 \AA wide at a surface density of about 100 per square micron. It was considered that the channels permit anion exchange to penetrate deep into the crystal following screw dislocations and indicating the distribution of defects on the crystal faces. In better crystals, the relation

$$\{100\}_{\text{CaCO}_3, \text{Rh}, Z=4} \parallel \{110\}_{\text{CaF}_2, \text{cubic}, Z=4}$$

$$\langle 0\bar{1}1 \rangle_{\text{CaCO}_3} \parallel \langle 100 \rangle_{\text{CaF}_2}$$

was found and the reaction was concluded to be epitaxial.

Projections of $\{100\}_{Z=4}$ are illustrated below for KNO_3I and KNO_2I .



Relation [1] is similar to those of Schultz⁽¹⁵³⁾ in that $(011)_{\text{KNO}_3\text{I}, Z=4}$ and hence $(0\bar{1}1)_{\text{KNO}_3\text{I}, Z=4}$ planes differ by 2° from $(011)_{Z=4}$ and $(0\bar{1}1)_{Z=4}$ of KNO_2I . It differs in that the $\{100\}$ planes of projection are not parallel, while $\langle 100 \rangle$ directions which correspond to the beam direction, are. The angle

$$(100) \wedge [100] = 8^\circ \text{ in } \text{KNO}_3\text{I, Rh, } Z = 4.$$

Relation [2] is the same as that found by Gard for the pseudomorphic fluorite.

Reports of thermal and radiation-induced decompositions of the isostructural carbonates and hydroxides discuss the topotactic nature of the reactions. MgCO_3 ,⁽¹³¹⁾ FeCO_3 ,⁽¹³²⁾ $\text{Fe}(\text{OH})_2$,⁽¹³²⁾ $\text{Ca}(\text{OH})_2$,⁽¹⁷⁵⁾ and $\text{Mg}(\text{OH})_2$ ^(133,134,109) all decompose in the orientation, in $Z = 4$ cells,

$$[111]_{\text{Rh}} \parallel [111]_{\text{cubic}}, \quad (1\bar{1}0)_{\text{Rh}} \parallel (1\bar{1}0)_{\text{cubic}}$$

that is, relation [3]. The triangular etch pits observed by

Kennedy (Section 3.1) may be compared to pseudomorphic MgO crystallites

lying on (111) planes. Resulting from magnesium and basic carbonate and hydroxide decomposition in the above orientation, the crystallites have a tendency for hexagonal and trigonal outlines.

Irradiation of aragonite in an electron microscope produces calcite and $\text{CaO}^{(135)}$ in the orientation

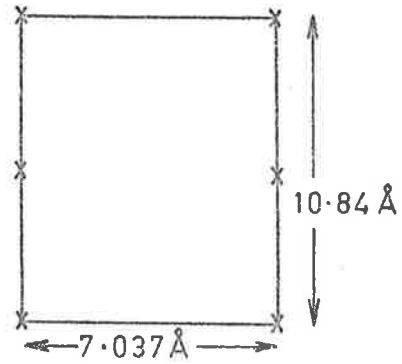
$$[11\bar{2}0]_{\text{calcite}} \parallel [100]_{\text{aragonite}}, (0001)_{\text{calcite}} \parallel (001)_{\text{aragonite}}$$

and

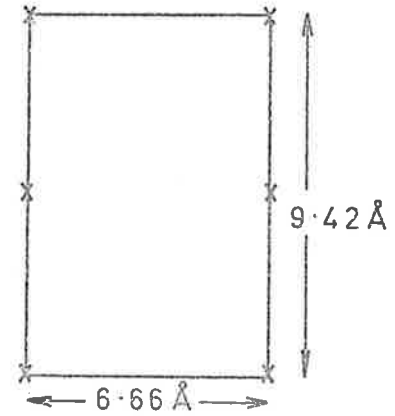
$$[1\bar{1}0]_{\text{CaO}} \parallel [100]_{\text{aragonite}}, (111)_{\text{CaO}} \parallel (001)_{\text{aragonite}}$$

with no direct correlation between CaO and aragonite. Relations [3], [4] and [5] for the radiative decomposition of KNO_3 are consistent with the above finding. The pseudomorphic replacement of calcite by fluorite⁽¹³⁷⁾ is a useful application of the topotaxy of this analogous structure change in the fields of micropaleontology and biology.

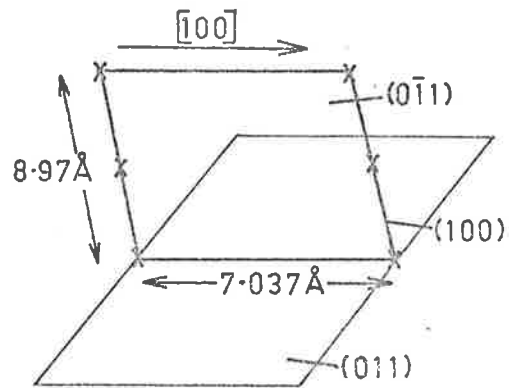
An alternative explanation for relations [1] to [5] is that best fit occurs on certain low index planes and directions while other planes in the crystal undergo appropriate changes conducive to lowest energy and good fit. This is clearly evident in relation [3]. In relation [1] best fit occurs on $(011)_{Z=4}$ and $(0\bar{1}1)$ planes and $[100]$ and $[0\bar{1}1]$ directions as illustrated below.



KNO_3I (011)_{Z=4} plane
Rh

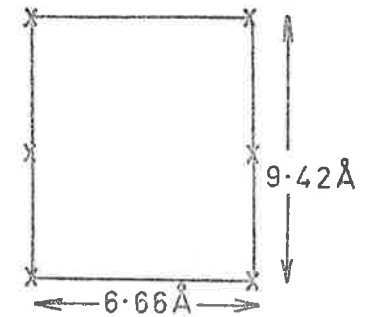


KNO_2I (011)_{Z=4} plane
cubic



KNO_3I (011)_{Z=4} plane
Rh

→
 $\frac{1}{2}$ twinning shear
 + expansion
 + contraction



KNO_2I (011)_{Z=4} plane
cubic

The mechanism involves (100)[100] type shear on the twin plane by an amount equal to only half the twinning shear, coupled with appropriate contraction and expansion of the plane of shear and twin plane (011) respectively. The amount and angle of shear for KNO_3I are 0.573 and 18° respectively, compared to 0.694 and $19^\circ 8'$ for calcite.⁽¹⁵⁷⁾

Another explanation for the observed relations could be that when a main zone axis of the parent is parallel to the beam, it will persist as a parallel zone axis of the product. Fujita et al⁽¹⁶⁶⁾ consider that the amount of secondary defects formed on electron radiation strongly depends on the crystallographic conditions of the specimen, as well as on the electron accelerating voltage. This does not appear to be the case in relation [2] however.

No conclusive evidence was found for an intermediate phase between KNO_3I and KNO_2I , like that postulated for the thermal decomposition of CaCO_3 .⁽¹⁵⁸⁾ An intermediate phase may be expected in view of the composition change, but in three separate experiments the two compounds coexisted without a phase of intermediate lattice parameters.

Stringer, Warble and Williams⁽¹⁰⁹⁾ observed the more disruptive process of magnesium hydroxide and basic magnesium carbonate decomposing to magnesium oxide by heat and radiation, in an electron microscope. Reviewing other reports, they concluded that a simple orientation relation between precursor and oxide exists, on the basis of the faithful retention of shape, high degree of orientation, and a strong tendency to assume hexagonal and trigonal shapes in magnesite platelets. This occurs despite the simultaneous primary decomposition, carbonate

recrystallization and conversion to oxide. Stringer et al⁽¹⁰⁹⁾ suggested that magnesium ions retain their two-dimensional arrangement throughout the decomposition and recrystallization stages, perhaps with some transient "rumpling" within the layers while the expulsion and rearrangement of anions take place.

Some orientation relations for carbonate decomposition reactions were also reported by A.G. Freeman,⁽³¹⁾ but to the writer's knowledge they have not yet been published.

In accordance with a similar argument by Kennedy,⁽¹⁵¹⁾ (see also Chapter 4) the distinction was considered between a real and an apparent orientation due to an "instrumental rotation". In relation [1] trigonal axes are tilted by 8.6° . If the rhombohedral to cubic structure change occurred by a Buerger deformation⁽⁴⁴⁾ observation of the orientation relation might depend on its physical position in space. Thus a crystal lying on a $\{100\}_{\text{Rh}, Z=4}$ face, on structure change, continues to lie on this face rather than move to an unbalanced position. The shape change involves a tilt by the amount that the old $\{100\}$ plane moves to its new position. Since the observation point is fixed, however, one interprets a false parallelism of planes. When relation [1] was re-examined in this light, it was still not the same as relation [3].

During the process $\text{KNO}_3\text{II} \rightarrow \text{I}$ and $\text{KNO}_3\text{I} \rightarrow \text{KNO}_2\text{I}$ "extra reflections" appeared at $\pm 19^\circ$ ($\pm 1^\circ$) to hexagonal $\{a\}$ reflections. They were streaked parallel to $\langle a \rangle_{\text{hex}}$ directions, figure 1(a) to (c). They are not explicable as superimposed twins or options of [3], or the

usual electron microscope phenomena^(159,106) of double diffraction, twinning or curvature of specimen resulting in the appearance of primary and close secondary zones. The "extra reflections" therefore may be interpreted as follows.

In terms of cation arrays, the process $\text{KNO}_3\text{II} \rightarrow \text{KNO}_3\text{I} \rightarrow \text{KNO}_2\text{I}$ represents a change in stacking sequence of h.c.p. \rightarrow distorted c.c.p. \rightarrow c.c.p.; in terms of anion arrays it is simple hexagonal \rightarrow distorted c.c.p. \rightarrow c.c.p. If one neglects the latter composition change the above structure changes may be achieved by partial dislocations or stacking faults. In Shockley partials⁽¹³⁸⁾ single layers of hexagonal arrays shear in alternative $\langle 11\bar{2} \rangle$ directions by an amount not equal to a lattice vector, and produce a resultant atomic displacement of $a/\sqrt{2}$ in $[10\bar{1}]_{Z=4}$. Other combinations of intrinsic and extrinsic stacking faults or Frank partial may also be found.⁽¹⁶⁴⁾ Basinski and Christian⁽¹⁸⁵⁾ propose a dislocation of the type

$$c[00.1] = \frac{a}{2} [110] + \frac{a}{2} [011] + \frac{a}{6} [1\bar{2}1]$$

for the f.c.c. to h.c.p. transformation.

In illustrating different types of deformations in martensite transformations, Christian⁽¹⁷⁴⁾ states that stacking faults may be considered as lattice invariant deformations. Faults of very low energy are regularly spaced so that a superstructure of the unfaulted structure is produced. Electron microscopy provides evidence of such faulted regions.

Anderson⁽¹⁶³⁾ discusses several examples of "extra reflections" in electron microscopy. He concludes that they are due to the superstructure of an intermediate metastable phase.

Possibly related to the above, another explanation considers the reaction with its composition change, as an exsolution phenomenon, such as in spinodal decomposition.⁽¹⁷⁴⁾ In reviews^(167,168) exsolution phenomena are graded with reference to thermodynamics, as proceeding by a classical nucleation and growth mechanism, referred to as continuous exsolution, through to spinodal decomposition. In continuous exsolution the compositional difference between the nucleus and matrix, that is, the fluctuation, is large, but its extent or volume is small. Discontinuous exsolution, for example, in a eutectoidal reaction, occurs where the new phase is accompanied by another which has an appropriate equilibrium composition with the host, and duplex or cellular precipitation is observed.

Spinodal decomposition differs from nucleation and growth in that it proceeds from a compositional perturbation which is small in degree but large in extent. The perturbation grows and a new phase gradually emerges which is structurally coherent with its surroundings across a diffuse interface and there is no clear stage at which the second phase appears. In its initial stage it gives rise to a sinusoidal wave in composition along some direction which grows with a preferred wavelength which may be several times the critical wavelength. It depends on several factors, but typically the wavelength is of the order of 10-500 Å.

Mechanisms of spinodal decomposition have been observed in certain minerals, such as alkali, and mixed and intermediate plagioclase, feldspars. Incipient exsolution and inversion phenomena in $KAlSi_3O_8$

and $\text{Na Al Si}_3\text{O}_8$ were observed by Laves,^(160,169) McConnell^(161,162) and others. In X-ray and electron diffraction patterns, diffuse streaks were found on or through Bragg reflections, often with asymmetry of intensity. They were considered to be evidence of a sinusoidal perturbation which McConnell⁽¹⁷²⁾ calculated as approximately 100 \AA . The extra reflections of figures 1 and 2 are distinctly separated from $\{1\bar{1}0\}_{Z=4}$ Bragg reflections, and are randomized to a small extent only, as are the main reflections. They are parallel to $\langle 1\bar{1}0 \rangle_{Z=4}$ directions in the Brillouin zone. On the other hand, paired (e) maxima symmetrically disposed about (b) superlattice positions were noted in the intermediate plagioclase feldspar, ornthite.⁽¹⁷³⁾ Similar effects may be occurring in other members of the mineral series.

McConnell⁽¹⁷²⁾ evaluated experimental X-ray and electron-optic data for alkali feldspars, and proposed a theory of metastable behaviour in a system subject to symmetry constraints, irrespective of a simultaneous composition change. He suggested that the theory has wider application than only to spinodal phenomena.

SECTION 3.5 CONCLUSION

Electron microscopy is a powerful technique in elucidating transformation mechanisms and reactions in the solid state, by enabling close observation of local behaviour in small specimens. This is done through a study of extinction contours, bright and dark field images which may contain lamellae, dislocations or twins, and by selected area diffraction patterns.

However, this assumes that a specimen is comfortably amenable to examination. Potassium nitrate is not, and so the full benefits of electron microscopy were not available. The necessary minimum beam intensity required longer photographic exposure times, and the reaction was usually completed in a few minutes. Thus the time taken for data collection was almost the same as the duration of the reaction. High resolution microscopy could not be considered.

In conclusion therefore, five orientation relations were reported in this study, of which one describes the $\text{KNO}_3 \text{ II} \rightarrow \text{I}$ transformation, and one the $\text{KNO}_2 \text{ I} \rightarrow \text{K}_2\text{O}(\beta)$ decomposition. The three orientations indicate that $\text{KNO}_3 \text{ I} \rightarrow \text{KNO}_2 \text{ I}$ is a topotactic reaction in that there is a three-dimensional correspondence between rows of ions in parent and product structures. Relation [3] is that found in several other analogous reactions previously reported. Relation [1], with the crystallographically related [2], however, corresponds to a martensitically predicted orientation, based on a shear system of $(100)[011]_{\text{I,Rh,Z=4}}$. This system was ^{considered} ~~shown~~ (in Chapter 2) to apply in the reverse but analogous transformation in $\text{RbNO}_3 \text{ I} \rightleftharpoons \text{II}$. The decomposition therefore,

may be viewed as a transformation accompanied by a small composition change. No shape change was observed, however, and the process is only assumed to be discontinuous. On the other hand, the reaction may be an example of a spinodal decomposition and hence a continuous transformation.

"Extra reflections" accompanying the process $\text{KNO}_3\text{II} \rightarrow \text{KNO}_3\text{I} \rightarrow \text{KNO}_2\text{I}$ were discussed (i) in terms of a metastable, intermediate phase with a superlattice structure, and (ii) as effects accompanying continuous exsolution phenomena. The fact that "extra reflections" were observed during the transformation as well as the decomposition, however, suggest that the process $\text{KNO}_3\text{II} \rightarrow \text{KNO}_3\text{I} \rightarrow \text{KNO}_2\text{I}$ be classified as a discontinuous transformation which could be categorized at an intermediate stage between martensite and non-martensitic.

The ambiguity as to whether the decomposition of the nitrate is continuous or discontinuous arises from the speed of the reaction, due to its sensitivity to the electron beam, and hence unsuitability for comprehensive electron microscopy. Nevertheless it has been shown that there is a complete decomposition on electron radiation in an electron microscope, and that by an ordered structure change the substance decomposes to potassium nitrite and then potassium oxide.

CHAPTER 4

CHAPTER 4THE II → I TRANSFORMATION IN POTASSIUM NITRATE

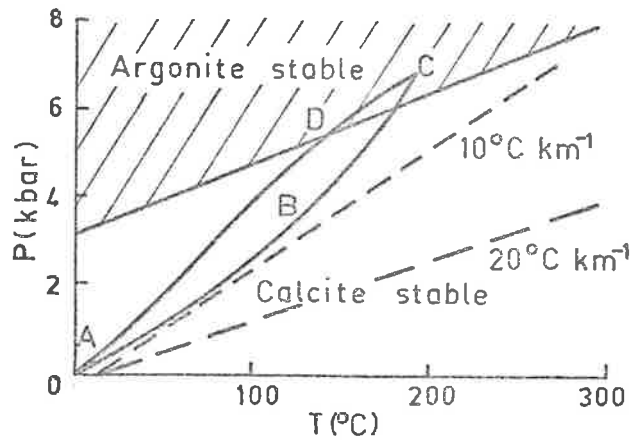
	Page
SECTION 4.1 INTRODUCTION	167
4.2 EXPERIMENTAL APPARATUS AND TECHNIQUES	181
4.3 RESULTS	184
4.3.1 $\{110\}_{II}$ Twinning and Premonitory Effects	184
4.3.2 Optical Microscopy	190
4.3.3 Scanning Electron Microscopy	200
4.3.4 Transmission Electron Microscopy	203
4.3.5 X-ray Diffraction	207
4.4 CALCULATION OF THE REGION OF COHERENT RE-ARRANGEMENT BY THE METHOD OF ARKHAROV	215
4.6 INTERPRETATION AND DISCUSSION	223
4.6.1 Analysis of Previously Reported Orientation Relations	223
4.6.2 Discussion	230
4.7 CONCLUSION	245

SECTION 4.1 INTRODUCTION

In the oceans of the world, reactions involving calcium and dissolved carbon dioxide take place.⁽¹⁹⁷⁾ As with oxygen, the balance of CO_2 is vital to the thermal stability and biological equilibrium of the environment. Most of the carbon in the earth's crust occurs as carbonate sediments (CaCO_3 , MgCO_3) and as the remains of organic materials (oil, coal, etc.) About 2% of freely available carbon dioxide is in the atmosphere, while the rest is in the oceans. In a geological sense, near-surface waters are more-or-less saturated with calcium carbonate. The bulk of carbonate precipitation occurs in marine organisms, (e.g. coral, molluscs) which, depending on their cell chemistry, grow the thermodynamically stable calcite, or the high pressure, metastable aragonite polymorph.

When calcium carbonate is synthesized in solution at low temperatures and one atmosphere pressure, either form can be obtained depending on solution chemistry and nucleation kinetics. Equilibrium tends to be obtained at temperatures over 100°C , in geological time.

Thus, when calcareous sediments containing both forms are buried, metastable aragonite is soon converted to calcite. In certain tectonic regions of the crust, calcite marbles are compressed to become aragonite marbles. Referring to the figure on the following page calcite marbles must follow the path A-B-C during burial. However, if the crustal thermal gradient was normal, (say $20\text{-}30^\circ\text{C km}^{-1}$, P increases at about 280 bars km^{-1}), then this transformation should never occur at all. Since it does, it indicates that the thermal gradient is



Phase diagram for CaCO_3 showing the stability fields of the polymorphs calcite and aragonite. The dashed lines show P-T variation in the crust for thermal gradients of 10 and $20^\circ\text{C}/\text{km}$. After Fyfe (197)

abnormally low in this geological region. From kinetic studies, it is seen that aragonite, formed at depth, could only reach the surface again if it returned along a path such as C-D-A where the thermal gradient is less than 10°C km^{-1} . Such a thermal gradient in the crust is possible only where material is rapidly descending into the mantle. Such a descending slab is associated with complex seismic activity, the region being termed a Benioff zone. Most of the world's destructive earthquakes and volcanos are associated with this convective motion.

In this way, a simple phase transformation such as calcite \rightleftharpoons aragonite records a major tectonic event. This type of information

is useful in recording fossil convective structures billions of years old.

However, for low-grade metamorphic rocks associated with shallow burial metamorphism, Newton, Goldsmith and Smith⁽¹⁹⁸⁾ caution the use of the calcite \rightleftharpoons aragonite equilibrium as a geobarometer to the earth's crust. Culminating with various studies⁽¹⁹⁹⁻²⁰²⁾ on deformed calcite, they observed aragonite crystallizing from strained calcite and showed that it can grow at reduced pressures in nature.

At one atmosphere, aragonite is the metastable polymorph compared to calcite.²⁵¹ Due to its propensity for mechanical twinning calcite can accumulate deformational energy in the form of internal strain. Thermochemical data show that at least 836 Joules mole⁻¹ of strain energy can be produced in calcite by mild deformation. This would lower the pressure requirements of aragonite relative to the strained calcite by more than 3 Kbars. The deformed calcite becomes unstable relative to aragonite which grows either during the deformation or, at least at temperatures below 400°C, faster than the strain recovery of calcite.

This hypothesis is confirmed in many natural specimens where aragonite seems to have selectively replaced highly-strained calcite. Suggestions of rhombohedral outlines in some of the aragonite batches provide further evidence for the "replacement" nature of the aragonite.

Other thin sections commonly show a fine pattern of rhombohedral tracings in the aragonite areas, suggestive of an inherited cleavage or twinning texture from the host calcite. In this crystal, the optical extinction of the aragonite "bands" is parallel to the length

of the crystals and they extinguish simultaneously. The proposed explanation is that aragonite is formed from the most highly energized stretched calcite crystals in the pre-existing calcite aggregate. The simultaneous extinction is due to crystallization in a stress field, or an orientation inherited from the fabric of the original calcite.

An alternative interpretation considers that the simultaneous extinction of the aragonite sections is due to their former connection as a single large aragonite crystal which became traversed by elongated areas of back-reaction calcite. Petrographic evidence is inadequate to unambiguously decide whether the aragonite replaced the calcite or vice-versa. If the latter case were true, two quite distinct types of back-reaction calcite should exist, since most of the back reaction calcite thermodynamically anticipated from calcite is very fine grained and different from the observed first-formed calcite.

The analysis of Newton et al, ⁽¹⁹⁸⁾ here paraphrased, of the inversion of deformed calcite to aragonite has involved only considerations of thermodynamic plausibility. On balance, petrographic and microprobe evidence suggests that the degree of calcite deformation rather than chemical variation, is the controlling factor in producing the selective nature of inversion to aragonite.

However, the actual atomic mechanisms by which aragonite could grow from strained calcite or Mg-oversaturated calcite remains obscure. One of the aims of this work therefore, was to study structurally the

mechanism of the aragonite-calcite transformation, in the iso-structural, inorganic compound, KNO_3 .

The geological relevance of this transformation having been ascertained, the direction of numerous studies of these wide-spread minerals may be outlined. The recognition that calcite and aragonite have the same chemical composition, CaCO_3 , marked the discovery in 1798, by Klaproth, of polymorphism.⁽²⁰⁷⁾ The orthorhombic structure of aragonite was first elucidated by W.L. Bragg,⁽²⁰⁸⁾ with subsequent refinements.^(209-212,239) Bragg also determined the structure of calcite,⁽²¹³⁾ later refined,⁽²⁵⁰⁾ and it is widely known and described in textbooks.⁽⁹⁹⁾ RbNO_3 II, illustrated in Section 2.3 of this thesis, has a calcite-type structure.

The fact that aragonite which is thermodynamically metastable at one atmosphere and ambient temperatures,⁽²⁰³⁻²⁰⁶⁾ is nevertheless found unchanged after geologically long periods of time, or only partially transformed in some samples, is explained by kinetic studies.⁽²¹⁴⁻²¹⁹⁾ The rate of transformation is both pressure and temperature dependent,⁽²¹⁵⁾ and there is general agreement that the process occurs by nucleation and growth, nucleation being the rate determining step. Providing the linear temperature gradient is less than or about 10°C per Km, up to a depth of 20 Km in the earth's crust, the rate of transformation to calcite is negligible.⁽²¹⁸⁾ Aqueous solvents, however exert a strong catalytic influence and lower the energy of activation for the transformation. The presence of impurity cations also affects the rate of transformation and growth precipitation

of aragonite. Mg^{2+} , Sr^{2+} , Pb^{2+} stabilize aragonite relative to calcite, whilst Na^+ or Li^+ decrease its stability. (219,201)

In view of its slow, "sluggish" rate, the aragonite \rightleftharpoons calcite transformation was considered by Buerger^(44,34) to be an example of a "reconstructive" transformation, as opposed to a "displacive" one. First coordination bonds are broken, so that high activation energies are involved. No symmetry relation necessarily exists between the two polymorphs, and there is a discontinuity in all physical properties. It was the aim of this work to confirm various subsequent suggestions^(210-221,105,120,) that the aragonite-calcite transformation as observed in KNO_3 is not necessarily reconstructive, but may proceed by two distinct mechanisms. As well as a "reconstructive" process, the structure change may occur by a mechanism which is similar to martensite transformations in metal alloys, and which results in a definite orientation relation. As was found for thallic nitrate,⁽³⁶⁾ the choice of mechanism may depend on the amount of imperfection and may be sensitive to small changes in the differences between structures.

Several orientation relations have already been reported for the aragonite-calcite transformation in $CaCO_3$, as observed by X-rays and electron microscopy,^(135,218,220,220-225) and these will be discussed in more detail in Section 4.6.1. For an orientation

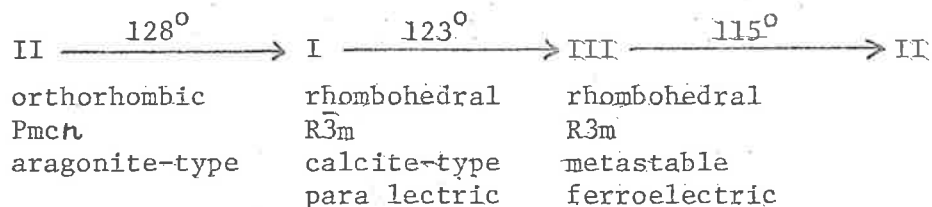
$$\begin{array}{l} [c]_{\text{aragonite}} \quad || \quad [c]_{\text{calcite, hex, (Z=3)}} \\ [a]_{\text{aragonite}} \quad || \quad [a]_{\text{calcite,}} \end{array}$$

Kozu and Kani⁽²²³⁾ propose a mechanism based on rotation of $\text{CO}_3=$ groups in relation to neighbouring cations, coupled with a weak displacement of the $\text{CO}_3=$ along the [c] axis. Hiragi et al⁽²¹²⁾ found this orientation by electron microscopy and discuss it on the basis of a non-diffusion martensite-type mechanism. Recently, Craido and Trillo⁽²²⁶⁾ observed that the aragonite and calcite phases can be interconverted by mechanical grinding of CaCO_3 . They speculated on a mechanism involving dislocations moving on $(11\bar{1})_{\text{Rh}, Z=4}$ calcite or (001) aragonite phases. Observations on experimentally deformed limestones however, concluded that the calcite to aragonite phase change under certain conditions is diffusive and non-martensitic.⁽²³⁰⁾

As well as grinding, deformation, and other such experiments on CaCO_3 ,^(199-202, 226-230, 249) the slip and twinning systems in calcite have been investigated through dislocations and decomposition processes.^(123-127, 165, 182, 229) In terms of the $Z=4$ rhombohedral cell, twinning occurs on $\{110\}\langle 001\rangle$ and slip on $\{100\}\langle 011\rangle$ and $\{11\bar{1}\}\langle 011\rangle$. There is no evidence of slip on either (110) or (111). In pseudo hexagonal aragonite, twinning on (110) is very frequent, and natural single crystals are rare.⁽²⁰⁸⁾ The angle $(110) \wedge (1\bar{1}0)$ is $63^\circ 48'$ compared to 60° if the structure was hexagonal. Cahn⁽¹⁸⁰⁾ classifies it as twinning by reticular pseudo-merohedry.

Potassium nitrate has the following modifications at one atmosphere:

[4.1]



The structure of KNO_3 II was determined at room temperature; (232,233) generally in this investigation, lattice parameters at 125°C were used, (225) Table 1(a),(b). Thermal expansion coefficients for various temperatures are known. (234-237) As in aragonite, the plane of the nitrate groups is slightly tilted with respect to the $(001)_{\text{II}}$ basal plane. (238)

The structure of phase I was determined at 152°C in terms of the rhombohedral $Z=2$ cell (240) and re-analysed in rhombohedral, $Z=1$ or hexagonal, $Z=3$. (118) The calcite-type structure is discussed in Section 2.3 of this thesis, and Table 1(b) presents the lattice parameters for the different sub-cells in KNO_3I . The thermal expansion is linear over the whole temperature range of phase I, with a predominant expansion along the $[c]$ axis, and a contraction in directions perpendicular to it. (241) The specific heat was carefully measured calorimetrically both during heating and cooling. (242)

By studying X-ray diffuse scattering Shinnaka (243) analysed the disordered structure of phase I in relation to the ferroelectric phase III. The transformation $\text{I} \rightarrow \text{III}$ is considered to be an order-disorder phenomenon. (118,243-245) In melt-grown single crystals cooled to 130°C , diffuse scatterings containing discrete maxima were observed at reciprocal lattice points of the primitive rhombohedral

TABLE 1(a)

LATTICE PARAMETERS OF KNO_3 , PHASE I, II AND III

Phase	Parameters	Temp (°C)	Reference
II	Orthorhombic, Z = 4 a = 5.414 b = 9.164 c = 6.431 Å	26°	Swanson et al ⁽²³³⁾
	a = 5.426 b = 9.169 c = 6.550 Å	125°	Davis and Oshier ⁽²²⁵⁾
I	rhombohedral X-ray cell, Z = 2 a = 7.181 ± 0.01 Å, α = 44°8.5'	152°	Tahvonen ⁽²⁴⁰⁾
	hexagonal, Z = 6 a = 5.396 Å, c = 19.410 Å	152°	"
	hexagonal, Z = 3 a = 5.42 Å c = 9.705	152°	Strømme ⁽¹¹⁸⁾
III	rhombohedral, Z = 1 a = 4.365 Å, α = 76°56'	120°	
	hexagonal, Z = 3 a = 5.43 Å, c = 9.11 Å	120°	Strømme ⁽¹¹⁸⁾

TABLE I(B)

SUB-CELLS OF PHASE I

(corresponding to Table 6, Section 2.3, for RbNO_3 II)

Z	Crystal System	Lattice Parameters	Reference
1	rhombohedral	$a = 4.50 \text{ \AA}$, $\alpha = 74.067^\circ$	Calculated from data in Strømme (118) by method in (99)
3	hexagonal	$a = 5.420 \text{ \AA}$, $c = 9.705 \text{ \AA}$	Strømme (118)
2	rhombohedral	$a = 7.181 \text{ \AA}$, $\alpha = 44.142^\circ$	Tahvonen (240)
6	hexagonal	$a = 5.396 \text{ \AA}$, $c = 19.410 \text{ \AA}$	Tahvonen (240)
4	rhombohedral	$a = 7.037 \text{ \AA}$, $\alpha = 100^\circ 46'$	Odlyha (105)
12	hexagonal	$a = 10.846 \text{ \AA}$, $c = 9.639 \text{ \AA}$	calculated from data in Odlyha(105) by method in(99)

cell. The disordered structure is produced by nitrate ions oscillating or rotating-librating at $\pm 30^\circ$ to formal calcite positions. KNO_3I is isostructural with NaNO_3 ,^(102,26) and melts at 334°C .

Phase III has an ordered structure with respect to phase I,^(263,118) and is of interest as a ferroelectric compound.⁽²⁴⁶⁻²⁴⁸⁾ The primitive rhombohedral unit cell has space group $R3m$. Thermal expansion coefficients are known.⁽²⁵²⁾

Electrical and thermal conductivities for the three phases have been studied, and transformations thus noted.^(245,253-255) A phase IV exists at high pressures, and thermodynamic properties of the transformations are listed.⁽²⁶²⁾ The conditions of growth from aqueous solution determine the phase and morphology of crystals.^(122, 256-259) Infra-red and ultra-violet absorption spectra are reported.^(260,261) In this summary of literature on KNO_3 , earlier papers are not noted, but may be found referenced in those papers quoted.

Like RbNO_3 , the transformations in KNO_3 have been studied by members of this laboratory prior to the work for this thesis.^(108,105, 120,221) Kennedy, Ubbelohde and Woodward⁽²⁷¹⁾ examined crystals of KNO_3 II by X-rays before and after heating to phase I. They noticed that the pseudomorphic product was composed of sub-units which were randomized by up to 5° . In "normal", non-rigorously dried crystals the $[b]_{\text{II}}$ axis (S.G. $Pbnm$ corresponding to the $[c]_{\text{II}}$ axis, S.G. $Pm\bar{c}n$) tended to persist within a small angle, while the other axes adopted random directions. In rigorously dried crystals all axes

adopted random directions after transformation. The product was often polycrystalline, and X-ray evidence was found for thermal twinning on $\{110\}_{II}$ after the transformation. In the work of Kennedy et al⁽²⁷¹⁾ "dry" crystals were heated to 100°C under high vacuum for several days, while "normal" crystals were dried for several days on filter paper open to the atmosphere.

Kennedy and Odlyha^(105,221) studied the transformations by polarized light microscopy. They discovered surface tilts or slip lines parallel to the basal plane of II during the II \rightarrow I transformation, and the crystals sometimes suffer a shape change or kinking of up to 7° successively in different directions. The transformation usually proceeded via a straight interface parallel to the basal plane, and if kept stationary for some hours, a row of etch pits developed, indicating a semicoherent interface.

In a total of 80 microscopy measurements the observed angles between initial and final extinction directions were 6°, 13°, 19°, 26°, 34°, 39°, 44°, 89° and 0°; all \pm 2° because of deformation of the specimens. Some products are also finely twinned. For the transformation, Odlyha and Kennedy⁽¹⁰⁵⁾ reported five orientation relations; two determined by X-rays and three by single-surface and two-surface analysis. One of the X-ray orientations was identical with that found by Davis and Oshier for KNO_3 .⁽²¹⁵⁾ These orientations are discussed later in Section 4.6.

Recrystallization and grain growth occurred in the vicinity of

190°C. When crystals are annealed at this temperature and subsequently cooled, phase III forms as twin bands, and is preserved to room temperature, finally transforming in a random fashion to form II.

Following the submission of thesis work by Odlyha,⁽¹⁰⁵⁾ Asadov and Nasirov⁽²⁶⁴⁻²⁶⁷⁾ published optical microscopy observations of the nucleation and "rhythmic" growth of KNO_3 I from phase II. Their photographs of surface tilts and resultant shearing parallel to the basal plane of II illustrate clearly, as do those of Kennedy and Odlyha, the shape change and bending of crystals.

Other early studies⁽²⁶⁸⁾ observe an interface and polycrystalline product, but no regular surface effects. Dufy⁽²¹⁹⁾ noticed a small number of black lines accompanying the aragonite to calcite transformation in thin elongated crystals viewed in an optical microscope.

The study of the II \rightarrow I transformation in KNO_3 formed part of the requirements for an Honours thesis⁽¹²⁰⁾ by the writer. By evaporating a thin layer of gold on orthorhombic crystals, the techniques of multiple beam interferometry⁽²⁶⁹⁾ and Nomarski interference contrast⁽²⁷⁰⁾ were successfully used to study surface effects accompanying the transformation, whilst specimens were still amenable to conventional optical microscopy, transmitting plane polarized light.

As well as surface tilts parallel to the basal plane, fainter, oblique surface effects were found, sometimes superimposed on the above, and often inclined at 44° to the basal (II) plane. Many unheated crystals showed a few lines or fine bands parallel to $[c]_{\text{II}}$ on

the $\{b\}_{II}$ face. On gradual heating the number increased above about 76°C , and they persisted on the surface of the transformed product. This fact, together with their displacement of polarized light interferometry fringes, indicated that these longitudinal lines were surface effects.

In the work for this thesis, studies on these surface effects accompanying the transformation were continued, with the aim of understanding its mechanism. The structure change was independently followed by X-ray diffraction, electron microscopy and diffractometry methods.

SECTION 4.2 EXPERIMENTAL APPARATUS AND METHODS

Optical microscopy was done with a Reichert Austria, Zeotopan research microscope which enabled a quick interchange between transmitted and reflected light, both normal, or plane polarized. The associated attachments for Nomarski interference contrast⁽²⁷⁰⁾ and polarization interferometry⁽²⁶⁹⁾ were used for surface studies. During the latter part of the work, an automatic exposure meter, the "Photomatic" facilitated photography using 35mm film, usually Ilford HP4 or FP4. Black and white films were developed and printed in the laboratory. Prints were enlarged in a Durst D659 Synchronized Twin Automat enlarger, monitored by a CdS enlarging meter. Crystals were coated with a thin layer of gold evaporated in a "Speedivac" vacuum coating unit.

The microscope heating stage consisted of a transparent conducting glass slide of resistance 5 ohms previously used in this laboratory by M. Odlyha.⁽¹⁰⁵⁾ The slide was supported in an asbestos holder made in the departmental workshop. The heating circuit was the same as for RbNO_3 studies, Chapter 2 and contained a voltage stabilizer. A temperature calibration graph for the heating stage was prepared by Mr A. Iversen of this laboratory by means of noting known melting points of various inorganic compounds. At high magnifications an uncertainty occurred in the temperature, due to the proximity of a high power, relatively cool microscope objective.

For X-ray diffraction experiments the same circuit was used with crystals being heated on a Matsunami glass coverslip on which was

painted a heating circuit such as is illustrated here. A colloidal



suspension of bright gold from Degussa (Frankfurt am Main) was applied to the slide and heated for a few hours in a furnace at about 450°C , with free passage of air. This left a deposit of shiny metal. The coverslip was carefully clasped in an asbestos support fixed to a goniometer, in contact with fine 30 s.w.g. copper wire terminals, via small copper screws. A paper asbestos shield was attached with water glass to minimize drafts, and the resulting heater was fragile. On the glass-only side of the coverslip, crystals were stuck on by high vacuum silicone grease which was generally found to be a satisfactory support for the temperature range, and so constraints imposed on crystals by growing directly from solution on to the glass, and which may possibly affect the transformation mechanism, were avoided.

During the decomposition study the transformation was occasionally observed. The electron microscope specimens were prepared and observations recorded as described in Chapter 3.

Crystals of Analar grade KNO_3 were usually grown from doubly-distilled, deionized water and dried over silica gel in a desiccator for about one day. They were further dried at room temperature in a moderate vacuum with a liquid nitrogen air trap, for several hours or overnight. Crystals grown from aqueous solution at room temperature usually adopted a flat, elongated acicular habit, about 0.1 mm wide

and lying on $\{010\}_{II}$.

Early replicas of the high temperature surface were examined in a Cambridge S600 Steroscan scanning electron microscope which was demonstrated and serviced by Mr. Leonard Green of the Metallurgy Department of the South Australian Institute of Technology, Levels Campus. Later examinations were made in an E.T.E.C. Siemens Autoscan S.E.M. maintained in the Geology Department of the University. The writer gratefully acknowledges a lecture concerning the principals, and a short course of instruction on its operation, by Dr. K. Bartusek. For a type of araldite replica, a Reichert OMU3 ultra microtome was demonstrated by Mr. Ross Crocker and used by the writer in the Zoology Department of the University.

Electron diffraction patterns were collected on Ilford Fine Grain Safety Positive film, 35 mm roll film, or flat plates. X-ray diffraction patterns were recorded mostly on Ilford Industrial G film. Polaroid type 57 film was also used.

Computing was done on the University CDC 6400 machine using the same programs as for $RbNO_3$, Chapter 2. For assistance with interpreting electron micrographs, particularly in Chapter 3, and X-ray precession photographs, a computer program, SORT, was written. The program was not completed, but could be used in an initial analysis. Most calculations were made using a Hewlett-Packard 45 electronic calculator.

SECTION 4.3 RESULTS4.3.1 $\{110\}_{II}$ Twinning and Premonitory Effects

Elongated, prismatic, room temperature crystals were thinly gold coated for Nomarski interference contrast microscopy. Table 2 summarizes optical observations, usually at magnifications X450, of fine bands parallel to the $[c]_{II}$ axis, and referred to as "longitudinal lines". It is seen that in normal crystals of reasonable but not thorough drying, longitudinal lines developed below the transformation temperature, and were first noticed at about 80°C. Where crystals were better dried, longitudinal lines were fainter, and in experiment number 8 of Table 2, no longitudinal lines were observed, either at room temperature or at any stage before the transformation. The mechanism of structure change was unusual in that the crystal bent up out of the plane of the slide and moved to one side. This shape change was reversible with cycling of temperature above and below the transformation point.

The longitudinal lines were clearly visible as fine surface effects, under Nomarski interference contrast and polarization interferometry.⁽¹²⁰⁾ Their width varied in the range 0.6×10^{-3} to 1.9×10^{-3} cms, as measured from photographic prints. The effect was reversible. Lines produced by heating disappeared on gradual or sudden cooling to form II again, whilst the few originally present, remain.

As already noted,⁽¹²⁰⁾ in transformed and untransformed regions of crystal, longitudinal lines were clearly apparent, and remain parallel

to the needle axis irrespective of any other transverse or oblique surface markings, in pseudomorphic crystals of relatively small shape change.

An interesting observation was made, which may be an experimental artefact. Under Nomarski interference contrast the lines disappeared when the crystal is rotated at $+45^{\circ}$ with respect to the needle axis, and were clearly evident or even more so at -45° .

On a $\{b\}_{II}$ face longitudinal lines were similar to $\{110\}_{II}$ pressure twins which were formed by gently rocking a new razor blade parallel to the basal plane until the crystal cleaved. A particular crystal was well-shaped with no surface imperfections or inclusions, had parallel extinction, and was dried under vacuum for $1\frac{1}{2}$ hours with a liquid nitrogen air trap. The crystal was originally untwinned, but both twinned and untwinned sections could be cut from it. Figures 1(a),(b) show the mechanically produced twin lamellae in $\{010\}_{II}$ and $\{001\}_{II}$ projections respectively, using transmitted, polarized light. In a $\{c\}_{II}$ face lamellae were not discernible in dark field conditions, in comparison to cleavage lines which were. With transmitted polarized light, the twins were inclined at 60° to a $\{b\}_{II}$ face.

Twinned directions

Six specimens of $\{b\}_{II}$ and $\{c\}_{II}$ projections were examined by X-ray precession, Laue and 15° oscillation photographs during heating to 120°C . $\{b\}_{II}$ projections were mounted with silicone grease, and $\{c\}_{II}$ with a drop of glue, Tarzan's Grip. The specimens were not rigorously dried, $1\frac{1}{2}$ hours in vacuum/liquid nitrogen.

Figure 1(a). KNO_3 II, $\{010\}$ face with lamellae \parallel to $[c]$, due to mechanical twinning. Negative magnification X65.

Figure 1(b). KNO_3 II, $\{001\}$ face with lamellae at 60° to $[b]$. Negative magnification X65. Optical microscopy; transmitted, polarized light.

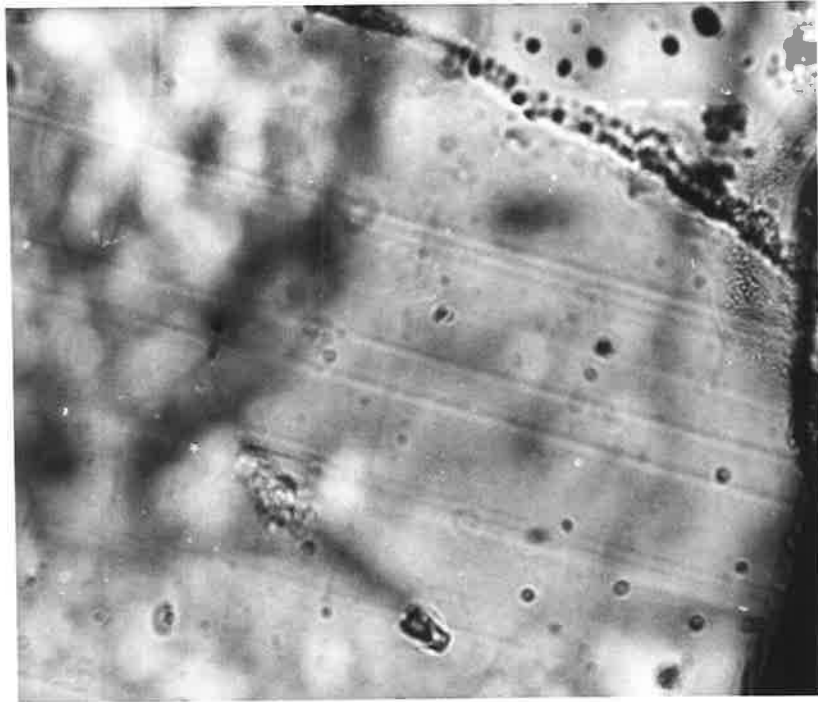


Figure 1(a)

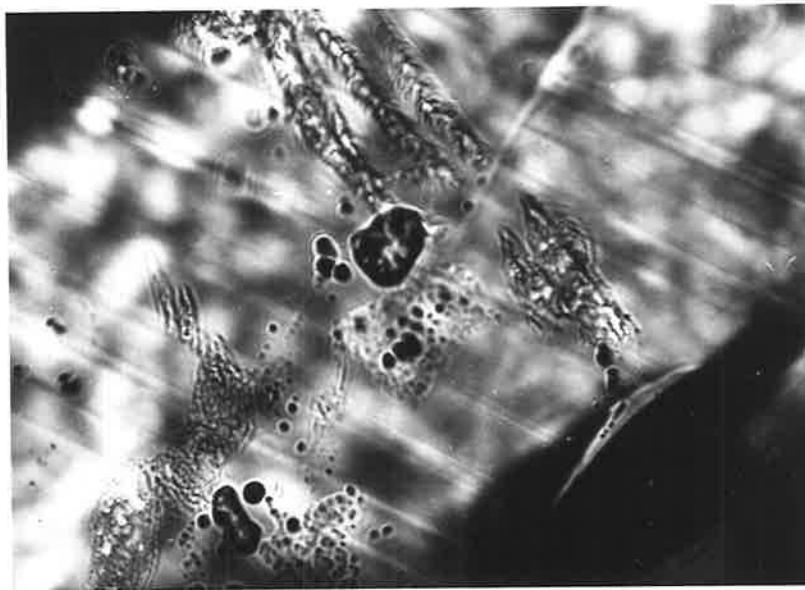


Figure 1(b)

TABLE 2
SUMMARY OF EXPERIMENTAL OBSERVATIONS
ON LONGITUDINAL LINES

Experiment Number	Method of Drying	Longitudinal lines before heating	Temp. when more LL's first appeared or whether LL's developed at all
1	Standing in atmosphere	-	developed LL's
2	½ hr in vac/ liq N ₂	-	developed LL's
3	overnight in vac/liq N ₂	-	LL's on other crystals, but none or any regular surface features on crystal under study; sudden transformation
4	39 hours over silica gel; 5¼ hours in vac/liq N ₂	Yes, faint	98°C
5	1 hr vac/ liq N ₂	no	80°C
6	3 days over silica gel; 5 hrs in vac/liq N ₂	yes	80°C
7	4½ hrs in vac/ liq N ₂	yes	beneath transforma- tion temperature.
8	4 hrs over silica gel; 12 hrs in vac/liq N ₂	no LL's	no LL's (unusual behaviour in that crystal moved).
9	standing in atmosphere	yes	76°C

TABLE 2 (Cont)

Experiment Number	Method of Drying	Longitudinal lines before heating	Temp. when more LL's first appeared or whether LL's developed at all
10	several months over silica gel	one well-defined wide band	others appeared but fainter than usual.
11	standing in atmosphere	-	yes
12	1½ hrs in vac/ liq N ₂	yes	yes

Figure 2(b). Laue photo of KNO_3II strained by mechanical twinning

Figure 2(a). X-ray precession of (001) level of KNO_3II mechanically twinned showing non-lattice point twin reflections.

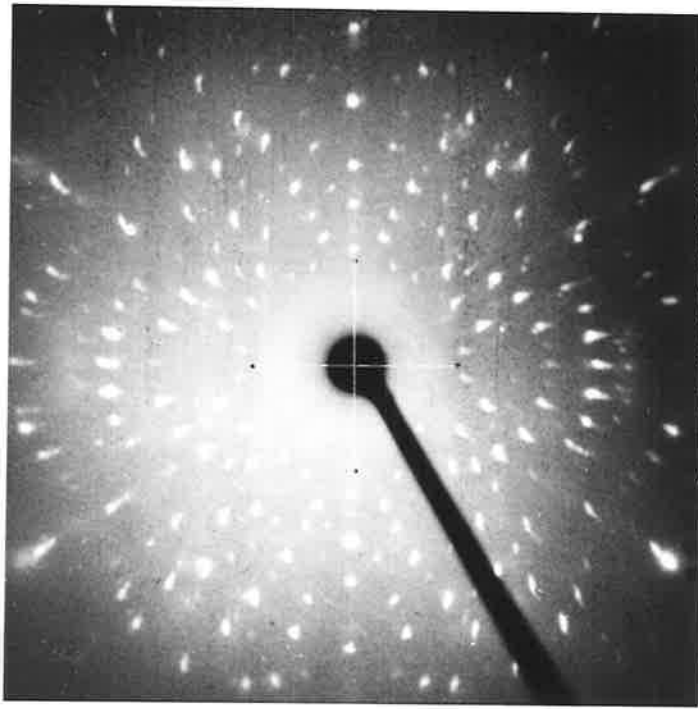


Figure 2(b)

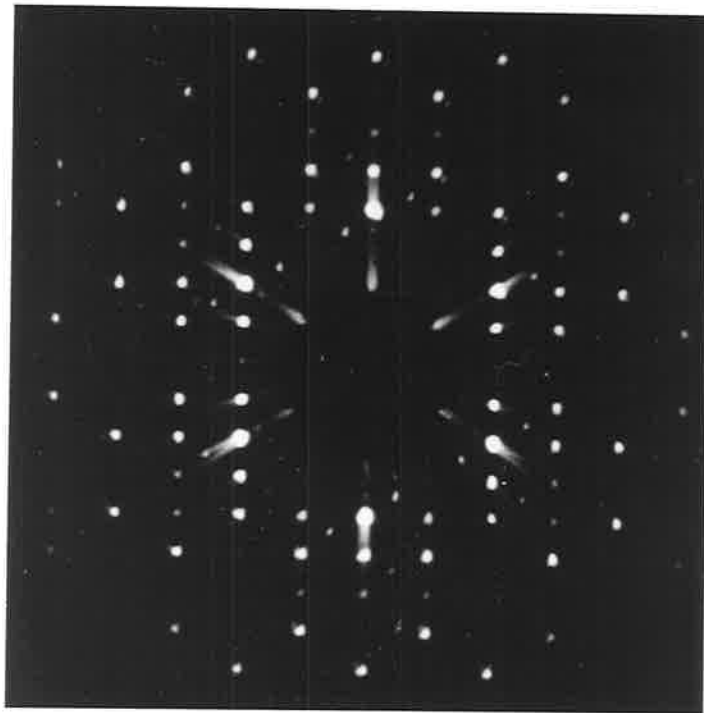


Figure 2(a)

Parent, $\{110\}_t$ and $\{\bar{1}10\}_t^{(180)}$ reciprocal nets of the $(001)_{II}$ layer were prepared. Due to systematic extinctions in the (hko) projection, a twin was more clearly seen in a (hkl) precession photograph, such as in figure 2(a), where twins produced satellite reflections to reciprocal lattice point reflections, and at extra non-lattice point sites. Streaked and split reflections in the corresponding Laue, figure 2(b) testified to the strained nature of the twinned crystal. $\{110\}$ twinning in KNO_3 is the same as in aragonite, $^{(208)}$ with an angle $(110) \wedge (1\bar{1}0)$ of 61.14 degrees.

In three experiments where a single, untwinned, crystal fragment in a $\{b\}_{II}$ or $\{c\}_{II}$ projection was heated to about $120^\circ C$, there were no indications of thermal $\{110\}_{II}$ type twinning, as compared to the remaining three experiments on pressure twinned specimens. Hence no conclusive evidence could be found that the longitudinal bands are due to thermal twinning, unless the proportion of the twin was so small as not to be discernible on the generously exposed X-ray photographs.

A possible explanation for the longitudinal lines may be that they are "water modified structure domains". In the aragonite-type orthorhombic structure hexagonal layers of cations are separated by nitrate anion layers, which are not exactly coplanar but slightly displaced in opposite directions along the $[c]_{II}$ axis, and are slightly tilted with respect to the basal plane.

In non-rigorously dried crystals, water molecules are trapped in the lattice of the relatively dense phase II. They may be hydrogen bonded to anions and electrostatically attracted to cations, or their

mere mechanical presence may alter the structure and cause it to adopt a configuration which is not the equilibrium one for the space group. The direction of longitudinal lines suggests that the water molecules disturb the structure in a small way, probably through the nitrate group, and cause some alignment with respect to the $[c]_{II}$ axis. Micro-domains of the modified structure are formed, similar to ferroelectric or anti-ferroelectric domains. ⁽²⁷²⁾

With increasing temperature the existing domains alter the lattice dynamics of the crystal and cause the formation of further modified structure domains. This is consistent with their disappearance on cooling. Kennedy et al.'s ⁽²⁷¹⁾ observation that the $[c]_{II}$ (S.G. Pmcn) often persist in "normal" crystals after transformation may therefore be associated with the above effect.

Furthermore, this effect may be involved with the hydrothermal catalysis of the aragonite to calcite transformation mentioned earlier, in contrast to the extremely slow transformation geologically observed in metastable aragonite. In any case it is suggested that the appearance of longitudinal lines indicates the extent of crystal dryness.

SECTION 4.3.2 Optical Microscopy

In the following presentation of optical microscope observations, for the sake of simplicity, observations are classified approximately by the extent of crystal dryness. Leaving in the presence of silica gel is not considered to be an efficient method of drying in this case, as seen in the previous section.

"Normal" crystals are those left standing in the atmosphere, or left under vacuum for less than 12 hours; "normal/dry" refers to crystals left under vacuum with a liquid nitrogen air trap, overnight; and "dry" very approximately describes specimens left under vacuum at room temperature with a liquid nitrogen air trap for over 12 hours

During the work for this thesis, 9 transformation experiments were performed on "normal" crystals, 5 on "normal/dry" crystals and 3 on "dry" crystals. The method usually adopted was slowly to heat crystals over a period of up to two days, leave to anneal just below 128°C for several hours or overnight, and gradually to increase the temperature in very small increments. Specimens were thinly gold coated.

Experiments yielding interesting observations are summarized as follows, and in Table 3. The previously reported observations (105, 221, 120) of a straight interface parallel to the basal plane as viewed in a $\{b\}_{II}$ face, etch pits, undulose extinction and a variety of extinctions in the product phase, were noted.

In "dry" crystals shape changes tended to be pronounced, as seen for example in figure 3, corresponding to experiment number 16

Figure 3. KNO_3I , transverse surface tilts. Nomarski interference contrast. Negative magnification X450.

Figure 4(a). $KNO_3II \rightarrow I$. Transmitted polarized light and negative magnification X140.
Figure 4(b).

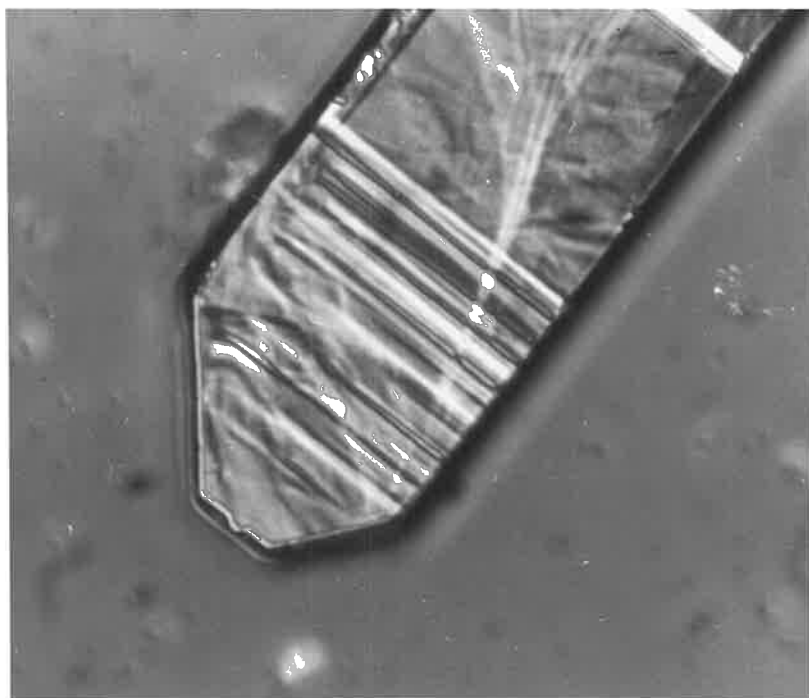


Figure 3



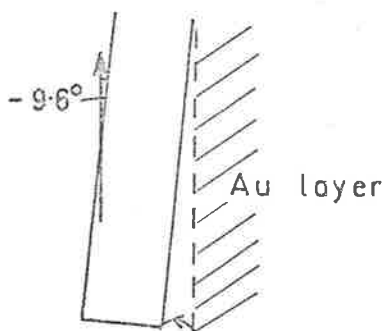
Figure 4(a)



Figure 4(b)

in Table 3, and the crystal referred to in experiment number 8 of Table 2 in Section 4.3.1. During the heating of this latter crystal no longitudinal lines were evident or appeared. Under Nomarski interference contrast the crystal surface showed some faint transverse effects after annealing below the transformation for $39\frac{1}{2}$ hours. An interface suddenly passed over the crystal leaving no regular surface markings. The entire crystal was extinct at -9.6° .

On suddenly switching off the heating current, the crystal moved out of the plane of the slide and across, as an interface flashed across it. The movement of the crystal was referenced against the gold layer boundary between the crystal and slide.



On cycling the temperature between room temperature and phase I temperature this shape change was immediately produced in alternating directions, each time accompanied by the passage of an interface.

Eventually due to the recyclings of temperature the crystal underwent a shape change so that its end stood out from the plane of the slide. It is to be noted that this crystal was relatively long and that the other end of the region observed was fixed. For discussion

this crystal is referred to a crystal A.

Crystal B of figure 4(a),(b) was "normal" and superheated to about 160°C . It was a small rectangular-shaped crystallite and apparently fixed at its end under the glass coverslip, and hence at a relatively higher temperature than normal at transformation. It transformed when a transverse interface, that is, one parallel to the basal (II) plane as seen in a $\{b\}_{\text{II}}$ projection, rapidly moved along its length, causing a zig-zag shape change. The extinction direction was measured perpendicular to the transverse lines, and hence apparently maintained.

In figure 4(a) the crystal kinks through 7° while in figure 4(b) angles of 12° and 15° are observed. Similar behaviour was noticed in acicular needles lying on each other or neighbouring crystallites, and hence not completely flat.

In two separate experiments, "normal" crystals transformed with a V shaped interface. The perpendicular interface bent 54° with respect to the $[c]_{\text{II}}$ axis, as shown below.

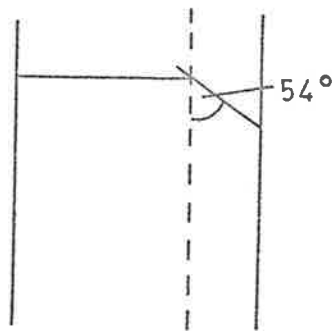


Figure 5. Phase I surface showing faint transverse traces and heavy oblique lines. Crystal corresponds to experiment number 1 of Table 3. Normarski interference contrast, neg. mag. X125.

Figure 6. The KNO_3I crystal corresponding to experiment 3 of Table 3. Transmitted, polarized light. The fine mixture of twins are regions of undulose extinction, as shown in figure 6(b). Neg. mag. X225.

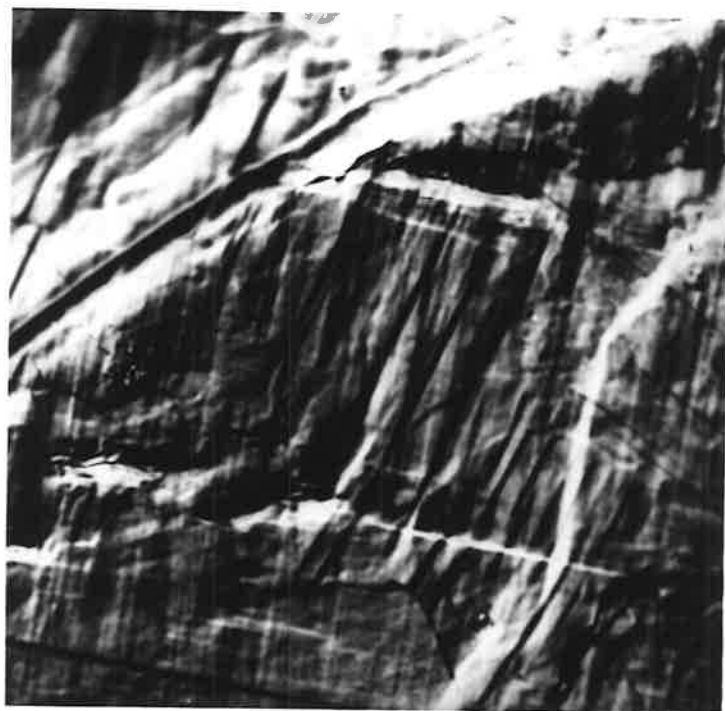


Figure 5.

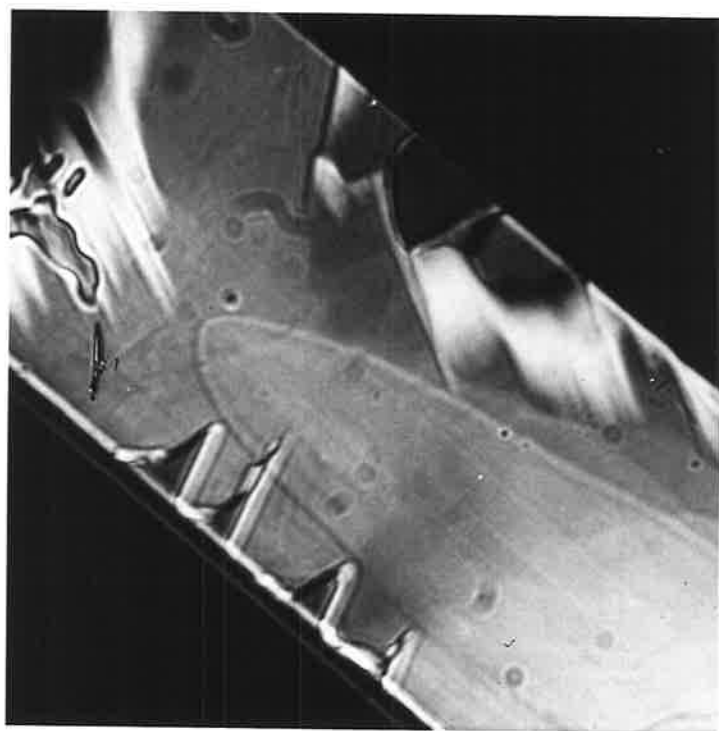


Figure 6.

[4.3.2]

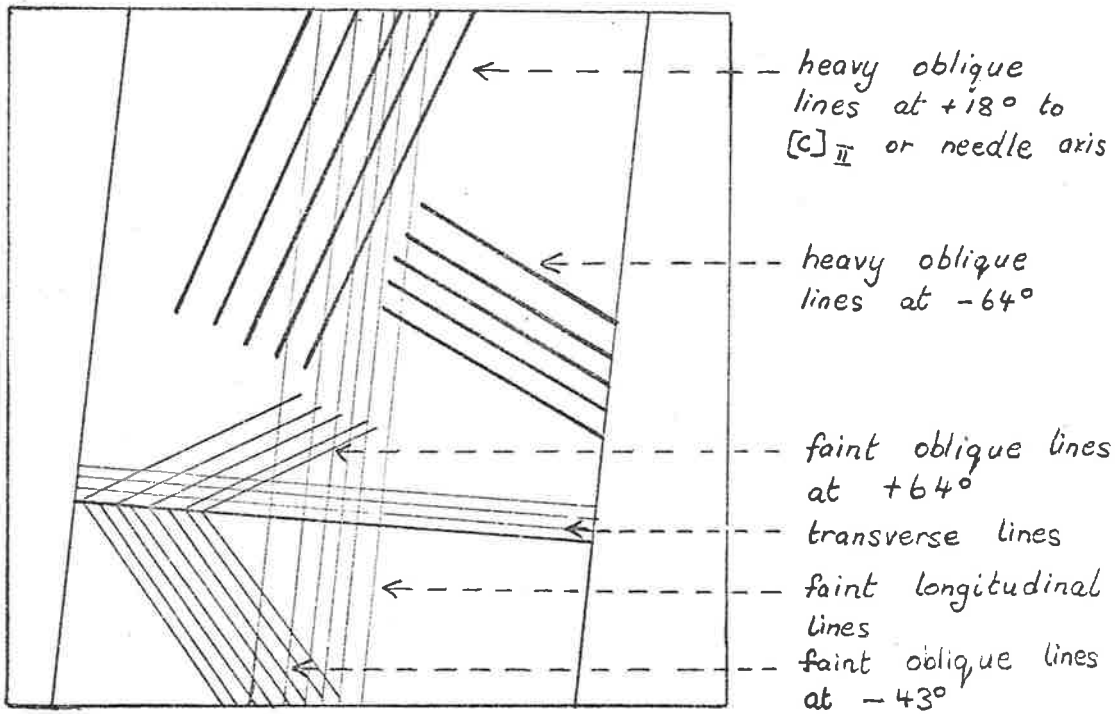


Figure 3.1 Orientation of surface traces in product KNO_3 I crystal of undulose extinction. Figure corresponds to Fig 5, and hence experiment 1 of Table 3.

[4.3.2]

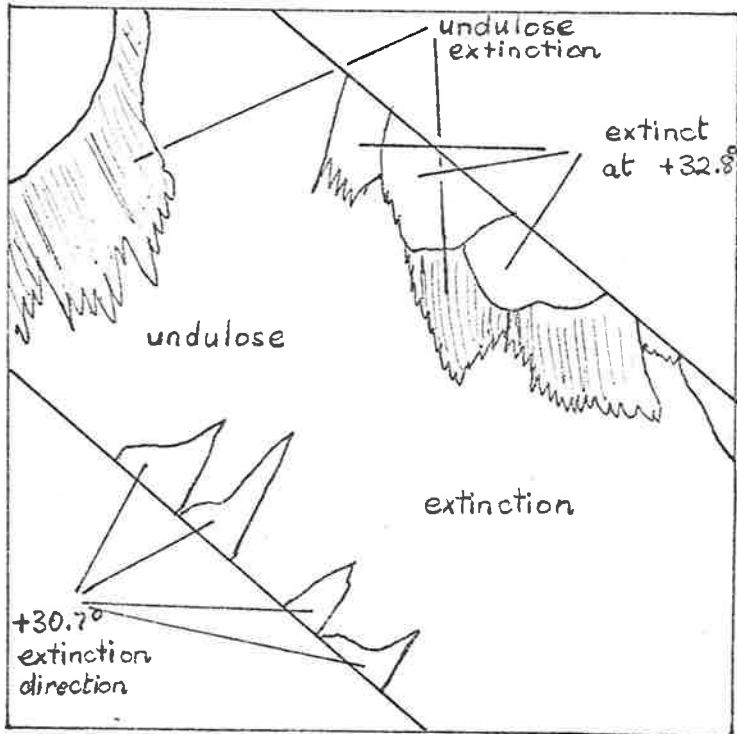


Figure 3.2 Extinction directions of phase I crystal, Figure 6 corresponding to experiment 3 of Table 3.

Phase I nucleated in another "normal" crystal in rectangular sites *not* parallel to the basal plane, the sites being inclined at 56° to the $[c]_{II}$ axis. On a stereogram, the 54° to $[c]_{II}$ interface lies on a zone 3° from $\{2k3\}_{II}$ and 5° from $\{1k2\}_{II}$, whilst the 56° interface lies on a zone 3° from $\{1k2\}_{II}$ and $\{5^0\}$ from $\{2k3\}_{II}$ zones.

As well as the relatively large surface tilts parallel to the basal (II) plane, regular, fainter surface changes were sometimes discernible on the $\{b\}_{II}$ face parallel and inclined to the basal plane. In some experiments, heavier oblique lines, possibly slip traces, were also found, figure 5.

Table 3 summarizes experimental observations of fainter surface effects on transformed $\{b\}_{II}$ and $\{c\}_{II}$ planes. As indicated, in some experiments extinction directions could not be determined accurately due to fine twins (such as in figure 6), compensation fringes as shown by use of quartz wedge, or a mixture of layers of different extinctions. A "normal", apparently untwinned crystal was sliced, mounted on a $\{c\}_{II}$ face and gold coated; the faint parallel markings following the transformation are also listed. The fast extinction direction was determined with a quartz wedge.

From Table 3 it is seen that surface traces were close to certain zones. Oblique traces are close (within the given average angular difference) to zones or planes of the type $\{1k2\}$ w/n $2\frac{1}{2}^\circ$, $\{3k2\}$ w/n $2-1/3^\circ$, $\{2k1\}$ w/n $3\frac{1}{2}^\circ$, $\{1k3\}$ w/n 3° , $\{3k1\}$ w/n 3° , $\{1k4\}$ w/n $1\frac{1}{2}^\circ$, and between $\{1k1\}$ by 5° and $\{2k3\}$ by 6° . Similarly, on the $\{c\}_{II}$ face markings are close to $\{12\bar{l}\}$ w/n 2° , $\{13\bar{l}\}$ w/n $\frac{1}{2}^\circ$, $\{23\bar{l}\}$ w/n 2° ,

{21 $\bar{1}$ } w/n 0°, {11 $\bar{1}$ } w/n 3-1/3°.

Figures 7 to 10 inclusive illustrate some of the crystals and effects described in Table 3. Figures 3.1 to 3.4 illustrate product orientations of various crystals corresponding to Table 3.

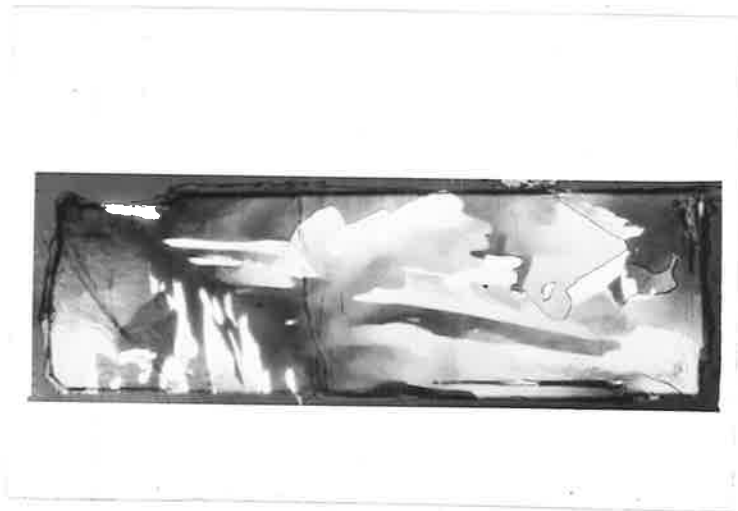


Figure 7. Polycrystalline KNO_3 with apparently overlapping layers of different extinction directions and undulose extinction. A "normal" crystal corresponding to experiment 1 of Table 3. Transmitted polarized light, neg. mag. X125, total mag. X330.

Figure 7(a). Interference contrast microscopy of KNO_3I surface. Faint oblique traces on crystal(i) of exp. no.7 in Table 3. Neg. mag. X225. Total mag. X900.

Figure 7(b). Interference contrast microscopy of KNO_3I surface. Faint transverse coexisting with oblique traces at -45° to $[c]_{\text{II}}$, in region of undulose extinction. Crystal corresponds to experiment 6 of Table 3. Neg. mag. X225. Total mag. X900.

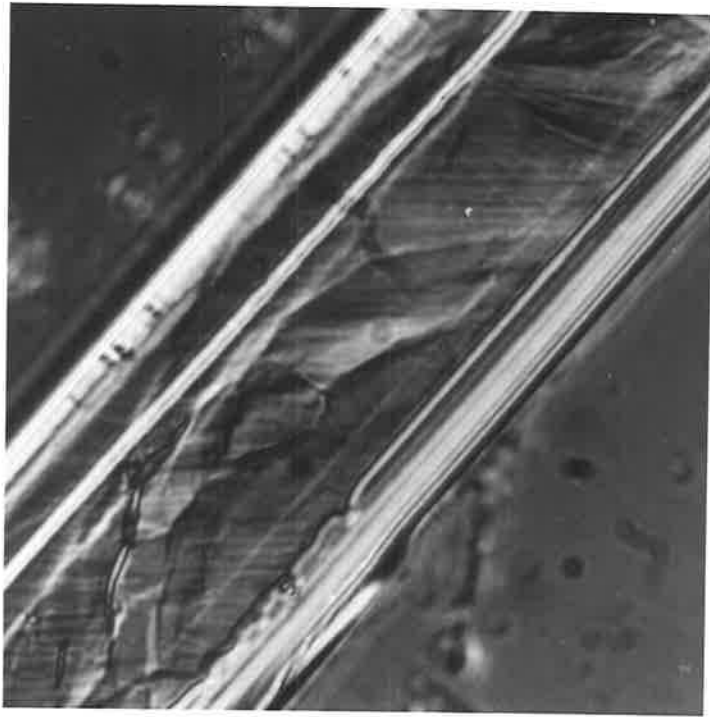


Figure 7(a)

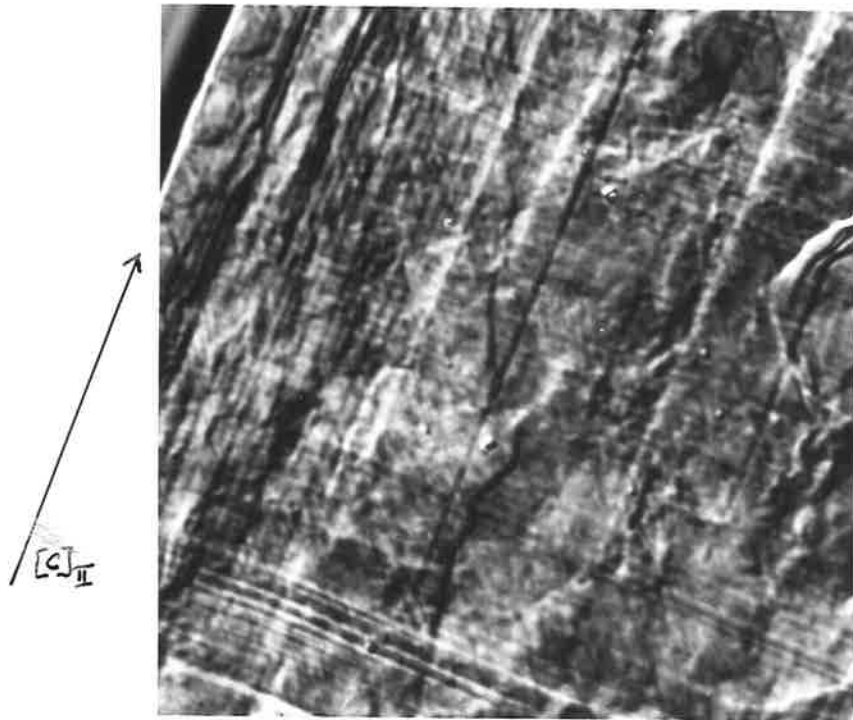


Figure 7(b)

Figure 8. Interference contrast of KNO_3 I.
When temp. was suddenly increased, this
"normal/dry" crystal transformed with
prominent surface tilts with subtexture.
Neg. mag. X450.

Figure 9. Interference contrast of KNO_3 II \rightarrow I.
Stationary interface with faint transverse
markings and longitudinal lines.
Crystal from exp. no. 5 of Table 3.
Neg. mag. X225.

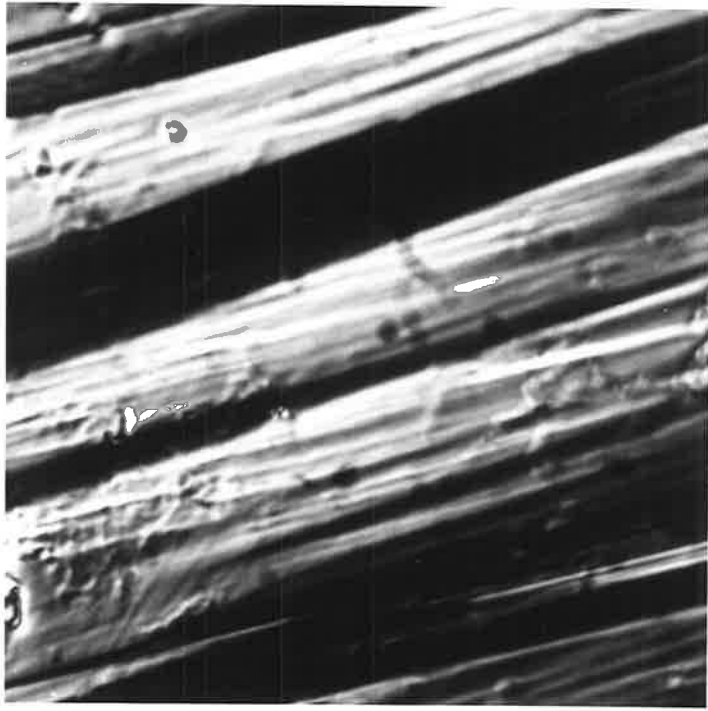


Figure 8.

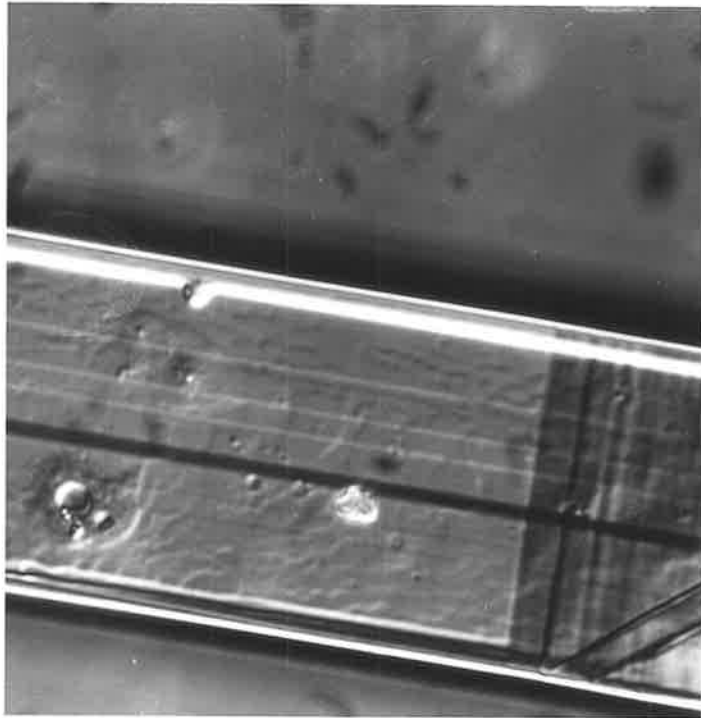


Figure 9.

Figure 10. $\text{KNO}_3\text{II} \rightarrow \text{I}$ by transmitted polarized light microscopy. Interface is irregular and diffuse in places. Crystal was dried only by standing in atmosphere. Corresponds to same batch as exp. no. 9 of Table 3. Neg. mag. X140.

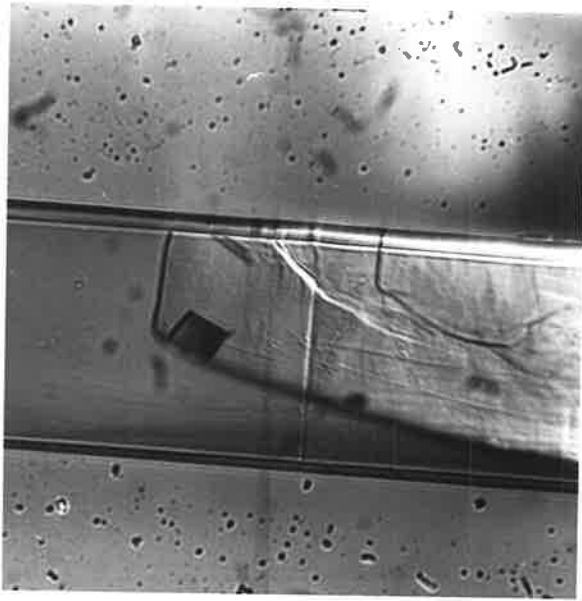


Figure 10(a)

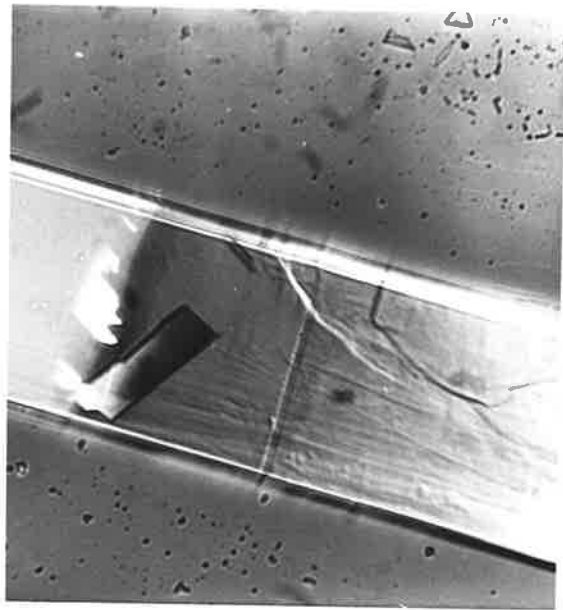


Figure 10(b)

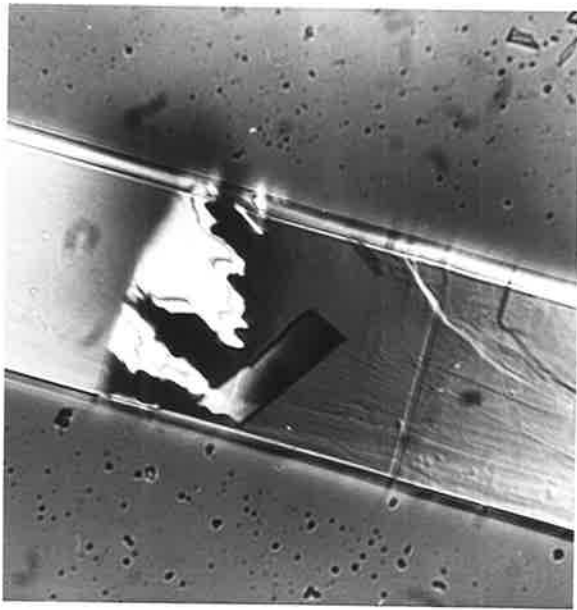


Figure 10(c)

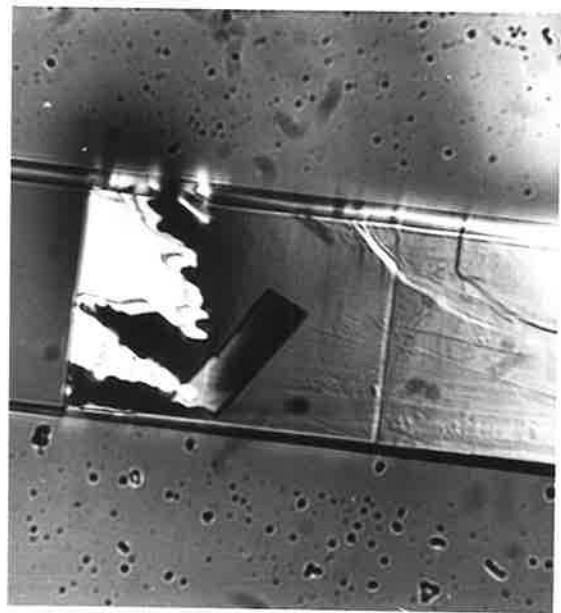


Figure 10(d)

[4.3.2]

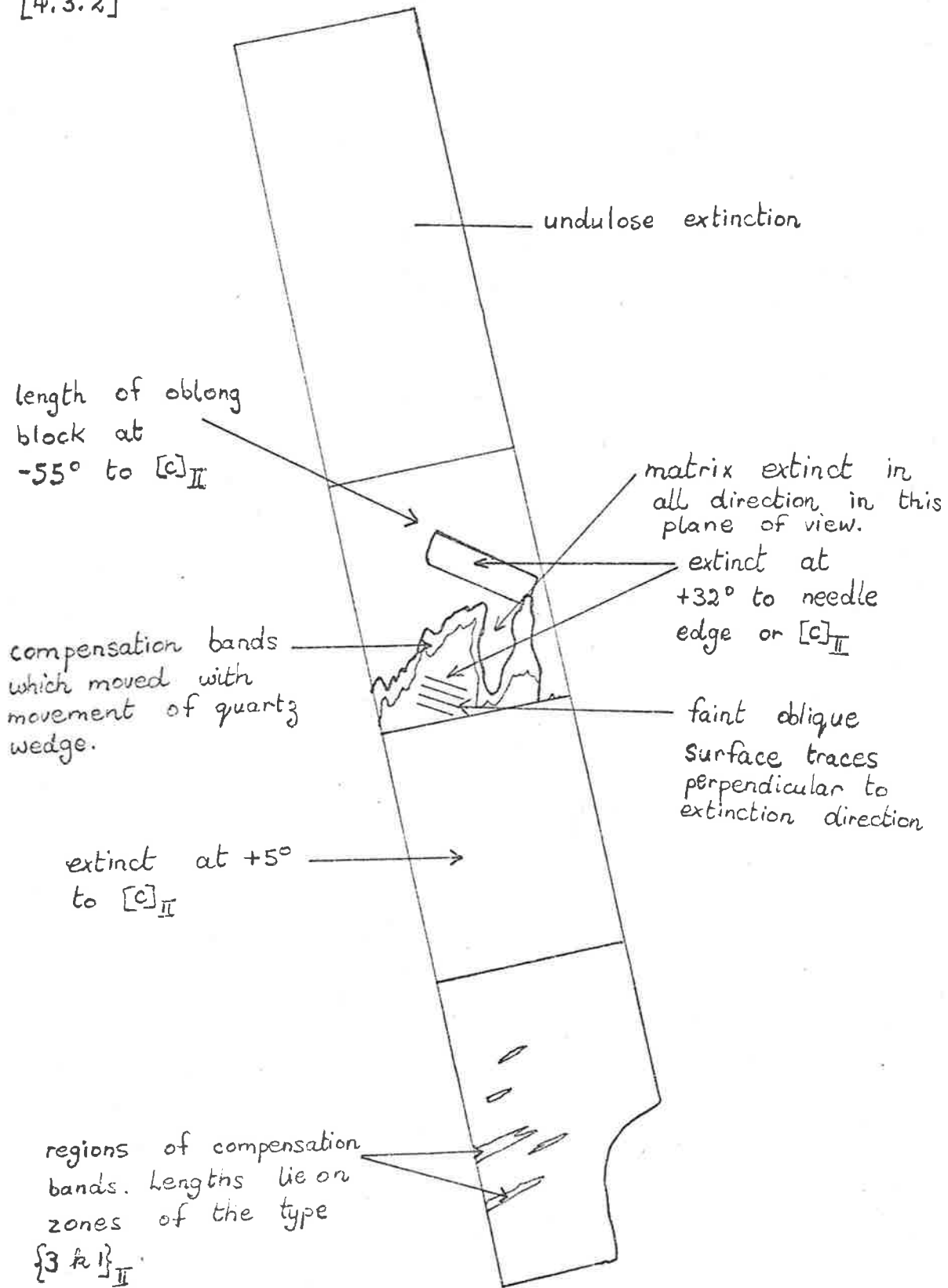


Figure 3.3 Product orientations of crystal corresponding to Figure 10 (a) to (d).

[4.3.2]

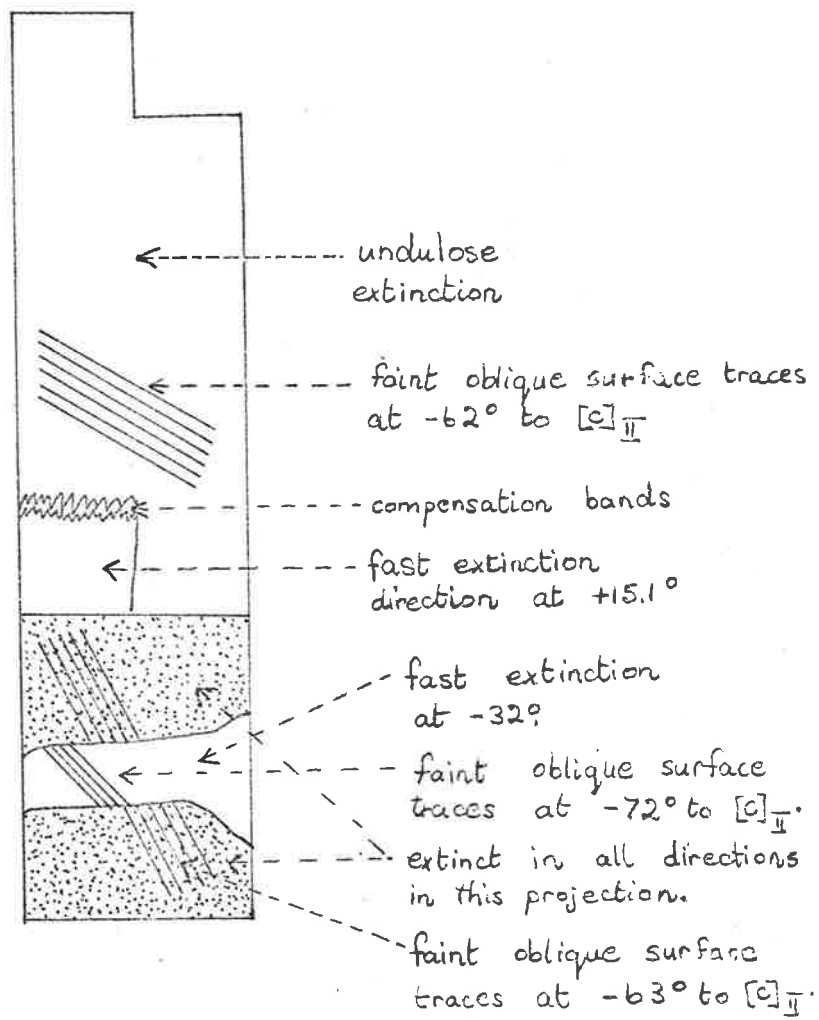


Figure 3.4 Product orientations and surface effects of crystal corresponding to experiment 10, Table 3.

TABLE 3

SURFACE EFFECTS ACCOMPANYING THE II \rightarrow I TRANSFORMATION IN KNO_3

{b} face: (a positive angle denotes the clockwise rotation of extinction direction)

Exp. No.	Extent of dryness	Description	Orientation w.r.t. $[\text{c}]_{\text{II}}$	Possible index in II (within x°)	Extinction direction	
1	normal	heavy lines	+18 $^\circ$	between $\{\bar{1}k4\}$ (1°) and $\{\bar{1}k3\}$ ($3\frac{1}{2}^\circ$)	undulose	
		heavy lines				not in same region
		faint oblique lines	co-exist- ing	-43 $^\circ$	between $\{2k3\}$ ($4\frac{1}{2}^\circ$) and $\{1k1\}$ (7°)	
		faint oblique lines				+64 $^\circ$
2	normal	faint transverse	-90 $^\circ$	$\{001\}$ or $\{0k1\}$	—	
		faint oblique	+58 $^\circ$	$\{\bar{3}k2\}$ (3°)	—	
		faint oblique only	+65 $^\circ$	between $\{\bar{2}k1\}$ ($2\frac{1}{2}^\circ$) and $\{\bar{3}k2\}$ (4°)	maintained	
3	normal	faint regular oblique markings	-55 $^\circ$	between $\{1k\bar{1}\}$ (5°) and $\{3k2\}$ (6°)	undulose & also comp- ensation bands	
		faint markings	-71 $^\circ$	between $\{2k1\}$ ($3\frac{1}{2}^\circ$) and $\{3k1\}$ ($3\frac{1}{2}^\circ$)		
		faint markings	+27 $^\circ$	between $\{\bar{1}k2\}$ ($4\frac{1}{2}^\circ$) and $\{\bar{1}k3\}$ (5°)	"	

continued/...

TABLE 3 (Cont)

Exp. No.	Extent of dryness	Description	Orientation w.r.t. [c] _{II}	Possible index in II (within x°)	Extinction direction	
4	normal	faint oblique lines	-56°	between $\{3k2\}$ (5°) and $\{1k1\}$ (6°)	-68°	
		heavy oblique lines	$+60^\circ$	$\{\bar{3}k2\}$ ($1\frac{1}{2}^\circ$)	undulose but about -16.8° in this region	
5	normal	relatively faint traverse lines	90°	$\{001\}$ or $\{0k1\}$	maintained, but also compensation bands.	
6	normal	traverse and faint oblique lines together	-45°	between $\{1k1\}$ (5°) and $\{2k3\}$ ($6\frac{1}{2}^\circ$)	overlapping, undulose	
7	normal crystal(i)	faint transverse	90°		-19.7°	
		faint oblique markings				} coexisting in parts
		faint oblique effects	$+50^\circ$	$\{\bar{1}k1\}$ (0°)	undulose but between -4.4° and -18.2° extinct in all directions	
crystal(ii)					fast extinction at $+14.0^\circ$	
crystal(iii)		a few transverse effects				

TABLE 3 (Cont)

Exp. No.	Extent of dryness	Description	Orientation w.r.t. $[c]_{II}$	Possible index in II (within x°)	Extinction direction
		faint oblique markings	$+47.5^{\circ}$	$\{\bar{1}k1\}$ (3°)	fast extinction at -55.5°
		faint transverse lines only	90°		fast extinction at -90°
8	normal	no regular effects			undulose
9	normal fig 4(a),(b)	transverse markings only	90°	$\{001\}$ or $\{0k1\}$	perpendicular to transverse effects
10	normal/dry crystal(i)	no regular surface effects			undulose, but about fast extinction -13.1°
	crystal(ii)	faint oblique markings	-63°	$\{3k2\}$ (2°)	extinct in all directions
		faint oblique markings	-72°	between $\{3k1\}$ ($2\frac{1}{2}^{\circ}$) and $\{2k1\}$ ($4\frac{1}{2}^{\circ}$)	-32.4°
		faint oblique markings	-62°	$\{3k2\}$ ($\frac{1}{2}^{\circ}$)	undulose, but between $+23.8^{\circ}$ and $+31.8^{\circ}$
11	normal/dry	no regular surface effects			undulose extinction

TABLE 3 (Cont)

Exp. No.	Extent of dryness	Description	Orientation w.r.t. [c] _{II}	Possible index in II (within x°)	Extinction direction
12	normal/dry	longitudinal lines present, faint transverse effects	90°	{001} or {0k1}	maintained
13	normal/dry	longitudinal lines, transverse effects	90°	{001} or {0k1}	undulose
14	normal/dry	well defined transverse tilts	90°	{001} or {0k1}	fast extinction maintained
15	dry	"crystal A' described earlier			
16	dry (42 hrs under vac/ liq N ₂) crystal(i)	part (a) faint longitudinal lines only, no other regular effects (b) faint transverse tilts (c) faint oblique lines (d) rows of markings similar to dislocation pits parallel to oblique lines rate of interface travel at constant temperature = 3.02 x 10 ⁻⁴ cms/min.	90° +21° +21°	{ $\bar{1}k3$ } (1°) { $\bar{1}k3$ }	fast extinction maintained

TABLE 3 (Cont)

Exp. No.	Extent of dryness	Description	Orientation w.r.t. $[c]_{II}$	Possible index in II (within x°)	Extinction direction
fig. 3	crystal(ii)	well defined transverse surface tilts			fast extinction direction maintained
		coexisting with faint oblique effects	-44°	{2k3} (5°)	
			$+62^\circ$	{1k1} ($6\frac{1}{2}^\circ$)	"
17	dry (48 hrs under vac/ liq N ₂)	no regular effects, faint longitudinal lines only.			fast extinction direction maintained
		faint oblique effects only	$+60^\circ$	{1k2} (0°)	
		faint transverse effects only	$+90^\circ$	{001} or {0k1}	
$\frac{[c]_{II}}{18}$	face : normal	faint, parallel effects	w.r.t. $[a]_{II}$		
			-20°	$\{\bar{1}5\bar{1}\}$ (1°), $\{\bar{1}4\bar{1}\}$ (3°)	
			-29°	$\{\bar{1}3\bar{1}\}$ ($1\frac{1}{2}^\circ$)	
			$+55^\circ$	$\{\bar{1}\bar{1}\bar{1}\}$ ($4\frac{1}{2}^\circ$)	
			-63°	$\{\bar{1}\bar{1}\bar{1}\}$ ($3\frac{1}{2}^\circ$)	
			-38°	$\{\bar{1}2\bar{1}\}$ (2°)	
			-66°	$\{\bar{3}2\bar{1}\}$ (2°)	
			$+58^\circ$	$\{\bar{1}\bar{1}\bar{1}\}$ (2°)	
			$+47^\circ$	$\{\bar{2}3\bar{1}\}$ (2°)	
			-73°	$\{\bar{2}1\bar{1}\}$ (0°)	

SECTION 4.3.3 Scanning Electron Microscopy

It was considered desirable to examine the surface of KNO_3I at higher magnifications such as in a scanning electron microscope. The microscopes available however, were not sufficiently versatile to contain a heating stage, so that a replica of the surface needed to be made. The idea essentially was to find a fluid which could be poured on the water-soluble crystals above 130°C , usually at about 160°C to allow for superheating prior to transformation, but less than 190°C to avoid recrystallization.⁽¹⁰⁵⁾ The fluid was allowed to polymerize in situ, faithfully replicating the surface. Crystals were washed away, preferably at the high temperature.

The replica was washed, dried, coated with a conducting surface, and examined in the scanning electron microscope. Only a moderate level of success was achieved, and various attempts are briefly outlined below.

Experiments were conducted on a hot plate whose temperature was set by means of an in-series variac (voltage transformer), and monitored by a thermometer suspended in a 50 ml beaker of silicone oil. This was used in preference to ethylene glycol whose vapour has some carcinogenic properties (Organic Chemistry Department). Crystals were transformed on a heating stage, transferred to the hot plate, and the polymer fluid applied.

The various monomers unsuccessfully tried were: araldite⁽²⁷³⁾ of various types, such as Araldite CY246 + Hardener HT976, Araldite AV8, which was supplied with other information by Mr Tom Kirkwood of Ciba-

Geigy Pty. Ltd., S.A. Crystals tended to be absorbed in the polymer matrix, and even with the use of microtomy to reveal the surface, it was found that the replica was not sufficiently sensitive to the surface effects.

A high molecular weight monomer prepared by Mr. Wally Dankiw of the polymer section of this department, ethylene glycol dimethyl methacrylate, was unsuccessful, as were attempts with various commercial products such as fibreglass, Canada balsam, Davis Fuller Resiweld, Estapol, plastic porcelain, new Apiezon Black Wax, Silastic E RTV moulding rubber, Dow Corning Silastic D. Similar results were obtained with monomers forming polystyrene, and polystyrene cross-linked with divinyl benzene, divinyl benzene alone, and an α -methyl methacrylate polymer dissolved in O-xylene, all of which were obtained from the polymer section of this department.

Attempts were made with inorganic polymers such as polyamides⁽²⁷⁴⁾ and siloxanes (both organic and inorganic),⁽²⁷⁵⁻²⁸⁰⁾ where eventually a suitable monomer fluid may have been developed if there was sufficient time to invest in this approach. A replica which was partly successful was a cellulose acetate film melted on at high temperature. The film was used in the S.A. Government Mines Department to replicate rock specimens. The rocks are coated with acetone, and an approximately 2 mm thick layer of film is applied and selectively etched.

The following method was developed to produce a room temperature replica. A piece of cellulose acetate film is thermally equilibrated

to 140°C on a glass slide on the hot plate, and then the slide and film are upturned on the KNO₃ specimen, and left for one minute. The crystals and slide are shock cooled in a thermos of liquid nitrogen, during which the coverslip supporting crystals and the slide separate easily; the cellulose acetate is washed several times in distilled water, dried, and coated with a thin layer of vacuum-evaporated gold, enabling examination by Nomarski interference contrast microscopy.

Unfortunately, however, when examined at higher magnifications in the scanning electron microscope, the heating and radiation effect of the electron beam caused destruction of the specimen. Some initial experiments were then made of a two stage replication technique⁽²⁸¹⁾ where a more stable replica of the first replica was made. However, due to time limitations, this avenue of investigation was discontinued, in anticipation of the advent of scanning electron microscopes fitted with internal specimen heating stages.

SECTION 4.3.4 Transmission Electron Microscopy

Potassium nitrate is very sensitive to electron radiation in the electron microscope, as described in Chapter 3 of this thesis.

However, by extremely careful observation, two orientations for the II \rightarrow I transformation were found, and they are described below. The specimen preparation and experimental procedure are given in Chapter 3, and the relations are numbered [n] in this and the next section.

Relation [1]

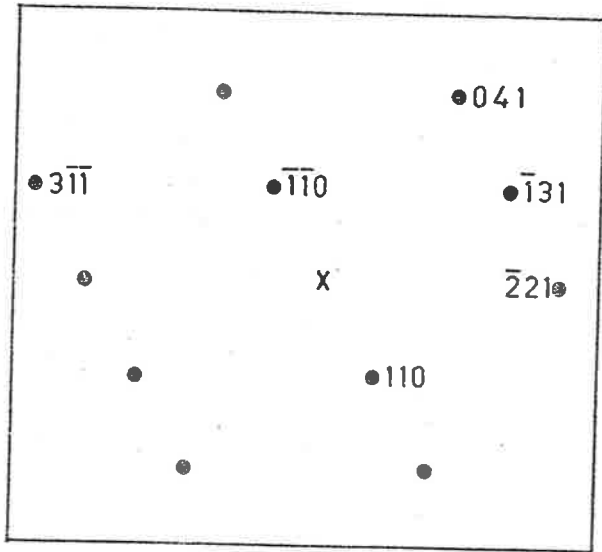
This is presented as relation [5], figure 2(a),(b) in Chapter 3, Section 3.2. It was accompanied by "extra reflections" and subsequently the nitrate decomposed to KNO_2I . The relation is:

$$\begin{array}{l} (001)_{\text{KNO}_3\text{II}} \parallel (111)_{\text{KNO}_3\text{I}, \text{Rh}, Z=4} \\ [100]_{\text{II}} \parallel [01\bar{1}]_{\text{I}} \text{-----} [1] \end{array}$$

In terms of the hexagonal $Z = 3$ or $Z = 6$ cells of phase I, relation [1] corresponds to $[c]_{\text{II}} \parallel [c]_{\text{I}}, [a]_{\text{II}} \parallel [a]_{\text{I}}$. It is the same as the aragonite-calcite orientation in the electron microscope, reported earlier⁽²²⁰⁾ but no "extra reflections" were noted.

Relation [2]

The parent, intermediate stage, and product diffraction patterns are given in figures 11(a),(b),(c). The parent projection was indexed, within an angular difference of 1° and an average difference of a spacing of 0.8%, as the $[1\bar{1}4]_{\text{II}}$ zone axis, or 5° from the $(1\bar{2}4)_{\text{II}}$ plane. The product diffraction pattern was previously observed during the aragonite-calcite transformation in the AEI M6G electron microscope, by



$\text{KNO}_3 \text{ II}$ Projection is 5° from $(\bar{1}\bar{2}4)$ or $[\bar{1}\bar{1}4]$

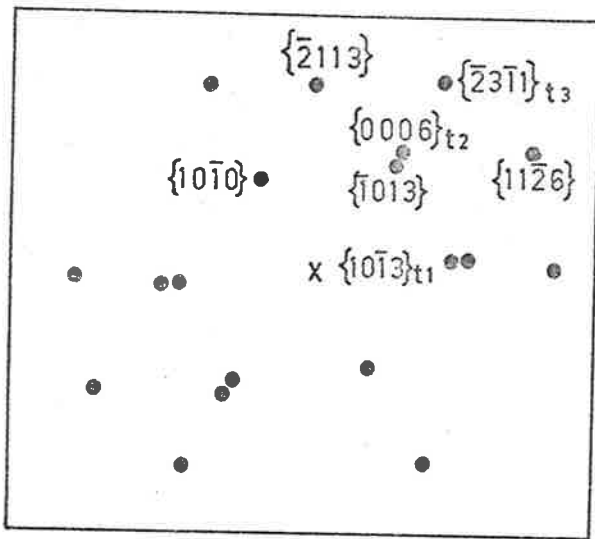


Fig. 12 (a)
 $\{\bar{1}\bar{2}19\}$ hex, $Z=6$
 projection of $\text{KNO}_3 \text{ I}$

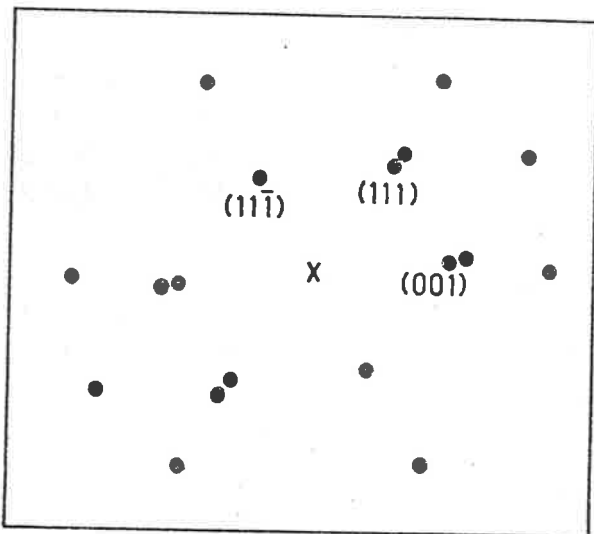


Fig 12 (b)
 $(\bar{1}\bar{1}0)$ Rh, $Z=4$
 projection of $\text{KNO}_3 \text{ I}$



Figure 11(a)
 $KNO_3 II$ in $[1\bar{1}4]$
projection



Figure 11(b)
 $KNO_3 II \rightarrow I$
intermediate
pattern.



Figure 11(c)
 $KNO_3 I$ twinned
product pattern.

S.W. Kennedy of this laboratory,⁽¹⁰⁸⁾ (see also Chapter 3). The carbonate pattern was unable to be indexed, which was also almost the case in KNO_3 ; in fact not all of the pattern was explained.

Two sets of indices were proposed for the product pattern, and are illustrated in figure 12(a),(b). In the first, (a), the average angular difference is less than 1° and the average ratio of $d(\text{obs})/d(\text{calc})$ is 2.6%. The projection is then $\{11\bar{2}9\}_{\text{I,hex},(Z=6)}$ with contributions from twins on $(10\bar{1}0)_{t_1}$, $(\bar{1}018)_{t_2}$, and $(10\bar{1}8)_{t_3}$. However, objections to this indexing arise from the fact that most of the untwinned pattern, including the double intense reflections, are attributed to indices which are supposed to be systematically extinct, even after brief consideration of the application of the dynamical theory of diffraction to this case.⁽²⁸⁸⁻²⁹¹⁾

Except for a maximum angular difference of 4° between expected and observed reflections for the projection considered, and an average $d(\text{obs})/d(\text{calc.})$ of 108.5%, the second, (b) indexing appears to be more satisfactory, although it is unable to explain the doublet intense reflections indicated in the figure. This difference in ratio of observed to calculated d spacings may not be significant, in view of a probability that the substance was simultaneously decomposing. Notwithstanding, Midorikawa et al⁽²⁸²⁾ found that no noticeable change in KNO_3 lattice parameters could be detected with up to 20% KNO_2 in $\text{KNO}_3(\text{II})$, in solid solution. If the second indexing is based on a thermally expanded cell at 335°C , just below the melting point, the maximum

angular difference is 1° , whilst the average $d(\text{obs})/d(\text{calc})$ is 106.0%. An advantage of the second indexing is that the intense reflections are attributed to $(100)_{\text{I,Rh,(Z=4)}}$ and $(111)_{\text{I,Rh,(Z=4)}}$ planes which theoretically diffract as the most intense and of relatively strong intensity, respectively. The second proposed indexing is a $(\bar{1}10)_{\text{I,Rh,(Z=4)}}$ projection with possibly some other form of twinning which produces the doublet intense reflections.

On the basis of the second indexing therefore, the intermediate photograph indicates a movement of planes in the zone containing the

$[111]_{\text{I,Rh}}$ axis. The orientation relation is

$(110)_{\text{II}} \parallel (11\bar{1})_{\text{I,Rh,(Z=4)}}$ such that

$[1\bar{1}4]_{\text{II}} \parallel [1\bar{1}0]_{\text{I}} \text{ --- --- --- --- --- --- --- --- --- } [2]$

giving $[021]_{\text{II}} \wedge [111]_{\text{I}} = 4\frac{1}{2}^\circ$.

SECTION 4.3.5 X-Ray diffraction

Orientation relations were determined mostly by X-ray precession, but also by Laue photography.

Relation [3]:

A basal section of a "normally" dried crystal was mechanically twinned on $\{110\}_{II}$ by slicing with a razor blade, and mounted with a drop of Tarzan's Grip on the heating, glass slide, in a $\{c\}_{II}$ projection. The strained nature of the crystal was apparent in the Laue photograph, seen in figure 2(b) of Section 4.3.1. In figure 2(a) non-lattice point twin reflections are clearly apparent in the corresponding first level precession photographs. During the slow heating to transformation, $\{110\}_{II}$ twinning remained. Following an intermediate stage in which both phases coexisted, as illustrated in figure 13(a), a single crystal product resulted, figures 13(b) to (f), in the orientation

$$(001)_{II} \parallel (0001)_{I,hex,(Z=3)}; [010]_{II} \parallel [11\bar{2}0]_I \text{ ----- [3]}$$

$$\text{that is, } [c]_{II} \parallel [c]_I, [b]_{II} \parallel [a]_I.$$

In terms of $Z = 4$ cells,

$$(001)_{II} \parallel (111)_{I,Rh,(Z=4)}; [010]_{II} \parallel [01\bar{1}]_{I,Rh,(Z=4)}$$

The product orientation was determined on the basis of zero, first, second and third level precession photographs, where the precession

Figure 13(a). (001) projection of $KNO_3II \rightarrow KNO_3I$
Laue, Mo radiation.

Figure 13(b). $(0001)_{hex, Z=3}$ projection of KNO_3I ,
the transformation product.
Laue, Mo radiation.

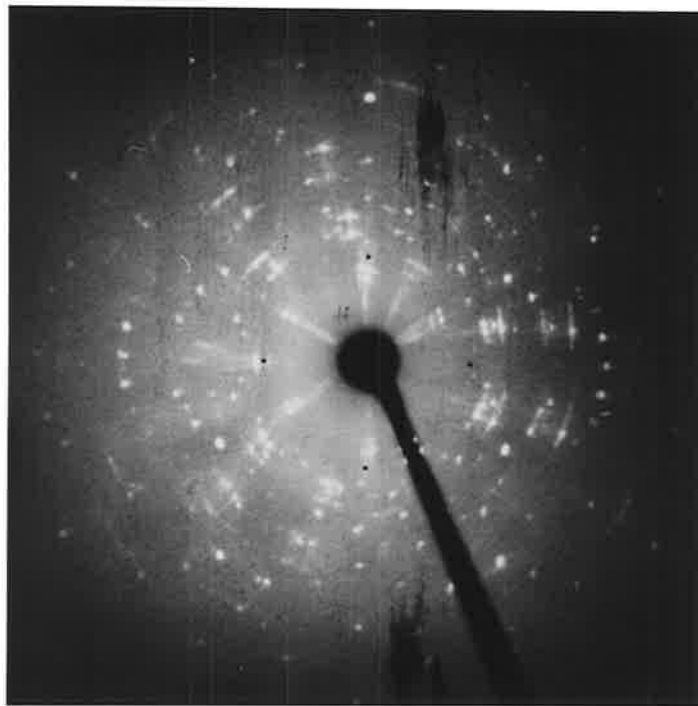


Figure 13(a). (001) projection of $KNO_3 II \rightarrow KNO_3 I$. Laue, Mo radiation.

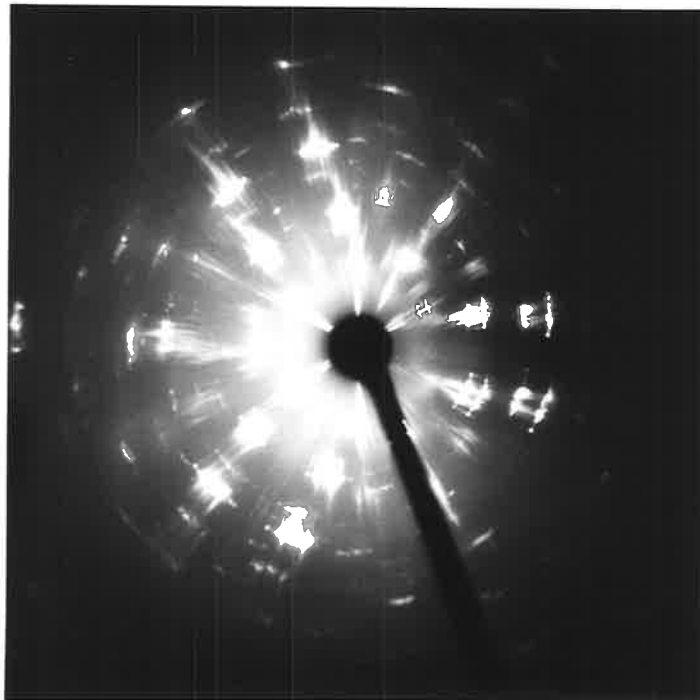


Figure 13(b). $(0001)_{hex, Z=3}$ projection of $KNO_3 I$, the transformation product. Laue, Mo radiation.

Figure 13(c). KNO_3I , $(0001)_{hex, Z=3}$ projection
Zero layer precession photo, Mo
radiation/Zr filter.

Figure 13(d). KNO_3I , $(0001)_{hex, Z=3}$ layer precession
photo. Mo/Zr filter.

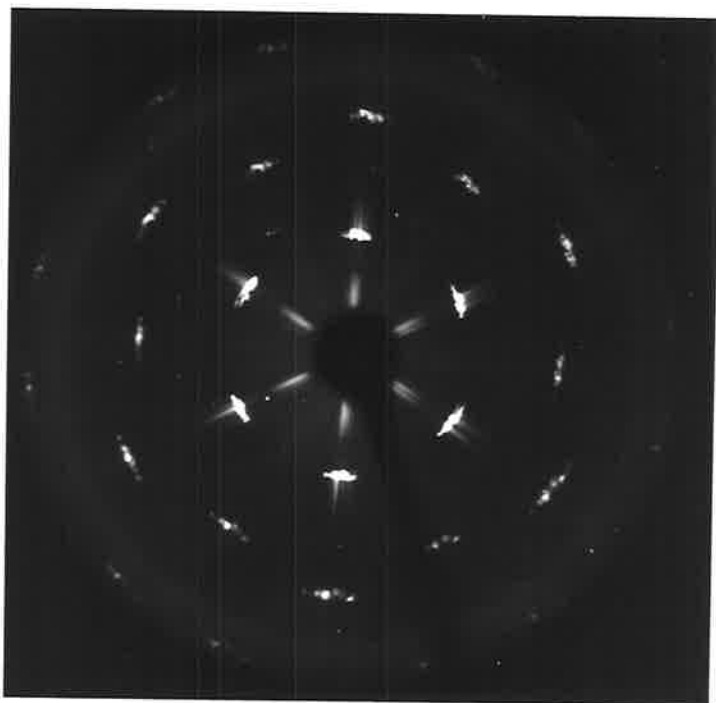


Figure 13(c)

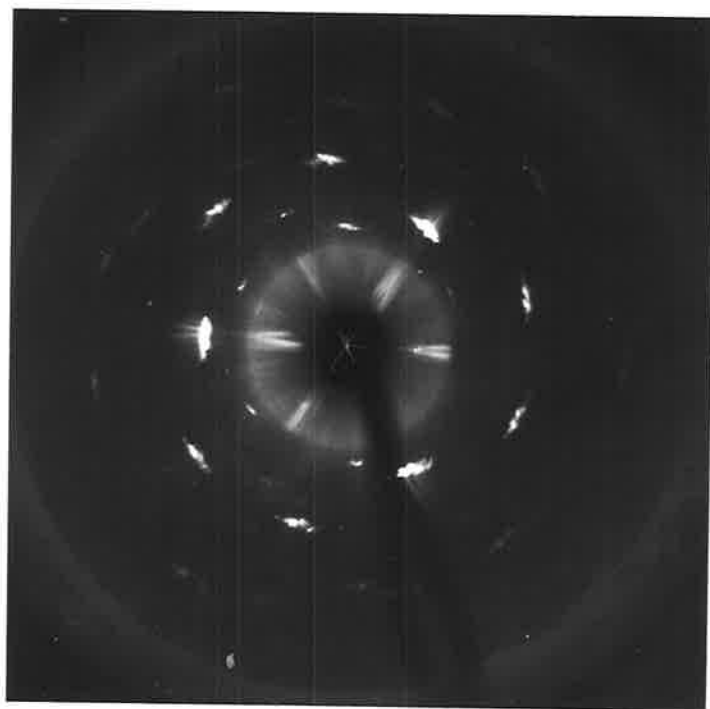


Figure 13(d)

Figure 13(e). KNO_3I , $(0002)_{hex, Z=3}$ layer precession
photo. Mo/Zr filter.

Figure 13(f). KNO_3I , $(0003)_{hex, Z=3}$ layer precession
photo. Mo/Zr filter.

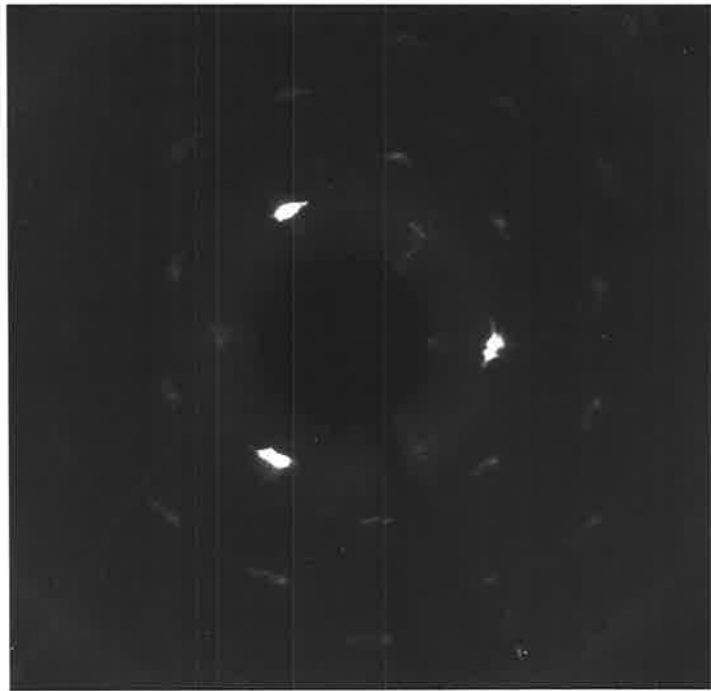


Figure 13(e)

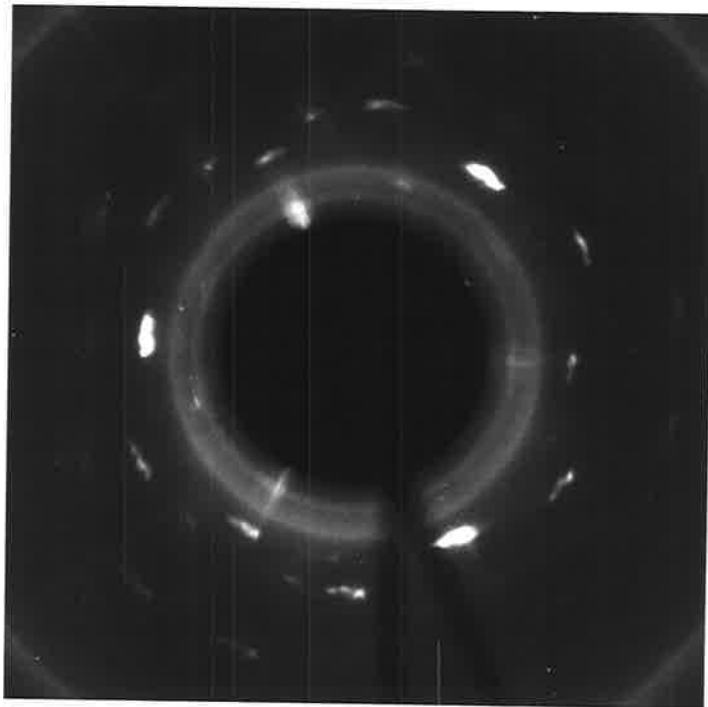
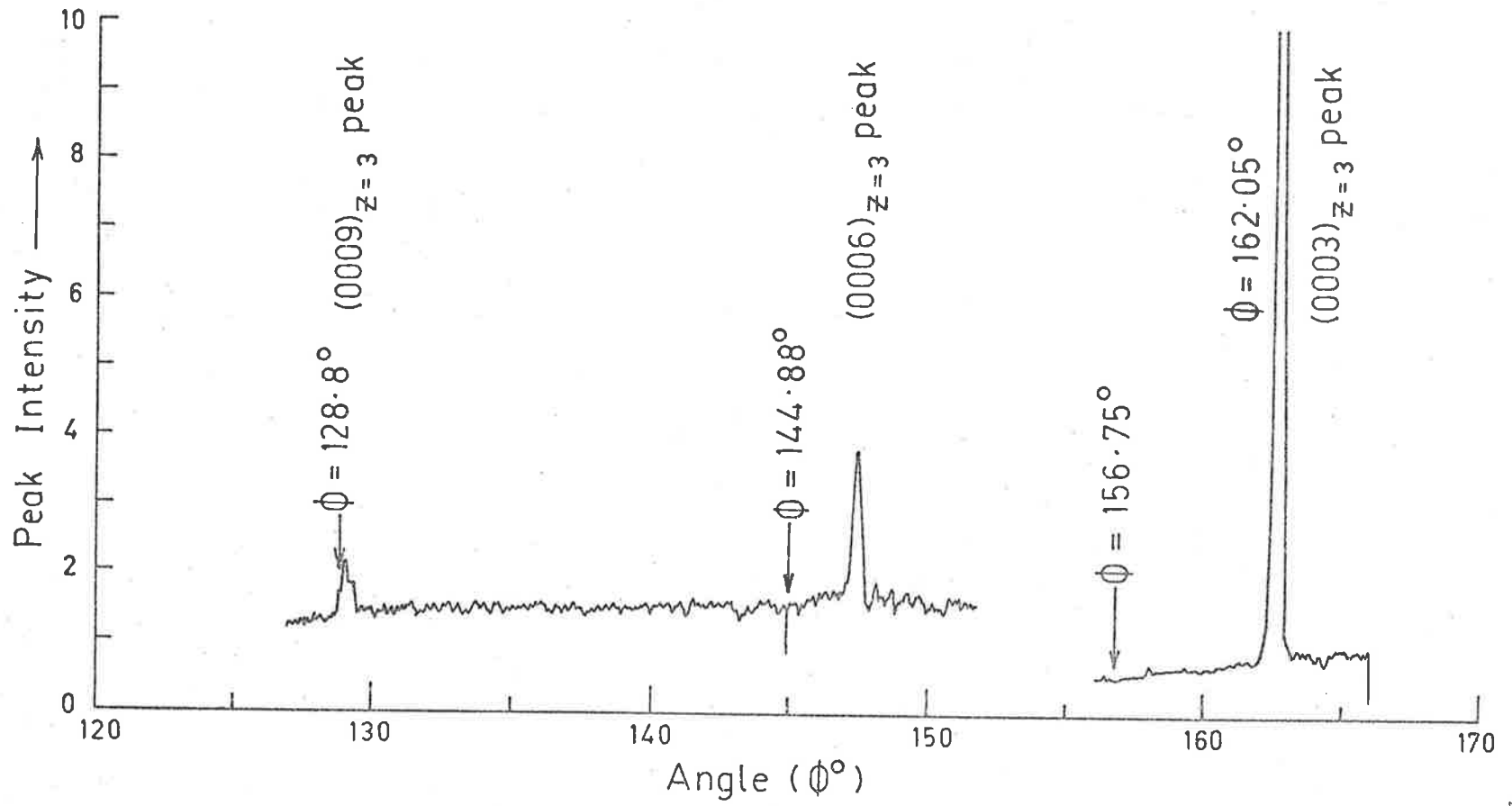


Figure 13(f)

[4.3.5]

Fig. 14. X-ray Diffractometry of Product Phase I on Transformation from $(001)_{II}$.



[4.3.5]

Figure 15(a). KNO_3 II cooled from I(\leftarrow II) (001)
projection. Zero layer precession.
Mo/Zr filter.

Figure 15(b). KNO_3 II cooled from I(\leftarrow II) (001)
layer precession. Mo/Zr filter.

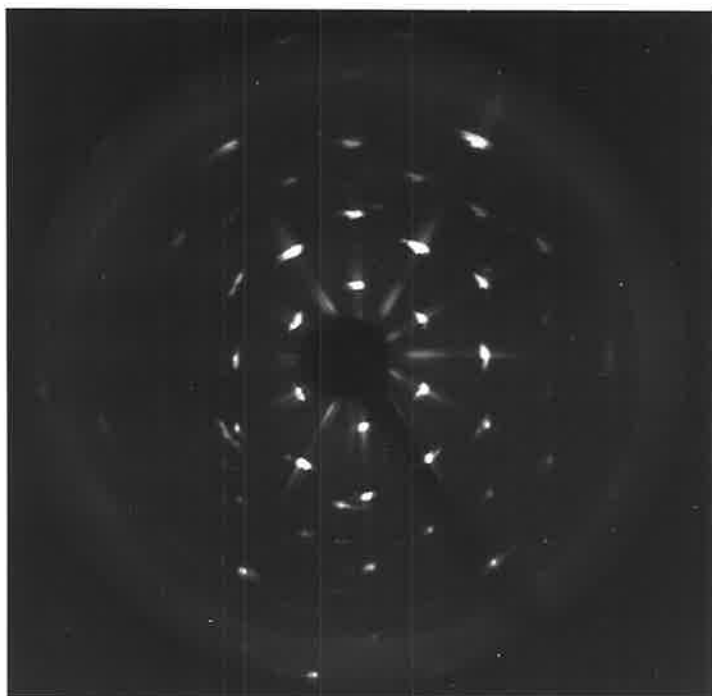


Figure 15(a)

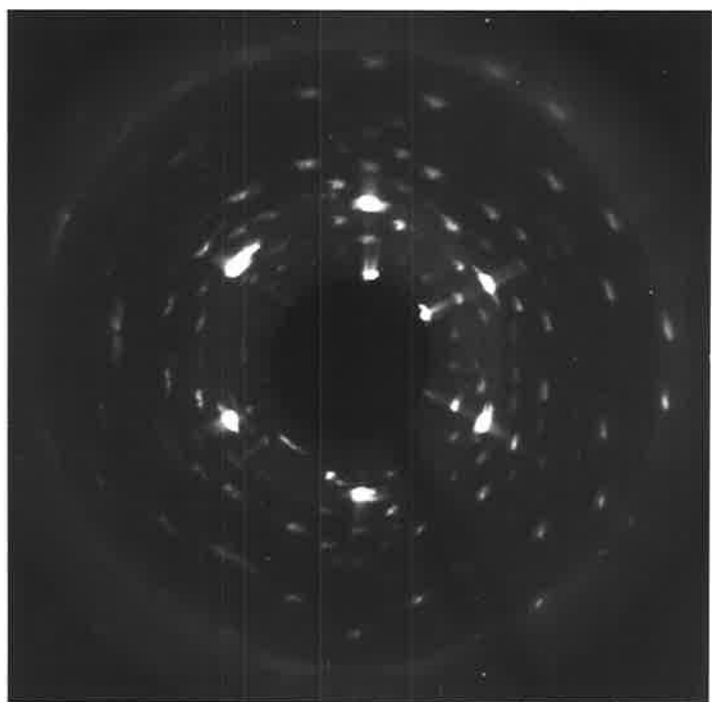


Figure 15(b)

camera was set for the hexagonal, $Z = 3$ unit cell lattice parameters. The reflections in each layer were indexed by d spacings and comparison of interplanar angles with standard $(0001)_{I,Z=3}$ stereograms.

The basal plane projection was confirmed when the X-ray heater was transferred to the diffractometer where the (0003) (0006) and (0009) peaks of $I_{\text{hex}(Z=3)}$ were located and scanned at the appropriate θ and $\Delta\theta$ settings, figure 14. The following table summarizes the experimental accuracy.

<u>Peak</u>	<u>θ°(obs) setting</u>	<u>θ°(calc) setting</u>	<u>Difference ($^{\circ}$)</u>
(0003)	162.05	161.70	.350
(0006)	146.18	146.06	.120
(0009)	128.5	128.95	.45

On cooling, the original $(001)_{II}$ orientation reappeared together with two equivalent projections mutually rotated at $\pm 60^{\circ}$ to it, as shown in figure 15(a),(b). Hence relation [3] was shown to be reversible and the cycled room temperature orientation can be interpreted as each of the three $[a]_{I,Z=3}$ axes returning to phase II to become a $[b]_{II}$ axis, while the basal plane remains parallel in both phases.

Phase I precession photographs, particularly figure 13(c), clearly showed randomization of reflections mostly along powder rings. In the zero layer it was measured as 15° . Second order reflections were split into discrete spots, suggesting a slight scatter of orientation.

Relation [3] was shown not to be that of Davis and Oshier⁽²²⁵⁾ where the calcite-type twin plane $\{01\bar{1}8\}_{I,Z=6}$ is parallel to $(001)_{II}$. Whilst the $\{02\bar{2}16\}_{I,Z=6}$ peak and $\{0003\}_{I,Z=3}$ peaks occur at closely similar θ values, the $\Delta\theta$ between the peaks of higher multiples of the $\{01\bar{1}8\}_{I,Z=6}$ plane do not coincide. Furthermore, comparison of the two types of $\{01\bar{1}8\}_{I,Z=6}$ reciprocal lattices with the experimentally observed lattice showed no match.

The fact that $[b]_{II} \parallel [a]_{I,Z=3 \text{ or } 6}$ was reaffirmed when zero and upper level precession photographs of phase I were superimposed according to Buerger's analysis of the difference between a hexagonal and rhombohedral lattice.⁽²⁸³⁾ Examination of figures 13(b) to (f) indicates that triangles formed by joining reciprocal lattice points, as in first and second level photographs, are displaced. Registry occurs in every fourth layer, that is, after a separation of two layers. This indicates a rhombohedral crystal, rather than a hexagonal one with registry in every second layer.

Now, the reciprocal of a hexagonal lattice is another hexagonal lattice whose orientation is rotated 90° from that of the first. However, the reciprocal of a hexagonal coordinate system to which a rhombohedral crystal has been referred, which is the case here, is another hexagonal coordinate system of identical orientation. This is because the reciprocal of a rhombohedral lattice is another rhombohedral lattice of different dimensions but identical orientation.

Hence, in figures 13(b) to (f), the reciprocal $[a]_{\text{hex},Z=3}^*$ axis

and the real $[a]_{\text{hex}, Z=3}$ axis, and $[b]_{\text{II}}$ axis are both vertical, being perpendicular to $\{b\}_{\text{II}}$ plane reflections. Hence with parallel parent and product basal planes, the $[a]_{\text{hex}, Z=3}$ axis of phase I was parallel to the $[b]$ axis of II.

In this experiment, the crystal itself was optically examined at magnifications of about 20X. Pronounced markings parallel to the basal plane were found, on which the crystal had visibly sheared. The X-ray relation [3] was observed in two further experiments, making a total of three.

Relation [4]

A "dry" crystal subject to vacuum with liquid nitrogen air trap for 21 hours was mounted in a $\{b\}_{\text{II}}$ projection, shown in figure 16(a). The single crystal transformation product, figure 16(b), (c), was irrational, but slightly off an $(0\bar{1}1)_{\text{I}(Z=4)}$ projection by rotation of $\pm 8^\circ$ about the $(100)_{\text{I}, (Z=4)}$ pole. Nevertheless it was seen that the $[c]$ axes of parent and product structures were mutually tilted by 8° or with consideration of missetting, by 10° deduced to be about the $(\bar{1}30)_{\text{II}}$ pole. In terms of the $Z = 4$ cell, the orientation relation was

$$\begin{aligned} [010]_{\text{II}} & \wedge [01\bar{1}]_{\text{I}, \text{Rh}, (Z=4)} & 8^\circ, & \text{(irrational product)} \\ (\bar{1}01)_{\text{II}} & \wedge (100)_{\text{I}} & = 3.5^\circ, & \text{(in plane of projection)} \\ (001)_{\text{II}} & \wedge (111)_{\text{I}} & = 8^\circ & \text{----- [4]} \end{aligned}$$

The crystal cooled to the polycrystalline product of figure 16(d), with reflections randomized along powder rings.

Of particular interest were the non-radial diffuse reflections in

Figure 16(a). KNO_3 II, (010) projection Laue photo.
Mo radiation

Figure 16(b). KNO_3 I transformation product,
(0 $\bar{1}$ 1)_{Rh, Z=4} projection. Laue.



Figure 16(a). KNO_3II , (010) projection
Laue photo. Mo radiation.

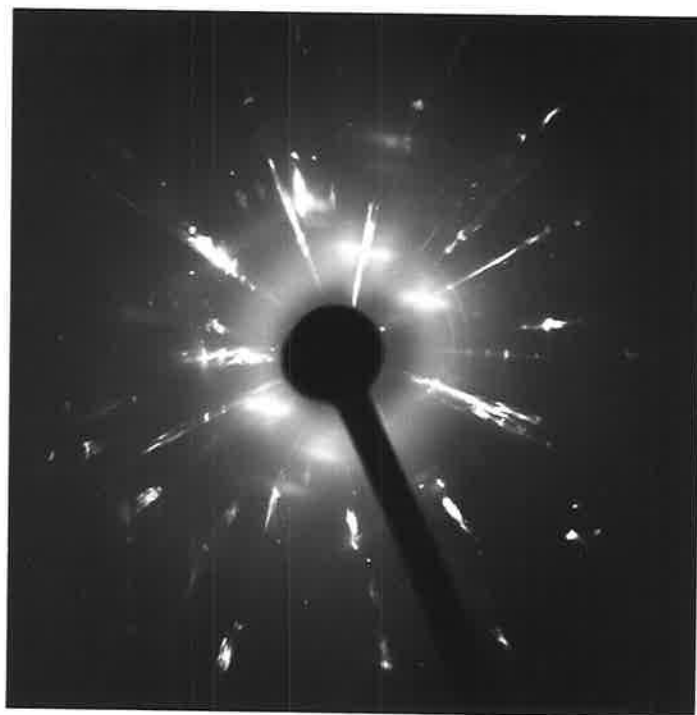


Figure 16(b). KNO_3I transformation
product, $(0\bar{1}1)_{\text{Rh}, Z=4}$
projection. Laue.

Figure 16(c). KNO_3I , approx. $(0\bar{1}1)_{\text{Rh}, Z=4}$ projection.
Zero layer precession. Mo/Zr filter.

Figure 16(d). Polycrystalline KNO_3II cooled from I.
Zero layer precession. Mo/Zr filter.

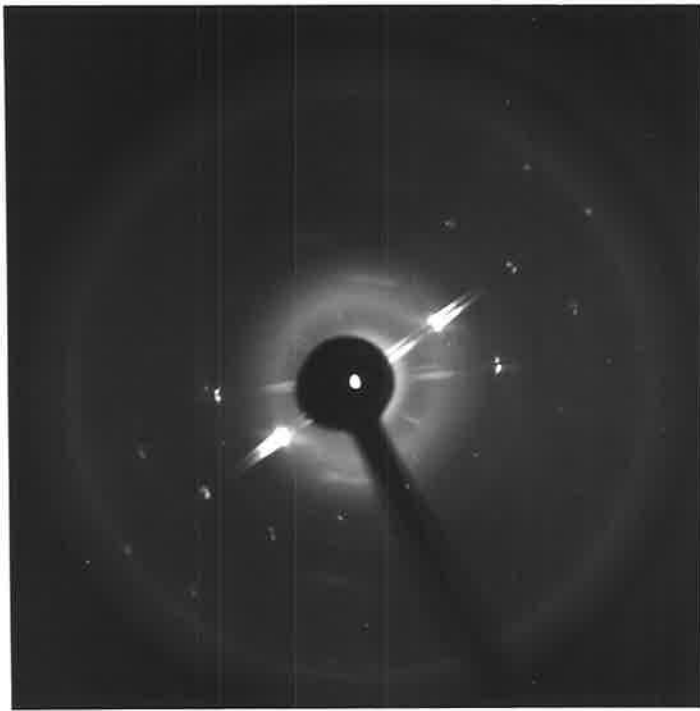


Figure 16(c)

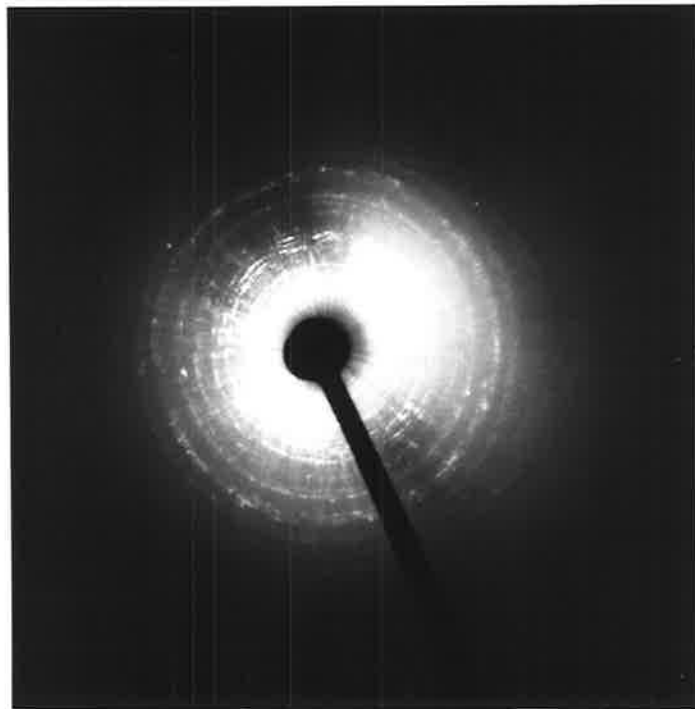


Figure 16(d)

$$(ii) \quad (1\bar{1}0)_{II} \parallel (01\bar{1})_{I, Rh, Z=4},$$

$$[001]_{II} \wedge [111]_I = 4^\circ \text{ ----- [5]}$$

Relations [6] [7] [8] [9]

An untwinned basal section was cut and mounted from a "dry" crystal subject to vacuum/liquid N₂ for 21 hours. No twin reflections were observed before transformation. Four orientations were found in the product, and identified from zero and upper level precession photographs. Expressed in the Z = 4 rhombohedral phase I cell, they are:

$$(i) \quad (001)_{II} \parallel (111)_{I(Z=4)},$$

$$[010]_{II} \wedge [01\bar{1}]_I = 10^\circ \text{ ----- [6]}$$

$$(ii) \quad [001]_{II} \parallel [211]_{I(Z=4)}, \text{ within } 1^\circ$$

$$(110)_{II} \wedge (0\bar{1}1)_I = 6^\circ \text{ ----- [7]}$$

giving $(001)_{II} \wedge (111)_I = 27^\circ$

$$(iii) \quad [001]_{II} \parallel [0\bar{1}1]_{I(Z=4)},$$

$$(100)_{II} \wedge (100)_I = 25^\circ$$

$$(100)_{II} \wedge (111)_I = 22^\circ$$

----- [8]

giving $(001)_{II} \wedge (111)_I = 90^\circ$

(iv) the rotation twin of (iii),

$$[001]_{II} \parallel [01\bar{1}]_{I, (Z=4)},$$

$$\begin{array}{l}
 (0\bar{1}0)_{II} \wedge (100) \text{ } (111)_I = 10^\circ 28^\circ \\
 (100)_{II} \wedge (111)_I = 17^\circ \\
 (001)_{II} \wedge (111)_I = 90^\circ \text{ --- [9]}
 \end{array}$$

The product patterns of relations [6] and [7] were readily indexed, whilst [8] and [9] were indexed by matching reflections with a superimposed reciprocal net of an appropriate scale.

Relation [10]

A "normal" crystal of 8 hours under vacuum/liq N₂, was cut and mounted in a $\{c\}_I$ projection, and found to be untwinned. In the product, two orientations were found, relation [1] again, and

$$\begin{array}{l}
 [001] \parallel [100]_{I(Z=4)}, (\pm 5^\circ \text{ due to irrational product}) \\
 (010)_{II} \parallel (01\bar{1})_I \text{ --- [10]}
 \end{array}$$

giving $(001)_{II} \wedge (111)_I = 63^\circ$. This latter relation was deduced by matching reflections with a superimposed reciprocal lattice of the anticipated projection, drawn to the scale of the photograph.

SECTION 4.4 THE ARKHAROV ESTIMATION OF THE REGION OF COHERENT REARRANGEMENT

On examination of relations [1] and [3], the question arose as to whether there is any significance in the fact that in the electron microscope, KNO_3 transformed according to relation [1], viz.

$$[c]_{\text{II}} \parallel [c]_{\text{I,hex,Z=3}}, [a]_{\text{II}} \parallel [a]_{\text{I}},$$

whilst the X-ray specimen gave the relation $[c]_{\text{II}} \parallel [c]_{\text{I,hex,Z=3}}, [b]_{\text{II}} \parallel [a]_{\text{I}}$ [3]

A possible explanation may be that this is due to the size difference of the transforming matrix, which influences the product orientation.

The following calculations therefore, were made by the method devised by Arkharov, ⁽²⁸⁴⁾ to determine the region of coherent rearrangements in a transforming crystal. By considering individual atoms and rows of atoms in one plane, and then repeating the process in turn for subsequent planes above and below this zero plane, a three dimensional model is built up of the area enclosed by the criterion that no atom is displaced by more than one lattice spacing. The algebraic method is based on the assumption that somewhere in this region is a starting point which is fixed and defined as 0_{000} .

The Arkharov method was studied and example calculations were repeated for heuristic purposes.

In potassium nitrate the structure change is considered in terms of the $Z = 4$ orthorhombic cell of II and the $Z = 3$ hexagonal cell of I.

The calculations are given in Appendix A, where symbols and notations are the same as in the original text.⁽²⁸⁴⁾ Figure 2 in the Appendix depicts the zero plane which is seen to be a very extended type of ellipse. Approximating it to a rectangle, its area is 1.9×10^{-4} cm by 4.5×10^{-6} cm, which is 8.55×10^{-10} cm². The height of the ellipse is about 5.7×10^{-6} cms, so that in view of the large dimension in length the ellipsoid can further be approximated to a rectangular solid of volume 4.87×10^{-15} cms³.

Relation [1] was found in a triangular crystallite which was photographed at magnification X13,100. The approximately equilateral triangle of sides 1.20, 1.30 and 1.25 cm had an area of about 2.6×10^{-6} cm². The crystallite was quite transparent at the low beam intensity, but allowing for a maximum thickness of $1000 \overset{\circ}{\text{A}}$, the volume of the solid is 2.6×10^{-11} cm³.

Hence the area and volume of crystal in which relation [1] was observed is significantly greater than the region of coherent re-arrangement calculated by the Arkharov method. The relation observed in the electron microscope, therefore, cannot be explained on the basis of lattice dimensions, as resulting from an Arkharov-type coherent re-arrangement, but is produced by a more complicated transformation mechanism. In conclusion, therefore, this case implies that a martensite transformation can occur in a particle of the size suitable for electron microscopy.

SECTION 4.6 INTERPRETATION AND DISCUSSIONSECTION 4.6.1 Analysis of Previously Reported Orientation Relations

Several orientations have already been reported for the aragonite-calcite transformation in CaCO_3 and KNO_3 , as mentioned in the introductory section of this Chapter. Due to the variety of calcite-type cells used in their expression however, they were re-analysed in terms of the rhombohedral $Z=4$ calcite cell, and orthorhombic $Z=4$ aragonite cell. This was facilitated by the use of bronze metal skeleton structure models constructed by the departmental Workshop.

A more detailed phase II structure was constructed on a polystyrene base, with thin metal rods and polystyrene balls of diameter 25 cms, and matches trigonally joined to represent nitrate groups. Another type of model was made by joining table-tennis sized balls into hexagonal array layers, representing rotating-librating nitrate groups of radius 1.9 \AA .⁽⁵¹⁾ The layers were separated by hexagonal arrays of smaller 25 cm plastic balls, joined by wire pipe cleaners, and representing K^+ ions. As described in Chapter 3, in phase II the stacking sequence in $[\text{c}]_{\text{II}}$ nitrate ions is simple hexagonal, with K^+ ions in h.c.p. In distorted NaCl-type rhombohedral phase I, both sets of ions adopt a c.c.p. sequence. Orientation relations were examined by superposition of computed stereograms in appropriate projections.

In (1933) Shôji⁽²²²⁾ and later Kennedy, Ubbelohde and Woodward (1953),⁽²⁷¹⁾ reported, on the basis of X-ray studies that the trigonal

[c] axis was maintained but a polycrystalline species usually resulted. Brown, Fyfe and Turner (1962)⁽²¹⁸⁾ however, noted five orientation relations in naturally occurring aragonite transforming to calcite. Dasgupta (1964)⁽²²⁴⁾ heated natural untwinned aragonite to observe, by rotation photographs, the orientation of a single crystal calcite product. Davis and Oshier (1967)⁽²²⁵⁾ made numerous X-ray diffractometric and optical observations on CaCO_3 and KNO_3 . They reported on orientation in which [c] axes tilt by 26° . With the rate of temperature increase of 0.3 to $0.5^\circ\text{C}/\text{min}$, they noted a pronounced incubation period before transformation and measured the transformation temperature for $\text{KNO}_3 \text{ I} \rightleftharpoons \text{II}$ to be 127.5°C .

Hiragi, Kachi, Takada and Nakanishi (1966)⁽²²⁰⁾ transformed synthetic aragonite in an electron microscope with beam intensity of 50 KV, and reported an orientation relation for which they proposed a non-diffusive martensite mechanism (see later). Burrage and Pitkethley (1969)⁽¹³⁵⁾ found a violent reaction to 100 KV electrons in an electron microscope, but noted that during the change aragonite to calcite to CaO , the trigonal $[\text{c}]_{\text{II}}$ axis was maintained between consecutive products. Odlyha and Kennedy⁽¹⁰⁵⁾ of this laboratory, found at least five orientations, two by X-ray oscillation and Laue photographs, and three by single- and double-surface analysis.

The following account summarizes relations in terms of $Z = 4$ cells.

Odlyha and Kennedy (by optical microscopy):

$$[c]_{II} \wedge [c]_I = 90^\circ$$

(with rotations about $[a]_{II}$ and $[b]_{II}$).

Dasgupta : $[001]_{II} \parallel [111]_{I, Rh, Z=4}$

$$(010)_{II} \parallel (1\bar{1}0)_I$$

(i.e. $[c]_{II} \parallel [c]_{I, Z=3}$, $[b]_{II} \parallel [a]_I$)

Brown, Fyfe and Turner - I: $(100)_{II} \parallel (10\bar{1})_I$

$$(021)_{II} \text{ i.e. } [011]_{II} \parallel [111]_I$$

$$[c]_{II} \wedge [c]_I = 54.5^\circ \text{ in } (10\bar{1}) \text{ plane}$$

Brown, Fyfe and Turner-II: $(100)_{II} \parallel (10\bar{1})_I$

$$(010)_{II} \parallel (010)_{I, Z=4} \text{ ie. } (\bar{1}104)_{Z=6}$$

$$[001]_{II} \parallel [101]_I$$

$$[c]_{II} \wedge [c]_I = 44.2^\circ \text{ in } \{10\bar{1}\}_{I, Z=4} \text{ plane}$$

Brown, Fyfe and Turner-III: $(100)_{II} \parallel (10\bar{1})_I$

$$(001)_{II} \parallel (010)_I \text{ ie. } (\bar{1}104)_{Z=6}$$

$$[010]_{II} \parallel [101]_I$$

$$(101)_{II} \parallel (11\bar{1})_I$$

$$[c]_{II} \wedge [c]_I = 45.8^\circ \text{ in } (10\bar{1})_{Z=4} \text{ plane}$$

Brown, Fyfe and Turner-IV: $(010)_{II} \parallel (10\bar{1})_I$

$$[001]_{II} \parallel [101]_I$$

$$(100)_{II} \parallel (010)_I \text{ ie. } (\bar{1}104)_{Z=6}$$

$$[c]_{II} \wedge [c]_I = 44.2^\circ \text{ in } (10\bar{1})_{Z=4} \text{ plane.}$$

Brown, Fyfe and Turner - V:

$$\begin{array}{l} (110)_{II} \parallel (2\bar{1}\bar{1})_I \\ (203)_{II} \parallel (11\bar{2})_I \\ (322)_{II} \parallel (10\bar{1})_I \\ (\bar{1}31)_{II} \parallel (111)_I \\ [c]_{II} \wedge [c]_I = 67.5^\circ \end{array}$$

Hiragi, Kachi, Takada, Nakanishi: (220)

$$\begin{array}{l} (001)_{II} \parallel (111)_I, \\ [\bar{1}10]_{II} \parallel [\bar{1}10]_I \\ \text{(i.e. } [c]_{II} \parallel [c]_{I(Z=3)}, [a]_{II} \parallel [a]_{I}.) \end{array}$$

Odlyha and Kennedy - I :

$$\begin{array}{l} [010]_{II} \parallel [01\bar{1}]_I \\ (001)_{II} \parallel (311)_I \\ [c]_{II} \wedge [c]_I = 21^\circ \text{ in } (01\bar{1})_{Z=4} \\ \text{plane} \end{array}$$

giving $(100)_{II} \parallel \{1\bar{1}1\}_{I(Z=4)}$

Davis and Oshier, Odlyha and Kennedy - II:

$$\begin{array}{l} [010]_{II} \parallel [10\bar{1}]_I \\ (001)_{II} \parallel (101)_I \\ [c]_{II} \wedge [c]_I = 27^\circ \text{ in } (10\bar{1})_{Z=4} \\ \text{plane.} \end{array}$$

Odlyha and Kennedy - III:

$$\begin{array}{l} [100]_{II} \parallel [\bar{1}01]_I \\ (010)_{II} \parallel (101)_I \\ [c]_{II} \wedge [c]_I = 60^\circ \text{ in } (\bar{1}01) \text{ plane.} \end{array}$$

Odlyha and Kennedy-IV:

$$\begin{array}{l} (\bar{2}\bar{3}0)_{II} \parallel (511)_{I,Z=4} \\ (\bar{1}10)_{II} \parallel (3\bar{4}10)_{Z=6} \\ (010)_{II} \wedge (\bar{1}\bar{1}1)_I = 5^\circ \\ (100)_{II} \wedge (1\bar{1}0)_I = 20^\circ \\ [c]_{II} \wedge [c]_I = 27^\circ \end{array}$$

$$\begin{aligned}
 \text{Odlyha and Kennedy - V:} \quad & (010)_{\text{II}} \parallel (22\bar{1})_{\text{I}(Z=4)} \text{ i.e. } (01\bar{1}4)_{Z=6} \\
 & (\bar{1}10)_{\text{II}} \quad (3\bar{1}\bar{1})_{\text{I}} \\
 & (100)_{\text{II}} \wedge (1\bar{1}0)_{\text{I}} = 12^\circ \\
 & (010)_{\text{II}} \wedge (110)_{\text{I}} = 19^\circ.
 \end{aligned}$$

Odlyha⁽¹⁰⁵⁾ points out that her third orientation is slightly off that of Brown, Fyfe and Turner I. Both orientations can be interpreted as a twin in form I of $[a]_{\text{II}} \parallel [a]_{\text{I,hex,Z=6}}$, $[c]_{\text{II}} \parallel [c]_{\text{I}}$ which is then twinned on the twin plane $(\bar{1}108)_{\text{I,Z=6}}$. $[c]$ axes thus tilt by twice the phase I twinning shear angle; that is, $2 \times 27.44^\circ = 54.9^\circ$. Brown, Fyfe and Turner gives $[c]_{\text{II}} \wedge [c]_{\text{I}(Z=6)} = 56^\circ$ with $[a]_{\text{II}} \parallel [a]_{\text{I}(Z=6)}$ while the orientation Odlyha and Kennedy - III has $[a]_{\text{II}} \wedge [a]_{\text{I}(Z=6)} = 4^\circ$, $[c]_{\text{II}} \wedge [c]_{\text{I,Z=6}} = 60^\circ$.

The relations Brown, Fyfe and Turner-III and Odlyha and Kennedy V are similar and differ only in that the latter is rotated with respect to the former by 8° around $[b]_{\text{II}}$ and 2.5° around $(2\bar{1}\bar{1}0)_{\text{I}(Z=6)}$.

Examination of the above orientations shows that a certain observation was consistently made, with the exception of those orientations to be mentioned. Most of the relations conform to the criterion that the hexagonal (Z=3 or Z=6) $[a]$ axis of phase I is parallel to a main axis ($[a]$, $[b]$) in phase II. Since $\{10\bar{1}\}_{Z=4}$ is parallel to $(100)_{\text{II}}$ or $(010)_{\text{II}}$, from the crystallography there is a rotation of $[c]_{\text{II}}$ axes through various angles but always in the $\{10\bar{1}\}_{\text{I,Z=4}}$ plane. The orientations which do not conform to the above criterion are Brown, Fyfe and Turner V, and Odlyha and Kennedy IV where $(1\bar{1}0)_{\text{I}(Z=4)} \wedge$

TABLE (6)

POSSIBLE CRYSTALLOGRAPHIC INTERPRETATIONS OF PREVIOUSLY
REPORTED ORIENTATION RELATIONS

$[c]_I \wedge [c]_{II}$	Orientation and Author	Possible Interpretation (I, (Z = 6), hexagonal cell)
0°	Dasgupta	$[c]_I \parallel [c]_{II}, [a]_I \parallel [b]_{II}$
21°	O. & K. - I	$[a]_I \parallel [b]_{II}$
27°, 26°	O. & K. - II,	$[a]_I \parallel [b]_{II} + \frac{1}{2}$ twin shear so that
	D. & O.	$(101)_{I, Z=4} \equiv (01\bar{1}8)_{I, Z=6} \parallel (001)_{II}$
55°, 60°	B.F.T. - I,	$[a]_I \parallel [a]_{II}, [c]_I \parallel [c]_{II}$
	O. & K. - III	then twinned on $(101)_{I, Z=4}$ $\equiv (01\bar{1}8)_{I, Z=6}$
		(B.F.T. - I is 0.35° from twin position)
		(O. & K. - III is 5.12° from " ")
45.8°, 45°	D. & K. - V,	$[a]_I \parallel [a]_{II}$ and $[c]_I \parallel [b]_{II}$, then
	B.F.T. - III	twinned on twin plane of I.
		(O. & K. - V has $[c]_I \wedge [c]_{I,t} = 10^\circ$)
		(B.F.T. - III has $[c]_I \wedge [c]_{I,t} = 11^\circ$)
44°	B.F.T. - II	$[a]_I \parallel [a]_{II}, [c]_I \parallel [c]_{II}$ then twinned
		($[c]_I \wedge [c]_{I,t} = 12^\circ$ off position)
44°	B.F.T. - IV	B.F.T. - II rotated through 90°
67°	B.F.T. - V	-

$(100)_{II} = 20^{\circ}$. The latter orientation was found by ~~single~~^{two} surface analysis. Table 6 briefly summarizes possible interpretations for the relations.

Dasgupta⁽²²⁴⁾ heated natural aragonite crystals as did Shoji⁽²²²⁾. Davis and Oshier (225) make no mention of rigorous drying so that one may assume that "normal" crystals were observed. Brown, Fyfe and Turner⁽²¹⁸⁾ studied natural aragonite but Davis and Oshier⁽²²⁴⁾ suggest that some of their orientations may be due to hydrothermal replacement by calcite. The reports of Kennedy and Odlyla do not mention for how long needles were left under vacuum with liquid nitrogen air trap. It may or may not be relevant therefore, that in general, one cannot conclude that the previously reported orientations were observed in rigorously dry crystals.

SECTION 4.6.2 DISCUSSION

Some discussion has already been made with presentation of results. Briefly recapitulating, mechanical twinning of phase II on $\{110\}_{II}$ causes the appearance of non-lattice point twin reflections in $(001)_{II}$ level X-ray precession photographs. Longitudinal lines on the $\{b\}_{II}$ face are similar to $\{110\}_{II}$ twin lamellae. However, there is no conclusive evidence that longitudinal lines are twin lamellae; this is based on X-ray examination and optical microscopy of $\{b\}_{II}$ and $\{c\}_{II}$ faces during heating.

Alternatively, longitudinal lines may be interpreted as water-modified structure domains, and are indicative of the extent of crystal dryness. With increasing temperature their number increases, possibly due to the effect of the original domains on the lattice dynamics of the structure. Below the transformation temperature, the new domains disappear on cooling.

The shape change illustrated in crystals A and B of Section 4.3.2 introduces uncertainties in the determination of extinction directions and orientation relations. From the diagram in Section 4.3.2 it is seen that if crystal A had not altered its position, the extinction angle relative to the crystal edge would be less than -9.6° . The exact amount of shape change was not measured. Kennedy and Odlyha⁽²²¹⁾ allow a value of $\pm 2^\circ$ in measurements of extinction directions, due to specimen deformation. Odlyha⁽¹⁰⁵⁾ however, measured an angle of 7° in successive kinking of crystal in different directions. The crystal B of figure 4(a) kinks through 7° while in figure 4(b) angles of 12°

and 15° are observed. In such cases the extinction direction is measured with respect to the (II) basal shear lines. Similar behaviour was noticed in acicular needles lying on each other or crystallites, and hence not completely flat. For this reason, experimental studies were usually made on separate single crystals.

This question of real and apparent orientations has risen in other studies in this laboratory (Fraser,⁽⁴¹⁾ Kennedy⁽¹⁵¹⁾ and see Chapter 3, Section 3.4). Hence, measurements of some crystallographic transformation parameters in crystals undergoing large shape changes, are subject to this uncertainty.

The V-shaped interface and oblique nucleation sites indicate an alternative interface to that whose trace is parallel to the basal plane. The interface lies between $\{1k2\}_{II}$ and $\{2k3\}_{II}$, which is consistent with oblique surface traces lying close to such zones.

The appearance of fine twins and compensation bands in the optical microscope indicates that the product of transformation may be a complex mixture of orientations, probably due at least to the simultaneous occurrence of symmetry-related options. Definite crystallographic information may be found in a single crystal product. A postulated transformation mechanism or its options may be compared with experimental observations such as in Table 3, for consistency with the characteristics of the relation.

Previous optical observations^(105,221) were confirmed. In particular, in Section 4.3.2, Table 3, experiments numbered 2,5,9,12, 14,16 and 17 agree with $[c]_{II} \wedge [c]_{I,Z=3} = 0$, whilst experiments

7(ii), 7(iii) and 10(iii) confirm $[c]_{II} \wedge [c]_{I(Z=3)} = 90^\circ$ with rotations about $[a]_{II}$ and $[b]_{II}$. This may possibly be due to the similarity of the hexagonal array of ions in the basal plane with the vertical $\{10\bar{1}0\}$ pseudo-hex plane. McConnell and Lima de Faria⁽²⁵⁾ observed for goethite, that a small adjustment on a vertical plane will convert it to a h.c.p. plane. Minor rearrangements of the phase II lattice accompanying tilting of nitrate ions may therefore be a path to relations where $[c]_{II}$ tilts 90° to become parallel to the previous $[b]_{II}$.

The electron microscope orientation [1] of Section 4.3.4 is $[c]_{II} \parallel [c]_{I,hex,Z=3}$, $[a]_{II} \parallel [a]_I$. As discussed in Chapter 3 the ions in both phases form hexagonal arrays. In phase II cations are h.c.p. and anions, simple hexagonal. Phase I is a distorted NaCl-type structure with both types of ions in a c.c.p. sequence.

With respect to the cation lattice, the transformation may be regarded as analogous to the f.c.c. to h.c.p. structure change in cobalt.^(138,185) ΔV is -0.3% and the relation $(111)_{f.c.c.} \parallel (0001)_{h.c.p.}$, $[1\bar{1}0]_{f.c.c.} \parallel [11\bar{2}0]_{h.c.p.}$ is obtained via stacking faults or partial dislocations.

In terms of hexagonal, Z=12 cells for both phases, the relation is $[c]_{cubic} \parallel [c]_{h.c.p.}$, $a_{cubic} \parallel a_{h.c.p.}$. As suggested in Chapter 3, the "extra reflections" accompanying the II \rightarrow I transformation, as in the $KNO_3I \rightarrow KNO_2I$ decomposition, may be due to partial dislocations which constitute the mechanism of transformation.

Several other mechanisms for relation [1] have already been

postulated. Kôzu and Kani⁽²²³⁾ hypothesize that aragonite to calcite proceeds by 30° rotations of planar anions, accompanied by $\pm \frac{1}{12} [c]_0$ shifts. This is followed by slight and regular displacements of these atoms by $2.4 \overset{\circ}{\text{Å}}$ and $1.5 \overset{\circ}{\text{Å}}$ in [a] and [b] directions respectively. A total of 12 layers describe the mechanism.

"Layer transposition theory" was discussed with C.W. Allen⁽²⁹³⁾ who was investigating defects, transformations and polymorphism in Laves phases. When one hypothetically shears layers above one another, one assumes that a moving layer carries with it to a new position, the layer above it, whose relative position to the moving layer is unchanged. In view of this, the writer has found Kôzu and Kani's⁽²²³⁾ mechanism questionable since it appears to assume that when one layer moves, the layer above it remains stationary or unchanged in space. As a result, the moving layer needs to pass directly under ions of the superlying layer, even though these are oppositely charged. This may be energetically prohibitive in comparison to other mechanisms.

Hiragi, Kachi, Takada and Nakanishi⁽²²⁰⁾ reported relation [1] in the electron microscope, observing a tiny synthetic crystal of aragonite transforming to calcite. They described the two structures in detail and proposed a non-diffusive martensite-type mechanism consisting of three operations:

- (i) the h.c.p. Ca^{++} ions of aragonite shear on the basal (II) plane to c.c.p. positions, in a manner analogous to the martensite transformation of cobalt,^(138,185) mentioned earlier;
- (ii) $\text{CO}_3 =$ ions of phase II similarly shear to three types of

positions (abc...) in a c.c.p.-type calcite;

(iii) anions rotate to adopt calcite configurations.

Essentially, therefore, a cooperative movement takes place on an

$(001)_{II}$ plane in a $[310]$ arag. or $[0\bar{1}0]$ arag. direction.

During the writing of this chapter Swaminathan and Srinivasan⁽²⁹⁴⁾ proposed detailed mechanisms for the $II \rightarrow I \rightarrow III \rightarrow II$ transformation involving "shuffles" and rotations of nitrate groups; that is, small rearrangements which they maintain are martensitic. The product orientation in $II \rightarrow I$ appears to be $[c]_{II} \parallel [c]_{I,hex,Z=3}, [a]_{II} \parallel [a]_I$; that is, relation [1].

Electron microscope relation [2] indicates a mechanism involving shear in a zone containing the $[111]_{I,Rh}$ axis. The observation that $(11\bar{1})_{I,Rh,Z=4} \parallel (110)_{II}$ is significant in light of Craido and Trillo's⁽²²⁷⁾ conclusion that movement of dislocations occurs on $(11\bar{1})_{I,Rh,Z=4}$ planes.

X-ray relation [3] is a novel type of relation for the h.c.p. to c.c.p. type of structure change, such as in cobalt, mentioned earlier.

Several explanations were considered, as follows.

The first hypothesis is that the phase II structure shears in an oblique direction accompanied by tilting of nitrates so that $[c]_{II} \parallel [c]_I$ with $[b]_{II} \parallel [a]_{I,Z=3}$. In Sections 4.1 and 4.3.2 it was described how

faint, oblique surface effects were often observed inclined at 44° or 45° to the basal (II) plane. If the crystal transformed to phase I in the above relation, these oblique markings would be parallel to $\{1\bar{1}1\}$ or $\{100\}_{I,Z=4}$ planes. This suggests that the mechanism of transformation was martensite-type with deformation of the cation lattice and tilting of nitrate groups. $\{100\}\langle 011\rangle_{I,Z=4}$ was considered as a lattice invariant twinning shear system in isostructural RbNO_3I (Chapter 2). However, it must be noted that in the experiment giving relation [3], transverse striations were clearly evident and the X-ray optical arrangement did not enable sensitive Normarski interference contrast observation of the crystal surface to find 45° markings.

A second explanation focuses on the anion framework.^(298,20)
 H. Megaw⁽²⁹⁸⁾ discusses observed thermal vibrations and a lattice mode in calcite and NaNO_3I . Oxygen atoms from the planar anions may be described in terms of octahedra whose interstices are filled with C or N atoms causing octahedra to behave as rigid bodies. The filled octahedra share corners in a three-dimensional framework. Deviations from this ideal structure occur when filled octahedra rotate about their triad axes by positive and negative amounts. Examples of inorganic compounds show varying values of this azimuthal tilt. VF_3 and LiNbO_3 have positive values of 7° and 10° respectively, whilst CaCO_3I and NaNO_3I have negative values of -12° and -14° respectively. For a tilt of $+30^\circ$ the cation-oxygen bonds of two neighbouring octahedra are collinear and an ideal perovskite framework results. The ideal

h.c.p. structure has a tilt angle of 0° and is found in RhF_3 and PdF_3 . One may visualize the ideal perovskite framework as contracting or undergoing negative rotation so as to overshoot the ideal close-packed state to adopt the calcite-type position.

Empty octahedra also present in the structures are less rigid, and in fact rather "soft" with respect to compression or elongation along the triad axis. This is largely due to Ca-C type repulsive forces. The resulting lattice mode causes oxygen atoms to move in a line inclined at about 45° to the (0001) plane, and perpendicular to the C-O bond. The previously-mentioned faint oblique surface markings at 44° or 45° to the basal plane may be due to such movements of anion octahedra. Relation [3] may result when such octahedra rotate and tilt in some coordinated manner.

A third explanation is based on the fact that relation [3] was observed in a non-rigorously dried crystal. Water molecules are trapped in the phase II lattice and hydrogen bond to nitrate groups, which thus become bulkier. The difference between the aragonite and calcite structure is usually discussed in terms of rotation of the nitrate group, as illustrated below: (19,118,208,102,223,224,18)



The structure of calcite (a) and aragonite (b), and positions of calcium atoms around the CO_3^- groups in both structures.

The structures are usually drawn so that $[a]_{\text{II}}$ is parallel to $[a]_{\text{I,hex}}$ and the anions are changed in this projection. The writer suggests that in rigorously dry crystals the transformation mechanism is determined by the cation lattice with the anions rotating and tilting. As will be discussed later, this corresponds to a displacive, martensite-type mechanism similar to that in RbNO_3 $\text{I} \rightleftharpoons \text{II}$ (Chapter 2). In the presence of water, however the mechanism is modified or dependent on the now bulkier nitrate groups. Since they are less able to rotate to calcite positions as shown above, the cation frame rotates by $\pm 30^\circ$ about the stationary anions and relation [3] in which $[b]_{\text{II}} \parallel [a]_{\text{I}}$, results.

Figure 13(b) of Section 4.3.5 shows that there is a small scatter of product orientations about the $[c]_{\text{I},Z=3}$ axis. This arises from the fact the phase II is pseudo-hexagonal and in this case, also twinned on $\{110\}_{\text{II}}$. Figure 13(a) in the same section shows an intermediate stage in the transformation in which both phases coexist. It is comparable to Ubbelohde's "hybrid state".⁽³⁾ A single crystal

hybridizes with coexistence of domains of either form suitably oriented to minimize strains. This leads to "thermodynamic indeterminacy" or spread in the intersection of free energy curves (see Chapter 1). In KNO_3 pseudo-hexagonal (II) and hexagonal [a] axes lengths change negligibly in the basal plane. There is a rotation of axes through 30° in this plane, but the fit on the basal plane when $[b]_{\text{II}} \parallel [a]_{\text{I},Z=3}$ is comparable to that when $[a]_{\text{II}} \parallel [a]_{\text{I},Z=3}$ which would minimize the strains in terms of lattice parameters.

Phase I in relation [3] cooled in the reverse orientation of $[a]_{\text{I},Z=3} \parallel [b]_{\text{II}}$ together with two coexisting orientations of $[b]_{\text{II}}$ at $\pm 60^\circ$ to the original. As stated in Section 4.3.5 this may be interpreted as each of the three $[a]_{\text{I},Z=3}$ axes becoming $[b]_{\text{II}}$, or as evidence of $\{110\}_{\text{II}}$ twinning on cooling as suggested by Kennedy et al. (271)

The irrational X-ray relation [4] in which $c_{\text{II}} \hat{=} c_{\text{I,hex},Z=3} = 8^\circ$ is similar to relation [5] found from a $\{\bar{1}10\}_{\text{II}}$ projection identified by systematic extinctions in precession photographs, and assymetry in the Laues. It emphasizes the pseudo-hexagonal nature of phase II, and indicates that for the purpose of the transformation $[010]_{\text{II}}$ and $[\bar{3}10]_{\text{II}}$ are equivalent.

X-ray relations [6] to [9] are consistent with optical microscopy in that the product is composed of more than one orientation. Relation [7] in which the [c] axes tilt by 27° is a pseudo-equivalent of the previously reported orientation of Davis and Oshier,⁽²²⁵⁾ where $[010]_{\text{II}} \parallel [10\bar{1}]_{\text{I}(Z=4)}$. In [7] $(0\bar{1}1)_{\text{I}(Z=4)}$ is 6° from $(110)_{\text{II}}$ which

corresponds to $[130]_{II}$ and hence a pseudo $[010]_{II}$ axis. Relation $[10]$ in a "normal" crystal conforms to the criterion gathered from the analysis of previously reported orientations, and this work, that a hexagonal $[a]_I$ axis is parallel to $[a]_{II}$ or $[b]_{II}$.

The electron microscope and X-ray orientation relations are significant since they indicate that the aragonite-type to calcite-type transformation in KNO_3 does not necessarily proceed by shearing of layers along the basal plane. Relation [1] where $[c]_{II} \parallel [c]_{I,hex,Z=3}$, $[a]_{II} \parallel [a]_I$, is the same as that for the h.c.p. f.c.c. structure change in cobalt⁽¹³⁸⁾ involving stacking faults. The relations [3] and [2] - [7] cannot be achieved simply by shearing on the basal $(001)_{II}$ plane. The previously reported orientations of Davis and Oshier⁽²²⁵⁾ and others (Section 4.6.1) also show this. Hence, cooperative movements occur on other planes.

The results of optical microscopy briefly summarized in Table 3, Section 4.3.2 show that surface traces in KNO_3I are often observed close to certain zones. In experiment number 16, crystal (ii) two sets of faint oblique traces at -44° and $+62^\circ$ to $[c]_{II}$ coexisted with well-defined transverse surface tilts. The fast extinction direction of the crystal was maintained, as shown by use of a quartz wedge. The origin of the oblique traces may be explained as follows. Standard stereograms of $(010)_{II}$ and $(01\bar{1})_{I,RhZ=4}$ are superimposed according to relation [3] which was experimentally observed by X-rays as $[c]_{II} \parallel [c]_{I,hex,Z=3}$, $[b]_{II} \parallel [a]_I$. Traces would be found at $+63^\circ$ by planes which lie on zones of the type $\{0k\ell\}$, including $\{00\ell\}$. At -44.5°

traces correspond to a zone of the type $\{hkh\}$ which includes $(\bar{1}\bar{1})_I$ and $(100)_I$, but does not include any other $\{110\}_I$ planes. $\{110\}_{I, Rh, Z=4}$ twinning in calcite is well known, but the other set of $(100)_I$ or $(\bar{1}\bar{1})_I$ traces has not been previously observed by optical microscopy, in association with the $II \rightarrow I$ transformation.

This observation was repeated in experiment numbers 17 and 2 for the 63° to $[c]_{II}$ traces. Similarly, in experiment number 1, faint oblique surface traces at $+64^\circ$ and -43° to $[c]_{II}$ were noted in a crystal of undulose extinction. This indicates a variety of twinned product orientations.

In experiment 10, crystal (ii), faint oblique markings at -63° to $[c]_{II}$ were found in a $KNO_3 I$ crystal which was extinct in all directions. This implied that the $[c]_{II}$ axis tilted 90° about $[a]_{II}$ to become parallel to $[b]_{II}$ as was already previously observed (reference 105 and Section 4.6.1). When two standard stereograms of $(010)_{II}$ and $(111)_{I, Rh, Z=4}$ are superimposed according to the correspondence $[b]_{II} \parallel [c]_{I, hex, Z=3}$, $[c]_{II} \parallel [a]_I$, traces might be anticipated from planes lying a zone of the type $\{11\bar{l}\}$ which includes the planes $\{110\}$, $\{11\bar{1}\}$, $\{001\}$. These possibilities are consistent with those discussed above for the previous lattice correspondence. Hence, considerable information concerning the transformation mechanism may be gained by the optical microscopy of surface tilts, to complement X-ray and electron microscope data.

The apparent equivalence of types of zones producing traces on $\{b\}_{II}$ and $\{c\}_{II}$ faces, might lead to the speculation that in the trans-

formation there is a stage where the lower, orthorhombic symmetry is disregarded, in favour of a higher-symmetry, cubic-type, intermediate structure. During the second stage of this hypothetical mechanism, the rhombohedral product is formed.

BaCO_3 (witherite)⁽²⁹⁵⁾ transforms from aragonite-type orthorhombic to the calcite-type rhombohedral phase at 803°C . At 976°C it adopts an NaCl-type structure, S.G. $\text{Fm}\bar{3}\text{m}$.^(296,297) Strontianite (SrCO_3)⁽²⁹⁶⁾ similarly transforms directly from aragonite-type to calcite-type structure. Calcite-type RbNO_3 II becomes NaCl-type phase I on heating (Chapter 2). Hence a hypothetical cubic intermediate is unlikely.

At this stage, it is apparent that the aragonite-type to calcite-type transformation in potassium nitrate is not necessarily reconstructive as was generally considered.^(34,44) This is implied by reproducible, ordered, surface effects and X-ray and electron microscope orientations. This conclusion is consistent with Kennedy and Patterson's⁽³⁶⁾ finding that the orthorhombic to rhombohedral transformation in thallos nitrate may proceed by two distinct mechanisms, one reconstructive, and the other similar to a martensite-type process.

The transformation in KNO_3 may be compared with transformations in ammonium nitrate⁽²⁹⁹⁻³⁰¹⁾ which has five polymorphs at normal pressure. In rigorously dried crystals the II \rightarrow IV transformation occurs at 50.85°C .⁽³⁰²⁾ In moist crystals it proceeds via phase III at 80°C and 29°C on cooling and 37°C and 86°C on heating. The transformation involves a process of dissolution and recrystallization.

In potassium nitrate the reproducible, ordered surface effects

are due to shape changes in the transformed crystal. The observed superheating beyond 128°C in the optical microscope, is consistent with previous reports. (225) This, together with the variety of rational and irrational orientation relations indicate that the transformation should be examined as a martensite mechanism. The previous hypotheses of such a type of mechanism deal only with relation [1], discussing along the lines of stacking faults and shear on the basal plane only.

It is now clearly evident that there is cooperative movement of atoms along other non-basal planes, which leads to the variety of orientation relations. Such movements are being considered along the lines of deformational relationships between sub-cells and the true cell (references 303, 37 and from understanding of the mechanisms operating in RbNO_3 transformations. (360)) In terms of a martensite mechanism, suitable lattice correspondences and deformations need to be found.

Strain axes parameters may be obtained by the matrix algebra formulation of martensite theory, such as presented by Bowles and Mackenzie. (27-29) The structure change here is complicated in that a lattice correspondence producing the irrational relations is not readily apparent. A clue to choosing appropriate shear systems however, may lie in understanding the lattice dynamics of the structure. (20-22,358) One may postulate that lattice perturbations described in phonons, resonate with increasing energy, and at transformation precipitate into a shear system. In impure or highly imperfect

crystals such cooperative behaviour is retarded, and the transformation is achieved by an alternative mechanism.

A martensite-mechanism may involve a sub-cell or polyhedron of phase II which shears on one of its low index planes to become a sub-cell of phase I. The plane of shear may have a relatively high index in the orthorhombic (II) or rhombohedral (I) cell. In KNO_3 II the hexagonal arrays of cations in h.c.p. sequence define polyhedra which are similar to an acute rhombohedron, and which are stacked alternatively facing $[010]_{\text{II}}$ and $[0\bar{1}0]_{\text{II}}$ directions. Two sides of a polyhedron have lengths $\frac{1}{2}[110] = 5.334 \text{ \AA}$ while the third is 4.483 \AA determining its height. The polyhedra contain almost planar trigonal nitrate groups slightly tilted with respect to the basal (II) plane, and they are connected by faces parallel to (001) on which they lie.

One may postulate that at transformation the structure unfolds, probably accompanied by tilting of nitrate groups. The polyhedra of II becomes rhombohedral $Z=1$ cells of I, and irrational orientations result.

A systematic consideration of deformational relationships between sub-cells and a true cell is given by Kennedy⁽³⁰³⁾ for the structure types MX , MX_2 , MXO_3 . Kennedy points out that many structures are related by deformations of the cation cage with corresponding tilts of anions and "shuffles". Structural analysis of TlNO_3 , III is consistent with this interpretation.⁽²⁴⁾

Hence, such deformations with consequent misregistry and transformation shear systems need to be found to fully explain the aragonite-type to calcite-type mechanism.

SECTION 4.7 CONCLUSION

In conclusion, therefore, this work has examined the transformation from the points of view of optical microscopy, X-ray diffraction, electron microscopy and computing. Calculations of the Arkharov estimation of the region of coherent rearrangement for the given orientation in KNO_3 showed that its size is much smaller than that of a crystallite suitable for electron microscopy.

At least 7 reliable and reproducible orientation relations were found, including 2 by electron microscopy. Together with a few previously reported relations^(225,105) they indicate that there is cooperative movement of ions on non-basal , planes as well as on $(001)_{II}$. The latter shearing only was hitherto usually discussed. Optical microscopy of faint surface tilts reveal oblique as well as transverse tilts. Complementing X-ray orientations, the oblique traces may be produced from shearing by twinning or slip on such planes as $\{110\}$, $\{1\bar{1}1\}$, and $\{001\}$ of the rhombohedral, $Z=4$ calcite-type cell of KNO_3I . Experimental observations suggest that the aragonite to calcite transformation may proceed by a displacive, martensite-type mechanism. Further quantitative analyses along these lines are suggested.

CHAPTER 5

CHAPTER 5PART A - A MARTENSITE ANALYSIS OF THE TETRAGONAL TO
MONOCLINIC TRANSFORMATION IN ZIRCONIA

	Page
SECTION 5.1 INTRODUCTION	247
5.2 RESULTS	250
5.3 DISCUSSION AND CONCLUSION	267

PART B - ELECTRON MICROSCOPY OF MERCURIC SULPHIDE

5.4 INTRODUCTION	270
5.5 OBSERVATION	271

CHAPTER 5

PART A - A MARTENSITE ANALYSIS OF THE TETRAGONAL TO MONOCLINIC TRANSFORMATION IN ZIRCONIA

SECTION 5.1 INTRODUCTION

At atmospheric pressure zirconia exists in three modifications:⁽⁴¹⁾



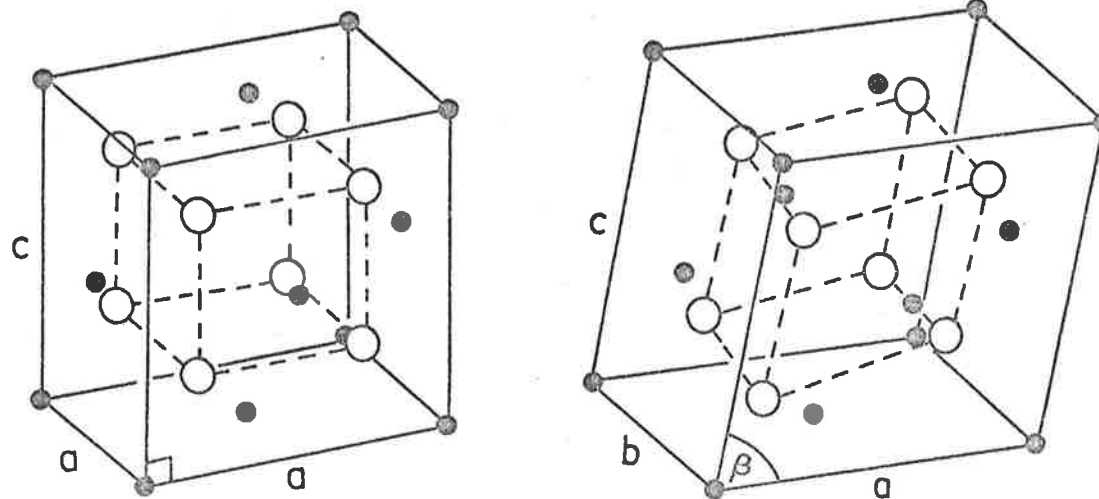
The tetragonal to monoclinic transformation in zirconia was considered to be martensitic,^(304,308,23) although until about 1974, no comprehensive analysis appeared, to explain the observed habit planes and shear systems. Fraser and Kennedy⁽⁴¹⁾ then fully described the transformation mechanism in terms of three lattice correspondences and a variety of slip and twin lattice invariant shear systems. The lattice parameters of the two phases at the transformation temperature were calculated from parameters and thermal expansion coefficients of Patil and Subbarao.⁽³⁰⁵⁾

Due to the nature of the structure change, the determination of the magnitudes and directions of the principal deformation axes was considered in two parts. A two dimensional homogeneous strain is coupled with an expansion or contraction perpendicular to it. Fraser adapted an analytical geometry method⁽³⁰⁹⁾ which factorizes the homogeneous shear into an expansion or contraction of the cell edge together with a simple shear. The method is characterized by two of the deformational directions being irrational, and the magnitude of η_3 varies by only $\sim 1\%$ from unity for all three lattice correspondences. The method was verified by calculations using the Bowles and

Mackenzie⁽²⁷⁻²⁹⁾ method. The information was then analysed in the CDC 6400 computer, using program MRTNST supplied by Ledbetter and Wayman.⁽³⁰⁾

Shortly afterwards Bansal and Heuer⁽³⁰⁸⁾ published results of a martensite analysis by the matrix algebra method of Bowles and Mackenzie. Fraser of this laboratory, however, noticed that some of the details of their calculation appeared to be erroneous. For a particular lattice correspondence a metric is assymmetric. By definition^(27,46) it is a symmetric, square (3 x 3) matrix relating vectors in basis A to the reciprocal basis A*. Secondly, the volume increase determined from unit cell lattice parameters is 1.9030% which differs from 1.8356% and 1.8360% which were calculated from principal distortions of the two lattice correspondences. Fraser⁽⁴¹⁾ concluded that errors in the initial stages of their work could be serious.

This section of the thesis, therefore, describes a martensite analysis of the transformation using Bansal and Heuer's⁽³⁰⁸⁾ lattice parameters, the purpose being to determine the effect of the above errors. The shorter method of Fraser was used to find the magnitude and directions of the principal deformation axes. The various shear systems in the three lattice correspondences were likewise analysed by PROGRAM MRTNST. Essentially, therefore, Fraser's calculations were repeated with slightly different lattice parameters, so that the effect of small changes in lattice parameters on predicted orientations and habit planes, was investigated. The results of calculations are tabulated.



II (Tetragonal)

III (Monoclinic)

Fig. 1. Crystal structures of zirconia II and III. ⁽⁴¹⁾

● zirconium atoms

○ oxygen atoms

SECTION 5.2 RESULTS

TABLE 1

LATTICE PARAMETERS (Å)

(at 1000°C, from Bansal and Heuer^(307,308))

Tetragonal (phase II)	a = 5.1358
	b = 5.2609
Monoclinic (phase III)	a = 5.1538
	b = 5.2100
	c = 5.3263
	$\beta = 81.385^\circ$

TABLE 2(a)

LATTICE CORRESPONDENCES

(from Fraser⁽⁴¹⁾)

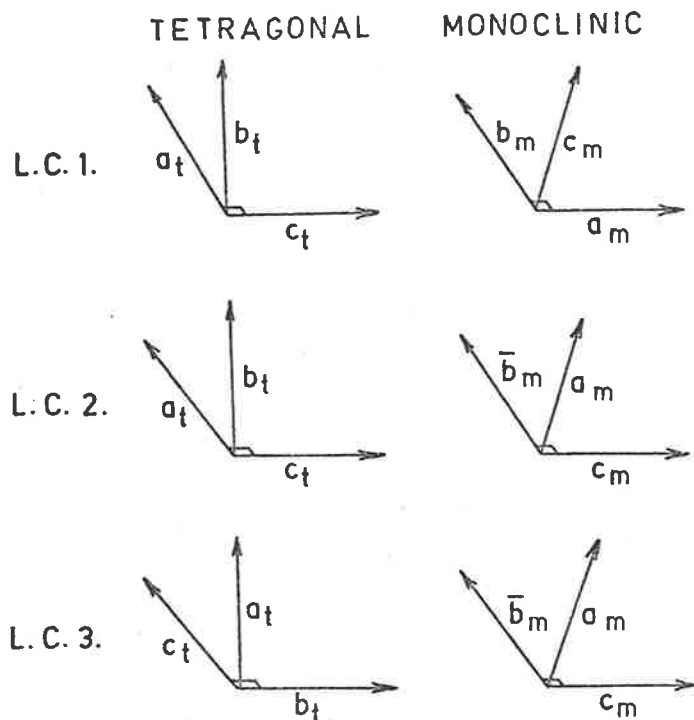


TABLE 2(b)
LATTICE CORRESPONDENCE MATRICES ⁽⁴¹⁾

LC1	$\begin{vmatrix} 0 & 0 & 1 \\ 1 & 0 & 0 \\ 0 & 1 & 0 \end{vmatrix} *$	or	$\begin{vmatrix} 0 & 0 & 1 \\ 0 & \bar{1} & 0 \\ 1 & 0 & 0 \end{vmatrix}$	
LC2	$\begin{vmatrix} 0 & 1 & 0 \\ \bar{1} & 0 & 0 \\ 0 & 0 & 1 \end{vmatrix} *$	or	$\begin{vmatrix} 1 & 0 & 0 \\ 0 & 1 & 0 \\ 0 & 0 & 1 \end{vmatrix} \otimes$	
LC3	$\begin{vmatrix} 0 & 1 & 0 \\ 0 & 0 & 1 \\ 1 & 0 & 0 \end{vmatrix} \otimes$	or	$\begin{vmatrix} 1 & 0 & 0 \\ 0 & 0 & \bar{1} \\ 0 & 1 & 0 \end{vmatrix} *$	

* matrices used by present authors

⊗ matrices used by B&H

(Two sets of matrices arise because of equivalence of $[a_1]$ and $[a_2]$ tetragonal axes).

TABLE 3

PRINCIPAL DEFORMATIONS

(Indices are referred to an orthonormal basis, with axes parallel to the base axes of the tetragonal lattice).

	LC1	LC2	LC3
η_1 (direction)	[0, .8233, .5676]	[0, .7277, -.6859]	[.7565, -.6540, 0]
(magnitude)	1.0865	.9293	.9390
η_2 (direction)	[0, -.5676, .8233]	[0, .6859, .7277]	[.6540, .7565, 0]
(magnitude)	.9245	1.0809	1.0959
η_3 (direction)	[100]	[100]	[001]
(magnitude)	1.0144	1.0144	.9903
$\Sigma \eta_i^{2-3}$.0644	.0611	.0633

TABLE 4

LATTICE CORRESPONDENCES, PRINCIPAL DISTORTIONS AND SHEAR SYSTEMS
USED BY BANSAL AND HEUER (307,308)

	<u>Type 2 (LC3)*</u>	<u>Type 3 (LC2)</u>
<u>Lattice Correspondence Matrix</u>	$\begin{vmatrix} 1 & 0 & 0 \\ 0 & 0 & 1 \\ 0 & 1 & 0 \end{vmatrix}$	$\begin{vmatrix} 1 & 0 & 0 \\ 0 & 1 & 0 \\ 0 & 0 & 1 \end{vmatrix}$
* (LC3) of the writer		
<u>Principal Deformations</u>		
η_1 (direction) (magnitude)	$[\ .6288, \ -.7775, \ 0]$ 1.0978	$[.6849, \ 0, \ .7286]$ 1.0829
η_2 (direction) (magnitude)	$[.7775, \ .6288, \ 0]$.9367	$[.7286, \ 0, \ \-.6849]$ 1.01444
η_3 (direction) (magnitude)	$[001]$.9903	$[001]$.9270
<u>Shear systems (slip)</u>	$(1\bar{1}0)[001]$ $(111)[1\bar{1}0]$ $(100)[001]$ $(100)[011]$	$(1\bar{1}0)[001]$ $(1\bar{1}0)[110]$ $(10\bar{1})[010]$ $(111)[1\bar{1}0]$

TABLE 5
COMPARISON OF SOLUTIONS REPORTED BY B.&H. (307,308)
AND THE WRITER

B.&H. reported 32 solutions, for the two lattice correspondences, each shear system giving 4 solutions. The writer reports only the following 20:

	<u>Shear system</u>	<u>No. of solutions</u>
LC3 (type 2)	(1 $\bar{1}$ 0)[001]	0
	(111)[1 $\bar{1}$ 0]	4
	(100)[001]	0
	(100)[011]	4
LC2 (type 3)	(1 $\bar{1}$ 0)[001]	2
	(1 $\bar{1}$ 0)[110]	2
	(10 $\bar{1}$)[010]	4
	(111)[1 $\bar{1}$ 0]	4
		—
		20
		—

TABLE 6
COMPARISON OF SOLUTIONS REPORTED BY
FRASER⁽⁴¹⁾ AND THE WRITER

Fraser⁽⁴¹⁾ obtained 42 solutions from the three lattice correspondences, while the writer found only 38, for the same shear systems. Not all of Fraser's shear systems gave solutions, while some extra habit planes were found by the writer. Habit planes of both sets of solutions were numbered and plotted on a stereogram using PROGRAM HPPLØT. The angles between corresponding habit planes are listed below.

Fraser(1974)

no. of plane	Angle (^o)	no. of plane	Angle (^o)	no. of plane	Angle (^o)
1	3	16	39	31	7
2	5	17	-	32	14
3	2	18	-	33	3
4	2	19	1	34	5
5	4	20	3	35	-
6	2.5	21		36	5.5
7	4	22	2.5	37	-
8	1	23	3	38	9
9	4	24	1	39	1
10	-	25	3	40	-
11	1.5	26	5	41	1.5
12	2	27	8	42	4
13	1.5	28	8	43*	4.5
14	2.5	29	8		
15	3	30	8.5		

*extra habit plane obtained by present authors
 -no solutions found by present authors.

TABLE 7ORIENTATION RELATIONS IMPLIED BY THE LATTICE DEFORMATIONS

(obtained by the writer)

LC1 : (0, .8233, .5676) _t	(.5676, 0, .8233) _m , [100] _t	[010] _m
LC2 : (0, .7277, -.6859) _t	(.7277, 0, -.6859) _m , [100] _t	[0 $\bar{1}$ 0] _m
LC3 : (.7565, -.6540, 0) _t	(.7565, 0, -.6540) _m , [001] _t	[0 $\bar{1}$ 0] _m

TABLE 8

DETAILS OF SOLUTIONS OBTAINED BY THE WRITER

(Symbols correspond to those published with the description of PROGRAM MRTNST by Ledbelter and Wayman.⁽³⁰⁾).

Lattice Correspondence 3:

Lattice Invariant Shear	No.	Angle	Rotation Axis [u]	Rigid Body Rotation (THETA) (°)	Habit Plane Indices (P1)	Direction of Shape Strain [D1]	Magnitude of Shape Strain (M1)
(1 $\bar{1}$ 0)[001]							no solution
(111)[1 $\bar{1}$ 0]	1	2.98	[.383 .082 -.898] ~[10 $\bar{2}$]	8.06	(.144 -.979 .151) ~(1 $\bar{7}$ 1)	[-.916 -.277 -.284] ~[3 $\bar{1}$ 1]	.197
	2	2.98	[-.191 .496 .827] ~[1 $\bar{2}$ 4]	.349	(-.889 -.368 -.279) ~(3 $\bar{1}$ 1)	[.234 -.956 .172] ~[151]	.197
	3	2.56	[-.602 .143 -.767] ~[415]	3.24	(-.245 -.937 -.257) ~[141]	[-.973 .076 .213] ~[401]	.170
	4	2.56	[-.019 -.367 .908] ~[013]	6.86	(-.981 -.003 .199) ~(501)	[-.164 -.948 -.264] ~[126]	.170
(100)[001]							no solution
(100)[011]	5	7.60	[-.031 .584 -.792] ~[045]	18.464	(-.185 -.862 -.483) ~(142)	[-.986 .077 .142] ~[701]	.396
	6	7.60	[.225 -.007 .951] ~[104]	4.44	(.995 .092 -.051) ~(100)	[-.007 .869 .483] ~[021]	.396

TABLE 8 (Cont.)

Lattice Invariant Shear	No.	Angle	Rotation Axis [u]	Rigid Body Rotation (THETA) (°)	Habit Plane Indices (P1)	Direction of Shape Strain [D1]	Magnitude of Shape Strain (M1)
(100)[011]	7	2.12	[-.223 .002 .952] ~[104]	4.48	(.938 .303 .170) ~(621)	[-.024 .869 -.483] ~[021]	.120
	8	2.12	[.252 -.899 -.350] ~[141]	3.49	(-.032 -.877 .491) ~(021)	[-.947 -.254 -.192] ~[511]	.120
Lattice Correspondence 2:							
(110)[001]	9	3.54	[.990 .022 -.135] ~[701]	4.42	(-.802 -.586 -.118) ~(751)	[-.165 .123 -.955] ~[118]	.110
	10	3.54	[.135 .987 .083] ~[170]	4.97	(-.207 .090 -.998) ~(105)	[-.799 .598 -.061] ~[110]	.110
(110)[110]	11	0.82	[.982 .007 .182] ~[501]	4.33	(-.014 .997 .084) ~(010)	[.002 .043 .975] ~[001]	.153
	12	0.82	[-.982 -.007 .185] ~[501]	4.40	(.001 .118 1.017) ~(019)	[-.015 1.000 .007] ~[010]	.153
(101)[010]	13	2.90	[-.393 -.235 -.868] ~[214]	7.90	(.444 -.860 .258) ~(231)	[-.826 -.442 .341] ~[211]	.187

continued/.....

TABLE 8 (Cont.)

Lattice Invariant Shear	No.	Angle	Rotation Axis [u]	Rigid Body Rotation (THETA) (°)	Habit Plane Indices (P1)	Direction of Shape Strain [D1]	Magnitude of Shape Strain (M1)
(10 $\bar{1}$)[010]	14	2.90	[-.341 .538 .753]	3.45	(.774 .516 -.377)	[-.523 .823 -.216]	.187
			\sim [$\bar{1}22$]		\sim (21 $\bar{1}$)	\sim [$\bar{2}4\bar{1}$]	
	15	2.90	[.341 .538 -.753]	3.45	(.774 -.516 -.377)	[-.523 -.823 -.216]	.187
			\sim [12 $\bar{2}$]		\sim (2 $\bar{1}\bar{1}$)	\sim [$\bar{2}4\bar{1}$]	
	16	2.90	[.393 -.235 .868]	7.90	(.444 .860 .258)	[-.826 .442 .341]	.187
			\sim [2 $\bar{1}4$]		\sim (221)	\sim [$\bar{2}11$]	
(111)[1 $\bar{1}0$]	17	5.95	[-.042 -.994 -.098]	4.56	(-.740 -.670 -.064)	[-.616 .595 -.504]	.212
			\sim [0 $\bar{1}0$]		\sim ($\bar{1}10$)	\sim [$\bar{1}1\bar{1}$]	
	18	5.95	[-.403 -.041 .892]	10.86	(-.684 .516 -.527)	[-.679 -.734 -.009]	.212
			\sim [$\bar{1}02$]		\sim ($\bar{1}1\bar{1}$)	\sim [$\bar{1}\bar{1}0$]	
	19	1.02	[-.985 .006 -.167]	4.38	(-.009 -.108 -1.018)	[.077 -.997 -.006]	.168
			\sim [$\bar{6}0\bar{1}$]		\sim (0 $\bar{1}9$)	\sim [010]	
	20	1.02	[.973 .157 -.163]	5.24	(.075 -.993 -.091)	[-.015 -.026 -.976]	.168
			\sim [61 $\bar{1}$]		\sim (0 $\bar{1}0$)	\sim [00 $\bar{1}$]	
(010)[101]	21	3.12	[.978 .199 -.066]	4.89	(.193 -.955 .232)	[.618 -.221 -.737]	.120
			\sim [5 $\bar{1}0$]		\sim (1 $\bar{5}1$)	\sim [3 $\bar{1}3$]	

TABLE 8 (Cont.)

Lattice Invariant Shear	No.	Angle	Rotation Axis [u]	Rigid Body Rotation (THETA) (°)	Habit Plane Indices (P1)	Direction of Shape Strain [D1]	Magnitude of Shape Strain (M1)
	22	3.12	[-.101 -.272 -.934] ~[139]	4.19	(.623 -.275 -.733) ~(213)	[.158 -.949 .267] ~[162]	.120
(110)[110]	23	13.83	[.037 .169 .961] ~[016]	27.58	(-.864 .474 -.174) ~(531)	[-.535 -.798 .270] ~[231]	.508
	24	13.83	[.002 -.994 .110] ~[091]	4.78	(-.725 -.651 .230) ~(331)	[-.715 .659 -.228] [331]	.508
	25	.82	[.986 -.006 -.165] ~[601]	4.79	(-.014 -.992 .127) ~(081)	[-.001 -.235 -.949] ~[014]	.169
	26	.82	[-.985 .006 -.167] ~[601]	4.85	(-.002 -.314 -.972) ~(013)	[-.014 -.978 .201] ~[051]	.169
(101)[101]	27	11.58	[.043 .981 -.186] ~[051]	22.43	(.552 -.328 -.785) ~(324)	[-.821 -.218 -.515] ~[412]	.402
	28	.88	[-.983 .185 .008] ~[510]	4.49	(.051 .227 .996) ~(014)	[.000 .993 -.114] ~[091]	.164
	29	.99	[.982 .187 -.008] ~[510]	4.56	(.008 -.999 .041) ~(010)	[.106 -.139 -.961] ~[119]	.180

TABLE 8 (Cont.)

Lattice Invariant Shear	No.	Angle	Rotation Axis [u]	Rigid Body Rotation (THETA) (°)	Habit Plane Indices (P1)	Direction of Shape Strain [D1]	Magnitude of Shape Strain (M1)
($\bar{1}11$)[110]	30	1.04	[.973 -.142 .180] $\sim[7\bar{1}1]$	5.71	(-.069 -.993 .102) $\sim(\bar{1}\bar{9}1)$	[.033 -.205 .955] [0 $\bar{1}5$]	.183
	31	1.04	[-.992 -.014 .122] $\sim[801]$	4.77	(.026 -.292 -.979) $\sim(0\bar{1}\bar{3})$	[-.073 -.979 .184] $\sim[051]$.183
	32	4.93	[-.401 -.171 -.879] $\sim[2\bar{1}5]$	7.87	(.640 .356 -.698) $\sim(21\bar{2})$	[.781 -.559 .271] $\sim[321]$.171
	33	4.93	[-.136 .981 -.132] $\sim[1\bar{7}\bar{1}]$	5.63	(.825 -.522 .222) $\sim(4\bar{2}1)$	[.577 .405 -.692] $\sim[11\bar{2}]$.171
Lattice Correspondence 2							
(110)[001]	34	3.54	[.135 -.987 -.083] $\sim[1\bar{7}0]$	4.97	(-.207 -.090 .998) $\sim(\bar{1}05)$	[-.799 .598 .061] $\sim[110]$.110
(010)[001]	35	3.54	[.990 -.022 .135] $\sim[701]$	4.42	(-.802 .586 1.180) $\sim(\bar{1}12)$	[-.165 -.123 .955] $\sim[1\bar{1}8]$.110
(110)[$\bar{1}10$]	36	.82	[-.982 .007 -.185] $\sim[10\bar{5}]$	4.40	(.001 -.118 -1.017) $\sim(0\bar{1}\bar{9})$	[-.015 -1.000 -.007] $\sim[0\bar{1}0]$.153
	37	.82	[.982 -.007 -.182] $\sim[50\bar{1}]$	4.33	(-.014 -.997 -.084) $\sim(0\bar{1}0)$	[.002 -.043 -.975] $\sim[00\bar{1}]$.153

continued/.....

TABLE 8 (Cont.)

Lattice Invariant Shear	No.	Angle	Rotation Axis [u]	Rigid Body Rotation (THETA) ($^{\circ}$)	Habit Plane Indices (P1)	Direction of Shape Strain [D1]	Magnitude of Shape Strain (M1)
(101)[$\bar{1}01$]	38	9.55	[-.009 .055 .975] $\sim[001]$	4.24	(-.639 -.299 -.726) $\sim(2\bar{1}\bar{2})$	[.679 -.170 -.697] $\sim[4\bar{1}\bar{4}]$.222
	39	.79	[-.982 .189 .007] $\sim[510]$	4.38	(.031 -.024 -1.024) $\sim(00\bar{1})$	[-.003 -.995 -.098] $\sim[0\bar{1}0]$.148
	40	.81	[.981 .192 -.007] $\sim[510]$	4.45	(.005 -.984 -.180) $\sim(05\bar{1})$	[-.041 .054 -.974] $\sim[00\bar{1}]$.151
($\bar{1}11$)[110]	41	5.95	[-.403 .041 -.892] $\sim[\bar{1}0\bar{2}]$	10.86	(.684 .516 -.527) $\sim(11\bar{1})$	[.679 -.734 -.009] $\sim[1\bar{1}0]$.211
	42	5.95	[-.042 .994 .098] $\sim[010]$	4.56	(.740 -.670 -.064) $\sim(1\bar{1}0)$	[.616 .595 -.504] $\sim[11\bar{1}]$.212
	43	1.02	[.973 -.157 .163] $\sim[6\bar{1}1]$	5.24	(-.075 -.993 -.091) $\sim(0\bar{1}0)$	[.015 -.026 -.976] $\sim[00\bar{1}]$.168
	44	1.02	[-.985 -.006 .166] $\sim[601]$	4.38	(.009 -.108 -1.018) $\sim(0\bar{1}9)$	[-.077 -.997 -.006] $\sim[0\bar{1}0]$.168
<u>Lattice Correspondence 3</u>							
(010)[$\bar{1}00$] (twinning)	45	5.19	[-.146 -.108 -.960] $\sim[\bar{1}\bar{1}8]$	5.26	(.483 -.721 -.509) $(3\bar{2}\bar{2})$	[.478 -.714 .499] $\sim[3\bar{2}\bar{2}]$.039

continued/.....

TABLE 8 (Cont.)

Lattice Invariant Shear	No.	Angle	Rotation Axis [u]	Rigid Body Rotation (THETA) (°)	Habit Plane Indices (P1)	Direction of Shape Strain [D1]	Magnitude of Shape Strain (M1)
	46	5.19	[.146 .108 -.960] ~[118]	5.26	(.483 -.721 .509) ~(232)	[.478 -.714 -.523] ~[232]	.039
	47	3.67	[.215 -.134 -.944] ~[217]	3.77	(-.483 -.721 -.509) ~(232)	[.478 .714 -.499] ~[232]	.039
	48	3.67	[-.215 .134 -.944] ~[217]	3.77	(-.483 -.721 -.509) ~(232)	[-.478 -.714 .499] ~[232]	.039
(010)[101]	49	3.12	[.997 -.079 -.009] ~[100]	4.56	(-.679 -.229 .715) ~(313)	[-.078 -.984 -.157] ~[061]	.114
	50	3.12	[-.037 .123 -.968] ~[018]	4.31	(-.116 -.986 -.122) ~(181)	[-.679 -.175 .696] ~[414]	.114
(011)[011]	51	.59	[-.124 -.005 -.969] ~[108]	4.41	(-.061 -.996 .060) ~(010)	[-.998 -.065 -.001] ~[100]	.148
	52	.56	[-.123 .005 .969] ~[108]	4.37	(-.990 -.140 .006) ~(710)	[.018 -1.000 -.011] ~[010]	.152
(101)[101]	53	13.03	[.166 -.985 -.036] ~[160]	26.87	(-.828 -.267 .505) ~(312)	[-.517 -.170 -.860] ~[318]	.512

continued/.....

TABLE 8 (Cont.)

Lattice Invariant Shear	No.	Angle	Rotation Axis [u]	Rigid Body Rotation (THEATA) (°)	Habit Plane Indices (P1)	Direction of Shape Strain [D1]	Magnitude of Shape Strain (M1)
	54	.50	[.004 .122 1.017] ~[018]	4.49	(.981 .194 .029) ~(510)	[-.082 .997 .003] ~[010]	.164
($\bar{1}11$)[01 $\bar{1}$]	55	4.93	[.899 -.017 .428] ~[201]	10.25	(-.498 -.701 .498) ~($\bar{2}\bar{3}\bar{2}$)	[.025 -.693 -.704] ~[0 $\bar{1}\bar{1}$]	.213
	56	4.19	[-.229 .972 -.047] ~[$\bar{1}40$]	4.31	(.064 .743 .682) ~(011)	[.376 .650 -.635] ~[12 $\bar{2}$]	.271
	57	.66	[-.099 -.112 -.965] ~[0 $\bar{1}\bar{8}$]	4.96	(.061 .996 -.065) ~(010)	[.999 .052 .013] ~[100]	.165
	58	.69	[-.139 .005 .967] ~[107]	4.38	(-.991 -.132 -.002) ~($\bar{8}\bar{1}0$)	[.017 -.999 .046] ~[0 $\bar{1}0$]	.161
<u>Lattice Correspondence 1</u>							
($10\bar{1}$)[010]	59	13.56	[-.786 .016 .603] ~[403]	30.49	(-.205 .962 .184) ~($\bar{1}51$)	[-.533 .234 .794] ~[$\bar{2}\bar{1}3$]	.618
	60	13.56	[-.962 -.274 .009] ~[$\bar{7}20$]	4.49	(.565 -.060 -.843) ~(20 $\bar{3}$)	[.042 -.997 .063] ~[010]	.618
	61	2.76	[.235 -.297 -.904] ~[1 $\bar{1}3$]	3.70	(.253 .923 -.296) ~(13 $\bar{1}$)	[.527 .274 .785] ~[213]	.124

TABLE 8 (Cont.)

Lattice Invariant Shear	No.	Angle	Rotation Axis [u]	Rigid Body Rotation (THETA) (°)	Habit Plane Indices (P1)	Direction of Shape Strain [D1]	Magnitude of Shape Strain (M1)
	62	2.76	.966 .243 -.088 $\sim \bar{4}10$	5.11	(-.537 -.327 -.797 $\sim (324)$	-.223 -.914 .332 $\sim \bar{2}83$.124
(010) 011	63	5.09	.154 -.131 -.956 $\sim 1\bar{1}\bar{7}$	3.93	(-.405 -.814 .427) $\sim (\bar{1}\bar{2}1)$.997 -.078 -.013 $\sim \bar{1}00$.355
	64	5.95	-.899 .017 .427 $\sim \bar{2}01$	10.28	(-.683 -.197 -.720) $\sim (\bar{7}\bar{2}\bar{7})$	-.025 -.692 .704 $\sim 0\bar{1}1$.285
	65	7.02	.905 -.019 .414 ~ 201	9.86	(-.683 -.197 .720) $\sim (\bar{7}\bar{2}\bar{7})$.025 -.708 .689 $\sim 0\bar{1}1$.373
	66	6.61	.099 .112 -.965 $\sim 01\bar{9}$	4.96	(.371 -.847 .391) $\sim (1\bar{2}1)$	-.999 -.052 .013 $\sim \bar{1}00$.384

The first 20 solutions of this table correspond to the twenty shear systems considered by Bansal and Heuer. The remaining solutions correspond to those considered by Fraser. (41)

TABLE 9

ORIENTATION RELATIONS
(Lattice correspondence 2)

Habit Plane Indices	Approx.	Planes and directions considered	Observed Angle	Predicted Angle	
				Writer	B&H
(-.802	$\bar{7}$	$(100)_t$ & $(100)_m$	$\sim 1^\circ$.62	.88
-.586	$\sim \bar{5}$	$[001]_t$ & $[001]_m$	$< 1^\circ$.15	.16
-.118)	$\bar{1}$	$[010]_t$ & $[100]_m$	$\sim 1^\circ$	8.72)	.85
		$[100]_t$ & $[010]_m$.62) *	
(-.014	0	$(100)_t$ & $(010)_m$	$\sim 1^\circ$.84	.95
-.997	~ 1	$[001]_t$ & $[001]_m$	$< 1^\circ$.03	.26
.084)	0	$[010]_t$ & $[100]_m$	$\sim 1^\circ$	8.62)	.91
		$[100]_t$ & $[010]_m$.81) *	

* The discrepancy is due to Bansal and Heuer's⁽³⁰⁸⁾ different labelling of axes.

TABLE 10

DIRECTION AND MAGNITUDE OF SHAPE DEFORMATION

No. of Solution	Habit Plane	Approx.	Direction	Magnitude
9	-.802	$\bar{7}$	-.165	.11021
	-.586	$\sim \bar{5}$.123	
	-.118	$\bar{1}$.955	
11	-.014	0	.002	.15261
	.997	~ 1	.043	
	.084	0	.975	

SECTION 5.3 DISCUSSION AND CONCLUSION

Bansal and Heuer^(307,41) observed two types of habit planes by transmission electron microscopy; type A, (671)_m, (761)_m corresponding to $\sim 7^\circ$ from $\{110\}_t$ and type B, (100)_t, (010)_t. Type A plates are within 2° of one of the predicted orientations, and type B are 4.5° from that predicted.

In the previous section, solutions obtained for the shear systems considered are given in Table 9 for comparison with Tables 3 and 4 respectively of Bansal and Heuer.⁽³⁰⁸⁾

The calculated angular difference between type A predicted habit planes and $(110)_t$ is

$$\begin{array}{l} (-.802 \\ -.586 \\ -.118) \end{array} \wedge (\bar{1}\bar{1}0) = 11.013^\circ \quad (\text{writer})$$

$$(\bar{6}\bar{7}1) \wedge (\bar{1}\bar{1}0) = 7.47 \quad (\text{Bansal \& Heuer})$$

In Table 9 it is seen that the predicted orientation calculated by the writer is slightly closer to the observed, than that of Bansal and Heuer. However, their habit plane predictions are closer to the observed, than those of the writer, given above. However, as seen in Table 8, there are several other shear systems and lattice correspondences which predict habit planes close to $\{110\}_t$ and $\{100\}_t$. A further consideration also is the experimental accuracy of habit plane determination.

When the solutions are compared with those of Fraser, as in Table 6 of the previous section, not all of Fraser's shear systems gave solutions,

whilst some extra habit planes were found by the writer. It is seen that the predicted location of habit planes is sensitive to the lattice parameters of the parent and product phases. Further conclusions from this work are briefly summarized below.

	B&H ^(307,308)	Fraser ⁽⁴¹⁾	Writer
Magnitude & direction of η 's	agree to 1st decimal place		
lattice parameters	1000°C	950°C	1000°C
Method of calculating η 's	different	same	same
Method of Analysis	stereographic	computational	computational
No. of predicted solutions	32		20
(for corresponding shear systems)		42	38
Total No. of Solutions	32	42	66

From Table 3 of Section 5.2, the volume change may be determined from principal deformations,⁽⁴¹⁾ according to ΔV (increase) = $100 - |1 - \eta_1 \eta_2 \eta_3|$. For lattice correspondences 1, 2 and 3, ΔV (increase) is 1.8934%, 1.8945% and 1.9068% respectively, whilst the volume increase calculated from unit cell lattice parameters by Bansal and Heuer, is 1.9030%. The analysis of Fraser⁽⁴¹⁾ based on lattice parameters of Patil and Subbarao,⁽³⁰⁵⁾ gave a value of 3.047% which was consistent with the value of the volume increase as calculated from lattice parameters.

In conclusion therefore, the writer's analysis was based on the

same lattice parameters as those of Bansal and Heuer.^(307,308) Their work however was thought to contain errors at an early stage in the analysis, so that it was repeated by a different method and using the computer. Comparison of results shows that as suggested by Fraser⁽⁴¹⁾ the errors have a significant effect on the number and position of predicted habit planes.

With the same method of analysis, the transformation was analysed using different sets of lattice parameters, Fraser using those of Patil and Subbarao⁽³⁰⁵⁾ and the writer using those of B&H.^(307,308) Comparison of results shows that the number and positions of predicted habit planes is sensitive to the lattice parameters. This indicates that in a martensite analysis great care should be taken to obtain the values of lattice parameters at the transformation temperature.

CHAPTER 5

PART B - ELECTRON MICROSCOPY OF MERCURIC SULPHIDE

SECTION 5.4 INTRODUCTION

Mercuric sulphide exists as two phases:

α -HgS	—————→	β -Hgs
cinnabar		metacinnabar
red, trigonal		black, cubic
Z = 3		Z = 4
a = 4.146 Å		a = 5.8157 Å
c = 9.497		
[refs.(310)-(312)]		[ref.(312)]

It occurs naturally as cinnabar and metacinnabar, respectively. (313)

The latter is the metastable form at one atmosphere. Hysteresis of the order of 100°C was observed in the transformation temperature. (314)

The thermal expansion coefficients of both phases are known. (314)

α -HgS is analogous to the trigonal elemental semiconductors selenium and tellurium, and consists of alternating Hg and S atoms along the trigonal, $[c]_{\text{hex}}$ axis. The rotatory power of cinnabar has been measured over a temperature range. (316) Several of the physical and chemical properties of mercuric sulphide have been determined. (317-324)

A few optical observations of the transformation have been made, but no orientation relations has yet been reported. The crystal morphology of α -HgS was studied in the electron microscope. (326)

In view of the high transformation temperature it was considered that HgS may be suitable for electron microscopy. The aim of this work therefore, was to find out if the transformation in which a structure containing -Hg-S-Hg-chains produces an oriented product.

SECTION 5.5 OBSERVATIONPreparation:

Several methods were considered for the preparation of HgS in small samples, which is difficult. (318,327-332) A diffusion growth method of Garner and White⁽³³⁰⁾ provided small and numerous crystallites of α -HgS suitable for electron microscopy. About 1.5 cms Hg at the bottom of a 25 mm pyrex test tube was covered by a 78.5% S: 21.5% Na₂S mixture and heated in an isothermal calorimeter type oven for 72 hours. On gradual cooling to room temperature the solidified flux was leached with methanol and numerous bright vermilion crystallites were washed many times with methanol and allowed to dry.

A vapour phase deposition method of Carlson⁽³²⁴⁾ was investigated with the assistance of Mr. T.G.K. Murty of the Physics Department, and apparatus therein. An inert crucible of red AR Grade HgS was heated to evaporation, in a vacuum chamber for over 6 hours. A thin layer of dark-coloured deposit collected on carbon-coated, unheated electron microscope grids placed at 20-25 cms from the crucible. The specimens thus obtained were mostly very thin giving powder rings in selected area diffraction patterns. However, a more solid, irregular mass gave a diffraction pattern which was identified as cubic metacinnabar.

Crystals of α -HgS prepared by the first-mentioned diffusion growth method, were ground with an agate mortar and pestle, and deposited on carbon-coated Au grids as a methanol suspension, by means of a 1 ml syringe. Specimens were examined in a Philips EM200 electron microscope calibrated by Au evaporation, on to Formvar-coated Cu grids.

In the electron microscope at 100 KV, triangular crystallites were quite stable under electron radiation. When a beam of maximum intensity was deflected for 15 minutes across a crystal, it caused movement of extinction contours, but no evidence of change was apparent in the image or diffraction pattern.

Specimens on a heating stage monitored by a Philips PW6310 Temperature Control Unit, were then examined. A liquid nitrogen anti-contaminator prevented any evolved gases from being deposited on the walls of the column. At an average beam intensity, the temperature was gradually increased until the crystal of α -HgS sublimed and the diffraction pattern disappeared. This observation was repeated twice. It was concluded therefore, that heating of cinnabar in the electron microscope caused possible decomposition and sublimation of the specimen prior to any transformation.

APPENDIX

APPENDIX A

THE ARKHAROV⁽²⁸⁴⁾ ESTIMATION OF THE REGION
OF COHERENT REARRANGEMENT

(See Chapter 4, Section 4.4)

Considering electron microscope orientation relation [1],

$$(001)_{II} \parallel (0001)_{I, \text{hex}, Z=3} ; [100]_{II} \parallel [11\bar{2}0]_I$$

In figure 1, the zero and first plane lattice nets defined by the cations are superimposed in the basal projection, and the differences in dimensions are slightly exaggerated for the purpose of illustration. Notations and symbols are the same as in the text⁽²⁸⁴⁾ to which equation numbers are referenced. Table 1 includes the lattice parameters while Table 2 lists the values of the main parameters for the calculation, defined in equations (4) to (12) of the text. The remaining tables are self-explanatory.

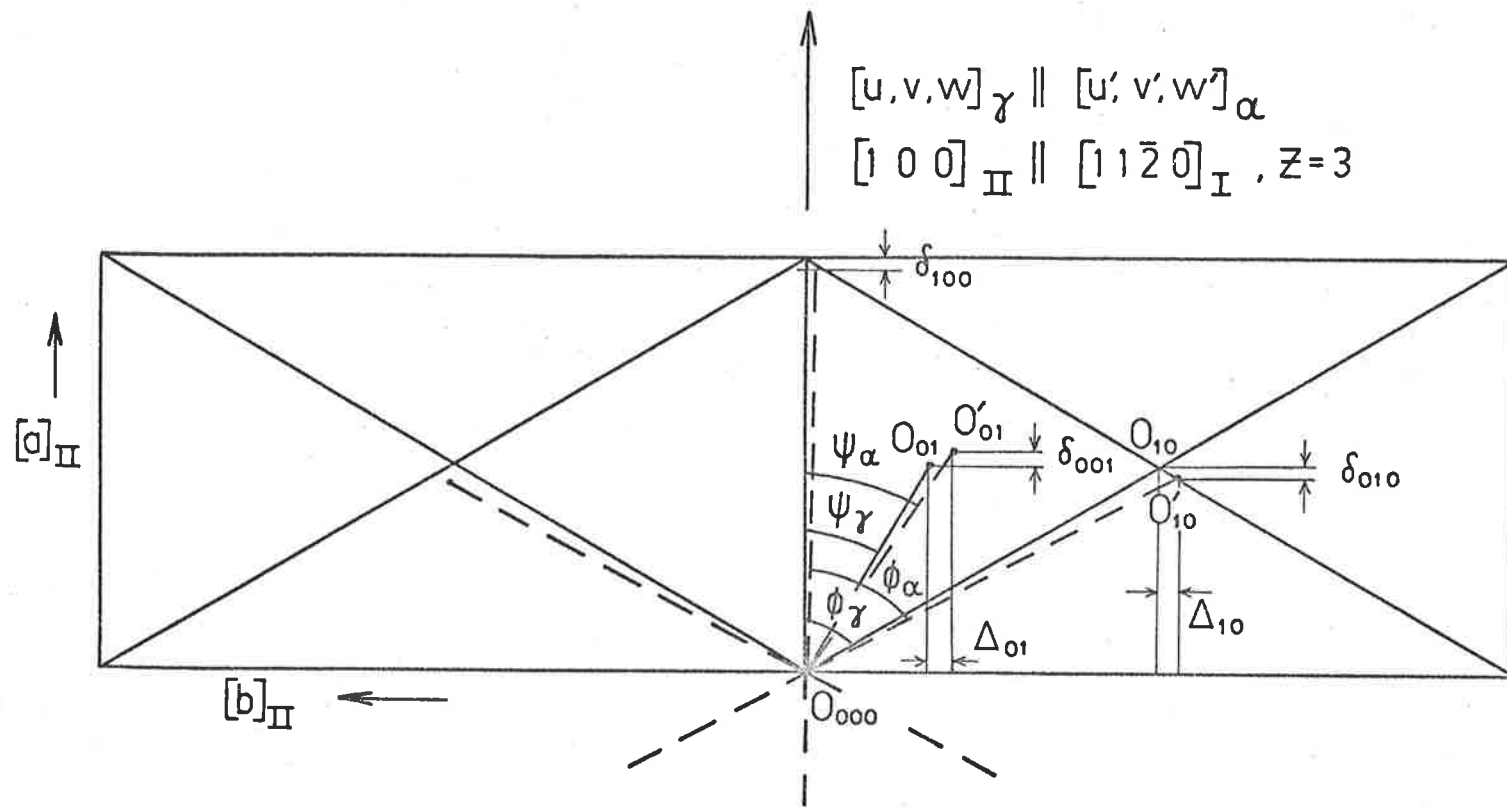


Fig. 1. Zero and first plane nets of KNO_3 II and I in orientation [1].

TABLE 1.Lattice Parameters (\AA) γ (II) at 125°C (225):

$$a = 5.426, b = 9.169, c = 6.550$$

 γ (II) at 128°C (corrected for thermal expansion by (237)):

$$a = 5.426, b = 9.169, c = 6.550$$

 α (I) at 128°C : (241)hexagonal, $z = 3$

$$a = 5.423 \quad c = 9.6385$$

Identify Period (\AA):

$$I_\gamma = [100]_{\text{II}} = 5.426$$

$$I_\alpha = [11\bar{2}0]_{\text{I}}, z = 3 = 5.423$$

Interplanar Distances (\AA):

$$d_{(001)}_{\text{II}} = 3.275_0$$

$$d_{(0001)}_{\text{I}} = 3.2128$$

$$D_1 = d_{(001)}_{\gamma} - d_{(0001)}_{\alpha} = 0.0621$$

$$S_\gamma = \frac{[110]}{2} = 5.3271 \quad (\text{\AA})$$

$$S_\alpha = 5.423 \quad (\text{\AA})$$

$$\phi_\gamma = \tan^{-1} \frac{[b]_{\text{II}}}{[a]_{\text{II}}} = 59.3837^\circ$$

$$\phi_\alpha = 60^\circ$$

$$v_\gamma = 3.1138 \quad (\text{\AA})$$

$$v_\alpha = \frac{\sqrt{3}}{3} I = 3.1309 \quad (\text{\AA})$$

$$\psi_\gamma = 90 - \phi_\gamma = 30.6162$$

$$\psi_\alpha = 30^\circ$$

TABLE 2.

MAIN PARAMETERS DEFINED BY EQUATIONS (4) - (12) ⁽²⁸⁴⁾ (Å).

$$\delta_{100} = I_{[100]\alpha} - I_{[1120]\alpha} = - 0.0031_0$$

$$\delta_{010} = - 0.001537$$

$$\delta_{001} = + 0.031739$$

$$\Delta_{10} = + 0.111928$$

$$\Delta_{01} = - 0.020347$$

per equation (20)) = 87.26 \approx 87

DIMENSIONS OF COHERENT SECTION IN ZERO PLANE $M_{cr} = \pm 48$ $p = 0$ (equations (15), (16) and (14))

No. of series (M)	No. of end atoms in the series N_{cr}^+ (Equation 15)	N_{cr}^-	Length of Coherent Section ($N_{cr}^+ - N_{cr}^-$) (Equation 16)	No. of atoms in row subject to minimum displacement (No) (Equation (14))
0	-1750.35	+ 1750.35	3500.70	0
1	-1750.48	+ 1749.49	3499.97	- 2.02
2	-1749.86	+ 1747.87	3497.73	- 4.03
3	-1748.49	+ 1745.51	3496.36	- 6.08
4	-1746.37	+ 1742.40	3488.77	- 8.07
5	-1743.50	+ 1738.54	3082.04	-10.08
10	-1717.67	+ 1707.75	3425.42	-20.17
15	-1671.90	+ 1657.02	3328.92	-30.25
20	-1604.37	+ 1584.54	3188.91	-40.34
25	-1512.05	+ 1487.26	2999.31	-50.42
30	-1389.82	+ 1360.07	2749.89	-60.51
35	-1228.47	+ 1193.76	2422.23	-70.59
40	-1008.74	+ 969.07	1977.81	-80.68
45	- 673.38	+ 628.76	1302.14	-90.76
46	- 575.31	+ 529.70	1105.01	-92.78
47	- 452.28	+ 405.68	857.96	-94.80
48	- 269.12	+ 221.518	49.6380	-96.81

$$p = 1, \quad M_{cr+} = +48.66, \quad M_{cr-} = -48.29$$

No. of row (M)	No. of end atoms in row		Length of Coherent Section ($N_{cr+} - N_{cr-}$)
	N_{cr+}	N_{cr-}	
+ 48	- 300.76	+ 273.64	574.40
+ 45	- 678.99	+ 654.84	1333.83
+ 40	-1007.82	+ 988.63	1996.45
+ 30	-1384.58	+1375.31	2759.89
+ 20	-1596.96	+1597.61	3194.57
+ 10	-1708.68	+1719.24	3427.92
+ 5	-1733.81	+1749.33	3483.14
0	-1739.99	+1760.47	3500.46
- 5	-1727.49	+1752.93	3480.42
- 10	-1696.00	+1726.39	3422.39
- 20	-1571.19	+1611.50	3182.69
- 30	-1344.49	+1394.72	2739.21
- 40	- 948.98	+1009.12	1958.10
- 45	- 601.58	+ 666.68	1268.26
- 48	- 158.28	+ 226.35	384.63

TABLE 5DIMENSIONS OF COHERENT SECTION IN 40th PLANE(EQUATIONS (15), (16) and (14))

$p = 40, M_{cr+} = +50.36, M_{cr-} = -35.82$

No. of row. M	Number of end atoms in row	
	N_{cr+}	N_{cr-}
+ 50	+ 184.20	+ 585.29
+ 40	- 622.18	+1401.58
+ 30	- 927.02	+1716.35
+ 20	-1086.68	+1885.92
+ 10	-1148.03	+1957.18
0	-1123.88	+1942.95
- 10	-1010.78	+1839.77
- 20	- 785.01	+1623.92
- 30	- 356.19	+1205.01
- 35	+ 125.45	+ 728.33
- 36	-	-

TABLE 6DIMENSIONS OF COHERENT SECTION IN 86th PLANE(EQUATIONS (15), (16) and (14))

$$p = 86, \quad M_{cr+} = +23.91, \quad M_{cr-} = +7.36$$

Number of Row (M)	Number of end atoms in row	
	N_{cr+}	N_{cr-}
- 23	- 677.94	+1005.64
+ 20	+ 616.56	+1124.61
+ 15	+ 574.97	+1171.16
+ 10	+ 656.43	+1094.65
+ 5	-	-
10	-	-
- 5	-	-
+ 7	-	-

TABLE 7DIMENSIONS OF COHERENT SECTION IN 87th PLANE(EQUATIONS (15), (16) and (14))

$$p = 87, \quad M_{cr+} = +19.71, \quad M_{cr-} = +11.92$$

Number of row (M)	Number of end atoms in row	
	N_{cr+}	N_{cr-}
+ 20	-	-
+ 19	+ 800.14	+ 962.49
+ 18	+ 765.24	+ 998.39
+ 17	+ 748.22	+1016.40
+ 16	+ 742.22	+1023.40
+ 15	+ 745.67	+1020.94
+ 14	+ 759.24	+1008.35
+ 13	+ 786.95	+ 981.64
+ 12	+ 855.94	+ 913.64

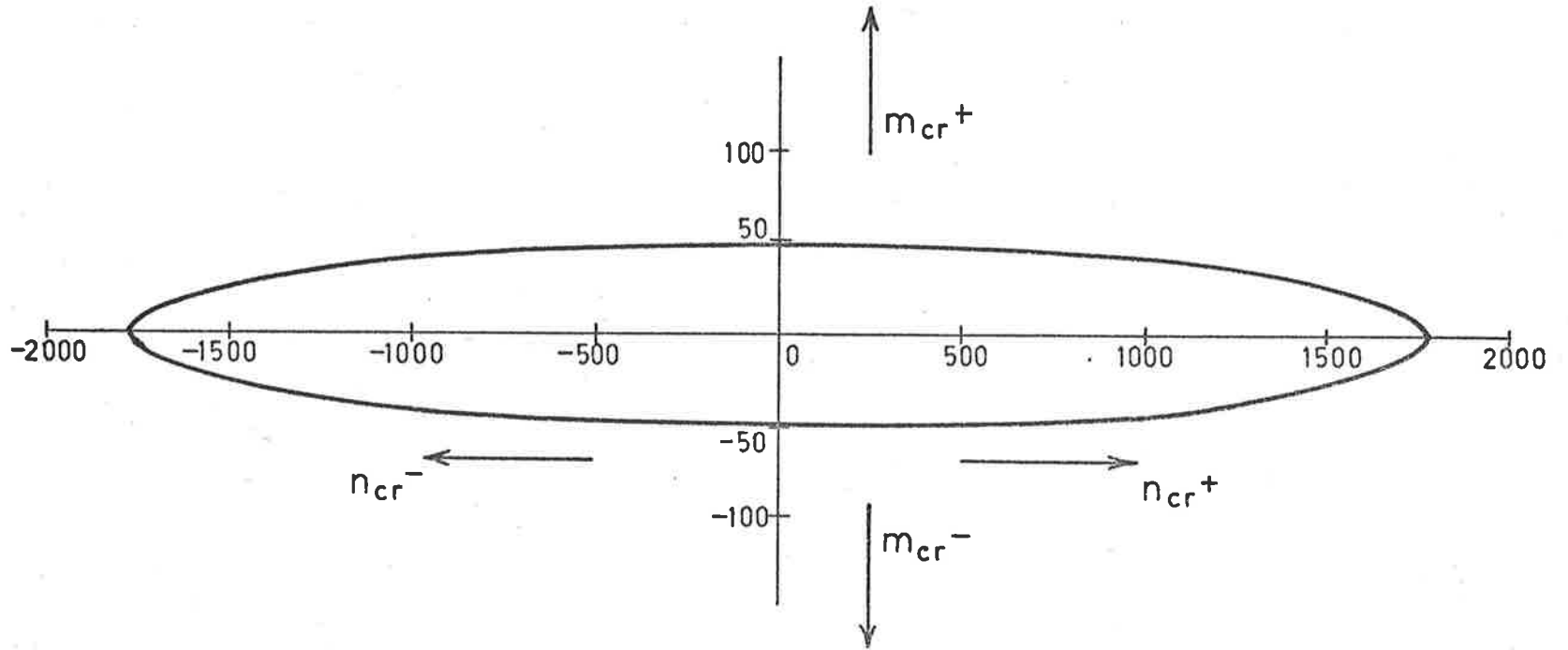


Fig. 2. Two dimensional Shape of Zero Plane.

TABLE 8
DIMENSIONS OF COHERENT REGION IN P PLANES

P Planes	M_{cr+}	M_{cr-}	No. of rows in coherent section $M_{cr+}-M_{cr-}$	No. of rows subject to minimum displacement M_0	No. of end atoms in row having number (M_0) $(N_{cr})_o$ $(N_{cr})_o$		No. of end atoms in row having number $(N_{moP})_o$	No. of atoms in row having number $/(N_{cr})_o/-/(N_{cr})_o/$
0	+48.48	-48.48	96.96	-	-1750.35	+1750.35	-	3500.70
1	+48.66	-48.29	96.95	-0.181787	-1739.96	+1760.62	+10.3285	3500.58
2	+48.83	-48.10	96.93	-0.363573	-1729.44	+1770.75	+20.6570	3500.19
3	+49.00	-47.90	96.90	-0.545360	-1718.78	+1780.75	+30.9855	3499.53
4	+49.15	-47.70	96.85	-0.727146	-1707.99	+1790.62	+41.31407	3498.61
5	+49.31	-47.49	96.80	-0.908933	-1697.07	+1800.35	+51.6425	3497.42
10	+49.98	-46.34	96.32	-1.817865	-1640.49	+1847.06	+103.285	3487.55
20	+50.82	-43.55	94.37	-3.635730	-1517.32	+1930.46	+206.570	3447.78
30	+50.98	-40.07	91.05	-5.453595	-1380.38	+2000.09	+309.855	3380.47
40	+50.36	-35.82	86.18	-7.271460	-1228.81	+2055.09	+413.141	3283.90
50	+48.83	-30.65	79.48	-9.089325	-1061.28	+2094.13	+516.426	3155.41
60	+46.12	-24.30	70.42	-10.907190	-875.72	+2115.15	+619.711	2990.87
70	+41.68	-16.23	57.91	-12.725055	-668.96	+2114.95	+722.996	2783.91
80	+33.93	-4.84	38.77	-14.542920	-435.77	-	+826.281	435.77
85	+26.47	-	26.47	-15.451853	-306.63	-	+877.924	306.63
86	+23.91	-	23.91	-15.633639	-279.59	-	+888.252	279.59
87	+19.71	-	19.71	-15.815426	-252.15	-	+898.581	259.12
88	-	-	-	-	-	-	-	-

BIBLIOGRAPHY

1. A.R. Ubbelohde, Quart. Rev. 11, (1957), pp 246 - 272.
2. A.R. Ubbelohde, Proc. Roy. Soc. A 159, (1937), pp 295 - 305.
3. A.R. Ubbelohde, Colloques Internationaux C.N.R.S. No. 205, (1972), "Étude des Transformations Cristallines à Haute Température".
4. J.W. Christian, "The Theory of Transformations in Metals and Alloys", Pergamon Press (1965).
5. J. Burke, "Kinetics of Phase Transformations in Metals", (1965), Pergamon Press.
6. M.E. Fine, "Phase Transformations in Condensed Systems", (1965), MacMillan.
7. K.C. Russell, ch. 6 in "Phase Transformations" (1968), American Society for Metals, Ohio.
8. W.T. Read, "Dislocations in Crystals", (1953) McGraw-Hill Publishers.
9. D. Hull, "Introduction to Dislocations", (1965), Pergamon Press.
10. R.W. Cahn (edit.), "Physical Metallurgy" (1965), ch. 13, North Holland Publ. Co.
11. P-Y. F. Robin, Amer. Mineral. 59, (1974), pp 1286 - 1298.
12. J.D. Bernal, "On Topotaxy", Schweizer Archiv. Jahrb. 26, (1960), pp 69 - 73.
13. L.S. Dent Glasser, F.P. Glasser and H.F.W. Taylor, Quart. Reviews 16, (1962), pp 343 - 360.
14. D.R. Dasgupta, Indian J. Earth Sciences 1, (1974), pp 60 - 72.
15. J.M. Thomas, Philosophical Trans. Royal Soc. London. 277, (1974), No. 1268, pp 251 - 286.
16. J.W. Christian, Inst. Met. Monograph, No. 33, (1968), pp 129 - 142.
17. L.S. Lieberman, in "Phase Transformations" (1968), American Soc. for Metals, pp 1 - 58.

18. L. Bragg and G.F. Claringbull, "Crystal Structures of Minerals", Vol. 4, (1965), pp 127 - 135.
19. I. Kostov, "Mineralogy" (1968), Oliver Boyd Publ., London, p. 529.
20. H.D. Megaw and C.N.W. Darlington, Acta Cryst. A31, (1975), pp 161 - 173.
21. A. Yamamoto, Y. Shiro, H. Murata, Bull. Chem. Soc. Japan 47 (2), (1974), pp 265 - 273.
22. M. Plihal, Phys. Stat. Sol. (6) 56, (1973), pp 495 - 506.
23. E.C. Subbarao, H.S. Maiti and K.K. Srivastava, Phys. Stat. Solidi (a) 21, (1974), pp 8 - 40.
24. W.L. Fraser, S.W. Kennedy and M.R. Snow, Act Cryst. B31, (1975), pp 365 - 370.
25. J.D.C. McConnell and J. Lima de Faria, Mineralog. Mag. 32, (1961), pp 898 - 901.
26. P. Cherin, W.C. Hamilton and B. Post, Acta Cryst. 23, (1967), pp 455 - 460.
27. J.S. Bowles and J.K. Mackenzie, III, Acta Met. 2, (1954), pp 224 - 234.
28. J.S. Bowles and J.K. Mackenzie, II, Acta Met. 2, (1954), pp 138 - 147.
29. J.S. Bowles and J.K. Mackenzie, I, Acta Met. 2, (1954), pp 129 - 137.
30. H.M. Ledbetter and C.M. Wayman, Mater. Sci. Eng. 7, (1971), pp 151 - 157.
31. A.G. Freeman, paper presented at Ninth Meeting of Australian Crystallographers, La Trobe University, Victoria, Australia, (1973).
32. M. DiDomenico and S.H. Wemple, Phys. Rev. 155, (1967), (2), pp 539 - 545.
33. J.S. Bowles and J.K. Mackenzie, Acta Met. 10, (1962), pp 623 - 636.
34. M.J. Buerger, Fortschr. Miner. 39, (1961), pp 9 - 24.
35. R.P. Zerwekh and C.M. Wayman, Acta Met. 13, (1965), pp 99 - 107.

36. S.W. Kennedy and J.H. Patterson, Proc. Roy. Soc. A, 283, (1965), pp 498 - 508.
37. S.W. Kennedy, J. Mat. Sci. 9, (1974), pp 1043 - 4.
38. S. Chatterji, A.L. Mackay and J.W. Jeffrey, J. App. Cryst. 4, (1971), p. 175.
39. M.S. Wechsler, D.S. Lieberman and T.A. Reid, Trans. A.I.M.E. 197, (1953), pp 1503 - 1515.
40. W.L. Fraser and S.W. Kennedy, Acta Cryst. A30, (1974), pp 13 - 22.
41. W.L. Fraser, Chemical Martensite Crystallography, Ph. D. Thesis, (1974).
42. W.L. Fraser and S.W. Kennedy, Acta Cryst. B28, (1972), p. 3101.
43. S.W. Kennedy, J.H. Patterson, R.P. Chaplin, A.L. Mackay, J. Solid State Chemistry 10, (1974), pp 102 - 107.
44. M.J. Buerger, "Phase Transformations in Solids", ed. R. Smoluchowski, J.E. Mayer, and W.A. Weyl, John Wiley (1951), p. 183.
45. S.W. Kennedy, Nature 210, (1966), pp 936 - 937.
46. C.M. Wayman, Intro. to the Crystallography of Martensite Transformations, (1964), MacMillan, New York.
47. A. Kelly and G.W. Groves, "Crystallography and Crystal Defects," Longman Group Ltd., (1970), p. 36.
48. S.W. Kennedy, G.F. Taylor, and (in part) J.H. Patterson, Phys. Stat. Sol. 16, (1966), pp K175 - 8.
49. R.N. Brown and A. C. McLaren, Acta. Cryst. 15, (1962), pp 974 - 6.
50. P.P. Salhotra, E.C. Subbarao, P. Venkateswarlu, Phys. Stat. Sol. 29, (1968), pp 859 - 64.
51. S.W. Kennedy, Phys. Stat. Sol. (a) 2, (1970), pp 415 - 8.
52. K.O. Stromme, Acta Chem. Scandinavica 25, (1971), pp 211 - 18.
53. Chr. Finbak, O. Hassel and L.C. Strømme, Zeit. Physik. Chem., B37, (1937), pp 468 - 71.
54. Chr. Finbak, O. Hassel, Zeit. Physik Chem. B35, (1937), pp 25 - 9.

55. U. Korhonen, Annales Acad. Scient. Fennicae AI., No. 102, (1951), pp 37 - 58.
56. W.H. Zachariassen, Skr. Norske Vid. - Akad. Oslo, I. Mat. -Natv. KI., (1928), pp 74 - 82.
57. L. Pauling and J. Sherman, Zeit. Krist. A.84, (1933), pp 213 - 216.
58. P.C. Bury and A.C. McLaren, Phys. Stat. Sol. 31, (1969), pp 799 - 806.
59. S.V. Karpov and A.A. Shultin, Phys. Stat. Sol. 39, (1970), pp 33 - 8.
60. T.P. Delacy and C.H.L. Kennard, Aust. J. Chem. 24, (1971), pp 165 - 7.
61. V.E. Plyushev, I.B. Markina, L.P. Shklover, Dokl. Akad. Nauk. SSSR. 108, (1956), P. 645.
62. A. Mustajoki, Annales Acad. Scient. Fennicae, AVI, (1958), No. 9.
63. A. Arell and M. Varteva, Annales Acad. Scient. Fennicae, AVI, (1961), No. 88.
64. B. Cleaver, E. Rhodes and A.R. Ubbelohde, Proc. Roy. Soc. A 276, (1963), pp 453 - 60.
65. K.J. Rao and C.N.R. Rao, J. Mat. Sci. 1, (1966), pp 238 - 48.
66. J.H. Fermor and A. Kjekshus, Acta Chem. Scandinavica 26, (1972), pp 2645 - 54.
67. A.N. Murin, I.V. Murin and B.S. Kornev, Russian J. Phys. Chem. 48, (1974), No. 7, pp 1042 - 3.
68. A. Ya. Dantsiger and E.G. Fesenko, Soviet Physics - Crystallography 8, (1964), No. 6, pp 717 - 720.
69. A. Ya. Dantsiger and E.G. Fesenko, Soviet Physics - Crystallography 10, (1965), No. 3, pp 272 - 274.
70. P.C. Bury and A.C. McLaren, Phys. Stat. Sol. 31, (1969), pp K5 - 7.
71. J.H. Fermør and A. Kjekshus, Acta Chem. Scandinavica 22, (1968), No. 6, pp 2054 - 5.
72. C.N.R. Rao, B. Prakash and M. Natarajan, National Bureau of Standards - N.S.R.D.S., No. 53, (1975).

73. S. Gordon and C. Campbell, Anal. Chem. 27, (1955), pp 1102 - 1109.
74. A.C. McLaren, Rev. Pure. Appl. Chem. 12, (1962), pp 54 - 71.
75. D.M. Newns and L.A.K. Staveley, Chem. Rev. 66, (1966), pp 267 - 278.
76. P.P. Salhotra, E.C. Subbarao, P. Venkateswarlu, Phys. Stat. Sol. 31, (1969), pp 233 - 6.
77. P. Cerisier and J. Guitard, C.R. Acad. Sc. Paris t 268 B, (1969), pp 1582 - 5.
78. F. Wallerant, Bull. Soc. fr. Minér. Cristallogr. 28, (1905), pp 311 - 374.
79. E.W. Courtenay and S.W. Kennedy, Aust. J. Chem. 27, (1974), pp 209 - 11.
80. Chr. Finbak and O. Hassel, J. Chem. Phys. 5, (1937), pp 460 - 461.
81. P.W. Bridgman, Proc. Am. Ac. Art. Sic. 72, (1937), p.46.
82. A.J. Iversen, Honours Report, University of Adelaide, (1970).
83. B. Cleaver and J.F. Williams, J. Phys. Chem. Solids 29, (1968), pp 877 - 880.
84. P.P. Salhotra, E.C. Subbarao and P. Venkateswarlu, J. Phys. Soc. Japan 27, (1969), pp 621 - 628.
85. M.H. Brooker, J. Chem. Phys. 59, (1973), pp 5828 - 29.
86. J.P. Devlin and D.W. James, Chem. Phys. Letters 7, (1970), pp 237 - 241.
87. T.P. Myasnikova and A.F. Yatsenko, Soviet Physics - Solid State 8, (1967), No. 9, pp 2252 - 3.
88. M.H. Brooker and D.E. Irish, Canadian J. Chem. 48, (1970), pp 1183 - 97.
89. R.A. Schreoder, C.E. Weir and E.R. Lippincott, J. Res. Nat. Bur. Stand. A.66, (1962), pp 407 - 434.
90. R.S. Halford, J. Chem. Phys. 14, (1946), pp 8 - 15.
91. J.H. Fermor and A. Kjekshus, Acta Chem. Scandinavica 27, (1973), pp 915 - 23.
92. J. Frenkel, Kinetic Theory of Liquids, Oxford Univ. Press, London, (1946).

93. L. Pauling, Phys. Rev. 36, (1930), pp 430 - 443.
94. J.J. Lander, J. Chem. Phys. 17, (1949), pp 892 - 901.
95. A.J. Iversen and S.W. Kennedy, Acta Cryst. B29, (1973), pp 1554 - 5.
96. A. Ya. Dantsiger, Soviet Physics - Solid State 7, (1966), pp 1845.
97. A.J. Dekker, Solid State Physics, MacMillan & Co. Ltd., London, (1965), pp 109 - 116.
98. C. Kittel, Intro. to Solid State Physics, John Wiley & Sons, (1968), pp 582 - 587.
99. N.F.M. Henny, H. Lipson and W.A. Wooster, The Interpretation of X-Ray Diffraction Photographs, MacMillan & Co. Ltd., (1960), pp 164 - 167, and appendices 1 and 2.
100. International Tables for X-Ray Crystallography, Vol. 1, (1952), Chapter 2.5.
101. H. Terauchi and Y. Yamada, J. Phys. Soc. Japan 33, (1972), pp 446 - 454.
102. Y. Shinnaka, J. Phys. Soc. Japan 19, (1964), pp 1281 - 90.
- 102a. R.G. Levesey, E. Lyford and H. Moore, J. Scientific Instrum. (J. Physics E) 1, Series 2, (1968), pp 1378.
103. R. Gomer, Rev. Sci. Instrum. 24, (1953), p. 993.
104. R.E. Aitchison, Aust. J. Appl. Sci. 5, (1953), pp 10 - 17.
105. M. Odlyha, M.Sc. Thesis, University of Adelaide, (1970).
106. K.W. Andrews, D.J. Dyson and S.R. Keown, Interpretation of Electron Diffraction Patterns, Adam Hilger Ltd., London (1971).
107. M.J. Buerger, The Precession Method in X-Ray Crystallography, John Wiley & Sons Inc., (1964).
108. S.W. Kennedy, private communication.
109. R.K. Stringer, C.E. Warble and L.S. Williams, Materials Science Research 4, Ed. by T.J. Gray and V.C. Fréchette, Kinetics of Reactions in Ionic Systems (1969).
110. C. Hennig, R. Lees and M.S. Matheson, J. Chem. Phys. 21, (1953), pp 664 - 668.

111. E.R. Johnson and J. Forten, Discussions Farad. Soc. 31, (1961), pp 238 - 246; J. Phys. Chem. Solids 15, (1960), pp 218 - 224.
112. C. Hochanadel and T. Davis, J. Chem. Phys. 27, (1957), pp 333 - 334.
113. J. Cunningham, H.G. Heal, Nature 179, (1957), pp 1021 - 1022; Trans. Farad. Soc. 54, (1958), pp 1355 - 1369.
114. D. Hall and J.N. Walton, J. Inorg. Nucl. Chem. 6, (1958), pp 288 - 294.
115. E.N. Ladov and E.R. Johnson, J. Am. Chem. Soc. 91, (1969), pp 7601 - 6.
116. L.W. Hamilton and M.D. Ingram, J. Chem. Soc., Faraday Transactions 68, (1972), pp 785 - 96.
117. H.B. Pogge and F.T. Jones, J. Phys. Chem., 74, (1970), pp 1700 - 1705.
118. K.O. Stromme, Acta Chem. Scand. 23, (1969), pp 1625 - 1636.
119. P. Touzain, F. Brisse and M. Caillet, Canadian J. Chem. 48, (1970), pp 3358 - 3361.
120. W.M. Kriven, Honours Report, University of Adelaide, (1970).
121. J.D.C. McConnell, Phil. Mag. 20, (1970), pp 1195 - 1202.
122. S.W. Kennedy, J. Crystal Growth 16, (1972), pp 274 - 276.
123. F.J. Turner, D.I. Griggs and H. Heard, Bull. Geol. Soc. America 65, (1954), pp 883 - 933.
124. J.M. Thomas and G.D. Renshaw, Trans. Farad. Soc. 61, (1965), pp 791 - 6.
125. R.E. Keith and J.J. Gilman, Acta Met. 8, (1960), pp 1 - 10.
126. G.D. Renshaw and J.M. Thomas, Nature 209, (1966), pp 1196 - 7.
127. J.M. Thomas and G.D. Renshaw, J. Chem. Soc. (A) (1967), pp 2058 - 2061.
128. W.E. Garner, "The Chemistry of the Solid State", Butterworths Scientific Publications, (1955), pp 223 - 8.
129. A.W.D. Hills, Chem. Engin. Sci. 23, (1968), pp 297 - 320.
130. D.A. Young, "Decomposition of Solids", Pergammon Press, (1966), pp 64.

131. D.R. Dasgupta, Indian J. Physics 38, (1964), pp 623 - 626.
132. D.R. Dasgupta, Indian J. Physics 35, (1961), pp 401 - 419.
133. J.F. Goodman, Proc. Roy. Soc. A 247, (1958), pp 346 - 352.
134. W.H. Rhodes and B.J. Wuensch, J. Amer. Ceramic Soc. 56, (1973), pp 495 - 496.
135. B.J. Burrage and D.R. Pitkethly, Phys. Stat. Solidi 32, (1969), pp 399 - 405.
136. K.O. Stromme, Acta Chem. Scand. 24, (1970), pp 1475 - 7.
137. J.F. Grayson, Micropaleontology 2, (1956), pp 71 - 8.
138. J.W. Christian, Proc. Roy. Soc. A 206, (1951), pp 51 - 64.
139. S.Z. Bokshiteyn, V.G. Ly tssau, I.M. Razumovsky, T.L. Svetlov, Yu M. Fishman, Fiz. Metal. Metalloved 33, (1972), pp 1277 - 1284.
140. R.F. Bartholomew, J. Phys. Chem. 70, (1966), pp 3442 - 6.
141. R.N. Kust and F.R. Duke, J. Am. Chem. Soc. 85, (1963), pp 3338 - 40.
142. S. Gordon and C. Campbell, Anal. Chem. 27, (1955), pp 1103 - 9.
143. L.K. Narayaswany, Trans. Farad. Soc. 31, (1935), pp 1411 - 1412.
144. P. Doigan and T.W. Davis, J. Phys. Chem. 56, (1952), pp. 764 - 766.
145. A.O. Allen and J.A. Ghormely, J. Chem. Phys. 15, (1947), p. 208.
146. H.G. Harrison and Ng Hok Nam, J. Chem. Soc., Farad. Trans. 8, (1973), pp 1432.
147. A.G. Maddock and S.R. Mohanty, Discussions Faraday Soc. 31, (1961), pp 193 - 202.
148. G.E. Boyd and M.H. Brooker, J. Am. Chem. Soc. 95, (1973), pp 4813 - 4821.
149. J. Cases - Casanova, Société Chimique de France, Bulletin. (1959), Nos. 77, 78, pp 429.
150. P. Pringsheim, J. Chem. Phys. 23, (1955), pp 369 - 375.
151. S.W. Kennedy, J. Appl. Cryst. 6, (1973), pp 293 - 5.

152. R. Le Hazif, P. Dorizzi and J.P. Poirier, Acta Met. 21, (1973), pp 903 - 911.
153. L.G. Schulz, Acta Cryst. 5, (1952), pp 264 - 265.
154. P.G. Partridge, Third European Conference on Electron Microscopy (Prague) (A), (1964), p 391.
155. E.D. Glover and R.F. Sippel, Amer. Min. 47, (1962), pp 1156 - 1165.
156. J.A. Gard, Third European Regional Conference on Electron Microscopy (Prague) (A), (1964), pp 333 - 334.
157. A. Kelly and G.W. Groves, Crystallography and Crystal Defects, Longman Group Ltd., (1970), ch. 10.
158. E.P. Hyatt, I.B. Cutler, M.E. Wadsworth, J. Amer. Ceramic Soc. 41, (1958), pp 70 - 74.
159. P.B. Hirsch, A. Howie, R.B. Nicholson, D.W. Pashley and M.J. Whelan, "Electron Microscopy of Thin Crystals," Butterworths, London, (1965).
160. F. Laves, J. Geol. 58, (1950), pp 548 - 571.
161. J.D.C. McConnell, Phil. Mag. 11, 8th. Ser. (1965), pp 1289 - 1301.
162. J.D.C. McConnell, Phil. Mag. 19, 8th. Ser. (1969), pp 221 - 229.
163. J.S. Anderson, Int. Symp. on "Reactivity of Solids", ed. by J.S. Anderson, W.M. Roberts, F.S. Stone (1972), pp 1 - 22.
164. A. Kelly and G.W. Groves, "Crystallography and Crystal Defects," Longman Group Ltd., (1970), Ch. 8.
165. V.N. Gurarii, N.I. Alyushina, V.N. Berezovskii, E.V. Danilova, (a) Fiz. Khim. Obrab. Mater. (1974) (6), pp 96 - 102, (in Russian); (b) Chem. Abstracts 82, (1975), No. 26, code No. 178424x.
166. H. Fujita, T. Tabata, K. Yoshida, N. Sumida, Japanese J. Appl. Phys. 11, (1972), pp 1522 - 1536.
167. J.W. Cahn, Trans. Met. Soc. A.I.M.E. 242, (1968), pp 168 - 180.
168. R.A. Yund and R.H. McCallister, Chem. Geol. 6, (1970), pp 5 - 30.
169. F. Laves, J. Geol. 60, (1952), pp 436 - 450.
170. J.B. Jones and W.H. Taylor, Acta Cryst. 14, (1961), pp 443 - 456.
171. W.S. MacKenzie and J.V. Smith, Amer. Miner. 41, (1956), pp 405 - 427.

172. J.D.C. McConnell, Min. Mag. 38, (1971) pp 1 - 20
173. M.C. Brown and P. Gay, Zeits. Krist 111, (1958) pp 1 - 14
174. J.W. Christian, The Theory of Transformations in metals and alloys, Pergammon Press (1965), CR XXI.
175. N.Datta, S. Chatterji, J.W. Jeffrey and A.L. Mackay Min. Mag. 37 (1969) pp 250 - 252.
176. A. Frances and E.R. Johnson, J. Phys. Chem. 79, (1975) pp 35 - 38.
177. L.P. Eremin, A.N. Oblavancev, Khim. Vys. Energ. 5 (3) (1971), pp 266 - 7.
178. H. Shôji, Zeit. für Kristallogr. 77, (1931), pp 381 - 410
179. W.L. Fraser, Honours Report, (1970), University of Adelaide.
180. R.W. Cahn, Advances in Physics 3, Phil Mag. Suppl., (1954), pp 363 - 445.
181. J.S. Bowles, J.K. Mackenzie, Acta Met. 2, (1954), pp 138 - 147.
165. V.N. Gurarii, N.I. Alyushina, V.N. Berezovskii, E.V. Danilova, (a) Fiz. Khim. Obrab. Mater. (1974) (6), pp 96 - 102, (in Russian); (b) Chem. Abstracts 82, (1975), no. 26, code no. 178424x.
182. D.J. Barber and H.R. Wenk, 8th Intern. Congress Electron Microscopy, Canberra (1974), 1, pp 480 - 481.
183. B.G. Hyde and M.O. Keefe (1973), Conference on Phase Transitions and their Applications in Materials Science, Penn. State. Uni., New York: Pergammon.
184. A.P. Janssen, R.C. Schoonmaker and A. Chambers, Surface Sci. 49, (1975) pp 143 - 160.
185. Z.S. Basinski and J.W. Christian, Phil. Mag. 44, (1953), pp 791 - 2.
186. M.J. Buerger, Amr. Miner 30, (1945), pp 469 - 482.
187. J.H. Van der Merwe, Surface Sci. 31, (1972) pp 198 - 228.
188. P.B. Hirsch, "Reactivity of Solids" (1972) pp 362 - 363, Ed. by J.S. Anderson, W.M. Roberts, F.S. Stone, (John Wiley and Sons).

189. R.W. Cahn, Progress in Metal Physics 2, (1950) Ed. B. Chalmers, Ch. 5.
190. J.E. Burke and D. Turnbull, Progress in Metal Physics 3, (1952), Ch. 7, Ed. B. Chalmers.
191. R.W. Cahn, "Physical Metallurgy", (1965), Ch. 19, (North Holland Publ. Co.).
192. American Society for Metals, Metals Park, "Recrystallization, grain growth and textures", (1965), Ch. 2.
193. J.S. Bowles, C.S. Barrett and L. Guttman, Trans. A.I.M.E. 188, (1950), pp 1478 - 1485.
194. Z.S. Basinski and J.W. Christian, Acta Met. 2 (1954), pp 101 - 116.
195. Z.S. Basinski and J.W. Christian, Acta Met. 2 (1954), pp 148 - 166.
196. S.W. Kennedy, J. Mat. Sci. 9, (1974), pp 1391 - 2.
197. W.S. Fyfe, "Geochemistry", (1974), Clarendon Press Oxford.
198. R.C. Newton, J.R. Goldsmith & J.V. Smith, Contr. Mineral and Petrol 22, (1969), pp 335 - 348.
199. J.H. Burns and M.A. Bredig, J. Chem. Phys. 25, (1956) pp 1281.
200. (a) F. Dacheville and R. Roy, (in) J.H. de Boer et al (eds.) "Reactivity of Solids", Elsevier, (1960) Amsterdam, pp 502 - 511; (b) and elsewhere.
201. J.C. Jamieson and J.R. Goldsmith, Amer. Mineral. 45, (1960), pp 818 - 827.
202. D.O. Northwood and D. Lewis, Canad. Mineral. 10, (1970), pp 216 - 224.
203. J.C. Jamieson, J. Chem. Physics 21, (1953), pp 1385 - 90.
204. G.J.F. MacDonald, Amer. Mineral. 41, (1956) pp 744 - 756.
205. J.C. Jamieson, J. Geol. 65, (1957), pp 334 - 343.
206. S.P. Clark, Amer. Mineral. 42, (1957), pp 564 - 6.

207. A.R. Verma and P. Krishna, "Polymorphism and Polytypism in Crystals", (1966), John Wiley and Sons, Inc.
208. W.L. Bragg, Proc. Roy. Soc. A 105, (1924) pp 16 - 39.
209. H.E. Swanson, R.K. Fuyat and G.M. Ugrinic, Nat. Bur. Stand. Circ. 539, III, (1954), pp 53 - 55.
211. Y. Hiragi, S. Kachi, T. Takada and N. Nakanishi, Bull. Chem. Soc. Japan 39, (1966) pp 2361 - 4.
212. B Dickens and J.S. Bowen, J. Res. Bur. Stand. 75A, (Phys. and Chem.), (1971), pp 27 - 32.
213. W.L. Bragg, Proc. Roy. Soc. A89, (1914), pp 468 - 489.
214. G. Chaudron, H. Mondange, M.M. Pruna, Proc. Int. Symp. on Reactivity of Solids, Gothenburg (1952), pp 9 - 20.
215. B.L. Davis and L.H. Adams, J. Geophys. Res. 70, no. 2, (1965) pp 433 - 441.
216. R.H. Kunzler and H.G. Goodell, Amer. J. Science 269, (1970) pp 360 - 391.
217. M Subba Rao, Indian J. Chem. 11, (1973) pp 280 - 283.
218. W.H. Brown, W.S. Fyfe and F.J. Turner, J. Petrol 3, (1962), pp 566 - 82.
219. Mondange - Dufy, Ann. de Chimie (Paris) 5, (1960), pp 107 - 163.
220. Y. Hiragi, S. Kachi, T. Takada, N. Nakanishi, J. Chem. Soc. Japan (Pure Chem. Section) 87, (1966), pp 1308 - 11.
221. S.W. Kennedy and M. Odlyha, Aust. J. Chem. 27, (1974). pp 1121 - 4.
222. H. Shôji, Zeit. fur Krist. 84, (1933), pp 74 - 84.
223. S. Kôzu and K. Kani, Imp. Acad. Japan Proc. 10, (1934); part II, pp 271 - 3; part I, pp 222-225.
224. D.R. Dasgupta, Min. Mag. 33, (1964), pp 924 - 9.
225. B.L. Davis and E.H. Oshier, Amer. Mineral. 52, (1967), pp 957 - 973.

226. J.M. Craido and J.M. Trillo, J. Chem. Soc., Faraday Trans. I 71, (1975), pp 961 - 6.
227. E. Fries and C. Marhic, Bull. Soc. fr. Minéral. Cristallogr. 96, (1973), pp 91 - 96.
228. R.N. Shock and S. Katz, Amer. Mineral. 53, (1968), pp 1910 - 1917.
229. D.J. Barber and H.R. Wenk, J. Mat. Sci. 8, (1973) pp 500 - 508.
230. H.R. Wenk, C.S. Venkitasubramanyan, D.W. Baker, Contr. Mineral. and Petrol 38 (1973) pp 81 - 114.
231. J.K. Solbakk and K.O. Strømme, Acta Chem. Scandinavica 23, (1969) pp 300 - 313.
232. D.A. Edwards, Zeit. fur Krist. 80, (1931), pp 154 - 162.
233. H.E. Swanson and R.K. Fuyat, Nat. Bur. Stand. Circ. 539. III, (1954), pp 58 - 59.
234. Nagatani Masanori, Sakata Kazuhiro, Yamazoe Noboru, Kagoshima Daigaku Koga Kubu Kenkyu Hokoku 15 (1973), pp 69 - 77; (also) Chem. Abstracts 80, (1974), no. 16, no. 88144 k.
235. J.K. Nimmo and B.W. Lucas, J. Physics C : Solid State Physics 6, (1973), pp 201 - 211.
236. J.L. Amoros, M. Gutierrez, M.L. Canut, Bol. R. Soc. Espanola Hist. Nat. (Geol.) 62, (1964), pp 23 - 29.
237. M.A. Lonappan, Proc. Indian Acad. Sci. A41, (1956) pp 239 - 44.
238. J.K. Nimmo and B.W. Lucas, Nature 237, (1972), no. 73.
239. A. Dal-Negro and L. Ungaretti, Amer. Mineral. 56, (1971), pp 768 - 72.
240. P.E. Tahvonen, Annal. Acad. Scient. Fennicae A.I. 44, (1947).
241. H.F. Fischmeister, J. Inorg. Nucl. Chem. 3, (1956), pp 182 - 6.
242. H. Miek - Oja, Annal. Acad. Sci. Fennicae A.I. 7, (1941).

243. Y. Shinnaka, J. Phys. Soc. 17, (1962), pp 820 - 8.
244. M.K. Teng, Journal de Physique 31, (1970), pp 771 - 777.
245. J.C. Souffi and P. Cerissier, C.R. Acad. Sc. Paris 274 (1972), pp 774 - 777.
246. S. Sawada, S. Nomura, S. Fujii, J. Phys. Soc. Japan 13, (1958), pp 1549.
247. T. Yanagi, J. Phys. Soc. Japan 20, (1965), pp 1351 - 1365.
248. A. Chen and F. Chernov, Phys. Review 154, (1967), pp 493 - 505.
249. L. Leiserowitz, G.M.H. Schmidt, A. Shamgar, J. Phys. Chem. Solids 27 (1966), pp 1453 - 57.
250. H.E. Swanson and R.K. Fuyat, Nat. Bur. Stand. Circ. 539, II, (1953), pp 51 - 54.
251. W.A. Crawford and W.S. Fyfe, Science 144, (1964) pp 1569 - 1570.
252. M. Kantola and T. Tarna, Annal. Acad. Scient. Fennicae, A, IV, Physica, (1970), no. 335.
253. Y. Asao, I. Yashida, R. Ando, S. Sawada, J. Phys. Soc. Japan 17, (1962), pp 442 - 446.
254. P. Weidenthaler, Collection of Czechoslovak Chem. Communications 30, (1965) pp 629 - 638.
255. I. Yoshida, J. Phys. Soc. Japan 15, (1960), pp 199 - 200.
256. E.V. Khamskii and D.V. Tsikaeva, Zh. Prikl. Khim, (J. Appl. Chem. USSR), 47, (1974) pp 724 - 7.
257. V.V. Sipyagin and A.A. Chernov, Soviet Physics - Crystallography, 17, (1973), pp 881 - 885.
258. E.V. Khamskii and N.S. Dvegubskii, J. Appl. Chem. USSR 44 (1971), pp 476 - 478.
259. J. Tuech and H. Patin, C.R. Acad. Sc. Paris 269, Serie C, pp 1539 - 42.
260. S.V. Karpov and A.A. Shultin, J. Phys. Chem. Solids 29, (1968) pp 475 - 480.
261. M. Kamada and R. Kato, J. Phys. Soc. Japan 35, (1973) p 1561.
262. F.R. Rossini et al, Nat. Bur. Stand. Circ 500 (1952) p 806.

263. T.F.W. Barth, Zeit. für Physik Chem. B43 (1959) pp 448 - 450.
264. Yu. G. Asadov, and V.I. Nasirov, Soviet Physics - Doklady 15 (1970), pp 324 - 6.
265. Yu. G. Asadov and V.I. Nasirov, Soviet Physics - Crystallography 15, (1971), pp 1052 - 6.
266. Yu. G. Asadov, V.I. Nasirov, and G.A. Jabrailova, J. Crystal Growth 15, (1972), pp 45 - 50.
267. Yu. G. Asadov, V.I. Nasirov, Soviet Physics - Crystallography 17, (1973), pp 871 - 3.
268. M. Midorikawa, Y. Ishibashi, Y. Takagi, J. App. Physics Japan 37, (1968), pp 30 - 33.
269. R.E. Smallman and K.H.G. Ashbee, "Modern Metallography" Pergammon Press, Ch 3, (1966).
270. S. Tolansky, "An Introduction to Interferometry" (1973) Longman, London.
271. S.W. Kennedy, A.R. Ubbelohde and I. Woodward, Proc. Roy. Soc. Ser A 219, (1953), pp 303 - 11.
272. F. Jona and G. Shirane, "Ferroelectric Crystals", (1962).
273. Bh. Krishnamurty, T.V. Kameswara Rao, P.V. Rao and T. Visweswar, Indian J. Pure and Applied Physics, 11, (1973) pp 214 - 215.
274. S. Temin, J. Applied Polymer Science 9 (1965), pp 471 - 481.
275. E.J. Rochow, W.F. Gilliam, J. Am. Chem. Soc. 63, part 1, (1941), pp 798 - 800.
276. E.G. Rochow, Chem. Eng. News 23, (1945) pp 613 - 616.
277. E.G. Rochow, "Introduction to the Chemistry of Silicones", 2nd edition (1951).
278. S.B. Speck, J. Organic Chemistry, 18, (1953) pp 1689 - 1700.
279. W.F. Gilliam, H.A. Liebhafsky, and A.F. Winslow, J. Am. Chem. Soc. 63, pt. 1, (1941), pp 801 - 803.
280. J.F. Hyde and R.C. De Long, J. Am. Chem. Soc. 63, pt. 1, (1941), pp 1194 - 1196.

281. D.E. Bradley, in "Techniques for Electron Microscopy", ed by D.H. Kay, 2nd Edit., (1965) Blackwell Publ., chapter 5.
282. M. Midorikawa, Y. Takagi, Y. Ishibashi, J. Phys. Soc. Japan 28, (1970), pp 1001 - 1005.
283. M.J. Buerger "X-ray crystallography", (1958) John Wiley & Sons, (Publ.), pp 498 - 504.
284. V.I. Arkharov, Fiz. metal. metalloved. 12, (1961), pp 853 - 859, (English Translation).
285. V.I. Arkharov and Z.V. Kovendyaseva, Fiz. metal. metalloved. 13 (1962), pp 97 - 106.
286. V.I. Arkharov, Fiz. metal. metalloved. 13, (1962), pp 567 - 571.
287. J. Gionnes and A.F. Moodie, Acta Cryst 19, (1965) pp 65 - 67.
288. J.M. Cowley, A.L.G. Rees and J.A. Spink, Proc. Phys. Soc. 64 part 1, (1951), pp 609 - 619.
289. J.M. Cowley and A.F. Moodie, Acta Cryst. 12, (1959), pp 360 -
290. P. Goodman and G. Lehmpfuhl, Zeit. fur Naturforschung 19, (1964), pp 818 - 820.
291. On discussion with Dr. G. Anstis of G.R. Anstis, D.F. Lynch, A.F. Moodie and M.A. O'Keefe, Acta Cryst. A29 (1975) pp 138 - 47.
292. N.H. Hartshorne and A. Stuart, "Practical Optical Microscopy", (1969) Edition, Arnold Publ., p 189.
293. C.W. Allen of C.W. Allen, P. Delavignette, and S. Amelinckx, Phys. Stat. Sol. 9, (1972), pp 237 - 246. Paper given at International Electron Microscopy Conference, Canberra, Australia, August 1974.
294. S. Swaminathan and S. Srinivasan, Acta Cryst. A31, (1975) pp 628 - 634; (arrived in Adelaide 18-11-75).
295. H.E. Swanson and R.K. Fuyat, Nat. Bur. Stand. Circular 539 vol. II, (1953), pp 54 - 6.
296. J.J. Lander, J. Chem Phys. 17, (1949), pp 892 - 901.

297. H.E. Swanson and R.K. Fuyat, Nat. Bur. Stand. Circular 539
10, (1960), pp 11 - 12.
298. H.D. Megaw, Acta Cryst. A26, (1970), pp 235 - 244.
299. R.N. Brown and A.C. McLaren, Proc. Roy. Soc. 266, (1962),
pp 329 - 343.
300. T. Seiyama and N. Yamazoe, J. Cryst. Growth 2 (1968), pp 255 -
266.
301. I Michaelis de Saenz, J.C. Tessore, R. Leone, Schweiz. Min.
Petr. Mitt. 50 (1970), pp 209 - 220.
302. M. Nagatani, M. Hayama, N. Yamazoe, T. Seiyama, Kogyo
Kagaku Zasshi 70, (1967), pp 1633 - 1637.
303. S.W. Kennedy, J. Mat. Sci. 9, (1974), pp 2053 - 2056.
304. J.E. Bailey, Proc. Roy. Soc. A 279, (1964), pp 395 - 412.
305. R.N. Patil and E.C. Subbarao, J. Appl. Cryst. 2, (1969),
pp 281 - 288.
306. R.N. Patil and E.C. Subbarao, Acta Cryst. A26 (1970),
pp 535 - 542.
307. G.K. Bansal and A.H. Heuer, part I, Acta Met 20, (1972),
pp 1281 - 1289.
308. G.K. Bansal and A.H. Heuer, part II, Acta Met. 22, (1974)
pp 409 - 418.
309. J.C. Jaeger, "Elasticity, Fracture and Flow", (1964),
Menthuen and Co. Ltd., London.
310. K.L. Aurivillius, Acta Chem.Scandinavica 4, (1950), pp
1413 - 1436.
311. P. Auvray and F. Genet, Bull. Soc. fr. Minéral. Cristallogr.
96, (1973), pp 218 - 219.
312. H.E. Swanson, R.K. Fuyat and G.M. Ugrinic, Nat. Bur. Stand.
Circ. 539, II, (1953), pp 17 - 23.
313. F.W. Dickson and G. Tunell, Amer. Mineral. 44, (1959), pp
471 - 487.

314. T. Ohmiya, J. Appl. Cryst. 7, (1974), pp 396 - 397.
315. K. Naukkarinen and T. Tuomi, Phys. Stat. Sol. (a) 16, (1973), pp K 85 - 87.
316. H. Langlois, B. Auyrault, F. Lefin, and Y. Toudic, Phys. Stat. Solidi (b) 60, (1973), pp 821 - 33.
317. J. Barcelo, M. Galtier, A. Montaner, C.R. Acad. Sci., Ser.B 274, (1972), pp 1410 - 1413.
318. K.J. Siemsen and H.D. Riccius, Phys. Stat. Solidi (d) 37 (1970), pp 445 - 451.
319. B. Auyrault, H. Langlois, M.C. Lecocq - Mayer and F. Lefin Phys. Stat. Solidi 17(a), (1973), pp 665 - 676.
320. R. Zallen, G. Lucovsky, W. Taylor, A. Pinczuk, and E. Burstein, Phys. Rev. B 1, (1970), pp 4058 - 4070.
321. Y. Marqueton, B. Auyrault, E.A. Decamp. and Y. Toudic, Phys. Stat. Solidi (b) 60, (1973), pp 809 - 820.
322. J. Sapriel, Appl. Phys. Letters 19 (1971) pp 533 - 535.
323. M.A. Nusimovici and A. Meskaoui, Phys. Stat. Solidi 58(b), (1973), pp 121 - 125.
324. P. Dawson, Spectrochimica Acta 28A, (1972) pp 2305 - 2310.
325. H.E. Merwin, Zeit fur Amorg. Chem. 2, (1913) pp 125 - 189.
326. K.N. Rai and O.N. Srivastava, Ind. Journal of Pure and Appl. Physics 10, (1972), pp 108 - 110.
327. Y. Toudic, R. Aumont, J. Cryst. Growth 10 (1971), pp 170 - 174.
328. E.H. Carlson, J. Crystal Growth 1, (1967) pp 271 - 277.
329. G. Masse, J.P. Aicardi, J. Barcelo, F. Bombe, and G. Debais, Thin Solid Films 8 (1971), pp 397 - 409.
330. R.W. Garner and W.B. White, J. Crystal Growth 7 (1970), pp 343 - 347.
331. O.L. Curtis, J. Appl. Physics 33, (1962), pp 2461 - 2463.

332. A. Pajaczkowska, J. Crystal Growth 7, (1970), pp 93 - 96.
333. B.A. Bilby and J.W. Christian, J. Iron and Steel Institute; (1961), pp 122 - 131.
334. N.D.H. Ross and A.G. Crocker, Acta Met. 18 (1970), pp 405 - 418.
335. "The Modern University Dictionary", (1961), Ed. by A.H. Irvine, Publ. by The Educational Book Co., Ltd., London.
336. J.M. Robertson and A.R. Ubbelohde, Proc. Roy. Soc. Lond. A 167 (1938) pp 122 - 147.
337. J.D.C. McConnell, Annual Rev. of Earth and Planetary Sciences", 3, (1975), pp 129 - 155.
338. G.J. Allpress, J. Solid State Chemistry 4 pp 173 - 185.
339. J.G. Allpress, E.A. Hewart, A.F. Moodie, J.V. Sanders, Acta Cryst. A28 pp 528 - 536.
340. S. Jijima, (a) Acta Cryst. A29 (1973), pp 18 - (b) 8th International Congress on Electron Microscopy, (1974), Canberra, pp 242 - 243.
341. P.R. Buseck and S. Iijima, Amer. Mineral. 59, (1974), pp 1 - 21.
342. J.M. Cowley and A.F. Moodie, Proc. Phys. Soc. 76, (1960), pp 378 - 384.
343. J.M. Brown, J.L. Hutchison and J.S. Anderson (1972) in "7th Intl. Symp. Reactivity of Solids", ed. by J.S. Anderson, F.S. Stone and W.M. Roberts, London, pp 116.
344. B.E.F. Fender in "Int. Rev. of Sci. (Solid State Chem.)", (1972), Ed. by L.E.J. Roberts, Butterworths, London.
345. R.J.D. Tilley, *ibid.*
346. J.S. Anderson, in "Surface and Defect Properties of Solids", (Chem. Soc. Specialist Periodical Report), (1972), 1, pp 1.
347. A. Magnéli, Arkiv. Kemi 2, (1950), pp 513.
348. A.D. Wadsley, in "Non-Stoichiometric Compounds", (1964), ed. by L. Mandelcorn, Acad. Press, Lond, ch 3.

349. L. Nagle and M.O'Keefe, Int. Rev. Sci. Inorg. Chem. Ser. 1, 10, (1972), pp 1 - 36.
350. A.F. Acton and M. Bevis, Acta Cryst. A27, (1971), pp 175 - 179.
351. W. Bollman, Surface Science 31, (1972), pp 1 - 11.
352. W. Bollman, in "Crystal Defects and Crystalline Interfaces", (1970), Springer - Verlag, Berlin.
353. P.G. Fox, J. Materials Science, 10, (1975) pp 340 - 360.
354. M. Cohen, in "Phase Transformations in Solids", edit. by R.Smoluchowski, J.E. Mayer, W.A. Weyl, John Wiley and Sons, (1951), ch 17.
355. L. Delaey, R.V. Krishnan, H. Tas and H. Warlimont, J. Mat. Sci. 9, (1974), pp 1521 - 1535.
356. P.C. Clapp, Phys. Stat. Sol. (b)57, (1973) pp 561 - 569.
357. M. Mori, Y. Yamada and G. Shirane, Solid State Communications 17, (1975), pp 127 - 130.
358. L. Merrill, "Proc. Int. Conf. High Pressure" (4th); published (1975); Edit. by Osugi Jiro, Phys. Chem. Soc. Japan: Kyoto, Japan.
359. P.C. Rowlands, E.O. Fearon, M. Bevis, J. Mater. Sci., 5 (1970), pp 769 - 776
360. S.W. Kennedy and W.M. Kriven, Letter to J. Mater. Sci., (1976), in press.

PUBLISHED PAPERS

Kennedy, S. W., & Kriven, W. M. (1972). Surface effects before and after the aragonite-type to calcite-like transformation in potassium nitrate in relation to mechanism. *Journal of Materials Science*, 7(9), 1092-1095.

NOTE:

This publication is included in the print copy of the thesis held in the University of Adelaide Library.

It is also available online to authorised users at:

<https://doi.org/10.1007/bf00550077>